Silica diagenesis, polygonal faulting, and shallow gas: implications for fluid migration, storage, and shallow hazards

A thesis submitted to The University of Manchester for the degree of Doctor of Philosophy in the Faculty of Science and Engineering

By

Mohammed Malah

2021

Department of Earth and Environmental Science

Basin Studies and Petroleum Geoscience Group

List of Contents

Word count: 56221

List of Figures

List of Tables

Abstract

By integrating 3D seismic data, petrophysical well logs and well cuttings samples, three (3) broad areas related to hydrocarbon plumbing systems and subsurface fluid flow in the eastern Central North Sea are investigated in this research, silica diagenesis, polygonal faulting, and shallow gas accumulations. Silica diagenesis which involves a two-step process of the conversion of amorphous biogenic silica (Opal-A) to crystals of cristobalite or tridymite (Opal-CT) and subsequently to crystals of quartz has been identified in sedimentary basins around the world. This process has the potential of significantly affecting the physical, mechanical, and fluid flow properties of the host rock and are important to the development of sedimentary basins. This study identifies for the first time, the presence of an Opal-A/CT reaction front in the Cenozoic mudstones of the eastern CNS by the use of a range of techniques including X-ray diffraction data (XRD) and the Quantitative Evaluation of Minerals by Scanning Electron Microscope (QEMSCAN) and conventional 3D seismic and well data interpretation techniques. Further, we analysed the impact the presence of salt diapir in the study area and conclude that it helped in elevating temperatures locally which led to the fossilization of the silica diagenetic reaction front. Furthermore, we investigate the relationship between silica diagenesis and polygonal fault systems hosted within the same interval. Recently, there has been a growing link between silica diagenesis in biosiliceous sediments and the evolution of polygonal faults. We investigated this link using conventional 3D seismic and well data through a spatial, temporal, and kinematic analysis of the polygonal fault systems within the sediments. We proposed a model for the nucleation, growth, and propagation of the polygonal fault system as a contemporaneous process happening alongside silica diagenesis and report that most of the faults are in-active at present, except for a few breaching the mid-Miocene unconformity surface and this is contemporaneous also, with the fossilization of the Opal-A/CT reaction front. Lastly, we investigated twenty-six shallow gas accumulations appearing as 'bright spots' on seismic data as seismic anomalies within the Cenozoic succession using conventional 3D seismic interpretation methods and geochemical methods for the evaluation of organic matter richness and thermal maturity from well cuttings sample within the shallow section. We classified the shallow gas accumulations based on their on their direct hydrocarbon indicator (DHI) characteristics, spatial and

temporal distribution, and their relationship with other focused fluid flow related features into two types, Type I & Type II. The Type I shallow gas anomalies are often found associated with the Zechstein salt diapirs while the Type II anomalies are found in discreet pockets within Delta Front sediments. Geochemical analysis from well cuttings samples indicates an average total organic carbon (TOC) content of 5% and with a very good generative potential, suggesting the possibility of the charging of shallow reservoirs hosting the shallow gas accumulations by biogenic gas in combination with deep thermogenic sources. We present a model for the shallow gas accumulations within the study area which may assist in mitigating risks associated with shallow gas accumulations whether they are considered as a shallow geohazard for the drilling of deeper targets or a potential new play where they are located near existing infrastructure. This study has implications for fluid migration, subsurface storage of carbon dioxide and nuclear waste and the assessment of shallow geohazards.

Declaration

I hereby declare that no portion of the work referred to in this thesis has been submitted in support of an application for another degree or qualification of this or any university or other institute of learning.

Mohammed Malah

Copyright Statement

Author

I hold a B.Sc. (Hons) degree in Geology from the University of Maiduguri (Nigeria, 2012) and an M.Sc. degree in Petroleum Geoscience from the University of Manchester (United Kingdom, 2015). I am a Chartered Geoscientist by the Nigerian Council of Mining Engineers and Geoscientists (COMEG) and a Fellow of the Geological Society of London (FGS). Currently, I work with the Department of Petroleum Resources (DPR), the Oil & Gas industry regulator in Nigeria. I work as an Upstream Energy Professional and an Assistant Data Manager with the National Data Repository (NDR) in a team responsible for day-to-day data operations and management activities of the repository. Before my current role, I have worked with the Chad Basin Development Authority (CBDA) and the Nigeria Geological Survey Agency (NGSA) as a Geologist. I have over a decade of combined experience in the Energy Industry, and I am a member of several professional bodies including the Energy Institute (EI), Society of Exploration Geophysicists (SEG), Nigerian Association of Petroleum Explorationists (NAPE), European Association of Geoscientists and Engineers (EAGE) and the American Association of Petroleum Geologists (AAPG). My research background is in the seismic imaging of fluids and fluid related hydrocarbon plumbing systems and their implications for petroleum systems and shallow geohazards. I currently live in Lagos Nigeria and in my free time, I mentor and provide academic & career guidance to young and upcoming Geoscientists. This led me to co-found Sirius Foundation, an educational trust platform for the promotion and funding of literacy and education especially in the Geosciences through mentorship and empowerment in Africa. I am a certified Drone Pilot and when I am not working, I enjoy reading or taking a walk.

Acknowledgements

I am grateful for people too numerous to mention, who have made an impact on me throughout the period of my studies for this Ph.D.

First off, I wish to extend my sincere appreciation and gratitude to my project supervisor, Prof. Mads Huuse, for his assistance and guidance and helping to craft and refine the theme of my research during my Ph.D. studies. Thank you for the cheerful outlook, the support and encouragement, flexibility and believing in me to finish this thesis despite the numerous challenges and roadblocks encountered during the period of these research.

I wish to thank the Petroleum Technology Development Fund (PTDF) and the Nigerian government for sponsoring and providing full funding for my studies and also Petroleum Geo-services (PGS) for providing me with the Seismic Data, TGS-NOPEC for providing well data, the Norwegian Petroleum Directorate (NPD) for providing me with well sample data and Schlumberger for providing me, through the University of Manchester, free Petrel software license for use in this research.

I like to give special thanks to all the technical and administrative staff at the University of Manchester and to all the Basin Studies group support staff especially, Dr. Kofi Owusu, Mike Turner and Claire Erskine who are always ready to listen and solve our issues.

I would like to acknowledge all my colleagues at the Basin Studies group, a group I take pride in being part of and having the opportunity to interact and gain insights from many talented graduate students. I thank you all for riding out this journey with me.

This thesis is dedicated to my late father Alhaji Malah Geidam and my late fiancée Maryam Umar Kassim (MUK), I am still undone.

Chapter 1

Introduction and Literature Review

1.1 Introduction

The following research work covers the broad field of ***'subsurface fluid flow phenomena & associated features'*** employing seismic data, petrophysical data and well cuttings to study the impact of seismically imaged subsurface hydrocarbon plumbing systems and associated fluid flow phenomena and their impact on the petroleum systems and shallow hazards in the Central North Sea (CNS). Such fluid flow phenomena investigated in detail in this dissertation include silica diagenesis, polygonal fault systems (PFS) and shallow gas accumulations in the Cenozoic unit of the Norwegian-Danish Basin (NDB) located in the eastern Central North Sea. This section briefly introduces the broad area of research, describes the location and the geological setting of the eastern CNS and adjacent areas within the context of the North Sea, the type, and characteristics of the dataset available for this research, the interpretation techniques employed, and equipment/software utilized as well as a literature review of silica diagenesis and fluid flow features. Finally, thesis synopsis is outlined, and the limitation of the study is highlighted.

1.2 Study Area Location & Geological Setting

The study area lies within the North Sea between 56° N and 59° N and 1° E to 6° E that forms part of the Atlantic Ocean and bordered by the United Kingdom, Norway, Denmark, Netherlands, and Germany (Figure 1.1). Water flows from east-to-west into the North Sea via the Skagerrak Strait and outlet into the Atlantic Ocean through the Baltic Sea where the North Sea merges with the Norwegian Sea above the Shetland Islands**.** The North Sea averages water depths of 100 m reaching its deepest towards the Norwegian Trench at 700 m and gently opening to the Atlantic Ocean above the Shetland Islands (Ducrotoy et al., 2000; Lamb et al., 2017). The Central North Sea is an epicontinental basin that developed from the Palaeozoic through to the Cenozoic along with the European and Paris Basins that are up to 300 km wide and 600 km long and about 5 - 8 km deep in places, they record a widespread period of deposition of sediments during active subsidence and graben formation. The Central North Sea (CNS) located within the North Sea basin forms part of the East Atlantic Margin and records its first graben formation since the Triassic and was subsequently filled by Palaeozoic to recent sediments often affected by regional subsidence, significant structural inversions and halokinesis (Sclater & Christie, 1980; Gowers & Sæbøe, 1985). Early works on structures and tectonic development of the CNS

by Sorgenfrei, (1969) and Ziegler, (1990) established the importance of post-rift subsidence, thermal relaxation of lithosphere and fluctuations in compressional stress field to the development of the present day North Sea basins while later works in the CNS focused much attention on the seismic sequence stratigraphy of the area and tried to establish the relationship between subsidence and basin fill and paleogeography for the North Sea (Gowers & Sæbøe, 1985; Jordt *et al.,* 1995; Michelsen et al., 1998; Huuse *et al.,* 2002). The changes in sedimentation, rates of deposition, sources and unconformities within the CNS is reflected by changes such as tectonics, eustatics and climatic that took place over time in the CNS and its margins (Rasmussen et al., 2005; Arnell et al., 2012). The Cenozoic of the CNS averages sediment thickness of 3 km (Figure 1.1) significantly dominated by siliciclastic sediments with reservoirs developed from the Palaeocene succession in the Norwegian-Danish Basin and adjacent areas within the CNS from southern Norway and offshore Denmark.

The onset of exploration in the North Sea since 1964 has made the region become one of the most prolific hydrocarbons producing provinces in the world. The discovery of the Palaeocene Siri Field in the Danish Sector of the CNS in 1995 ushered in a renewed interest for the characterization of the Paleogene and Neogene petroliferous sedimentary rocks in the Danish sector of the North Sea (Hamberg et. al, 2005; Schiøler et al., 2007). Some of the important producing fields from southern Norway include the Valhall field from Chalk reservoirs of the Hod and Tor formations and the Ekofisk field producing from lower Palaeocene Ekofisk formation and Danian Tor Formation. Important fields for the Danish sector include reservoirs from Upper Cretaceous Danian Chalk in the Dan field, Gorm and Tyra fields, and from the Palaeocene sandstones for such fields as Siri, Nini and Cecilie within the Siri canyon. Important fields for the Dutch sector include the shallow gas fields producing from Miocene and Pliocene reservoirs including A12-FA, F02a-B and B13-FA fields.

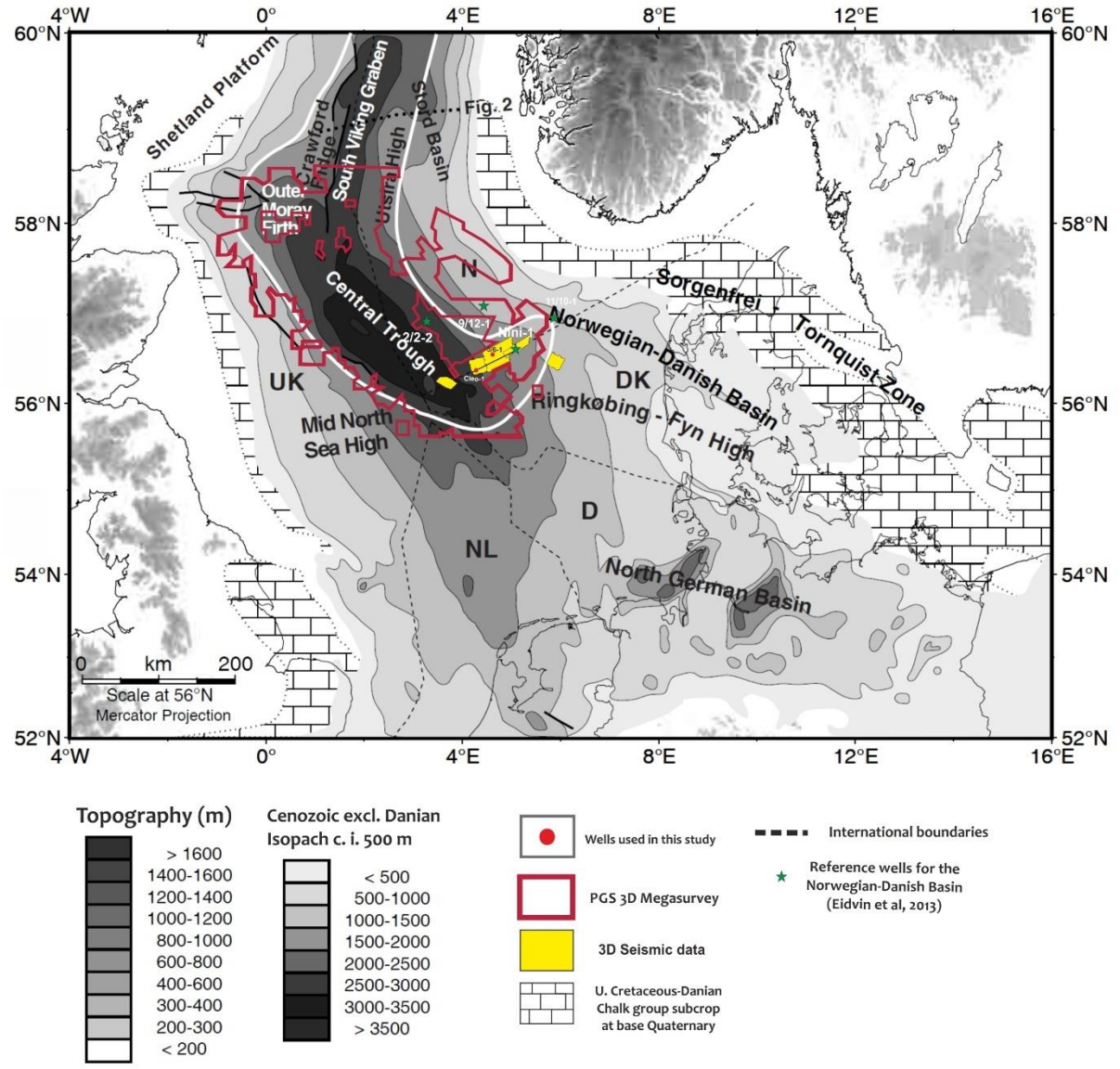

Figure 1.1: Location of the study area within the North Sea with some of the main structural elements and the depth to the top Cenozoic contour map and the outline of the PGS 3D MegaSurvey. (Modified from Huuse, 2002). N: Norway, UK: United Kingdom, NL: Netherlands, D: Germany, DK: Denmark.

1.2.1 The Cenozoic of the eastern Central North Sea

This study focuses from the top of the Lower Eocene Balder Formation to the top of the Oligo-Miocene Lark formation in the eastern Central North Sea. The Lark formation and underlying Horda Formation form the Hordaland Group of Deegan & Scull (1977) and the Westray Group and Stronsay Group of Knox & Holloway (1992). The Lark formation forms a large part of the Cenozoic mudstones with its depocenters in the North Sea and has been considered an effective seal in the Central North Sea. It is made of Oligo-Miocene

biosiliceous mudstones which were largely deposited in the North Sea prior to the Miocene silica switch in the North Atlantic (Cortese et al., 2004; Schiøler et al, 2007) (Figure 1.2). In the North Sea, the primary petroleum reservoirs exploited are the deeper Mesozoic sandstones and Cretaceous Chalks and the Cenozoic units. The Lark and Horda formation forms part of these uncharacterized Cenozoic units and hence the need to characterize it in this study. Exploration data since the Siri field was discovered has shown that the Lark formation has a high porosity and often released a large gas kick when penetrated (Hamberg et al., 2005; Schiøler et al., 2007). This makes the Lark formation a unit of economic importance within the Cenozoic of the CNS as recently in the Danish North Sea, the depleted reservoirs of the Nini West field is being targeted for carbon dioxide (CO_2) injection through the 'Greensand Project' (Rasmussen et al., 2005; Svendsen et al., 2010; https://www.maerskdrilling.com).

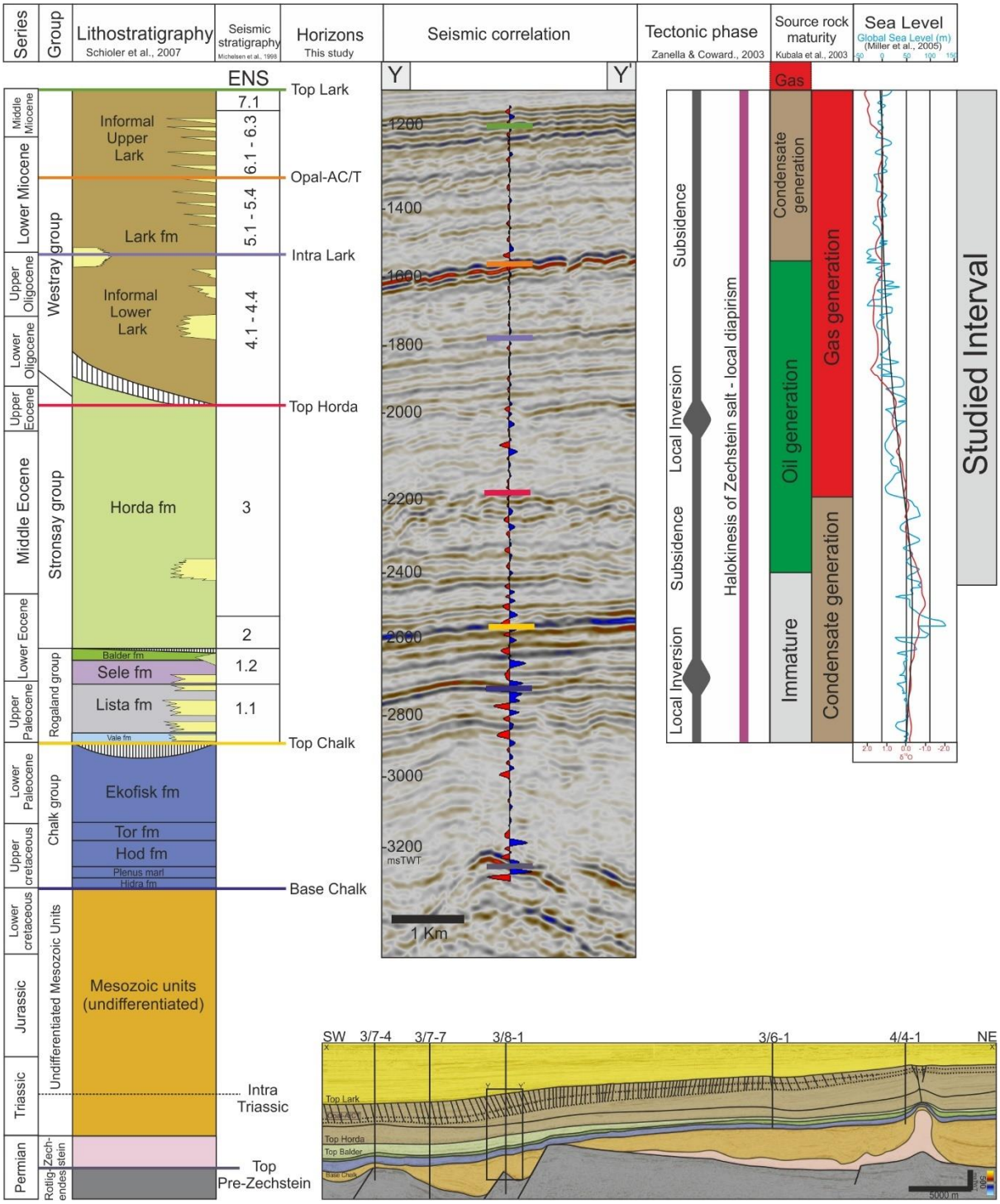

Figure 1.2: Stratigraphic position of horizons mapped and used in this study according to the lithostratigraphic subdivision of Schiøler et al., (2007) and seismic stratigraphy of Michelsen et al., (1998) by the aid of a seismic to well tie using well 3/8-1 (Inset: an interpreted seismic cross-section highlighting the position of the well 3/8-1, the key stratigraphic surfaces and other adjacent wells used in this study). (Note frequent thin sand stringers within the Westray Group Lark formation). Also shown are the local subsidence and inversion tectonics highlighting the tectonic evolution of the study area since the Cenozoic after Zanella & Coward., (2003), source rock maturation after Kubala et al., (2003) and the global sea level and $\delta^{18}O$ curves from Miller et al., (2005).

1.2.2 The Lark Formation: Westray Group

The Lark Formation represents the Westray Group of Knox & Holloway (1992) as one of the two groups to represent the Hordaland Group of Deegan & Scull (1977). The Lark Formation is a brownish grey mudstone-dominated lithofacies of the Westray Group which overlies the red-green-grey mudstones and silty mudstones and sandstones of the Horda Formation represented by the Stronsay Group and underlies the grey, sandy, and shelly mudstones, siltstones, and sandstones of the Nordland Group of Deegan & Scull (1977) in the Central North Sea (Schiøler et al., 2007). The Lark Formation was deposited in a sublittoral to upper bathyal water depth in the CNS and is an Oligo-Miocene biosiliceous mudstone which has been characterized as a regional seal and only studied from drill cuttings, well logs and subsurface data (Schiøler et al., 2007; Sulsbrück & Toft, 2018). The Lark formation is divided into four lithostratigraphic subunits (L1 - L4) based on seismic interpretations, well logs and biostratigraphy (Schiøler et al., 2007) and informally it is divided into the Lower Lark and Upper Lark formation according to inferred biosilica content with the top of the Lark formation approximately correlating with the mid-Miocene unconformity in the study area (Huuse & Clausen, 2001; Schiøler et al. 2007; Eidvin et al., 2014) (Figure 1.3). The Lower lark can be correlated to the Denmark onshore Oligocene Branden Clay and Brejning Formations and the Upper Lark is correlated to the onshore Vejle Fjord formation, Klintinghoved and Arnum formations all of which recorded delta progradations from the north and northeast (Rasmussen et al., 2005). The Lark formation, considered to be a regional seal, is uncharacterised in the study area and as such is hardly ever cored but exploration data from well reports indicates some anomalously high porosity and large gas kicks during penetration which makes it a unit of interest and economic significance. The Lark Formation covers extensively the Danish Sector of the North Sea and extends over the central and northern parts of the North Sea with its depocenter in the central and northern part of the Danish sector (Schiøler et al., 2007) (Figure 1.3). The three phenomena investigated in this study; silica diagenesis, polygonal faulting, and shallow gas accumulations (Figure 1.4) are all constrained by the Lark Formation within the datasets and the study area.

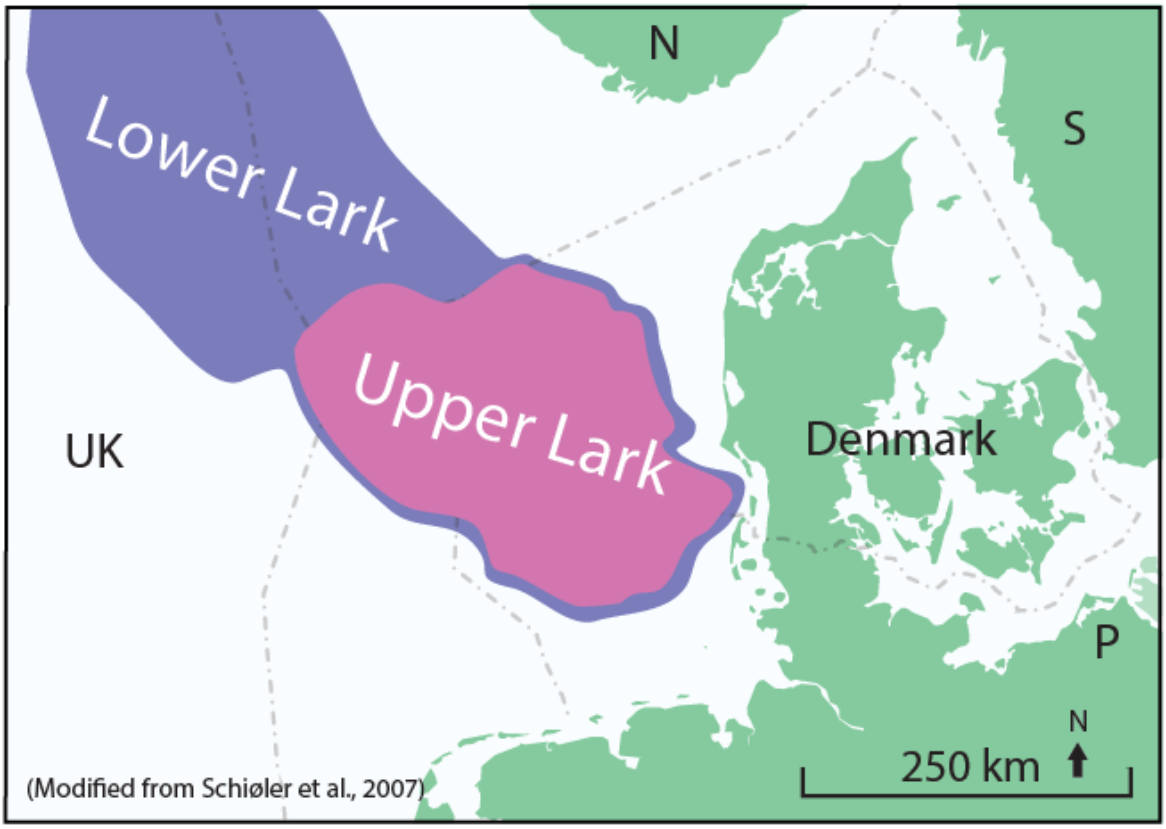

Figure 1.3: A general overview of the distribution of the Oligo-Miocene biosiliceous Lark formation within the Cenozoic section of the North Sea adapted from Mortimer-Lamb and Behl., (2018). The Lark formation is divided informally into the Upper and Lower Lark formations by biosilica content, and the Upper Lark is thought to contain up to 40% siliceous biosilica.

1.3 Rationale

This study is set out to study the genetic understanding of the links between silica diagenesis and polygonal faulting by studying the thinning out of a polygonally faulted wedge-tier and it's mineralogy and the significance for fluid flow and carbon capture and storage in the eastern Central North Sea.

Silica diagenesis, which is the transformation of amorphous biogenic silica (Opal-A) to low-crystalline lepisheres of cristobalite/tridymite has been documented by numerous borehole, seismic and field studies in sedimentary basins of the world. The transformation of Opal-A to Opal-CT is a dissolution precipitation process which affects the chemical and mechanical properties of the host rock lithology. Silica diagenesis, therefore, plays a significant role in the evolution of sedimentary basins post deposition. Despite the significance of silica diagenesis, the controlling factors are still a subject of debate. To

investigate silica diagenesis and infer the controlling factors for the eastern CNS, it is critical to know the overall mineralogy of the host rock succession.

Furthermore, silica diagenesis is inherently linked to compaction and deformation, as mineral dissolution and precipitation is known to significantly alter pore space and/or matrix volume of sediments and impact fluid flow within sedimentary basins. Recent developments in understanding polygonal fault systems (PFS) have highlighted links between silica diagenesis and the growth and propagation of such normal faults with a polygonal planform. Several theories on the origin of polygonal faults have been proposed and more recently, the initiation and propagation of polygonal fault systems through 'diagenetically induced shear failure' and 'gravitational loading' is most favoured. (Goulty., 2001; 2008; Shin et al., 2008; Cartwright., 2011). A systematic understanding of how silica diagenesis contributes to the nucleation and propagation of polygonal fault systems is a growing area of research. To investigate the link between silica diagenesis and polygonal faulting in the eastern CNS, it is crucial to understand the spatial and temporal distribution of the polygonal fault systems along with its evolution and kinematics.

Shallow gas within the Cenozoic succession of the CNS is well documented, imaged on seismic data as high amplitude anomalies. Many of the shallow gas accumulations are found associated with other focused fluid flow features such as polygonal faults and silica diagenetic reaction fronts, and all together they form the hydrocarbon plumbing systems of many sedimentary basins. These shallow gas accumulations are thought to have formed by migration of hydrocarbons from either thermogenic or biogenic sources or both. However, the role of the migration mechanism (conduits, faults) in charging the shallow gas reservoirs which form the shallow gas accumulations is still a subject of debate. Despite the significance of polygonal faults serving as potential migration pathways or seal impacting the accumulation of shallow gas in shallow reservoirs and assessing fault risk related with storage activities, they are still poorly understood. In order to investigate the relationship between shallow gas accumulations, and polygonal fault systems, it is crucial to assess and characterize the nature of several fault related shallow gas accumulations identified in the eastern CNS.

1.4 Aims and objectives

The aim of this research is to contribute to our understanding of overburden diagenesis and fluid flow in sedimentary basins by studying the tectonostratigraphy mineralogy and fluid occurrence in the eastern Central North Sea. The presence of shallow hydrocarbon accumulations is characterized and compared with similar accumulations from adjacent parts of the study area, the organic matter within the Cenozoic Mudstones is further characterized by means of Total Organic Carbon (TOC) and Rock-eval Pyrolysis and the charging of shallow reservoirs from biogenic sources or otherwise is considered. This is achieved by adopting an interdisciplinary approach that includes using 3D seismic & wireline data and analytical techniques such as X-ray Diffraction (XRD) and Quantitative Evaluation of Minerals by Scanning electron microscopy (QEMSCAN) to characterise the physical properties of the investigated unit within the Norwegian-Danish Basin (*More on analytical techniques and methods in subsequent sections*). The above approach allows for the following research aims to be addressed.

- To understand the controls on silica diagenesis in the eastern Central North Sea and identifying and documenting the extent of silica diagenesis.
- To determine the influence of silica diagenesis on the physical host rock properties and establish its relationship to polygonal faulting by means of spatial and temporal analysis.
- To understand the significance of polygonal faults as sub-vertical fluid flow conduits and/or baffles to stratal fluid flow (when offsetting aquifers) by mapping shallow gas accumulations in relation to underlying HC fairway and its overburden including polygonal faults.

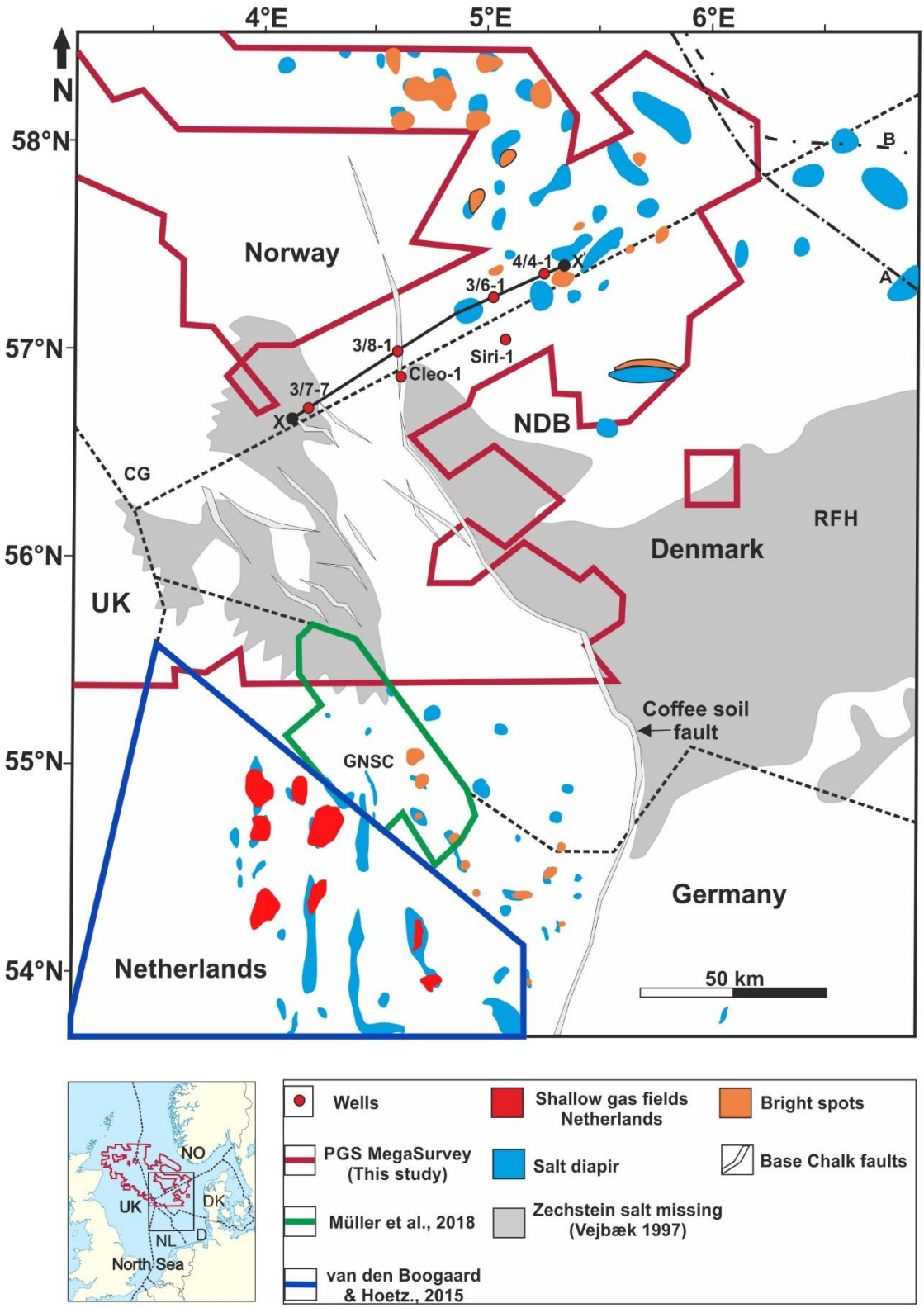

Figure 1.4: Main study area from the sub-crop of the PGS 3D MegaSurvey™ with references to previous studies within the area and the main structural elements within the eastern Central North Sea.

1.5 Thesis Structure and Synopsis

The thesis is written in a journal format and presented in five (5) chapters and a sixth (6) appendix and supplementary data chapter. The dissertation is organised in such a way that Chapter 1 is the main introduction and literature review section where chapters two (2), three (3) & four (4) make up the main body of the thesis with the three main papers while chapter five (5) gives a summary and conclusion of the dissertation and chapter six (6) is the appendix and supplementary data section. A summary of each chapter is given below:

Chapter One serves as an introduction to the dissertation, providing a brief background information on the study area and the rationale behind the studies including the aims and objectives of the research. This chapter also includes information on all the datasets available for this study and the methodologies and tools employed in conducting the analyses of these datasets detailing out all procedures and challenges encountered. This chapter further included a literature review on the fundamental areas and themes covered in detail in subsequent chapters of this dissertation.

Chapter Two is a paper titled "silica diagenesis in Cenozoic mudstones of the eastern CNS: Physical properties and the effect of salt diapirism" which identifies and characterize for the first time, a silica diagenetic boundary in the Cenozoic section of the eastern CNS. This paper will be sent for publication to the Basin Research journal and is co-authored by Mohammed Malah, Mads Huuse, Thilo Wrona and Kevin Taylor.

Chapter Three is a paper titled "Growth and propagation of polygonal normal faults due to silica diagenesis in the eastern Central North Sea" which considers the effects of sediment compaction on the geometry and controlling factors that led to the formation of polygonal fault systems (PFS) within Cenozoic mudstones of the CNS. This paper will be sent for publication in the journal of Marine and Petroleum Geology and is co-authored by Mohammed Malah, Mads Huuse and Thilo Wrona.

Chapter Four is a paper titled "Shallow gas accumulations, focused fluid flow features and geochemical characterization of Cenozoic mudstones in the eastern Central North Sea" which is a paper characterizing the occurrence of shallow hydrocarbon accumulations and other related fluid flow features in the CNS. This paper also considers the geochemical

characterization of the mudstones from sampled well cuttings. This paper will be sent to the Frontiers in Earth Science journal and is co-authored by Mohammed Malah, Mads Huuse and James Armstrong.

Chapter Five presents a summary and conclusion of the principal findings of this research work.

Chapter Six presents supplementary data and information that was used for this research.

1.6 Dataset and Methods

The database for this research includes the PGS 3D MegaSurvey™ and the TGS North Sea Renaissance 2D seismic, petrophysical well logs for all wells available for the Central North Sea from the Facies Map Browser by TGS. Well cuttings sample from well 3/7-7, 3/6-1 and 4/4-1 were obtained from the core store of the Norwegian Petroleum Directorate (NPD) covering the interval of interest and various analytical techniques including XRD, QEMSCAN, TOC and Rock-eval pyrolysis were undertaken on the samples (Table 1). A set of maps, supporting documents and well completion reports were accessed from the website of the Norwegian Petroleum Directorate (NPD). Additional description of datasets used for analysis will be further discussed under the applicable chapters in the thesis.

Table 1: Summary of main wells included in this study obtained from the NPD website.

Well	Water Depth (m)	Kelly Bushing (m)	WD + KB (m)	TD MD (m KB)	BHT ΔT°C	Oldest Age Penetrated	Oldest Formation/Group
3/7-4	66.0	25.0	91.0	3723.0	136	Late Permian	Zechstein GP
3/7-7	65.0	42.0	107.0	3930.0	127	Late Jurassic	Haugesund fm
3/8-1	65.5	42.0	107.5	4070.0	127	Early Permian	Rotliegend GP
3/6-1	64.0	34.0	98.0	2167.0	70	Late Cretaceous	Tor fm
4/4-1	62.0	43.0	105.0	2012.0	68	Late Cretaceous	Tor fm

All data taken from the website of the Norwegian Petroleum Directorate (NPD 2018), WD, water depth; KB, Kelly bushing; TD, total depth; MD, measured depth; BHT, bottom-hole temperature.

1.6.1 Datasets

1.6.1.1 *Seismic Data*

This study employed the use of the PGS 3D MegaSurvey™ seismic data that was created by merging many legacy 3D seismic cubes. The whole dataset covers an area of about 128,000 km^2 but a cropped 3D sub-volume of the PGS MegaSurvey™ covering an area of ~20,000 km^2 was mapped in detail for this study. The 3D survey has a sub-sampled bin spacing of 50 m by 50 m, a sampling rate of 4 msTWT with a maximum vertical resolution ($\lambda/4$) of c. 12 – 15 m and a horizontal resolution ($\lambda/2$) of 20 – 30 m according to a dominant frequency of 50 – 70Hz. The CNS MegaSurvey™ is a normal polarity (zero phase) data where a hard kick i.e., a positive reflection (peak) is represented by red and a soft kick i.e., a negative reflection is represented by a negative reflection (trough). The Cenozoic has an average interval velocity of 2km/s (+/- 10%) for the North Sea (Japsen, 1999) and a dominant frequency of 50Hz for the data in this study. The TGS North Sea Renaissance 2D survey covering parts in the Norwegian-Danish basin was employed to fill in gaps in the 3D seismic data coverage. Overall, the seismic data quality is good to moderate, although, quality deteriorates in the shallow section of the seismic data especially immediately below the seabed due to the influence of tunnel valleys and the fact that the acquisition of the data was initially optimised for imaging deeper sections of the CNS.

1.6.1.2 *Well Data*

This research enjoyed from wells available from the TGS Facies Map Browser (FMB™). The wells selected are those which are present in the research area and having good wireline log data including gamma ray, density, resistivity, neutron, sonic and other logs were selected (Table 1). All the wells were drilled targeting deeper Jurassic aged reservoirs and some do not have logs acquired for the Cenozoic section of the Norwegian Danish Basin which proved a challenge in some places during data analysis. A selection of wells within the CNS were selected and employed for the petrophysical analysis of the Norwegian Danish Basin, the wells were selected to ensure good correlation across the area of interest and for horizon interpretation and lithology delineation. The wells further selected for well cuttings sampling were selected based on cuttings availability from the Norwegian Petroleum Directorate (NPD).

1.6.1.3 *Drill Cutting Samples*

Drill cuttings are the first piece of information obtained about the lithology of a formation while drilling. Traditionally, after a first pass qualitative look, they are often not re-visited especially if wireline logs have been obtained. However, correct depth attribution for well samples cuttings during drilling is often an issue with analysing the samples. Recently, there has been a renewed interest in the oil and gas industry in the data available from drill cuttings since they are thought to provide valuable insight into the lithology of a formation in the absence of core data. This is especially driven by a focus on targeting unconventional plays and rejuvenating historic resources with the aim of saving cost and further insight into the physical characteristics of reservoirs for Carbon Capture and Storage (CCS). The physical characteristics of the formation such as its mineral components are important as they intrinsically control the fundamental Petrophysical parameters that directly or indirectly influence wireline log responses and the overall behaviour of a formation as a reservoir, seal, or source. Mudstone sections are hardly ever cored and cutting samples often not analysed for mineralogy or geochemistry. A total of one hundred and sixty (160) cutting samples from three wells were obtained from the NPD core store in Stavanger Norway according to data availability. The well cutting samples were from wells 4/4-1 (37 samples), 3/6-1 (50 samples) and 3/7-7 (73 samples) over a depth of 2km in the three wells with an average resolution of 10 m for samples analysed via XRD and 30 m for Rock-eval and QEMSCAN analysis. Below, a detailed sample database, depth sampled, and the type of analysis executed each well and sample are presented in Tables 8, 9 and 10 in the Appendix section. All efforts have been made to account for errors with respect to depth attribution of well cuttings samples analysed for this study and the consistency of the data over the sampled intervals indicates correct depth attribution for the referenced wells in this study.

1.6.2 Methods

A multidisciplinary approach was adopted for the analysis of all data available for this research within the Norwegian Danish Basin in the eastern Central North Sea. Specifically, the following techniques below were employed and will be elucidated further in this section. The methodology and technique employed for each specific study is further discussed extensively in subsequent chapters.

I. *Seismic Interpretation*
II. *Petrophysical Well Analysis*
III. *X-Ray Diffraction (XRD)*
IV. *Quantitative Evaluation of Materials by Scanning Electron Microscopy (QEMSCAN)*
V. *Total Organic Carbon Content (TOC)*
VI. *Rock-eval Pyrolysis (RE)*

1.6.2.1 *Seismic Interpretation*

The seismic data was integrated with well data from wells 3/6-1, 3/7-4, 3/7-7, 3/8-1, and 4/4-1 that cover the 3D sub volume obtained from the PGS MegaSurvey™ to achieve a seismic to well tie and petrophysical logs and completion reports from the NPD were used to determine lithology and perform investigations for the study area. Seismic sections were integrated with well data to establish the regional seismic horizons for the Cenozoic section and other intervals of interest. Conventional seismic interpretation technique for analysing the seismic data by earth visualization software like PETREL™ (2018) and GeoTeric™ (2018) was applied for this research and additional methodologies and tools for specific chapters are discussed further below and under each chapter. The analysis of the data with the aid of the software allows for stratigraphical mapping and feature identification via horizon picking and tracking across the 3D data through a systematic workflow (Figure 1.5). Horizon tracking parameters were optimised for quality results, an expansion quality of 'validated 3x3' which ensures the picking of the traces close to 24 seeding points against their neighbours in Petrel. A seed confidence of 85% was used to utilize the minimum tracking value for seismic amplitude as a percentage of seed points. Adjacent parent trace correlation quality of 0.75 – 0.80 picking peaks or troughs was used where applicable. A coarse gridding interval (cross line spacing of 50 and inline spacing of 50) was used and where necessary, a finer grid was employed as in such areas with poor resolution on the seismic cube to embrace more seed points. Two-way-time (TWT) surfaces were generated from the picked horizons which was subsequently 3D auto-tracked to fill in gaps in preference to wavelet tracking and correlation constraints prior to the generation of the time structure maps which was thus used to generate thickness maps in time. Were applicable, surfaces were sliced iso-proportionally to allow for a greater window of search away from a time surface or any two-time surfaces.

A systematic mapping/scanning of the 3D seismic cube was conducted using tools for assessing and mapping of seismic anomalies by identifying direct hydrocarbon indicators (DHI's) such as bright spots, flat spots, seismic attenuation, phase or polarity reversal, velocity pushdown, and gas chimneys according to Brown et al. (2011). Volume and surface attributes including RMS amplitude, variance edge, ant track and maximum/minimum amplitudes were also run on the seismic cube to derive more preferential seismic attributes that cannot be illustrated by regular seismic amplitude data.

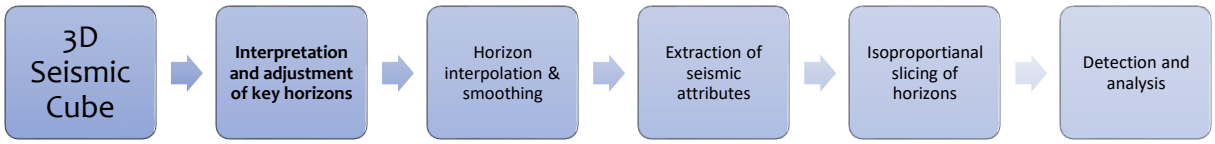

Figure 1.5: A systematic workflow employed for the analysis of the 3D seismic data in this study for the identification, definition, and interpretation of key features of interest.

For the interpretation, the key horizons mapped were based on the seismic stratigraphic framework of Michelsen et al., (1998) which subdivided the Cenozoic of the Central North Sea into 8 subsections CSSx – CSSxi based on the progradation or erosion of major surfaces and the lithostratigraphic subdivision of the Paleogene to Lower Neogene of the Central North Sea by Schiøler et al., (2007) based on lithological, sedimentological and biostratigraphic evidence into seven formations from the Top Chalk surface to the base of the Nordland group. Eight (8) key horizons tied from wells were mapped along with time significant boundaries identified based on seismic reflection terminations (onlaps, offlaps, toplaps, downlaps and truncations) based on seismic stratigraphic techniques by Mitchum et. al. (1977). Further to the key surfaces mapped, the identified Opal-A/CT reaction boundary and the detachment surface (base) of most of the Polygonal Faults within the study were also mapped.

1.6.2.2 *Petrophysical Well Analysis*

Wells established to have a good correlation and with available drill well cuttings for sampling were used for correlation with the seismic data and for the delineation of lithology. The correlation was achieved using Checkshot data available for the wells that was used to establish time-depth relationship especially for the Cenozoic section which

was used to estimate thickness maps across the NDB and adjacent areas. Completion logs and well reports publicly available from the NPD Fact Pages (last accessed in 2018) were also employed for this research alongside all data from the TGS Facies Map Browser (FMB).

The density and sonic logs obtained for the wells were employed to generate synthetic seismograms to allow for the calibration of the seismic to well and to accurately relate formation tops from wells to reflections on the seismic sections (seismic-to-well tie). The density and sonic logs were first used to generate reflection coefficients which was convolved with an extractive wavelet from the seismic cube to produce a synthetic seismogram with an equivalent acoustic impedance to the seismic cube at different stratigraphic intervals.

1.6.2.3 *X-Ray Diffraction (XRD)*

X-ray diffraction is a common technique often employed in studying the crystalline structure of sediments to determine mineralogy. The x-ray diffraction technique is non-destructive and requires only tiny amounts of samples to undertake semi-quantitative analyses of poly-mineral samples. The x-ray diffraction technique was applied to identify and quantify the composition of 160 well cuttings sample and involves the crushing of the 160 untreated mudstone cuttings samples obtained at a 10 m interval from the three wells 3/6-1, 3/7-7, and 4/4-1 in the Central North Sea (Table 8, 9 & 10) and the preparation of smear slides sample mounts for the x-ray powder diffraction. The sample preparation, analysis and identification are based on Brown & Brindley (1980), Moore and Reynolds (1997) and Hillier (2002). The diffraction measurements for phase identification were conducted using the Bruker D8 Advance™ diffractometer in the Williamson Research Centre at the University of Manchester operated via the DIFFRAC-Plus™ XRD Commander software. The measurements were conducted using 20 kV Cu radiations with the X-ray generator operated at 40 mA. The experimental set-up included a 4° divergence slit on both the primary and secondary side and with the diffracted beam collected at a 4-degree window positive sensitive detector lynx eye. Sample measurements start from the 2-theta of 5° and stop at the 2-theta of 69.9° with a step size of 0.020° and a step time of 30.60s. Sample analysis of the 160 samples from the 3 wells involved the use of the Bruker's Eva software for bulk rock mineralogy to understand the mineralogical changes within the Lark

Formation in the study area and RockJock™ software for the whole rock semi-quantitative XRD analysis with emphasis on clay mineralogy. Samples analysed indicates that the XRD patterns of the samples and mineralogy are mostly similar for the samples analysed and a representative sample is presented in Figure 1.6 & 1.7.

1.6.2.3.1 *XRD Peak Identification*

Clay mineral groups are identified for the following studies based on clay mineral identification in XRD data by Moore and Reynolds (1997). The presence of Illite is inferred on the XRD pattern of a non-oriented powdered sample with characteristic peaks around 9°, 18° and 26° (Figure 1.8). Smectite often occurs in a mixed Illite-Smectite layer in a diffuse manner rather than as a single peak and is inferred from the change of the 001 peak from ~5.2° in ethylene glycolated samples to ~6° in air dried samples to ~10° in heated samples (Figure 1.6). Kaolinite is inferred by peaks at 12.3° and 24.9° and often discerned from Chlorite based on the absence of a peak around 6.3° and the disappearance of the 001 peak when heated to 500°C (Figure 1.8). Quartz and quartz polymorphs opal-A and opal-CT were also identified on the x-ray diffraction data. Opal-A is usually identified as a diffuse band between ~10° - 40° and opal-CT is inferred from an asymmetric double-peak between 20° - 21.5° (Jones and Segnit, 1971; von Rad et al., 1978; Guthrie et al., 1995) and quartz is identified as a strong 001 peak at 26.6° (Moore and Reynolds, 1997) (Figure 1.8). The identified minerals and their characteristics features are summarised in the Table 2 below.

Table 2: Minerals identified, and their diagnostic feature compiled from various sources.

Mineral	**Diagnostic Feature**	**2 Theta (°)**	**d-spacing (Å)**	**References**
Quartz	001 Peak	26.6	3.343	Moore & Reynolds (1997)
Opal-A	Diffuse Band	~10 – 40	~2.2 - 8.8	Jones & Segnit (1971), von Rad et al., (1978)
Opal-CT	Asymmetric double-peak	20 & 21.5	4.13 - 4.44	Jones & Segnit (1971), Guthrie et al., (1995)
Illite	001 Peak 002 Peak 003 Peak	~9 ~18 ~26	~10 ~5 ~3.38	Moore & Reynolds (1997), Hillier (2002)
Kaolinite	001 Peak 002 Peak	12.3 24.9	7.17 3.58	Moore & Reynolds (1997), Hillier (2002)
Sylvite	Peak	28.3	3.15	Swanson et al., (1953)

Pyrite	002 Peak	33	2.709	Moore & Reynolds (1997)
Halite	Peak	31.7	2.82	Swanson et al., (1953)
Calcite	Peak	29.4	3.035	Moore & Reynolds (1997)
Barite	Peak	42.8	2.11	Swanson et al., (1953)

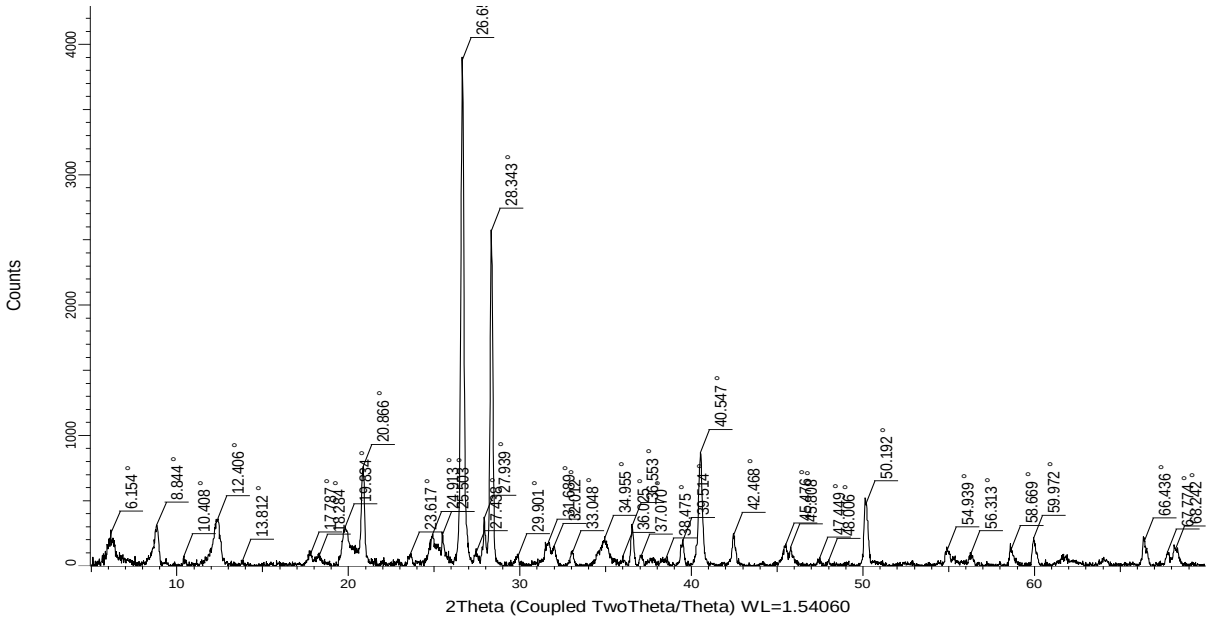

Figure 1.6: A typical peak search here depicted for sample 441-1 from well 4/4-1.

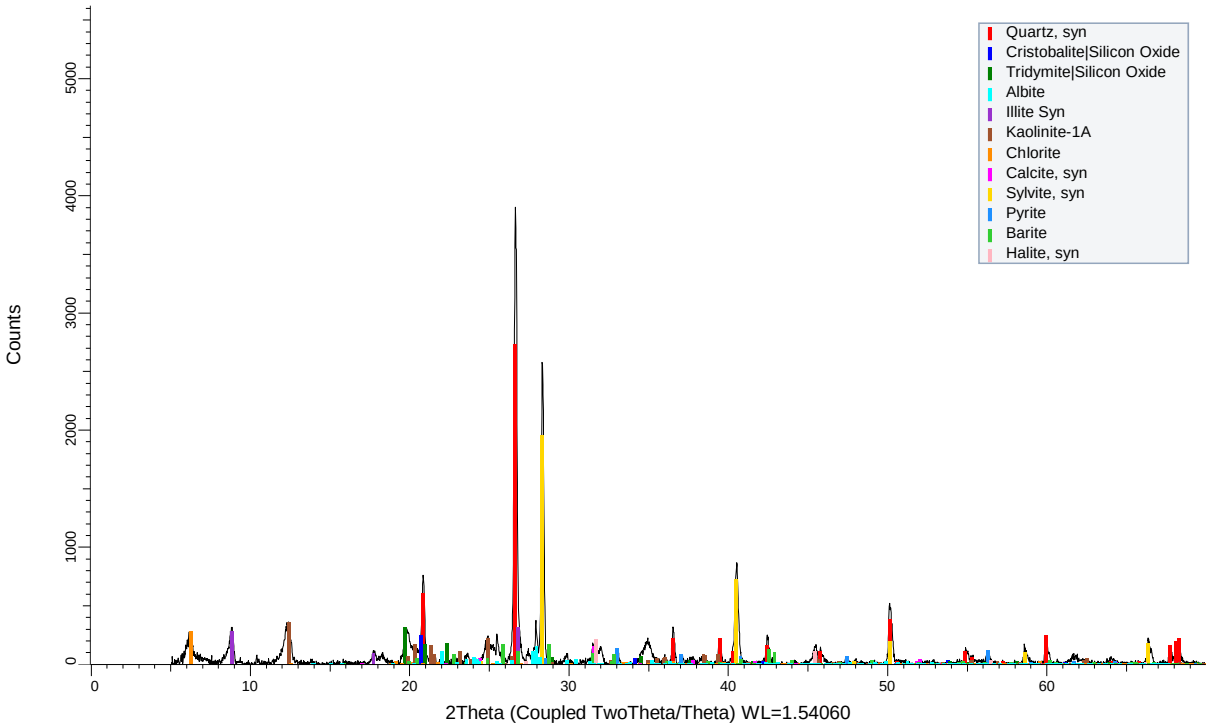

Figure 1.7: Minerals identified using the Bruker Eva Software for sample 441-1 from well 4/4-1 at 540m depth.

1.6.2.3.2 *XRD Quantification*

The quantification of the mineral phases including any amorphous material identified in each sample is further analysed using the Full Pattern Matching Technique (FullPat) developed by Chipera & Bish (2002). This method was executed using RockJock™ (V0.3) that allows for the quantitative analysis of powdered samples by comparing the integrated X-ray diffraction (XRD) intensities of individual minerals in complex mixtures to the intensities of known mineral standards against the natural sediments or even unknowns to estimate the proportions of minerals contained in the sample. This research employed the FullPat technique to quantify the proportion of Opal-A, Opal-CT and other minerals using the RockJock software. The X-ray data are first converted to a *.txt* file and then entered into the program and minerals or mineral groups likely to be present are selected in the optimization tab of the software after setting the background standard to quartz using an exponential background correction method. The program automatically fits the sum of the stored XRD patterns of pure standard mineral patterns to the measured patterns by varying the fraction of each mineral standard pattern, using the solver function in Microsoft Excel to minimize a degree of fit parameter between the calculated and measured pattern (Eberl D.D., 2003). The calculation analyses the patterns to find integrated intensities for the selected minerals and the intensities for each mineral is then determined to the proportion of each mineral standard and a best fit is achieved. The integrated intensities are then compared to the integrated intensity of the internal standard and the weight percentages of each mineral is calculated and the results are presented as a list of minerals with their corresponding weight percentages and stored on a spreadsheet for further processing. The diffractograms of the Cenozoic mudstones were analysed using the mineral standards Opal-A, Opal-CT, Quartz, Clays (Montmorillonite, Kaolinite, Chlorite), calcite, pyrite, barite, halite, sylvite.

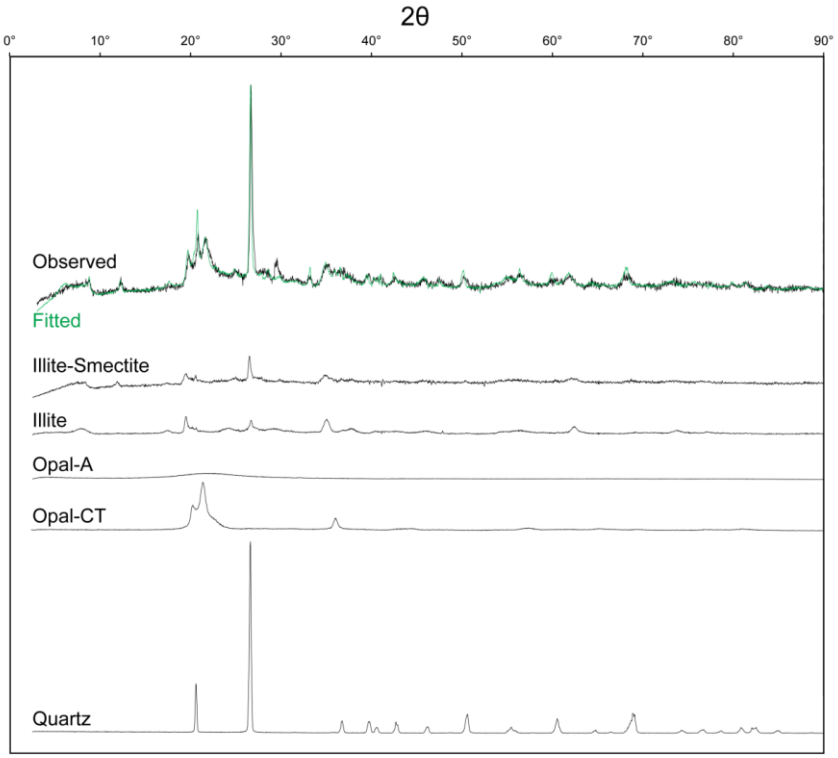

Figure 1.8: Examples of X-ray diffractogram patterns showing the observed pattern of identified minerals Quartz, Illite, Illite-smectite, opal-A and opal-CT from Wrona T., (2016).

1.6.2.4 *Quantitative Evaluation of Minerals by Scanning Electron Microscopy (QEMSCAN)*

Drill cuttings are the first piece of information obtained about the lithology of a formation while drilling. Traditionally, after a first pass qualitative look, they are often not re-visited especially if wireline logs have been obtained. Recently, there has been a renewed interest in oil and gas industry in the data available from drill cuttings since they are thought to provide valuable insight into the lithology of a formation in the absence of core data. This is especially driven by a focus on targeting unconventional plays and rejuvenating historic resources with the aim of saving cost and further insight into the physical characteristics of reservoirs. The physical characteristics of the formation such as its mineral components are important as they intrinsically control the fundamental petrophysical parameters that directly or indirectly influence wireline log responses and the overall behaviour of a formation as a reservoir, seal, or source. Although the QEMSCAN technique has a long history in the mining sector since it was initially developed by the Commonwealth Scientific and Industrial Research Organisation (CSIRO) in Australia during the 70's. The QEMSCAN technique has a long history in the in the mining industry to augment bulk chemical assay

with an earlier version tagged QEM*SEM™. Recently, its application has been broadly refined and modified to other industrial sectors including the oil and gas industry (Butcher and Botha, 2010). It is employed in the oil and gas industry for use as a form of rapidly automated mineral analysis of rock samples in combination with other techniques such as XRD, SEM, XRF etc. The QEMSCAN system uses a host of techniques including scanning electron microscope (SEM) and electron dispersive spectroscopy (EDS) with an automated analysis software that uses readings from backscattered electron intensity (BSE) and energy dispersive x-ray (EDX) to identify different mineral phases at each analysis point set according to the step interval (resolution) for each sample. A variety of quantitative information is often obtainable from QEMSCAN analyses, including mineral distribution, mineral composition, mineral angularity and the distribution of fabric, texture, and porosity of materials. In the following study, twenty-eight (28) samples at different depths covering an average depth of 1410 m between wells 4/4-1 and 3/7-7 were prepared by advance sample preparation technique of grain mount thin sections prior to running the analysis. A sampling resolution of 5 microns (µm) was determined to be sufficient to resolve elemental distribution and generate mineral maps at a high spatial resolution of 3 cm^2 on the grain mount thin section.

1.6.2.4.1 *QEMSCAN Methodology*

The analysis was conducted using the FEI QUANTA FEG 650 scanning electron microscope at the University of Manchester Williamson Research Centre laboratories. The QEMSCAN system is fully automated and enables the measurement of values along a predefined grid. Software used for the data acquisition is iMeasure V5.2 and iDiscover V5.2 software was used for data processing and analysis. The measurements were collected at a resolution of 5 microns (µm) particle map analysis (PMA) for overall mineralogy. (For more information about analytical methodology and modes for the QEMSCAN analysis, see Gottlieb et al., (2000) and Pirrie et al., (2004). Preliminary to running the sample analysis, standard instrument tuning including beam alignment, beam focusing, and the calibration of x-ray and back scatter sensors is performed. A measurement routine defining grid size and sample analysis per point is defined and the analyses is automated, operating at an accelerated voltage of 20 kV and a specimen current of 10 nA. The measurement routine includes defining a grid size using the FieldImage™ technique where an electron beam

moves across the sample on a field-by-field basis at a predetermined stepping interval of 5 µm. The FieldImage™ mode divides the surface of the sample into a virtual grid of fields according to the stepping interval of 5 microns and at each stepping interval, a mineralogical determination is made on the resultant back scattered electrons (BSE) and x-ray signals received from the point of analysis. The result is a mineralogical map of each stepping interval with a resolution equal to the beam at each interval step (Figure 1.9). A stepping interval of 5 microns was adopted for this study to optimise textural and modal mineralogical information. The iDiscover software was subsequently employed to stitch together all the field images for each sample to produce a mineral map during data processing (Figure 1.10).

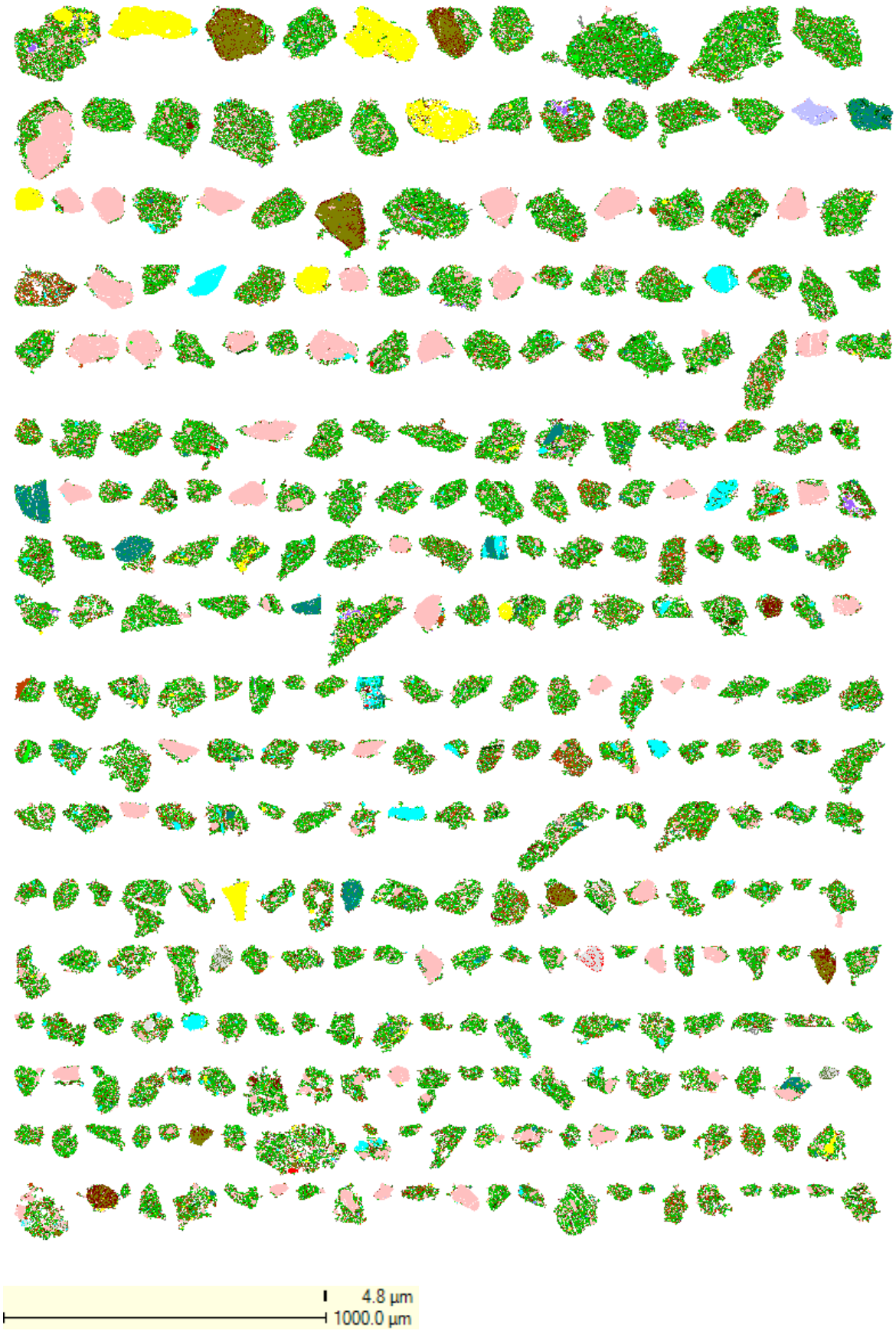

Figure 1.9: Particle map image of all particles mapped by QEMSCAN for drill cuttings from sample 441-1.

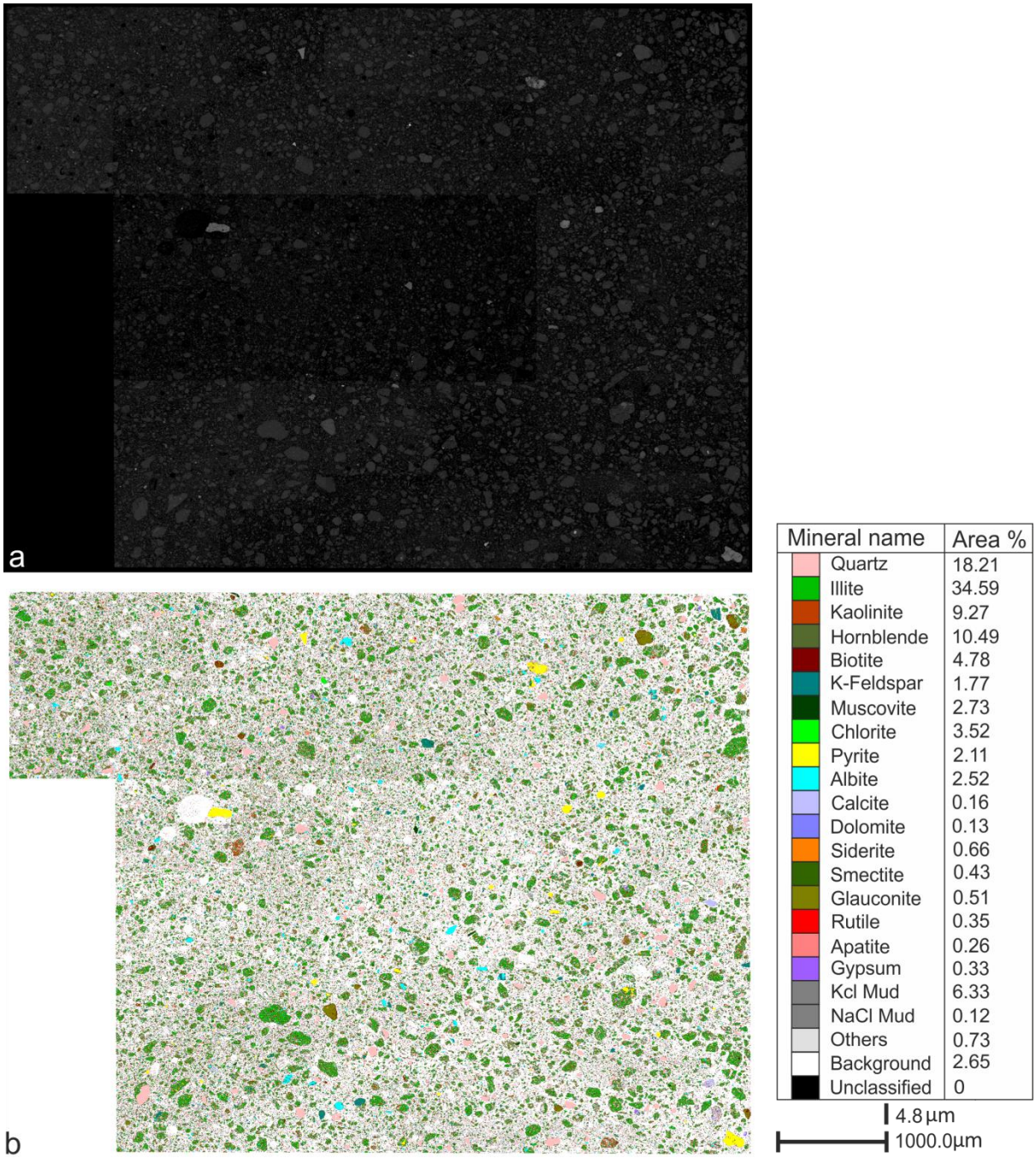

Figure 1.10: a) BSE map of polished section from drill cuttings of mudstone particles from a depth of 540m in well 4/4-1 and b) false colour map of the same polished thin section showing a mineralogical map and the distribution of main mineral species with Quartz in pink, Illite in green and Pyrite in yellow.

1.6.2.4.2 *Mineral Lists Classification for QEMSCAN Data Analysis*

A description of the mineralogy from the mineral list is essential to understand the mixture of mineral assemblages in the sample and to highlight specific mineral texture. The definition of the mineral list is the most critical step towards the analysis of the QEMSCAN

data obtained. The minerals are picked up by the analyser unit based on the backscatter electron intensity (BSE) and the x-ray spectrum that is compared with a table of known mineral and chemical compositions termed the species identification protocol (SIP) developed by CSIRO Minerals and the Federal Bureau of Investigation (Ward, 2000), a mineral or phase name is assigned to each pixel mapped. A description of mineral diversity that may be contained in each mineral assemblage in the samples analysed is listed in Table 3 below.

Table 3: Mineral assemblage identified using QEMSCAN

Mineral Assemblage	**Description**
Quartz	Silica group of minerals e.g., quartz, cristobalite, tridymite etc. and other silica minerals with a low backscattered electron coefficient such as such as hydrated silica minerals including opal and chert.
Illite & Illite-smectite	Illite and illite-dominant Illite-smectite. Including tiny amounts of ferroan-illite and ferroan Illite-dominant Illite-smectite and Illite finely intermixed with smectite and kaolinite.
Kaolinite	Kaolin group including halyosite and kaolinite ss. This mixture also represents pure kaolinite; kaolinite may also be present finely intermixed with a variety of other clays.
Biotite	Biotite mica and phlogophite.
K-Feldspar	K-rich alkali feldspar including microcline, orthoclase and sanidine.
Muscovite	Muscovite mica including white micas such as 'sericite.'
Chlorite	Fe-rich Chlorite including Fe-smectite and specific compositions of tourmaline and almandine garnet.
Pyrite	Pyrite and marcasite including pyrrhotite, jarosite and any other sulphides.
Calcite	Non-ferroan calcite and aragonite.
Dolomite	Non-ferroan dolomite.
Siderite	Siderite including Fe hydroxides such as goethite.
Smectite	Smectite and smectite-dominant Illite-smectite including physical mixtures of smectite and kaolinite.
Glauconite	Glauconite including specific trace compositions of biotite mica.
Rutile	Rutile and anatase including Ti-bearing phases including Titanite.
Apatite	Apatite and Ca-phosphates including hydro-apatite and bone.
Gypsum	Gypsum including anhydrite.
Unclassified	Undifferentiated mineral phases in trace quantities.

1.6.2.5 *Total Organic Carbon Content (TOC)*

1.6.2.5.1 *Traditional TOC Analysis*

Total organic carbon content (TOC) analysis was conducted using a Schimadzu TOC-V CPN analyser system in the Williamson Research Centre at the University of Manchester. The system included an SSM-5000A solid sample module that contained a Total Carbon (TC) and Inorganic Carbon (IC) unit. The TC is measured putting a measured amount of the crushed dry mudstone cuttings samples into a sample boat and into a sample port in the analyser unit. The port is connected directly to a furnace which has already been preheated to 680° C. Upon insertion into the furnace, all the carbon in the sample is converted to carbon dioxide (CO_2) and is carried in a stream of high purity air to an infrared detector. The detector produces a signal which is directly proportional to the concentration of the carbon in the carbon dioxide and is measured on the workstation as the Total Carbon (TC). The Inorganic carbon is measured in the same fashion as for the TC, but in this case, the sample is treated with Hydrochloric acid (HCL) to facilitate the liberation of the inorganic carbon from the sample once inserted into the TC port in the analyser unit. Prior to running the samples through the analyser for the following study, a calibration was done using three (3) different weigh outs of pure glucose ($C_6H_{12}O_6$) of 12.5 mg, 25 mg and 50 mg corresponding to 5 mg, 10 mg, and 20 mg of carbon in each sample before running for the Total Carbon (TC). In a similar fashion for the Inorganic Carbon (IC), a calibration of the analyser was conducted using sodium carbonate ($NaCO_3$) standards of 44.2 mg, 88.4 mg and 176.8 mg corresponding to 5 mg, 10 mg, and 20 mg of carbon in each sample. This initial calibration is to calibrate the '*calibration curve*' of the detectors to keep error margins below 3% and a calibration standard was run after every tenth sample analysed to ensure the analyser system consistency. All the data generated from the analyser system is stored on the TOC-V CPN software on a workstation and downloaded as an excel file for further processing.

For the following study, a total of forty-one (41) samples were analysed from three (3) wells 4/4-1, 3/6-1, and 3/7-7 from the CNS (Figure 1.2) for the samples collected from drill well cuttings from the Norwegian Petroleum Directorate (NPD) for the following analysis. The mudstone samples were dry crushed and measured out to 50 mg (+/- 5) using a metric balance accurate to four decimal places into the sample boat before onward insertion into

the analyser port unit. Results obtained for TOC values for the samples were analysed and a critical step of the analysis for the data prior to quantification included the correction of the carbon yield for the samples that might have been contaminated by drilling with an oil-based mud (OBM) (Charsky & Herron, 2013).

1.6.2.5.2 *CARPLOT*

This study further estimated TOC from log analysis of the sampled wells from digitised logs and to compare and validate values obtained from the laboratory analysis of the cuttings samples. The TOC results were obtained for log analysis using the CARPLOT software based on the methodology of Passey et al., (1990) (Figure 1.11). CARPLOT is a program which generates geochemical parameters such as total organic carbon (TOC) and pyrolysate (S2) yields from commonly available wireline log data. The software was developed to meet the need for accurate assessment of source richness to determine the prospectivity or otherwise of selected horizons in wireline data. Specialised logging tools capable of defining source richness are available but the CARPLOT system has the advantage of being applied retrospectively to wells where only a basic logging programme has been implemented. The methodology estimates TOC from either sonic/resistivity, neutron/resistivity or density/resistivity logs based on the log separation that occurs between the resistivity and other logs due to the presence of organic matter. The mathematical equation to quantify this separation is given in the equation below:

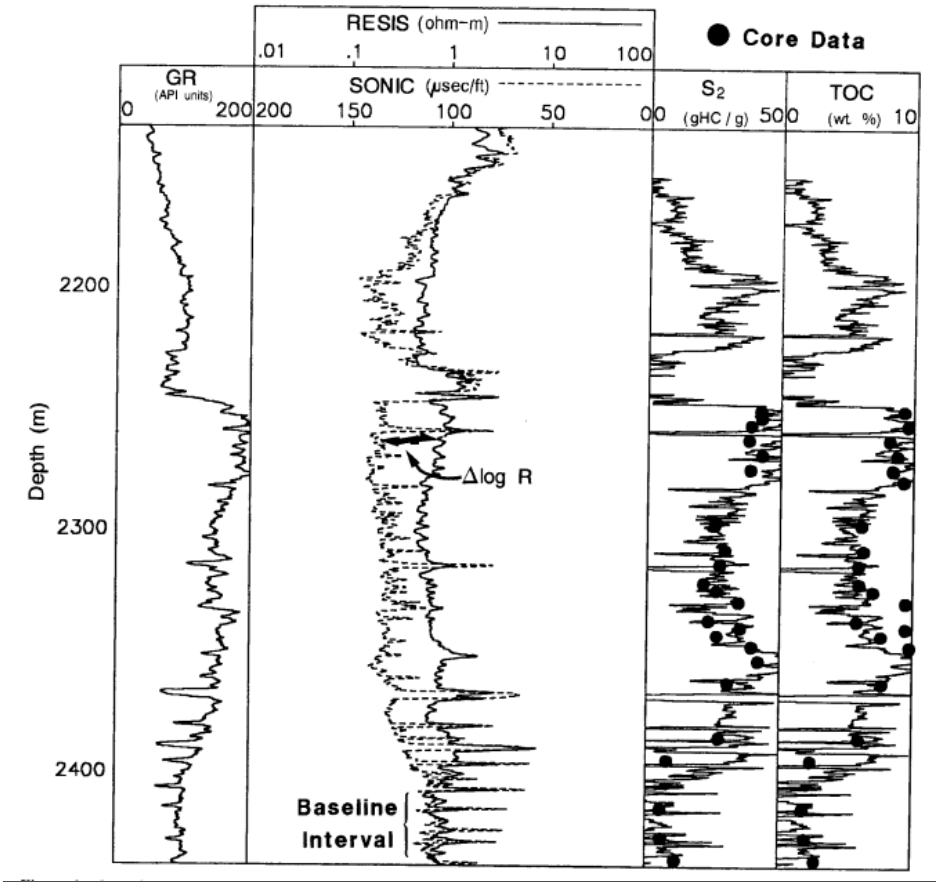

Figure 1.11: Well logs illustrating how to estimate ΔlogR from the separation between the sonic and deep resistivity logs outlined by the TOC estimation method of Passey et al., (1990).

$$\Delta logR = \log\left(\frac{R}{R_{baseline}}\right) - P(\Delta t - \Delta t_{baseline})$$

Where,

ΔlogR is the separation between the two logs measured in logarithmic resistivity circle.

R is the resistivity in Ωm

Δt is the sonic measurement in μs/ft.

P is the ratio of -50 μs/ft per one resistivity cycle.

$\Delta t_{baseline}$ is the sonic corresponding to $R_{baseline}$ in the lean shale interval (non-source rock).

With the log separation quantified, the TOC can be calculated using the equation below:

$TOC = \Delta logR \times 10^{[2.297 - (0.1688 \times LOM]}$

Where LOM is the level of maturity, for any specific *ΔlogR*, TOC decreases as Lom increases.

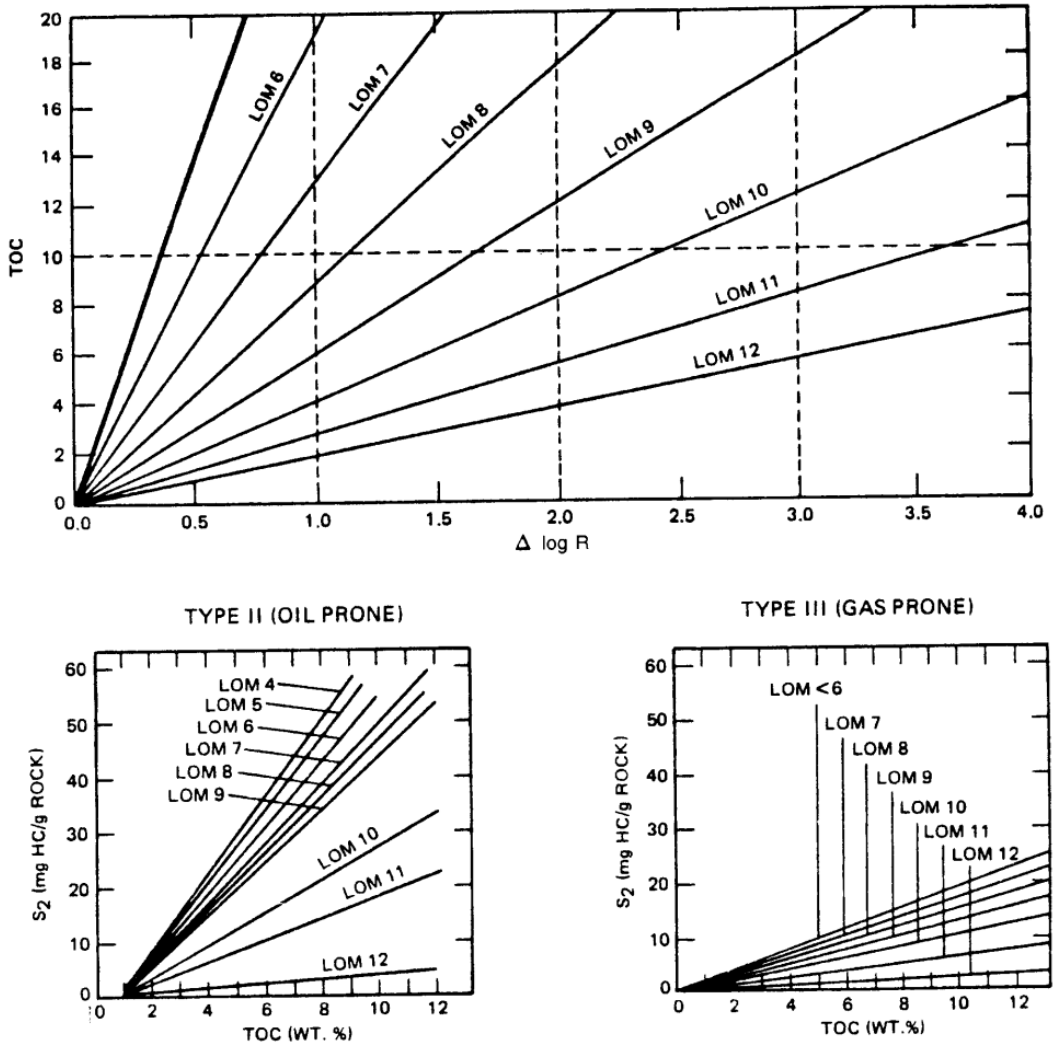

Figure 1.12 (a) ΔlogR diagram relating ΔlogR to TOC via maturity used for organic matter with <6 LOM. (b) TOC vs S_2 via maturity plot for Type II (Oil Prone) Kerogen used for both Type I and Type II kerogen. (c) TOC vs S_2 via maturity plot used for Type III (gas prone) kerogen. Sourced from Passey et al., (1990).

1.6.2.6 *Rock-eval Pyrolysis (RE)*

Seven samples where further selected (Table 4) for Rock-eval pyrolysis to determine the hydrocarbon potential of the Cenozoic mudstones and analysed at the Applied Petroleum Technology (APT) laboratories at Stavanger using a Rock-eval 6 and HAWK instruments according to procedures set by NIGOGA (4^{th} edition). Results from the analysis that include the following are presented below and in subsequent chapters.

S1: Amount of hydrocarbons thermally extracted at 300°C (Kg of free oil (unexpelled) /tonne rock).

S2: Amount of hydrocarbons produced from pyrolysis up to 550°C (Kg pyrolysate/tonne rock)

S3: Amount of CO2 released from organic matter at higher temperatures. (Kg CO2 from organic oxygen/tonne rock)

Tmax: Temperature at maximum S2 peak.

The primary data obtained above will be used to derive ratios as such:

Hydrogen Index = S2x100/TOC (mgHC/g TOC)

Oxygen Index = S3x100/TOC (CO_2/g TOC)

Production Index = S1/ (S1 + S2)

Table 4: Samples selected for Rock-eval pyrolysis and TOC values. (Note: TOC values for all wells and intervals sampled and detailed Rock-eval data analysis shown in appendix).

Sample ID	**UWI**	**Depth (m)**	**TOC (%)**
441-12	4/4-1	650	4.73
441-27	4/4-1	800	4.99
361-16	3/6-1	1050	4.85
361-36	3/6-1	1250	2.59
377-6	3/7-7	1400	6.82
377-46	3/7-7	1800	7.88
377-104	3/7-7	2380	5.04

1.7 Literature Review

1.7.1 Silica Diagenesis

Silica diagenesis involves a two-step process (i) the transformation of biogenic silica (opal A) to crystalline silica of cristobalite/tridymite (opal CT) and (ii) the transformation of opal CT to quartz (Behl., 2011). Both stage of transformation occurs through dissolution and precipitation which often releases significant amounts of water that affects the physical properties of host sediments (Williams et al., 1985; Davies et al., 2008). The rate and extent of these two-phase changes are primarily controlled by temperature and time, among other factors such as pressure, pH of the solvent and to some extent the content of the organic matter (Kastner et al., 1977; Williams et al., 1985; Isaacs, 1981; Keller & Isaacs, 1985; Hesse, 1988; Hinman, 1990; Dove & Rimstidt, 1994). These changes affect host rock strata as well as reducing its porosity which directly leads to an increase in p-wave velocity and bulk density (Isaacs, 1981; Tada & Iijima, 1983; Compton, 1991; Guerin & Goldberg, 1996; Chaika & Dvorkin, 2000; Kim et al., 2007; Spinelli et al., 2007; Thyberg & Jahren, 2011). Subsequently, these changes further cause an embrittlement within fine grained sediments which in turn affects the hydraulic properties of the formations leading to distinct seismic reflections that can be mapped and observed over several hundreds to thousands of kilometres (Davies & Cartwright, 2002; Volpi et al., 2003; Meadows & Davies, 2007; Davies et al., 2008; Neagu et al., 2010b; Ireland et al., 2011; Wrona et. al. 2017). Diagenesis plays a crucial role in reducing porosity and is often found to influence the style of deformation and fluid flow in sedimentary basins around the world (Figure 1.12; 1.13; 1.14).

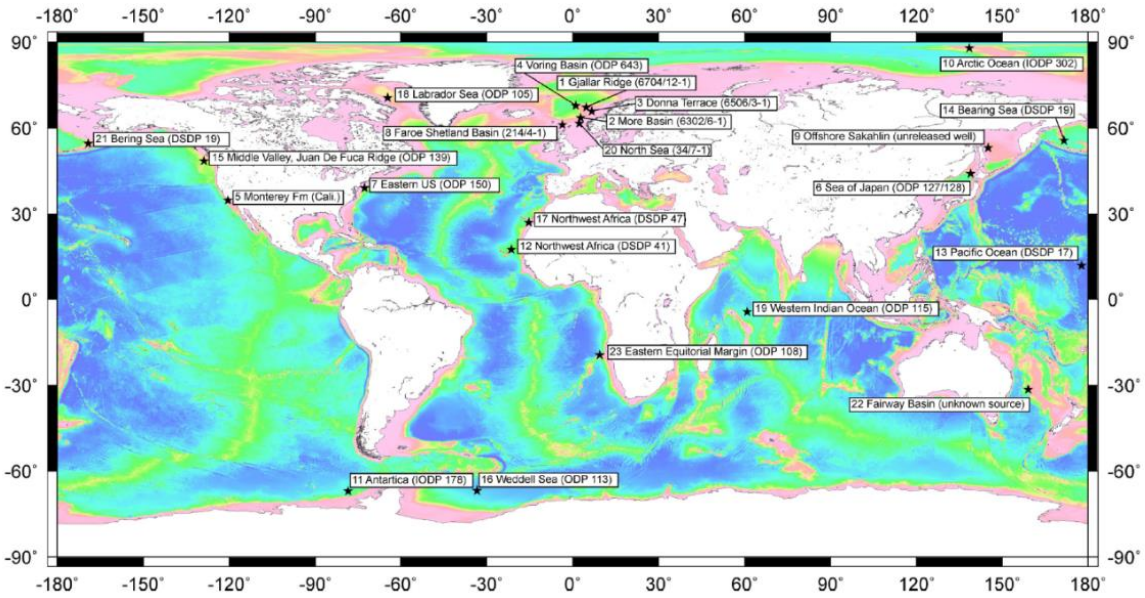

Figure 1.13: Map showing the global distribution of silica diagenetic transformation of opal-A to opal-CT confirmed by well data (After Ireland, 2011).

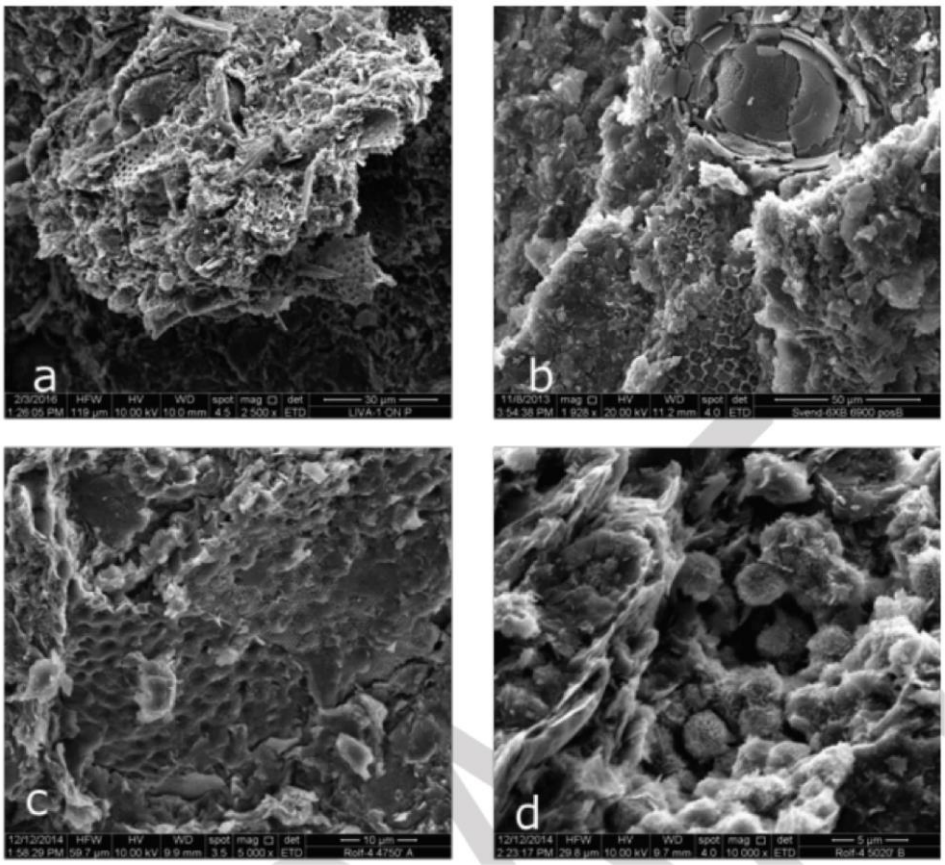

Figure 1.14: SEM images of (a) diatom fragments, (b) crushed diatom fragments from well cuttings, (c) Opal-CT lepisheres with some remnants of Opal-A and, (d) partially altered Opal-CT all from samples from the Central North Sea by Sulsbrück &Toft., (2018).

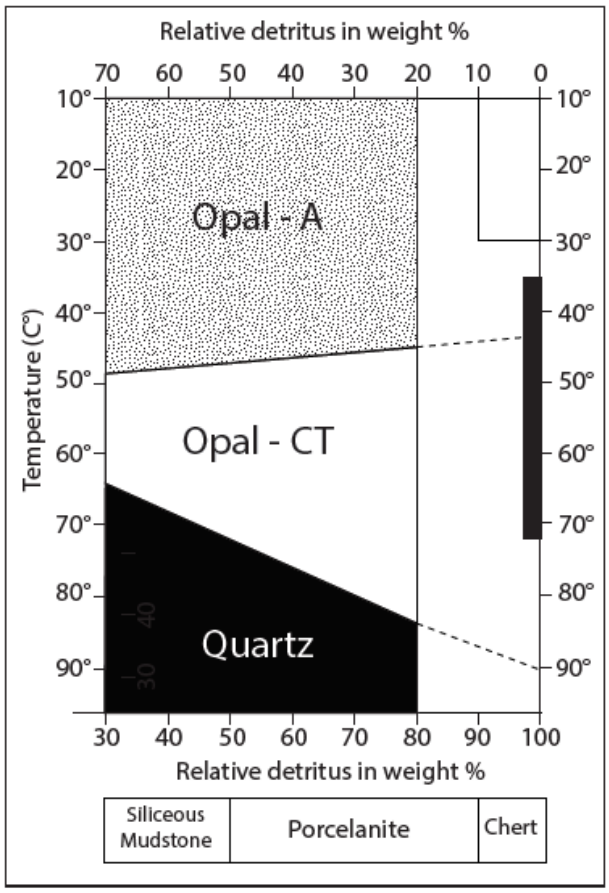

Figure 1.15: Phase diagram for the main phases involved in silica diagenesis (Behl., 2011)

1.7.2 Polygonal Fault Systems

As the name implies, polygonal faults are normal faults that appear with a polygonal geometry when viewed in plan form that are often layer bound have been reported in various sedimentary basins of the world (Figure 1.15). The geometry of these polygonal faults has been established but the processes controlling their nucleation are poorly understood. Several theories on the origin of polygonal faults have been proposed and recently, it is posited that the initiation of polygonal fault systems is linked to their host lithology where in clay-rich sediments, diagenesis can lead to shear fractures and normal faults under low confining stresses (Shin et al., 2008; Cartwright 2011, Wrona et al., 2017). Davies & Ireland (2011) before now linked the growth of polygonal normal fault systems to differential compaction associated with the transformation of Opal-A/CT. A much-debated question to date is the genesis of polygonal faults Cartwright (2011) (*and references therein*) and this research further analyses the role diagenesis plays in the nucleation of

such normal faults within the Central North Sea using 3D seismic data and borehole data (Figure 1.16).

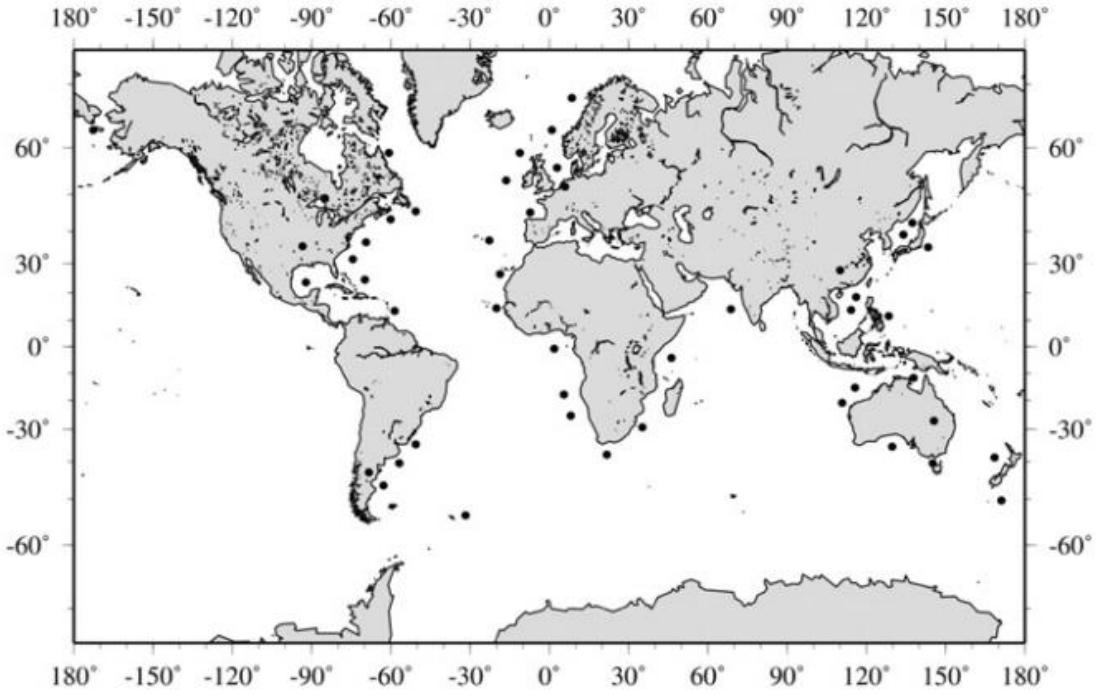

Figure 1.16: Global occurrence of polygonal fault systems identified on 2D, and 3D seismic data represented here by black dots on the map (From Cartwright 2011.)

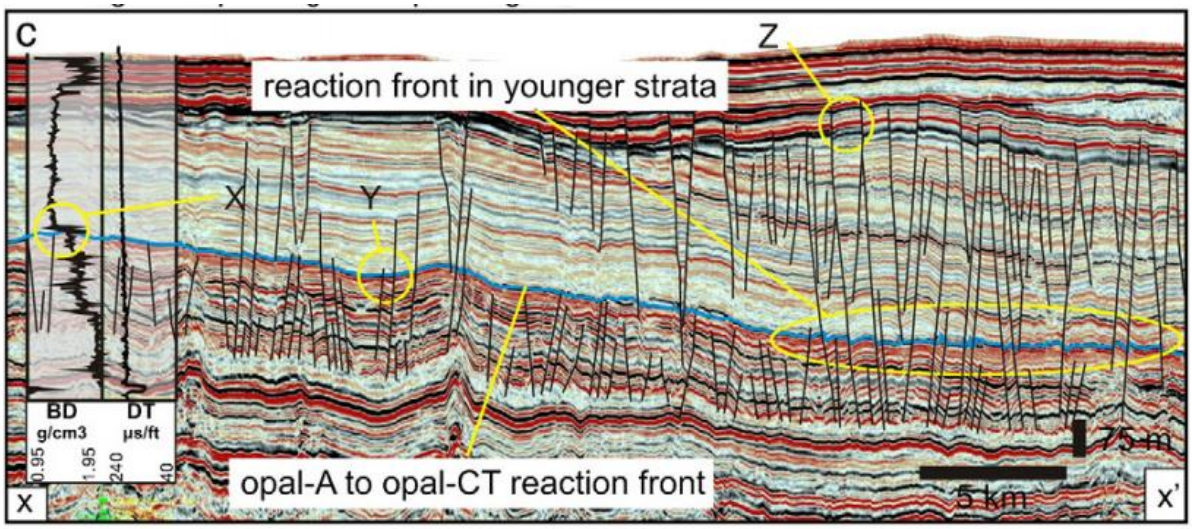

Figure 1.17: Example of a silica diagenetic boundary relationship with polygonal fault system in young strata in the VØring Basin offshore Norway, from Davies & Ireland, 2011.

1.7.3 Overview of Focused Fluid Flow Phenomena in Sedimentary Basins

Fluid flow features are a global phenomenon in sedimentary basins which have only come into light in recent years due to the advance in seismic imaging technology leading to better-imaging quality and more confident interpretation occurring along continental margins (Huuse et al., 2010; Figure 1.17). As Cartwright (2007) noted, the most exciting development in the Earth Sciences over the past century is the advance in seismic data acquisition which allows for visualisation of features in detail from over a few metres to a thousand square kilometres in 3D. Andresen (2012), proposed the application of the study of fluid flow features to the study of basin analysis, stating that fluid flow features such as mud volcano complexes, pockmarks and sandstone intrusions that developed due to the flow of fluids in the subsurface are underused tools which otherwise can be quantitatively and qualitatively integrated into analysing the petroleum system of a sedimentary a basin. Furthermore, Subsurface fluid flow processes and their associated features are increasingly being recognized as significant dynamic components of sedimentary basins. Fluid flow features have been classified in the past based on their lithology, geometry and the type of impact they impose on the hosting sediment (Huuse *et al.* 2010). Subsequently, Andresen (2012) grouped fluid flow features based on the cause of their formation into three major groups namely, i) subsurface sediment remobilization, ii) vertically focused fluid flow, and iii) laterally extensive fluid flow features summarised in (Figure 1.18).

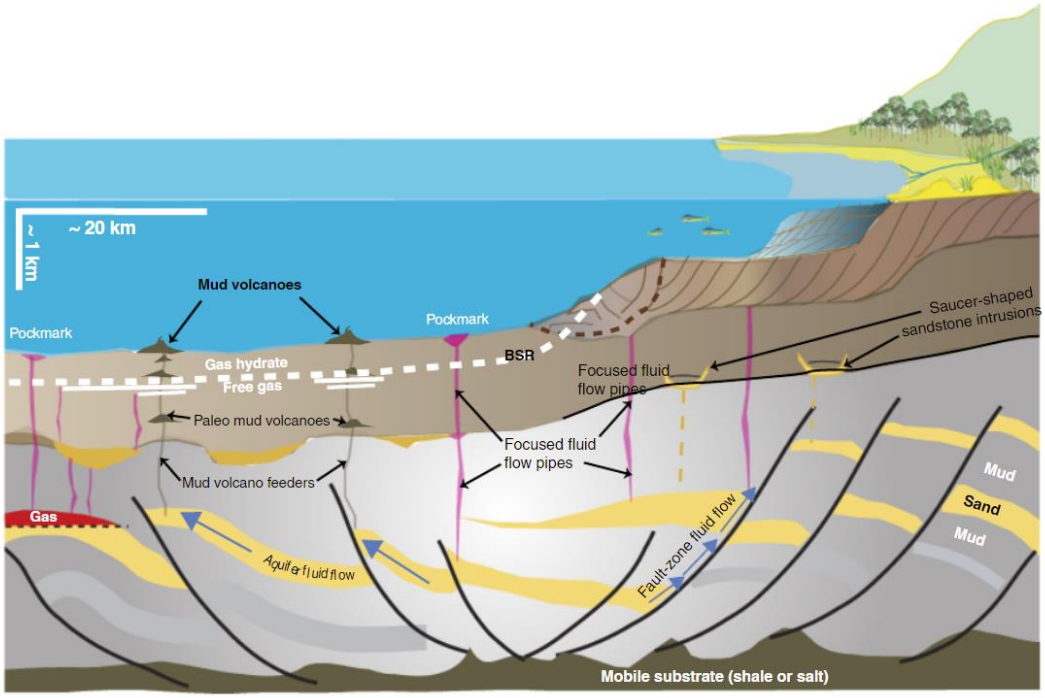

Figure 1.18: A diagram illustrating subsurface fluid flow phenomena highlighting examples of fluid flow features such as mud volcanoes, pockmarks, pipes, sandstone intrusions, bottom simulating reflectors related (BSR) to gas hydrates etc along continental margins from Huuse et al., (2010).

Fluid flow features that emanate from the subsurface remobilisation of sediments are often associated with overpressured aquifers often triggered by seismic activity and in some cases by recharge dynamics between the aquifer and fluid source (Huuse *et al.* 2010). Clastic sediment remobilization which may have resulted from the fluidization of a sand or mud source may be a pointer to seal failure and mud volcano systems forming biconic edifices from mud volcano feeder complexes (Roberts *et al.* 2010) as well. Expulsion of fluids to the seafloor leads to the development of pockmarks (Judd & Hovland 2007), chimneys are seismic artefacts that appear to be vertical regions of low amplitude and acoustic masking on a seismic profile, while pipes are narrow vertical zones of stacked high amplitude anomalies within a seismic section (Løseth *et al.* 2009, Figure 1.18). Methane Derived Authigenic Carbonate (MDAC) mounds are related to seepage of methane-rich fluids through fluid vents to the seafloor thus forming carbonate mounds on the surface of the seafloor. When fluid flow is focused horizontally within stratigraphic intervals in the subsurface, they give rise to laterally extensive fluid flow features such as gas hydrates, diagenetic fronts related with silica diagenesis, bottom simulating reflector (BSR), free gas

zones, gas hydrate stability zone (GHSZ) and hydrocarbon related diagenetic zone (HRDZ) (Berndt *et al.* 2004) (Figure 1.18).

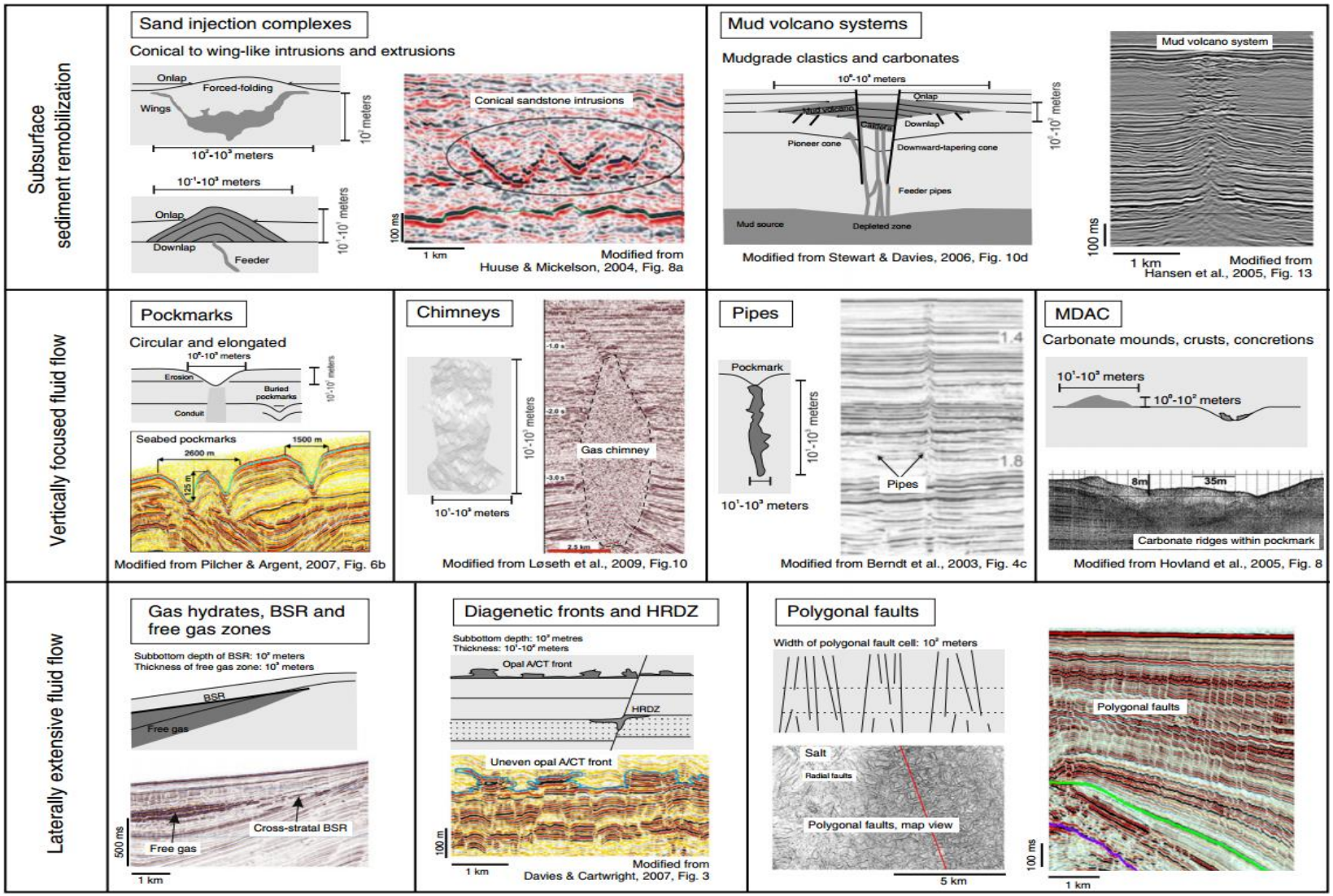

Figure 1.19: Schematic illustrations and examples of fluid flow features adopted from Andresen (2012) showing well the three classes of fluid flow features. MDAC= methane derived authigenic carbonates, BSR= bottom simulating reflection, HRDZ = hydrocarbon related diagenetic zones.

1.8 Additional Data and Limitation of Study

The 3D seismic data used is good and sufficient enough for the aims and objectives of this study. This study enjoyed the integration of a varied set of datasets and techniques, it is noteworthy to mention that there are still limitations to the integration of data from the seismic to the nano scale. Limitations in the study are first imposed by the quality of the seismic data, seeing that most of the data was optimised to only image deeper sections during the acquisition and the merging of different data types during the production of the PGS 3D MegaSurvey to cover a large part of the North Sea, some of the qualities where sacrificed to achieve a regional coverage. This proved to be a challenge in trying to interpret the polygonal faults within the study area due to the nature of the geometry of the polygonal fault system and the resolution of the seismic data.

The well data used in this study are good and sufficient. Critical well logs for this study such as sonic, density and resistivity logs were acquired for deeper sections of the study area although mostly missing for the shallow section under investigation, hence the limited use of well data from the TGS Facies Map Browser for this study.

The availability of well cuttings for the study gave insights into the physical properties of the Cenozoic section under investigation, albeit it should be noted that cuttings have issues to do with contamination and correct depth attribution. Care has been taken during data acquisition, processing, and interpretation to try to correct for the issue of contamination and the issues of caving, but this cannot be guaranteed 100%.

Furthermore, this study could have enjoyed from a basin modelling of the study area to constrain the timing of events, but no such modelling was conducted. As such, the timing of events such as the evolution of silica diagenesis and the polygonal fault system was constraint by the seismic interpretation of features such as the fluid flow features and other structural features within the study area.

1.9 References

Andresen, K. J., Huuse, M., & Clausen, O. R. (2008). Morphology and distribution of Oligocene and Miocene pockmarks in the Danish North Sea -implications for bottom current activity and fluid migration. *Basin Research*, *20*(3), 445–466. https://doi.org/10.1111/j.1365-2117.2008.00362.x

Andresen, K. J. (2012). Fluid flow features in hydrocarbon plumbing systems: What do they tell us about the basin evolution? *Marine Geology*, *332–334*, 89–108. https://doi.org/10.1016/j.margeo.2012.07.006

Anell, I., Thybo, H., & Rasmussen, E. (2012). A synthesis of Cenozoic sedimentation in the North Sea. *Basin Research*, *24*(2), 154–179. https://doi.org/10.1111/j.1365-2117.2011.00517.x

Behl, R. J. (2011). Chert spheroids of the Monterey Formation, California (USA): Early-diagenetic structures of bedded siliceous deposits. *Sedimentology*, *58*(2), 325–351. https://doi.org/10.1111/j.1365-3091.2010.01165.x

Berndt, C., Bünz, S., Clayton, T., Mienert, J., & Saunders, M. (2004). Seismic character of bottom simulating reflectors: Examples from the mid-Norwegian margin. *Marine and Petroleum Geology*, *21*(6), 723–733. https://doi.org/10.1016/j.marpetgeo.2004.02.003

Butcher, A. R., & Botha, P. W. S. K. (2010). Automated mineralogy derives key characteristics directly from reservoir rock. *The American Oil & Gas Reporter*, *January 20*, 4. https://scholar.google.com/scholar?lookup=0&q=Automated+Mineralogy+Derives+Key+Characteristics+Directly+From+Reservoir+Rock&hl=en&as_sdt=0,5

Caroline M. Isaacs. (1981). Porosity Reduction During Diagenesis of Monterey Formation, Santa Barbara, California: ABSTRACT. *AAPG Bulletin*, *65*. https://doi.org/10.1306/2f919f0d-16ce-11d7-8645000102c1865d

Cartwright, J. (2011). Diagenetically induced shear failure of fine-grained sediments and the development of polygonal fault systems. In *Marine and Petroleum Geology* (Vol. 28, Issue 9, pp. 1593–1610). Elsevier. https://doi.org/10.1016/j.marpetgeo.2011.06.004

Cartwright, J. (2007). The impact of 3D seismic data on the understanding of compaction, fluid flow and diagenesis in sedimentary basins. *Journal of the Geological Society*, *164*(5), 881–893. https://doi.org/10.1144/0016-76492006-143

Cartwright, J., & Huuse, M. (2005). 3D seismic technology: The geological "Hubble." In *Basin Research* (Vol. 17, Issue 1, pp. 1–20). European Association of Geoscientists & Engineers. https://doi.org/10.1111/j.1365-2117.2005.00252.x

Cartwright, J., Huuse, M., & Aplin, A. (2007). Seal bypass systems. *American Association of Petroleum Geologists Bulletin*, *91*(8), 1141–1166. https://doi.org/10.1306/04090705181

Chaika, C., & Dvorkin, J. (2000). Porosity reduction during diagenesis of diatomaceous rocks. *AAPG Bulletin*, *84*(8), 1173–1184. https://doi.org/10.1306/a9673c70-1738-11d7-8645000102c1865d

Charsky, A., & Herron, S. L. (2013). Accurate, direct Total Organic Carbon (TOC) log from a new advanced geochemical spectroscopy tool: comparison with conventional approaches for TOC estimation. In *Search and Discovery* (Vol. 41162).

Chipera, S. J., & Bish, D. L. (2002). FULLPAT: A full-pattern quantitative analysis program for X-ray powder diffraction using measured and calculated patterns. *Journal of Applied Crystallography*, *35*(6), 744–749. https://doi.org/10.1107/S0021889802017405

Cohen, R. E. (2019). *First-principles theory of crystalline SiO2*. Silica: Physical Behaviour, Geochemistry, and Materials Applications. https://doi.org/10.1515/9781501509698

Compton, J. S. (1991). Porosity reduction and burial history of siliceous rocks from the Monterey and Sisquoc Formations, Point Pedernales area, California. *Geological Society of America Bulletin*, *103*(5), 625–636. https://doi.org/10.1130/0016-7606(1991)103<0625:PRABHO>2.3.CO;2

Cortese, G., Gersonde, R., Hillenbrand, C. D., & Kuhn, G. (2004). Opal sedimentation shifts in the World Ocean over the last 15 Myr. *Earth and Planetary Science Letters*, *224*(3–4), 509–527. https://doi.org/10.1016/j.epsl.2004.05.035

Davies, R. J., & Cartwright, J. (2002). A fossilized Opal A to Opal C/T transformation on the northeast Atlantic margin: Support for a significantly elevated palaeogeothermal gradient during the Neogene? *Basin Research*, *14*(4), 467–486. https://doi.org/10.1046/j.1365-2117.2002.00184.x

Davies, R. J., Goulty, N. R., & Meadows, D. (2008). Fluid flow due to the advance of basin-scale silica reaction zones. *Bulletin of the Geological Society of America*, *120*(1–2), 195–206. https://doi.org/10.1130/B26099.1

Davies, R. J., & Ireland, M. T. (2011). Initiation and propagation of polygonal fault arrays by thermally triggered volume reduction reactions in siliceous sediment. *Marine Geology*, *289*(1–4), 150–158. https://doi.org/10.1016/j.margeo.2011.05.005

Deegan, C. E., & Scull, B. J. (1977). A standard lithostratigraphic nomenclature for the Central and Northern North Sea / compiled by C.E. Deegan and B.J. Scull. *A STANDARD LITHOSTRATIGRAPHIC NOMENCLATURE FOR THE CENTRAL AND NORTHERN NORTH SEA.*, 36.

Dove, P. M., & Rimstidt, J. D. (1994). Silica-Water Interactions. *Silica. Physical Behaviour, Geochemistry and Materials Applications. Reviews in Mineralogy & Geochemistry*, *29*, 259–308. https://pubs.geoscienceworld.org/msa/rimg/article-abstract/29/1/259/110563

Downey, M. W. (1984). Evaluating Seals for Hydrocarbon Accumulations. *American Association of Petroleum Geologists Bulletin*, *68*(11), 1752–1763. https://doi.org/10.1306/ad461994-16f7-11d7-8645000102c1865d

Ducrotoy, J. P., Elliott, M., & De Jonge, V. N. (2000). The North Sea. In *Marine Pollution Bulletin* (Vol. 41, Issues 1–6, pp. 5–23). Elsevier Ltd. https://doi.org/10.1016/S0025-326X(00)00099-0

Eberl, D. D. (2003). User's guide to RockJock - A program for determining quantitative mineralogy from powder X-ray diffraction data. *U.S. Geological Survey Open-File Report 03-78*, 1–47. https://pubs.usgs.gov/of/2003/of03-078/pdf/RockMan7.pdf

Edwards, G.V.; Butcher, A. R. (1999). *Edwards & Butcher, 1999 QemSCAN -*. https://scholar.google.com/scholar?hl=en&as_sdt=0%2C5&q=Edwards+%26+Butcher%2C+1999+qemscan&btnG=

Eidvin, T., Riis, F., & Rasmussen, E. S. (2014). Oligocene to Lower Pliocene deposits of the Norwegian continental shelf, Norwegian Sea, Svalbard, Denmark, and their relation to the uplift of Fennoscandia: A synthesis. *Marine and Petroleum Geology*, *56*, 184–221. https://doi.org/10.1016/j.marpetgeo.2014.04.006

Gottlieb, P., Wilkie, G., Sutherland, D., Ho-Tun, E., Suthers, S., Perera, K., Jenkins, B., Spencer, S., Butcher, A., & Rayner, J. (2000). Using quantitative electron microscopy for process mineralogy applications. *Jom*, *52*(4), 24–25. https://doi.org/10.1007/s11837-000-0126-9

Gowers, M. B., & Sæbøe, A. (1985). On the structural evolution of the Central Trough in the Norwegian and Danish sectors of the North Sea. *Marine and Petroleum Geology*, *2*(4), 298–318. https://doi.org/10.1016/0264-8172(85)90026-1

Guerin, G., & Goldberg, D. (1996). Acoustic and elastic properties of calcareous sediments across a siliceous diagenetic front on the eastern U.S. continental slope. *Geophysical Research Letters*, *23*(19), 2697–2700. https://doi.org/10.1029/96GL02188

Guthrie, G. D., Bish, D. L., & Reynolds, R. C. (1995). Modeling the X-ray diffraction pattern of opal-CT. *American Mineralogist*, *80*(7–8), 869–872. https://doi.org/10.2138/am-1995-7-823

Hamberg, L., Dam, G., Wilhelmson, C., & Ottesen, T. G. (2005). Paleocene deep-marine sandstone plays in the Siri Canyon, offshore Denmark-southern Norway. *Petroleum Geology Conference Proceedings*, *6*(0), 1185–1198. https://doi.org/10.1144/0061185

Hancock, P. L. (1983). Geological atlas of Western and Central Europe. In *Journal of Structural Geology* (Vol. 5, Issue 6). Shell. https://doi.org/10.1016/0191-8141(83)90079-2

Heggland, R. (1998). Gas seepage as an indicator of deeper prospective reservoirs. A study based on exploration 3D seismic data. *Marine and Petroleum Geology*, *15*(1), 1–9. https://doi.org/10.1016/S0264-8172(97)00060-3

Hesse, R. (1989). Silica diagenesis: origin of inorganic and replacement cherts. *Earth Science Reviews*, *26*(1-3 C), 253–284. https://doi.org/10.1016/0012-8252(89)90024-X

Hinman, N. W. (1990). Chemical factors influencing the rates and sequences of silica phase transitions: Effects of organic constituents. *Geochimica et Cosmochimica Acta*, *54*(6), 1563–1574. https://doi.org/10.1016/0016-7037(90)90391-W

Hoetz, M. van den B. and G. (2015). Seismic characterisation of shallow gas in The Netherlands. *Abstract FORCE Seminar Stavanger 8-9 April 2015*, *April 2015*, 1–3. http://www.force.org/Global/Seminars/2015/150408 - Underexplored plays/Presentations/Seismic Characterisation of Shallow Gas in The Netherlands.pdf

Huuse, M., Lykke-Andersen, H., & Michelsen, O. (2001). Cenozoic evolution of the eastern Danish North Sea. *Marine Geology*, *177*(3–4), 243–269. https://doi.org/10.1016/S0025-3227(01)00168-2

Huuse, M. (2002). Cenozoic uplift and denudation of southern Norway: Insights from the North Sea Basin. *Geological Society Special Publication*, *196*(1), 209–233. https://doi.org/10.1144/GSL.SP.2002.196.01.13

Huuse, M., Jackson, C. A.-L., Van Rensbergen, P., Davies, R. J., Flemings, P. B., & Dixon, R. J. (2010). Subsurface sediment remobilization and fluid flow in sedimentary basins: An overview. *Basin Research*, *22*(4), 342–360. https://doi.org/10.1111/j.1365-2117.2010.00488.x

Japsen, P. (1999). Overpressured Cenozoic shale mapped from velocity anomalies relative to a baseline for marine shale, North Sea. *Petroleum Geoscience*, *5*(4), 321–336. https://doi.org/10.1144/petgeo.5.4.321

Jeans, C. V. (1998). M OORE , D. M. & R EYNOLDS , R. C., Jr. 1997. X-Ray Diffraction and the Identification and Analysis of Clay Minerals , 2nd ed. xviii + 378 pp. Oxford, New York: Oxford University Press. Price £27.95 (spiral-bound paperback). ISBN 0 19 508713 5. . *Geological Magazine*, *135*(6), 819–842. https://doi.org/10.1017/s0016756898501501

Jones, J. B., & Segnit, E. R. (1971). The nature of opal I. nomenclature and constituent phases. *Journal of the Geological Society of Australia*, *18*(1), 57–67. https://doi.org/10.1080/00167617108728743

Jordt, H., Faleide, J. I., Bjørlykke, K., & Ibrahim, M. T. (1995). Cenozoic sequence stratigraphy of the central and northern North Sea Basin: tectonic development, sediment distribution and provenance areas. *Marine and Petroleum Geology*, *12*(8), 845–879. https://doi.org/10.1016/0264-8172(95)98852-V

Judd, A., & Hovland, M. (2007). Seabed fluid flow: The impact on geology, biology, and the marine environment. In *Seabed Fluid Flow: The Impact on Geology, Biology, and the Marine Environment*. Cambridge University Press. https://doi.org/10.1017/CBO9780511535918

Kastner, M., Keene, J. B., & Gieskes, J. M. (1977). Diagenesis of siliceous oozes-I. Chemical controls on the rate of opal-A to opal-CT transformation-an experimental study. *Geochimica et Cosmochimica Acta*, *41*(8). https://doi.org/10.1016/0016-7037(77)90099-0

Keller, M. A., & Isaacs, C. M. (1985). An evaluation of temperature scales for silica diagenesis in diatomaceous sequences including a new approach based on the Miocene Monterey Formation, California. *Geo-Marine Letters*, *5*(1), 31–35. https://doi.org/10.1007/BF02629794

Kim, G. Y., Yoo, D. G., Lee, H. Y., Lee, Y. J., & Kim, D. C. (2007). The relationship between silica diagenesis and physical properties in the East/Japan Sea: ODP Legs 127/128. *Journal of Asian Earth Sciences*, *30*(3–4), 448–456. https://doi.org/10.1016/j.jseaes.2006.11.011

Knox, R. W. O., & Holloway, S. (1992). Paleogene of the central and northern North Sea. In *Lithostratigraphic nomenclature of the UK North Sea* (p. 206). https://scholar.google.co.uk/scholar?hl=en&q=Paleogene+of+the+central+and+northern+North+Sea&btnG=&as_sdt=1%2C5&as_sdtp=

Lamb, R. M., Huuse, M., & Stewart, M. (2017). Early Quaternary sedimentary processes and palaeoenvironments in the central North Sea. *Journal of Quaternary Science*, *32*(2), 127–144. https://doi.org/10.1002/jqs.2894

Løseth, H., Gading, M., & Wensaas, L. (2009). Hydrocarbon leakage interpreted on seismic data. *Marine and Petroleum Geology*, *26*(7), 1304–1319. https://doi.org/10.1016/j.marpetgeo.2008.09.008

Meadows, D., & Davies, R. J. (2007). Morphological development of basin-scale silica diagenetic fronts revealed with 2D seismic reflection data: Offshore Sakhalin, Russian far east. In *Journal of the Geological Society* (Vol. 164, Issue 6). https://doi.org/10.1144/0016-76492006-163

Michelsen, O., Thomsen, E., Danielsen, M., Heilmann-Clausen, C., Jordt, H., & Laursen, G. V. (1998). Cenozoic Sequence Stratigraphy in the Eastern North Sea. *Mesozoic and Cenozoic Sequence Stratigraphy of European Basins*. https://doi.org/10.2110/pec.98.02.0091

Mitchum, R. M., Vail, P. R., & Thompson, S. (1977). Seismic Stratigraphy and Global Changes of Sea Level: Part 3. Relative Changes of Sea Level from Coastal Onlap: Section 2. Application of Seismic Reflection Configuration to Stratigraphic Interpretation. *AAPG Memoir*, *26*, 63–81.

http://archives.datapages.com/data/specpubs/seismic1/data/a165/a165/0001/0050/0063.htm

Morris, M. C., McMurdie, H. F., Evans, E. H., Paretzkin, B., Parker, H. S., Pyrros, N. P., & Hubbard, C. R. (1982). Standard X-Ray Diffraction Powder Patterns. In *NBS Monograph (United States)*. https://doi.org/10.1524/zkri.1970.131.1-6.159

Mortimer-Lamb, M., & Convention, R. B.-A. P. S. (2018). Quantitative Compositional Characterization of the Biosiliceous Miocene Lark Formation, Danish North Sea, and Norwegian Margin. *Searchanddiscovery.Com*. http://www.searchanddiscovery.com/abstracts/html/2019/longbeach-90339/abstracts/2019.PS.22.html

Müller, S., Reinhardt, L., Franke, D., Gaedicke, C., & Winsemann, J. (2018). Shallow gas accumulations in the German North Sea. *Marine and Petroleum Geology*, *91*, 139–151. https://doi.org/10.1016/j.marpetgeo.2017.12.016

Nail, S. L., White, J. L., & Hem, S. L. (1976). Structure of aluminium hydroxide gel I: Initial precipitate. *Journal of Pharmaceutical Sciences*, *65*(8), 1188–1191. https://doi.org/10.1002/jps.2600650814

Nail, S. L., White, J. L., & Hem, S. L. (1976). Structure of aluminium hydroxide gel I: Initial precipitate. *Journal of Pharmaceutical Sciences*, *65*(8), 1188–1191. https://doi.org/10.1002/jps.2600650814

Neagu, R. C., Cartwright, J., Davies, R., & Jensen, L. (2010). Fossilisation of a silica diagenesis reaction front on the mid-Norwegian margin. *Marine and Petroleum Geology*, *27*(10), 2141–2155. https://doi.org/10.1016/j.marpetgeo.2010.09.003

Passey, Q. R., Creaney, S., Kulla, J. B., Moretti, F. J., & Stroud, J. D. (1990). A practical model for organic richness from porosity and resistivity logs. In *American Association of Petroleum Geologists Bulletin* (Vol. 74, Issue 12, pp. 1777–1794). Geoscience World. https://doi.org/10.1306/0c9b25c9-1710-11d7-8645000102c1865d

Pirrie, D., Butcher, A. R., Power, M. R., Gottlieb, P., & Miller, G. L. (2004). Rapid quantitative mineral and phase analysis using automated scanning electron microscopy (QemSCAN); potential applications in forensic geoscience. *Geological Society Special Publication*, *232*, 123–136. https://doi.org/10.1144/GSL.SP.2004.232.01.12

Ragueneau, O., Tréguer, P., Leynaert, A., Anderson, R. F., Brzezinski, M. A., DeMaster, D. J., Dugdale, R. C., Dymond, J., Fischer, G., François, R., Heinze, C., Maier-Reimer, E., Martin-Jézéquel, V., Nelson, D. M., & Quéguiner, B. (2000). A review of the Si cycle in the modern ocean: Recent progress and missing gaps in the application of biogenic opal as a paleoproductivity proxy. *Global and Planetary Change*, *26*(4), 317–365. https://doi.org/10.1016/S0921-8181(00)00052-7

Rasmussen, E. S., VejbæK, O. V., Bidstrup, T., Piasecki, S., & DybkjæR, K. (2005). Late Cenozoic depositional history of the Danish North Sea basin: Implications for the

petroleum systems in the Kraka, Halfdan, Siri and Nini fields. *Petroleum Geology Conference Proceedings*, 6(0), 1347–1358. https://doi.org/10.1144/0061347

Roberts, K. S., Davies, R. J., & Stewart, S. A. (2010). Structure of exhumed mud volcano feeder complexes, Azerbaijan. *Basin Research*, 22(4), 439–451. https://doi.org/10.1111/j.1365-2117.2009.00441.x

Schiøler, P., Andsbjerg, J., Clausen, O. R., Dam, G., Dybkjær, K., Hamberg, L., Heilmann-Clausen, C., Johannessen, E. P., Kristensen, L. E., Prince, I., & Rasmussen, J. A. (2007). Lithostratigraphy of the Palaeogene - Lower Neogene succession of the Danish North Sea. In *Geological Survey of Denmark and Greenland Bulletin* (Issue 12). https://doi.org/10.34194/geusb.v12.5249

Sclater, J. G., & Christie, P. A. F. (1980). Continental stretching: An explanation of the Post-Mid-Cretaceous subsidence of the central North Sea Basin. *Journal of Geophysical Research: Solid Earth*, *85*(B7), 3711–3739. https://doi.org/10.1029/jb085ib07p03711

Shin, H., Santamarina, C. J., & Cartwright, J. A. (2008). Contraction-driven shear failure in compacting uncemented sediments. *Geology*, *36*(12), 931–934. https://doi.org/10.1130/G24951A.1

Sorgenfrei, T. (1969). *Geological perspectives in the North Sea area* (Vol. 19). http://2dgf.dk/xpdf/bull19-02-160-196.pdf

Spinelli, G. A., Mozley, P. S., Tobin, H. J., Underwood, M. B., Hoffman, N. W., & Bellew, G. M. (2007). Diagenesis, sediment strength, and pore collapse in sediment approaching the Nankai Trough subduction zone. *Bulletin of the Geological Society of America*, *119*(3–4), 377–390. https://doi.org/10.1130/B25920.1

Sulsbrück, H. & Toft, J. (2018). A new observation of a bio siliceous opal bearing sequence in the Miocene Lark Formation in the Danish North Sea.

Swanson, H. (1953). *Standard X-ray diffraction powder patterns*. https://books.google.co.uk/books?hl=en&lr=&id=kFAM9FKYsIkC&oi=fnd&pg=PA8&dq=SWANSON,+H.E.,+TATGE,+E.+%26+FUYAT,+R.K.+(1953)+Standard+X-Ray+Diffraction+Powder+Patterns.&ots=E_Q_e-4fRZ&sig=AKcLYyFmAJS1529IOyj9t1TTGxY

Tada, R., & Iijima, A. (1983). Petrology and diagenetic changes of Neogene siliceous rocks in northern Japan. *Journal of Sedimentary Petrology*, *53*(3), 911–930. https://doi.org/10.1306/212f82e7-2b24-11d7-8648000102c1865d

Thyberg, B., & Jahren, J. (2011). Quartz Cementation in Mudstones: Sheet-Like Quartz Cement from Clay Mineral Reactions during Burial. *Petroleum Geoscience*, *17*(1), 53–63. https://doi.org/10.1144/1354-079310-028

Vejbæk, O. V. (1997). Dybe strukturer i danske sedimentære bassiner. *Geologisk Tidsskrift*, *4*(4), 1–31.

Volpi, V., Camerlenghi, A., Hillenbrand, C. D., Rebesco, M., & Ivaldi, R. (2003). Effects of biogenic silica on sediment compaction and slope stability on the Pacific margin of the Antarctic Peninsula. *Basin Research*, *15*(3), 339–363. https://doi.org/10.1046/j.1365-2117.2003.00210.x

von Rad, U., Riech, V., & Rosch, H. (1978). Silica Diagenesis in Continental Margin Sediments off Northwest Africa. In *Initial Reports of the Deep-Sea Drilling Project, 41*. https://doi.org/10.2973/dsdp.proc.41.131.1978

Ward, D. (2000). Use of an X-Ray Spectral Database in Forensic Science. In *Forensic Science Communications* (Vol. 2, Issue 3, pp. 107-). Federal Bureau of Investigation. http://go.galegroup.com.manchester.idm.oclc.org/ps/anonymous?id=GALE%7CA137921503&sid=googleScholar&v=2.1&it=r&linkaccess=abs&issn=15288005&p=AONE&sw=w

Williams, L. A., Crerar, D. A., & Hall, G. (1985). SILICA DIAGENESIS, II. GENERAL MECHANISMS 1. In *pubs.geoscienceworld.org*. https://pubs.geoscienceworld.org/jsedres/article-lookup/55/3/312

Wrona, T. (2016). *Silica diagenesis and physical properties of Cenozoic rocks in the North Viking Graben, northern North Sea*. https://spiral.imperial.ac.uk/handle/10044/1/59966

Wrona, T., Jackson, C. A. L., Huuse, M., & Taylor, K. G. (2017). Silica diagenesis in Cenozoic mudstones of the North Viking Graben: physical properties and basin modelling. *Basin Research*, *29*, 556–575. https://doi.org/10.1111/bre.12168

Chapter 2

First Paper Titled: Silica Diagenesis in Cenozoic Mudstones of the eastern Central North Sea: Physical properties and the effect of salt diapirism

This paper will be submitted to the Journal of Basin Research.

Silica Diagenesis in Cenozoic Mudstones of the eastern Central North Sea: Physical properties and the effect of salt diapirism

Mohammed Malah[1, 2], Mads Huuse[1], Kevin Taylor[1] & Thilo Wrona[3].

1. Department of Earth and Environmental Science, University of Manchester.
2. Corresponding author: mohammed.malah@manchester.ac.uk
3. Department of Earth Science, University of Bergen, Bergen, Norway.

Abstract

Silica diagenesis, particularly the transition of amorphous Opal (Opal-A) to Cristobalite & Tridymite (Opal-CT) is known to impact the physical properties of siliceous sediments across sedimentary basins of the world. The impact to the physical properties of the host rock is associated with changes to the geomechanical properties of the host rock which affects compaction, deformation, and fluid flow during early burial. Using a combination of 3D Seismic data, Petrophysical well logs and well cuttings data, we identified and mapped an extensive silica diagenetic boundary termed the Opal-A/CT reaction front in the eastern Central North Sea (CNS) . We were able to identify and map a distinctive high amplitude reflection on the 3D seismic data across an area ~20,000 km^2 and analyse the lithology of the host rock using XRD and QEMSCAN techniques on well cuttings sample. The Opal-A/CT reaction front mapped is associated with polygonal faults and is not a Bottom Simulating Reflector (BSR) and is thought to be out of equilibrium with the present-day isotherms within the eastern CNS. The mapping of the reaction front showed a preferential propagation of the reaction front in relation with polygonal faulting and salt diapirism. We present a model showing the implication of local salt diapirism within the study area which might have elevated temperatures and led to the fossilization of the reaction front and the preservation of both Opal-A and Opal-CT within the host rock. The findings in this study have implications for both hydrocarbon resource exploitation and underground storage for cardon dioxide and nuclear waste.

2.1 Introduction

Silica diagenesis plays a vital role in understanding host rock properties of siliceous sediments and have been widely studied in different hydrocarbon basins of the world. Silica diagenesis which occurs in fine grained siliceous sediments is often associated with an ultimate change in the geomechanical properties of the host rock which leads to compaction and deformation during early burial. The intrinsic geomechanical properties of fine-grained siliceous sediments control the development of natural fractures and can influence how the host rock will transmit or retain fluids or even respond to hydraulic fracturing (Dong et al., 2017). The alteration of the microstructural properties of host rock lithology due to silica diagenesis has implications for mechanical behaviour such as contraction and hardness that affect compressiveness and brittleness which can be used to predict failure conditions of the host rock (Gross, 1995; Passey et al., 2010; Weller 2018). Silica Diagenesis is a two-step process that encompasses the conversion of biogenic silica (Opal A) to crystalline silica of cristobalite/tridymite (Opal CT) and subsequently, the conversion of Opal CT to quartz (Williams et al., 1985; Isaacs, 1981; Keller & Isaacs, 1985). Both stages of silica diagenetic transformation occur through dissolution and precipitation which often releases significant amounts of water that affects the physical properties of the host rock sediments (Williams et al., 1985; Davies et al., 2008). Physical geomechanical properties affected by silica diagenesis in the host rock include the Young's Modulus and Poisson's ratio which have been related to the mineralogical composition (e.g., clay, quartz, feldspar, carbonate & pyrite) and total organic carbon content of the host rock (Jarvie et. al. 2007; Harris et. al. 2011). The physical and chemical changes to the host rock due to silica diagenesis results in porosity reduction affecting pore connectivity, pore geometry and the grain-to-grain contacts increasing the density of the host rock which in turn leads to an increase in p-wave velocity (Isaacs 1981; Compton 1991; Guerin & Goldberg, 1996; Meadows & Davies, 2009; Ishii et. al. 2011; Thyberg & Jahren 2011). The changes to mineralogy due to diagenesis occurs over an interval within the host rock usually termed the 'transformation zone' and or 'reaction zone' (Berner, 1980; Ortoleva, 1994). The changes in density and ultimately p-wave velocity due to silica diagenesis produces distinct seismic reflections that can be observed and mapped over several hundreds to thousands of kilometres on seismic data with a distinct character and signature over the transformation zone usually termed the 'silica diagenetic boundary' or 'reaction front' or

the 'opal-A/CT boundary' (Davies & Cartwright, 2002; Cartwright & Huuse., 2005; Meadows & Davies, 2007; Ireland et. al. 2011; Wrona et. al. 2017). The changes at the silica diagenetic boundary leads to a geochemical rearrangement of minerals, fluid expulsion, formation of pressure compartments that often lead to overpressure within the host lithology, and other diagenesis related deformation (Behl 2011). The mapping of the silica diagenesis transformation zone on 3D seismic data across different petroleum basins of the world shows that silica diagenesis can influence fluid flow, overpressure and compaction and may trigger submarine slope failures, sediment remobilisation and injections and the formation of polygonal fault systems (Davies et al., 2006, 2008; Cartwright, 2007, 2011; Neagu et al., 2010; Davies & Ireland, 2011, Wrona et. al. 2017). Although silica diagenesis has been studied widely in different sedimentary basins, the factors influencing the evolution and propagation of the silica diagenetic front associated with silica diagenesis is poorly constrained and the use of 3D seismic data allows for spatial mapping of the diagenetic transformation in detail (Cartwright & Huuse., 2005).

In this paper, 3D seismic data and petrophysical data is combined with borehole and mineralogical data to define a silica diagenetic boundary (opal-A/CT transformation zone) in the eastern Central North Sea (CNS), characterise the influence of the of the boundary on the host rock properties of the Cenozoic mudstones and establish what the controls are and the evolution of the reaction front. The combination of seismic data, petrophysical well logs and well cuttings provide constraints on the propagation and geometry of the reaction front within the Cenozoic mudstones of the eastern CNS along the Norwegian-Danish offshore borders. These allows for the opportunity to analyse the controls on local variations in temperature (thermal conductivity), depositional systems and the structure and propagation of the diagenetic front (Neagu et. al. 2010). The recognition of a fossilized 'arrested' silica diagenetic boundary on seismic data is useful in the study of paleo-geothermal events and understanding of basin silica diagenetic processes which impact reservoir quality and mechanical properties of host strata important for basin analysis. Furthermore, Understanding the impact of silica diagenesis in siliceous sedimentary basins of the world has implications for hydrocarbon exploration, subsurface geohazards, and climate change. We identified and characterized the silica diagenetic boundary using 3D seismic data, petrophysical well logs and well cutting samples and introduce a new model

for the propagation and evolution of the silica diagenesis reaction front impacted by local tectonics and salt diapirism in the eastern CNS.

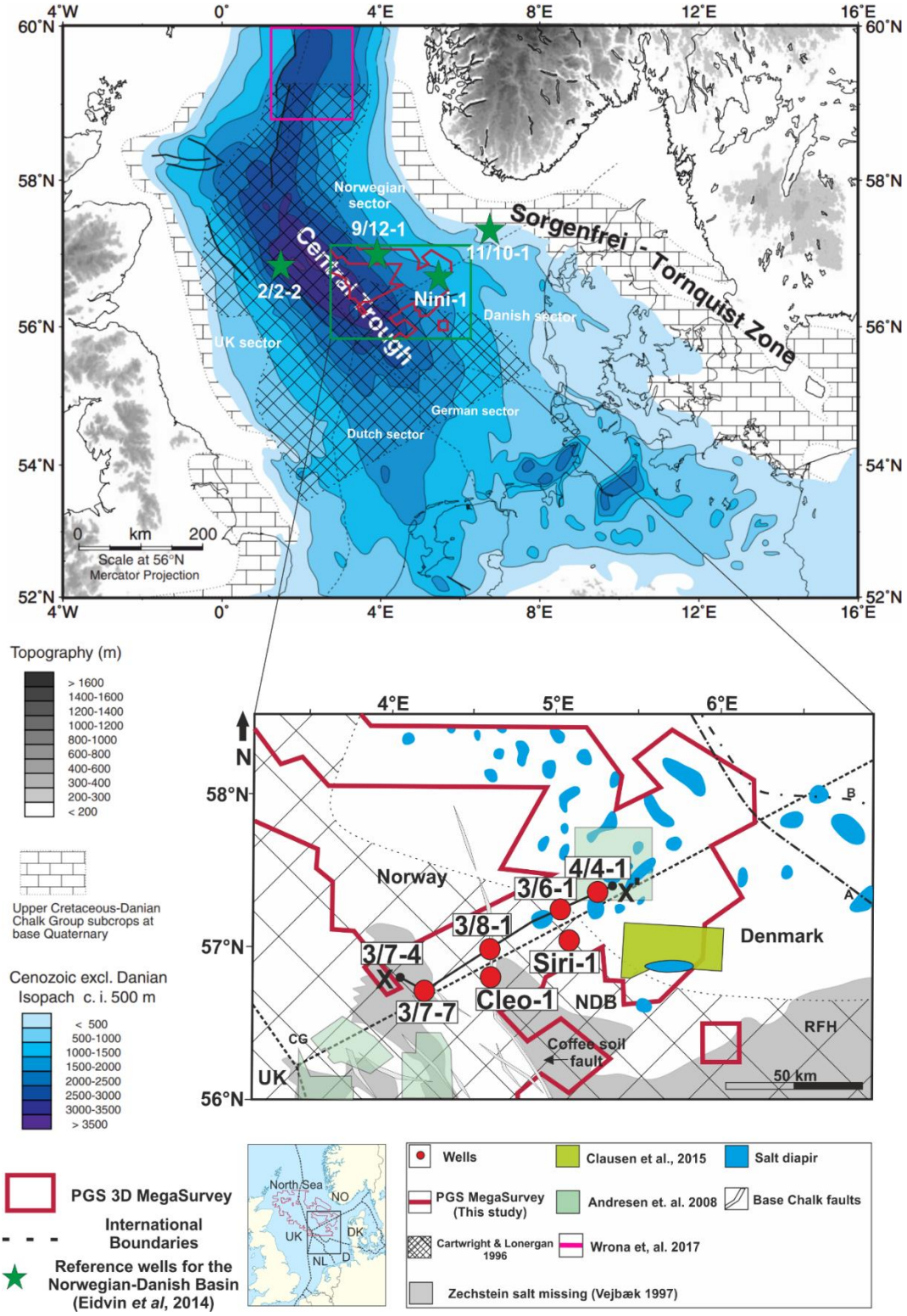

Figure 2.1: Location of study area in the (a) eastern Central North Sea and some of the main structural elements including the sediment thickness of the Cenozoic sediments excluding the Danian with the coverage of the PGS MegaSurvey™ 3D Data. (b) Indicated is the extent of Polygonal Faulting in part of the study area from Cartwright & Lonergan (1996), a zoom-

in to the study area highlights the positions of the wells 3/7-4, 3/7-7, 3/8-1, 3/6-1, and 4/4-1 employed for this study along with the local structural elements including the Coffee Soil Fault, The Ringkobing-Fyn High (RFH), the extent of the Permian Zechstein salt diapirism and mapped shallow gas anomalies. Also highlighted are relevant studies within the study area.

2.2 Geological Setting

This study is located along the Norwegian-Danish offshore borders in the Norwegian Danish Basin (NDB) and adjacent areas including the Central Graben (CG) area in the eastern Central North Sea (CNS). The CNS is an epicontinental basin which developed from the Palaeozoic through the Cenozoic centred on regional Mesozoic rift faults and is affected by regional subsidence and halokinesis (Ziegler, 1990; Fyfe et. al. 2003, Clausen et. al. 2012). The Norwegian-Danish Basin (NDB) is confined by the Central Graben to the southwest and west, the Ringkobing-Fyn-High to the south, the Fennoscandian Shield to the north and northeast and the Horda Platform to the northwest and contains up to 8 km thick successions of Palaeozoic to recent sediments (Ziegler, 1990). The Cenozoic succession reaches a thickness of 3 km in the CNS (Figure 2.1) and is characterised by Halokinesis induced faulting by the Zechstein evaporites with no major structural faulting affecting the Cenozoic unit but rather some inversion related pulses of uplift and halokinesis which is still presently active affecting parts of the basin (Michelsen et al., 1998; Zanella &Coward., 2003; Jordt et. al., 2005; Clausen & Huuse, 1999). Sediments supplied to the Cenozoic North Sea basin were influenced by tectonic movements of older structural elements and are sourced from Oligocene to Pleistocene clinoforms from the east (Jordt et al., 1995; Michelsen et al., 1998). The Cenozoic of the CNS preserves a complete record of Cenozoic sedimentation within depocenters characterised by prograding delta slope systems studied extensively by Jordt et al., (1995), Michelsen et al., (1998) and Thöle et al. (2014) and subdivided into units based on seismic sequence stratigraphic principles. Large prograding deltas are believed to have covered the entire CNS during the Oligo-Miocene and later times, with sediment influx from the Baltic River system and its environs (Overeem et al., 2001), which are partly controlled by subsidence and climatic conditions during later times that created accommodation space for sediments during glacial and interglacial cycles (Kuhlmann & Wong., 2008). The discovery of hydrocarbons in the Palaeocene - Eocene plays tagged the 'Siri Fairway' of the Norwegian-Danish basin outside the hydrocarbon-prone Central Graben demonstrates the importance of cross-stratal and lateral fluid migration from deeper and shallower source rocks of thermogenic and biogenetic fluids, coupled with pore fluid expelled by sediment compaction within the

Central North Sea (Hamberg et al., 2005; Ohm et al., 2006). The Paleogene to Lower Neogene of the Norwegian Danish Basin has been further divided in to seven (7) formations based on lithological, sedimentological and biostratigraphic study of well sections from the Danish North Sea by Schiøler et al., (2007) (Figure 2.2). The divisions from the top of the Chalk Group to the base of the Nordland Group is characterised by the Cenozoic Mudstones of the NDB known as the Stronsay Group and Westray Group represented by the Horda formation and Lark formation respectively (Deegan & Schull, 1977; Knox & Holloway, 1992; Schiøler et al., 2007). The Lark formation (Figure 2.2), deposited in a sublittoral to upper bathyal water depth in the CNS is an Oligo-Miocene biosiliceous mudstone which has been characterized as a regional seal and only studied from drill cuttings, well logs and subsurface data (Schiøler et al., 2007; Sulsbrück & Toft, 2018). The Lark formation is divided into four lithostratigraphic subunits (L1 - L4) based on seismic interpretations, well logs and biostratigraphy (Schiøler et al., 2007) and in this study, it is informally divided into the Lower Lark and Upper Lark formation according to inferred biosilica content with the top of the Lark formation correlating with the mid-Miocene unconformity in the study area. The Lower lark can be correlated to the Denmark onshore Oligocene Branden Clay and Brejning Formations and the Upper Lark is correlated to the onshore Vejle Fjord formation, Klintinghoved and Arnum formations all of which recorded delta progradations from the north and northeast (Rasmussen et al., 2005). The Lark formation is considered a regional seal in the Central North Sea and as such it is uncharacterised. Data available on the Lark formation is mostly from seismic data, wireline logs and well cuttings samples. Data from exploration wells according to well reports indicate anomalously high porosity and large gas kicks during penetration of the Lark Formation which makes it a unit of interest and economic significance. The silica diagenetic boundary in this study is currently fossilized in the upper Lark formation and we posit that the silica diagenetic boundary formed initially within the Eocene Horda formation and Lower Lark formation before migrating to be fossilized in its current position in the Upper Lark formation subparallel to the Top Lark (TL) formation within the study area.

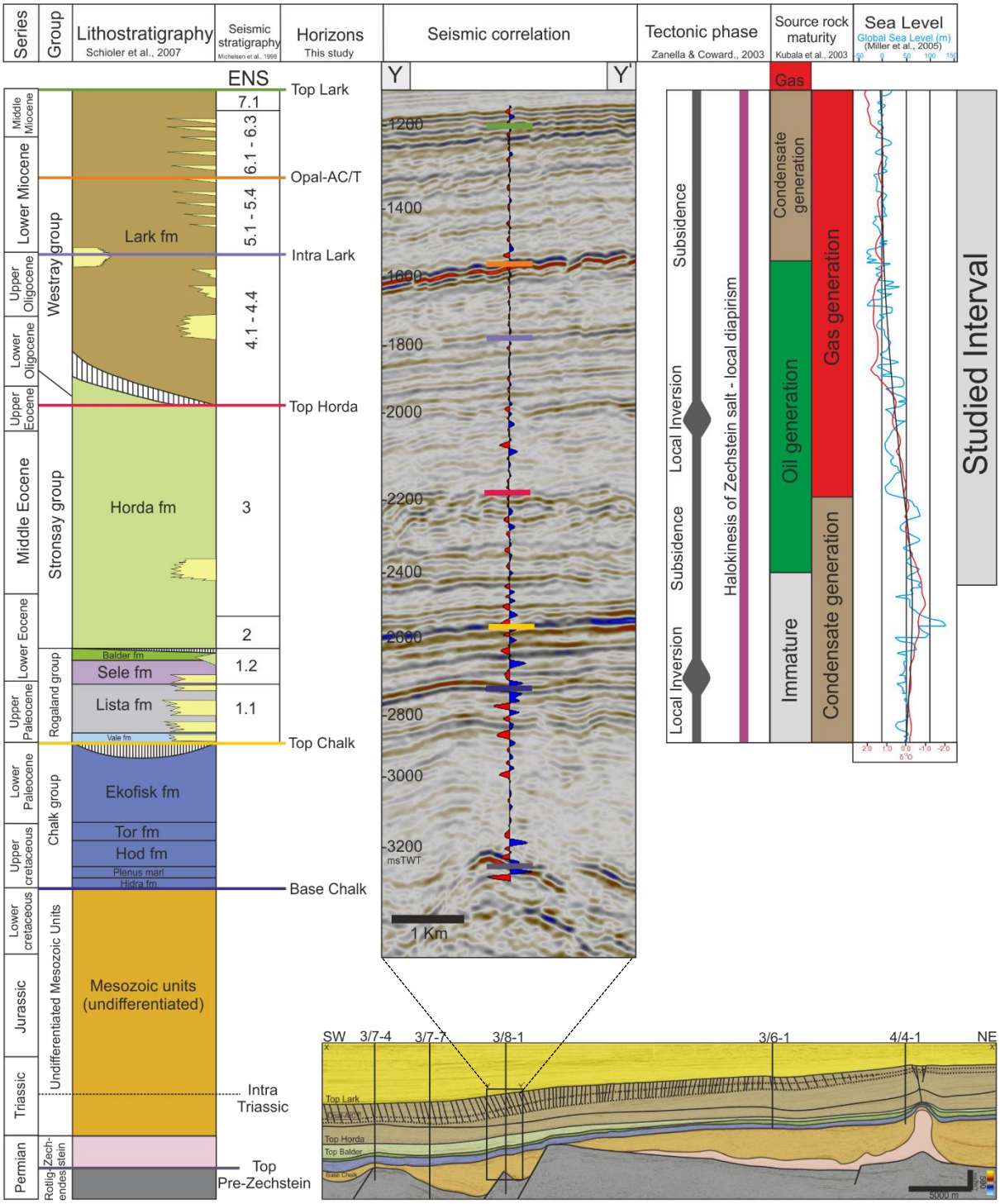

Figure 2.2: Stratigraphic position of horizons mapped and used in this study according to the lithostratigraphic subdivision of Schiøler et al., (2007) and seismic stratigraphy of Michelsen et al., (1998) by the aid of a seismic to well tie using well 3/8-1 (Inset: an interpreted seismic cross-section highlighting the position of the well 3/8-1, the key stratigraphic surfaces and other adjacent wells used in this study). (Note frequent thin sand stringers within the Westray Group Lark formation). Also shown are the local subsidence and inversion tectonics highlighting the tectonic evolution of the study area since the Cenozoic after Zanella & Coward., (2003), source rock maturation after Kubala et al., (2003) and the global sea level and $\delta^{18}O$ curves from Miller et al., (2005).

2.3 Data

2.3.1 3D Seismic Data

Data for this study is a cropped volume of the PGS 3D MegaSurvey™ which covers an area of ~20,000 km^2 in the eastern Central North Sea (Figure 2.1). The 3D survey has a sub-sampled bin spacing of 50 m by 50 m, a sampling rate of 4 msTWT with a maximum vertical resolution ($\lambda/4$) of c. 12 – 15 m and a horizontal resolution ($\lambda/2$) of 20 – 30 m according to a dominant frequency of 50 – 70Hz. The CNS MegaSurvey™ is a normal polarity (zero phase) data where a hard kick i.e., a positive reflection (peak) is represented by red and a soft kick i.e., a negative reflection is represented by a negative reflection (trough). The Cenozoic has an average interval velocity of 2km/s (+/- 10%), thus allowing for the vertical measurements made in milliseconds two-way time (ms TWT) to be directly converted to depth in meters (m) as a first order approximation for the interval of interest for the North Sea (Japsen, 1999; Huuse et al., 2001). The data is sufficient for resolving the silica diagenetic boundary within the study area; however, the 3D seismic data is of variable data quality and polarity due to the post-stack merging of variable seismic cubes to achieve the extensive MegaSurvey™ data by PGS. In places, a phase rotation is applied to improve the match between different versions of seismic data, including adjacent surveys that were merged. A phase rotation of 180° produces a reverse polarity version of the input trace while a +90° or -90° rotation alters the seismic trace in such a way that a peak or trough on the input trace becomes a zero crossing on the output trace and vice versa. The phase rotation allows for an improved seismic-to-well tie and comparison of seismic data with well logs in other parts of the study area.

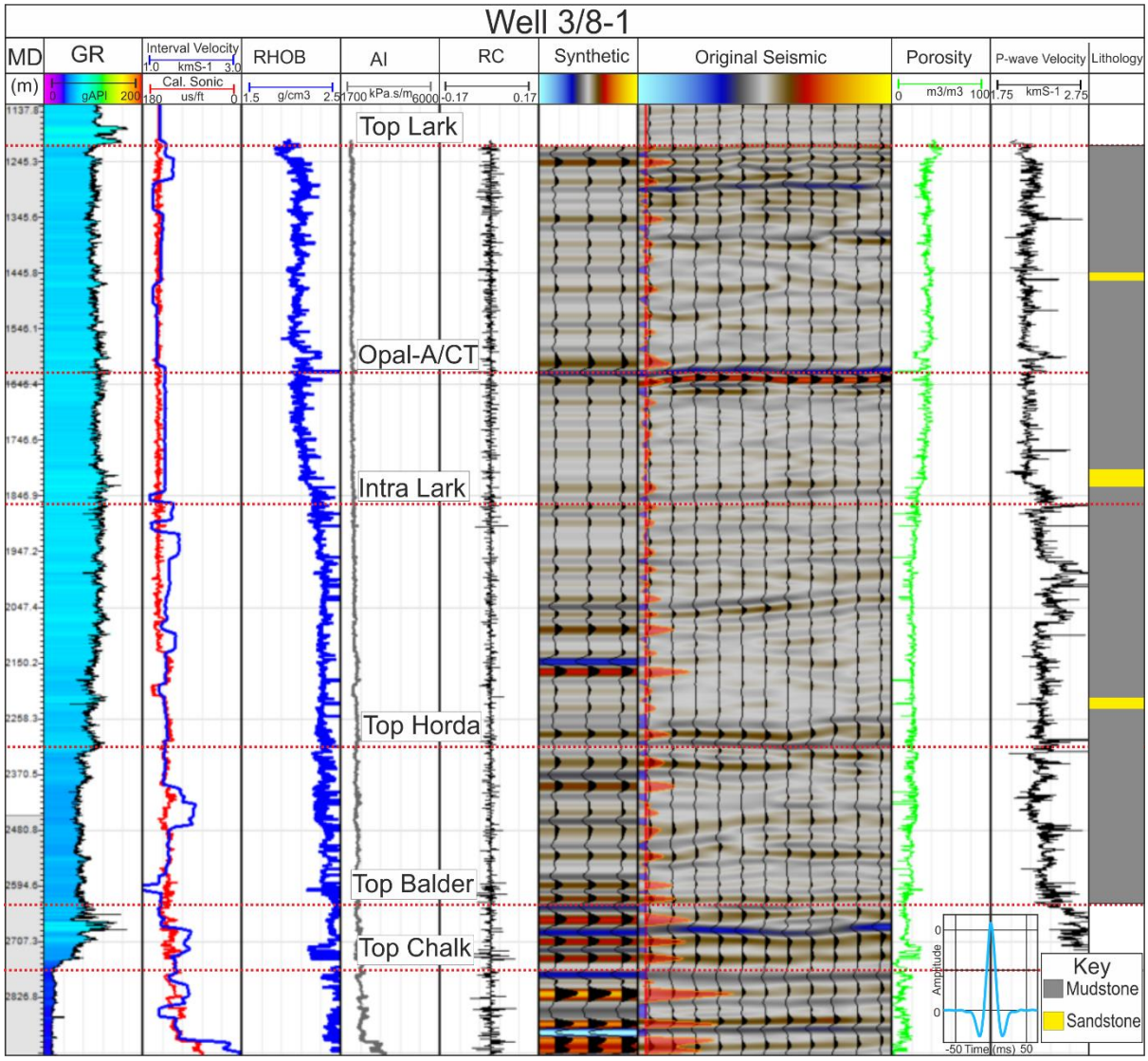

Figure 2.3: Seismic well correlation showing synthetic seismogram generated from well 3/8-1 and tied to the PGS 3D MegaSurvey™ Data. Also shown from left to right are the gamma ray log over the investigated section to the Top Chalk surface, the interval velocity, and the averaged sonic log over the interval as well as the density log over the interval. The acoustic impedance (AI) generated, and the wavelet (inset) convolved with the reflectivity coefficient (RC) to create the synthetic seismogram which aided with the seismic to well-tie at the well location. This was also used to model the synthetic response of the opal-A/CT boundary. An estimated porosity log (green) was generated from the Neutron log and a p-wave Velocity from the sonic log over the interval. A lithological interpretation of the log is shown in the last panel.

2.3.2 Well Data: Petrophysical & Well Cuttings

For this study, petrophysical logs from five exploration wells obtained from the TGS Facies Map Browser (FMB™) (Table 5) and well cutting samples for three wells **4/4-1, 3/6-1** and **3/7-7** were obtained from the Norwegian Petroleum Directorate (NPD) core store in Stavanger over the interval of interest. Lithology information, bottom-hole temperature, total depth, oldest penetrated formation, and other related information were obtained from well

reports from the Norwegian Petroleum Directorate (NPD) Factpages™ (2018) for the wells of interest (Table 5). A total of one hundred and sixty (160) samples were obtained from the NPD core store covering a total of depth of ~2000 m in the three wells 4/4-1 (360 m), 3/6-1 (580 m) and 3/7-7 (1050 m) analysed for this study. Mudstone sections are hardly ever cored and cutting samples proved valuable in this study, where we demonstrate that ample valuable microscopic information can be derived from well cutting samples. It is noteworthy though, that correct depth attribution of well cuttings due to caving can be an issue.

The one-hundred and sixty (160) cutting samples were obtained at an approximate resolution of 10 m in the wells and the wells were selected based on well cuttings availability for sampling from the NPD. The cutting samples were analysed for bulk whole rock mineralogy using X-ray diffraction (XRD) and Quantitative Evaluation of Materials by Scanning Electron Microscopy (QEMSCAN) for this study. Wireline data was analysed for petrophysical well logs and trends were extracted over the interval of interest from the sampled wells 3/7-7, 3/6-1 and 4/4-1 and the other adjacent wells including well 3/7-4 and 3/8-1 within the study area (Figure 1). Cuttings samples obtained and analysed are unwashed, thus, some level of contamination is expected 3/7-7 as well was drilled with oil-based mud (OBM) and well 3/6-1 partly by OBM and well 4/4-1 with seawater and this was taken into consideration during the analysis of data obtained from the well cuttings.

Table 5: Summary of wells included in this study compiled from the NPD Factpages™ website (2018).

Well	Water Depth (m)	Kelly Bushing (m)	WD + KB (m)	TD MD (m KB)	BHT ΔT°C	Oldest Age Penetrated	Oldest Formation/Group
3/7-4	66.0	25.0	91.0	3723.0	136	Late Permian	Zechstein GP
3/7-7	65.0	42.0	107.0	3930.0	127	Late Jurassic	Haugesund fm
3/8-1	65.5	42.0	107.5	4070.0	127	Early Permian	Rotliegend GP
3/6-1	64.0	34.0	98.0	2167.0	70	Late Cretaceous	Tor fm
4/4-1	62.0	43.0	105.0	2012.0	68	Late Cretaceous	Tor fm

All data taken from the website of the Norwegian Petroleum Directorate (NPD 2018).

WD, water depth; KB, Kelly bushing; TD, total depth; MD, measured depth; BHT, bottom-hole temperature.

2.4 Methods

2.4.1 Seismic Interpretation

The 3D Seismic data was integrated with data from ten exploration wells and a seismic-to-well tie is achieved using well 3/8-1 with a complete suite of logs for most of the Cenozoic section under investigation. Using conventional seismic interpretation techniques, Seismic sections were established based on the seismic-to-welltie after the establishment of key regional seismic horizons marking stratigraphic boundaries such as the Base & Top Chalk, Top Balder, Top Horda Formation and the Top Lark Formation (correlating with the mid-Miocene Unconformity in the study area) that were picked away from the borehole locations (Figure 2 and 3). The picking of the horizons away from the borehole allowed us to create a stratigraphic framework (Figure 2.3) of the Cenozoic section of the Central North Sea within the study area. We generated two-way-time (TWT) thickness maps within the sections based on the stratigraphic framework established which allowed us to investigate spatial variations in the thickness of the opal-A/CT transformation zone (Figure 2.8).

2.4.2 Petrophysical Well Log Analysis

Using the well logs in well 3/8-1, we generated a synthetic seismogram by the convolution of a wavelet with a reflection coefficient series estimated from the density and sonic logs to illustrate the detailed acoustic response of the opal-A/CT diagenetic boundary and other key stratal surfaces (Figure 2.3). A time-depth function generated from the convoluted wavelet and the reflectivity series of well 3/8-1 from the density and sonic logs was employed in re-calibrating the well logs in time. The resultant synthetic seismogram was aligned to seismic traces along the inline survey near the well and was subsequently manually calibrated to align with the seismic dataset (Figure 2.3). The silica diagenetic boundary (Opal-A/CT reaction front) is represented by a positive polarity (same as the seabed) and a high amplitude. The reaction front is also correlated with an increase in bulk density and p-wave velocity with a corresponding decrease in porosity over an interval averaging 50 m across the well transect within the transformation zone. At the well location on the seismic data, the silica diagenetic boundary is observed to be concordant

to the host strata and is crosscut by numerous polygonal normal faults terminating at the Top Lark surface (Figure 2.4).

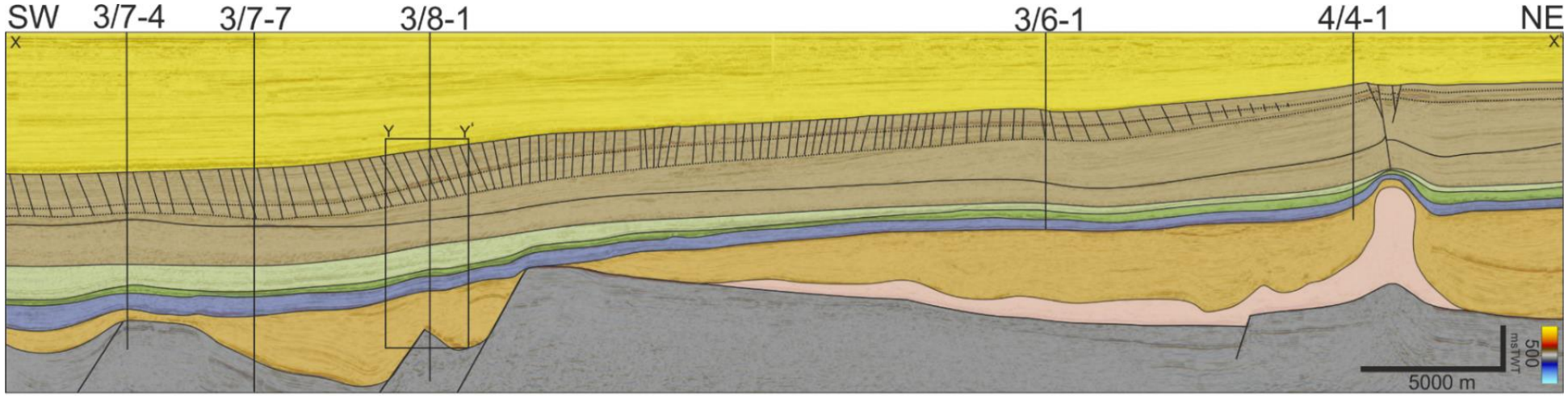
SW
3/7-4
3/7-7
3/8-1
3/6-1
4/4-1
NE
X
X'
Y
Y'
500
msTWT
5000 m

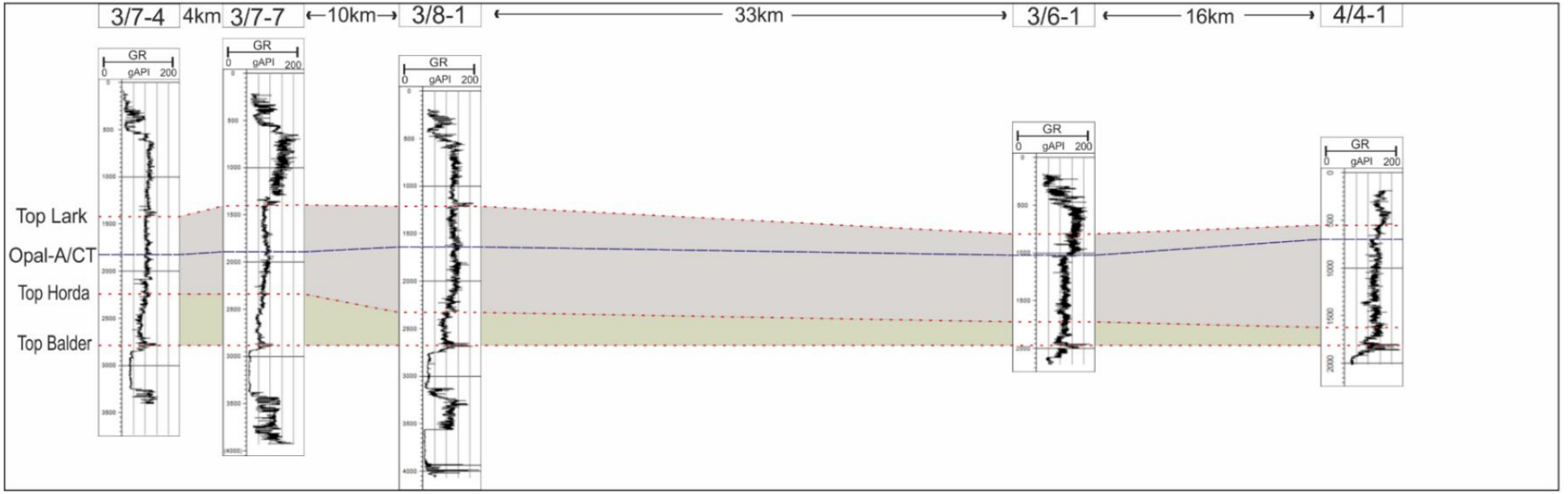
3/7-4
4km
3/7-7
10km
3/8-1
33km
3/6-1
16km
4/4-1
GR
0
gAPI
200
Top Lark
Opal-A/CT
Top Horda
Top Balder

Figure 2.4: Top: Interpreted seismic cross-section with positions of the wells used in this study and the major stratal surfaces mapped (See figure 1 for the location of cross-section within the study area), Note the position of the opal-A/CT boundary and the prevalence of polygonal faults within the interval that progressively decreases in off-set towards the NE of the study area. Bottom: A simplified well log correlation panel across the wells 3/7-4, 3/7-7, 3/8-1, 3/6-1, and 4/4-1 displayed along the seismic cross section at the top covering an approximate 65 km from the Central Graben through the NDB. Gamma ray log is used for the correlation of key surfaces within the Cenozoic Sediments including the Top Lark formation (equivalent to the middle-Miocene unconformity within the study area), the Top Horda Formation and Top Balder Formation. Note the almost flat nature of the mapped opal-A/CT boundary position identified within each of the wells and correlated.

2.4.3 X-ray Diffraction

Well cutting samples acquired from the Norwegian Petroleum Directorate (NPD) Core Store were analysed to determine whole rock (bulk) mineralogy using X-ray diffraction (XRD) technique of Cressey & Schofield (1996) and Batchelder & Cressey (1998). We applied the non-destructive XRD technique to one-hundred and sixty (160) well cutting samples from three wells 4/4-1 (37), 3/6-1 (50) and 3/7-7 (73) with an approximate resolution of 10 m. The samples were prepared on smear slides according to the methods of Batchelder & Cressey (1998) to ensure adequate particle statistics and help reduce primary extinction and preferred orientation of samples with clay minerals. The diffraction measurements were conducted using the Bruker D8 Advance™ diffractometer in the Williamson Research Centre at the University of Manchester operated via the DIFFRAC-Plus XRD Commander software. The measurements were conducted using 20 kV Cu radiations with the X-ray generator operated at 40 mA. The experimental set-up included a 4° divergence slit on both the primary and secondary side and with the diffracted beam collected at a 4-degree window positive sensitive detector lynx eye. Sample measurements start from the 2-theta of 5° and stop at the 2-theta of 69.9° with a step size of 0.020° and a step time of 30.60 s.

2.4.3.1 Quantification of Mineral Phases obtained by XRD

The mineral phases present in each sample were identified using the Bruker Eva Software and subsequently quantified by matching the diffraction pattern of the minerals and whole sample pattern using the RockJock™ whole pattern analysis software based on the methods of Chipera & Bish (2013). The RockJock™ software allows for the quantitative analysis of amorphous and crystalline phases within a complex mixture by comparing intensities of individual minerals against a standard (corundum or zircon) or standardless (quartz) intensity to quantify the proportion of Opal-A, Opal-CT, Quartz, Clays, Pyrite, and other minerals present (D.D. Eberl, 2003). The integrated intensities are then compared to the integrated intensity of the internal standard and the weight percentages of each mineral is calculated automatically and the results are presented as a list of minerals with their corresponding weight percentages and is stored on a spreadsheet for further processing. The standardless analysis is normalized automatically to 100% and the accuracy

of this method using the RockJock program is given at ±5% with a combined bias of 35.0 and for every sample analysed, the aim is for a degree of fit of <0.1.

2.4.4 Quantitative Evaluation of Minerals by Scanning Electron Microscope (QEMSCAN™)

A total of twenty-eight (28) samples from wells 4/4-1 (8) and 3/7-7 (20) were selected for further analysis by the quantitative evaluation of minerals by scanning electron microscope (QEMSCAN) technique. The QEMSCAN system allows for a fully automated quantitative chemical and mineralogical analysis of materials and generation of high-resolution mineral maps and images based on elemental chemistry of polished thin sections of samples of rock surfaces or grain mounts of loose cuttings or sediments (Pirrie et al., 2004). The QEMSCAN technique has been around since the Seventy's (70's) as a vital tool of mineralogical analysis of samples in the mining industry and has only recently been applied in other industries including the Oil & Gas industry (Butcher & Botha, 2012). The analysis was conducted using the FEI QUANTA FEG 650™ scanning electron microscope at the University of Manchester Williamson Research Centre. The QEMSCAN system is fully automated and enables the measurement of values along a predefined grid. Software used for the data acquisition is iMeasure™ V5.2 and iDiscover™ V5.2 software was used for data processing and analysis. The measurements were collected at a resolution of 5 microns particle map analysis (PMA) for overall mineralogy determined to be sufficient for this study (For more information about analytical methods and modes for the QEMSCAN analysis, the reader is referred to Gottlieb et al., 2000 and Pirrie et al., 2004). Preliminary to running the sample analysis, standard instrument tuning including beam alignment, beam focusing, and the calibration of x-ray and back scatter sensors is performed to obtain optimal results. A measurement routine defining grid size and sample analysis per point is defined and the analysis is automated, operating at an accelerated voltage of 20 kV and a specimen current of 10 nA. The measurement routine includes defining a grid size using the FieldImage™ technique where an electron beam moves across the sample on a field-by-field basis at a predetermined stepping interval of 5 µm. The FieldImage™ mode divides the surface of the sample into a virtual grid of fields according to the stepping interval of 5 microns and at each stepping interval, a mineralogical determination is made on the resultant back scattered electrons (BSE) and x-ray signals received from the point of

analysis. The result is a mineralogical map of each stepping interval with a resolution equal to the beam at each interval step (Figure 2.5). A stepping interval of 5 microns was adopted for this study to optimise textural and modal mineralogical information. The iDiscover software was subsequently employed to stitch together all the field images for each sample to produce a mineral map during data processing (Figure 2.5a). We used the global pre-processors within the iMeasure software including the FieldStitch™ to stitch together particles into a single field and the FieldImage™ (Particulator) to separate non-touching particles and the Boundary Phase to transform the boundary of phases based on adjacent phases and Touching Particles pre-processor to filter out and separate touching particles and the Filter particle pre-processor to delete contaminants such as barite and other background noise (Figure 2.5b).

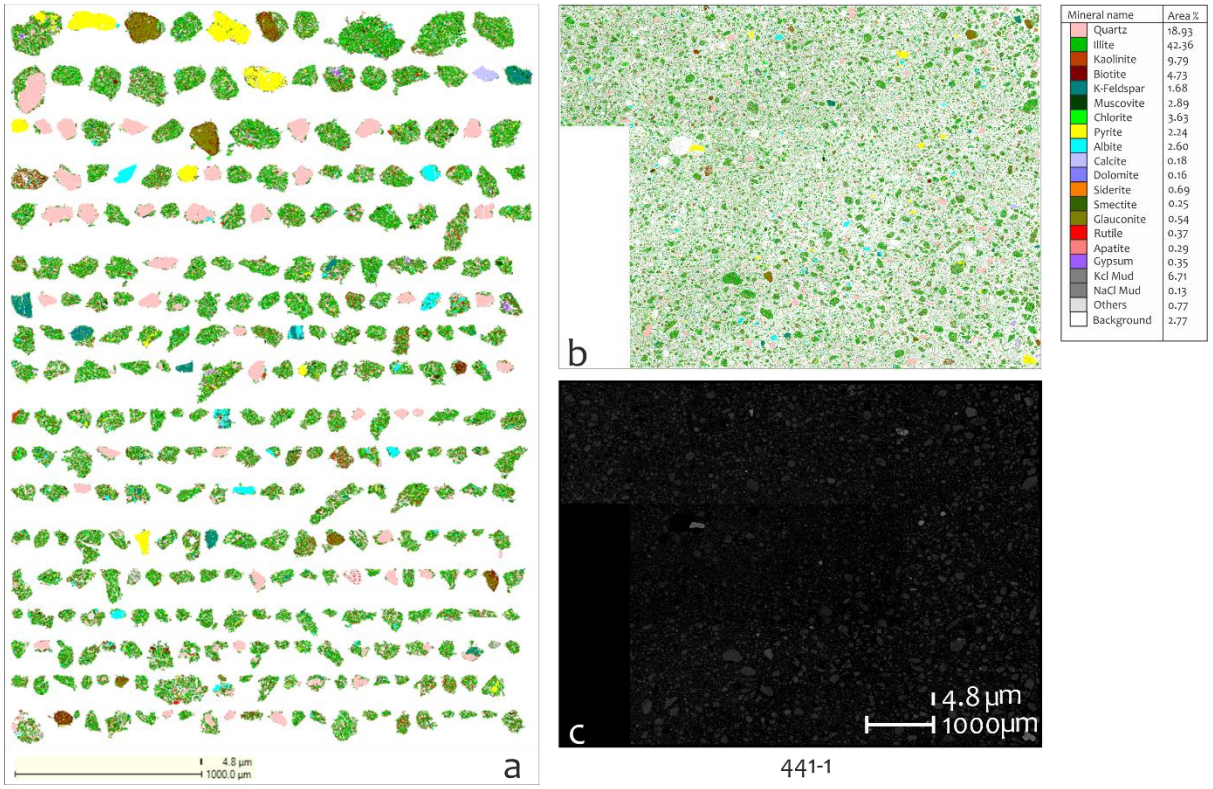

Figure 2.5: a) Particle map image of all mudstone particles mapped by QEMSCAN for drill cuttings of sample 441-1 obtained from well 4/4-1 at an approximate depth of 540m section showing a mineralogical map and the distribution of main mineral species with Quartz in pink, Illite in green and Pyrite in yellow. (b) Stitched false colour map of the particle map image obtained from the polished thin section. (c) BSE map of the same polished thin section from drill cuttings of mudstone particles.

2.4.4.1 *Mineral Lists (Species Identification Protocol: SIP™) in QEMSCAN*

A crucial step in analysing the QEMSCAN data entails the development of the mineral library especially for complex samples like mudstones which are composed of a significant amount of clays (Mogensen et al., 2014). Using the minerals obtained for the same samples from the XRD analysis, we were able to calibrate the mineral list in the QEMSCAN system for analysis using the QEMSCAN iDiscover software to calibrate the QEMSCAN data and significantly reduce the number of unclassified minerals in each sample analysed. The Spectral Analysis Engine (SAE™) of the iDiscover software allows for the fitting of the elemental spectra of all mineral phases contained within the samples based on the measurements obtained using the EDS detector. The detector measures the energy dispersive X-ray (EDX) count of each sample point and calculates the best match for each elemental concentration while recording the spectrum and quantifying the relative contribution of each spectra. The results are the X-ray count, backscatter image (BSE) brightness and the quality of each spectrum matched. We assigned a 'must have' and 'may have' elemental range for the mineral phases expected and the elemental compositions were compared to the Primary SIP list tagged ***'O&G 15 Kv v3.7'*** in the iDiscover software to develop a secondary SIP list suited for the classification of the Cenozoic mudstone samples analysed in this study. We defined multiple end member SIP entries for given mineral phases e.g., Clays and set thresholds for the X-ray count, BSE brightness and the spectral match quality. The Secondary SIP list is developed to allow for the classification of each individual measurement point according to elemental concentrations and once all phases have been identified on a pixel-by-pixel basis, the individual phases are grouped into minerals or phases and presented as a modal mineralogy reported in area or mass percentage contained in each sample. The development of the SIP list for the classification of the mineral phases contained in the samples was optimised fully to reduce the amount of unclassified phases without compromising the accuracy of the results. We adjusted the modified parameters of the SIP list to obtain an accurate estimation of the elemental and mineralogical contents of the samples which improved the hit rate of the SAE to identify and classify more sample points. We consider to be satisfactory for this study confidence values for elemental and mineral composition classification of the samples with values exceeding 90%. Although the data preparation and data acquisition protocols of XRD and QEMSCAN differ in principle, the fundamental difference between the two methods lies in

the ability of XRD to differentiate between mineral polymorphs (e.g., calcite and aragonite or quartz, tridymite and cristobalite) while QEMSCAN does not differentiate such polymorphs. Also, the quantified data from XRD is presented in volumetric mass fractions normalized to 100% and the QEMSCAN system data quantification is by default reported as the surface area fractions of minerals which is more directly comparable with optical mineralogy data and hence, we had to optimise the readings for the QEMSCAN data in this study to report in mass area fractions which is more directly comparable to XRD volumetric mass fractions.

2.5 Results

2.5.1 Physical properties of Cenozoic Mudstones in the eastern CNS

2.5.1.1 *XRD Data*

Whole rock X-ray diffraction analysis of well cuttings samples from the three (3) wells 3/7-7, 3/6-1 and 4/4-1 within the Cenozoic Mudstones of the CNS shows that the mudstones are composed primarily of clay minerals (illite and montmorillonite) and silica minerals (opal-A, opal-CT, and quartz) with minor amounts of pyrite and calcite and trace amounts of sylvite and halite with barite cement according to the mineral phase identification derived from the Bruker Eva Software. Also, based upon FullPat results obtained from the RockJock program, the Cenozoic Mudstones of the CNS from well cutting samples obtained from the representative Lark formation, are confirmed to be composed primarily of clay minerals, silica minerals, and other minerals (Figure 2.6). In well 4/4-1, the average clays and silica mineral content makes up about 90% of the total composition and 80% in wells 3/6-1 and 3/7-7, respectively. Although, it is noteworthy that the results/readings for wells 3/6-1 and 3/7-7 might have been affected by the presence of Barite from drilling fluid contamination of the cuttings sample. The average percentage for biogenic silica (opal-A + opal-CT) contained in the cutting samples of wells 3/7-7 and 3/6-1 are 33% and 28% respectively with a range of 20 – 48% for well 3/7-7 and 21 – 49% for well 3/-61. Well 4/4-1 contains an average composition of biogenic silica of 40%. In each of the three wells, other mineral abundances average 10% in well 4/4-1 and 20% for both wells 3/-61 and 3/7-7 of the total mineralogical compositions of the one hundred and sixty (160) well cutting samples analysed. The average biosiliceous composition for the three wells combined is 33% with a range of 28 -39% and 41% for the total clays with a range of 41 – 43%. The following results

from the XRD data of well cuttings samples for the Lark formation from the CNS is within the range of 3-38% quantification of biosiliceous silica obtained for the Lark Formation by Mortimer Lamb, (2018) using Core Data from three (3) wells from the CNS and from a similar studies conducted by Sulsbrück & Toft, (2018) that estimated an average content of up to 40% biogenic silica from core data for the Lark Formation in the Central North Sea. We see a gentle decrease in the amount of biogenic silica from the data analysed for wells 3/7-7 and 3/6-1 and an almost constant amount of quartz in both wells while we see only a slight decrease in biogenic silica content in well 4/4-1 and a slight increase in quartz content within the sampled interval.

T56r

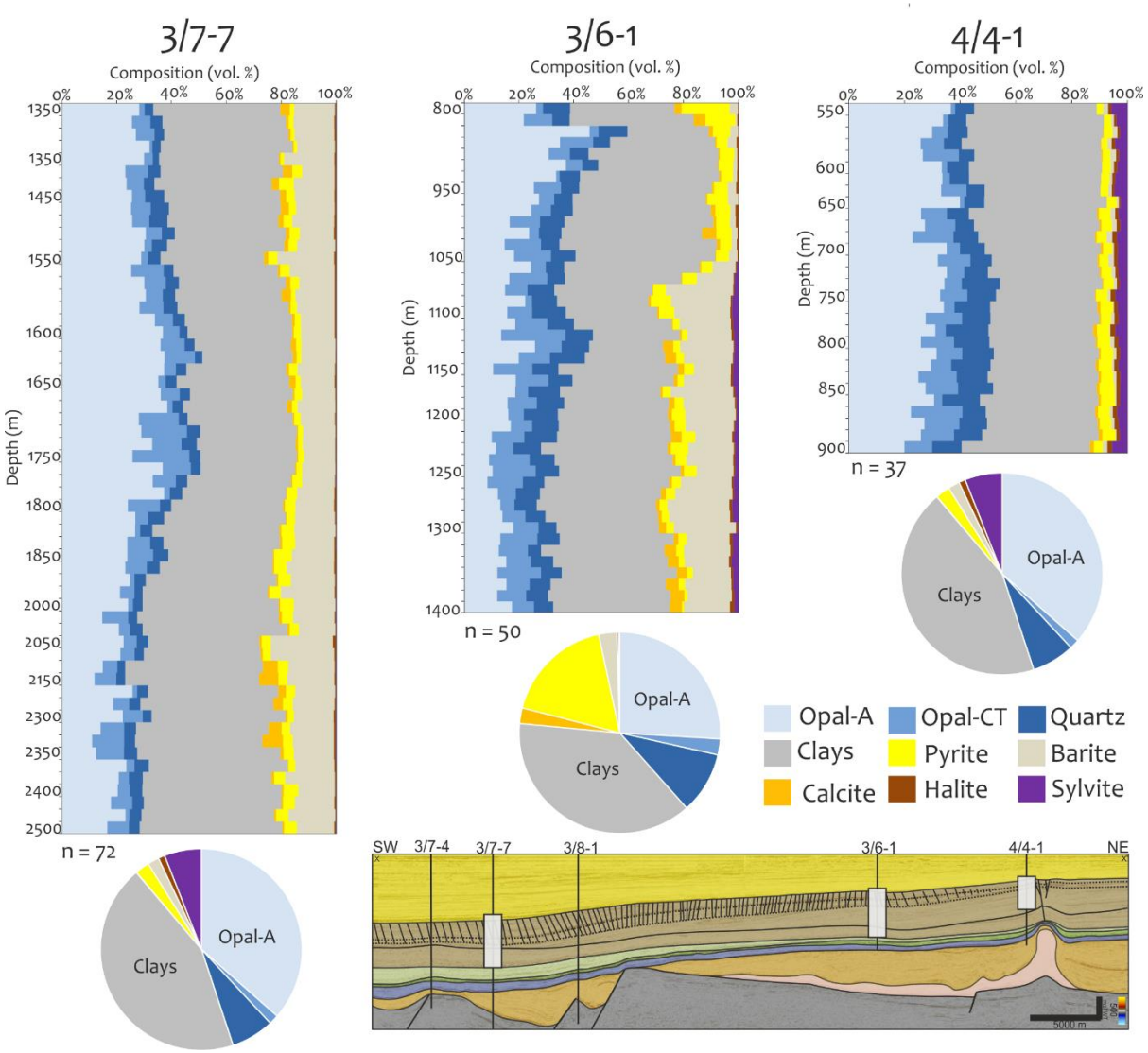

Figure 2.6: Quantitative XRD full pattern matching to determine mineral composition of well cuttings samples from well 3/7-7, 3/6-1 and well 4/4-1. Average of total clays and total silicates composition for the Lark formation is 80% for well 3/7-7 and 3/6-1 and 90% for well 4/4-1. Inset: Position of the wells and the sampled interval.

2.5.1.2 *QEMSCAN Data*

A total of twenty-eight selected samples analysed by QEMSCAN generated mineral maps, stitched particle image map and a BSE image of each sample (Figure 2.5). Mineralogical data obtained from the cuttings sample were compared to petrophysical logs such as gamma ray, calliper, and density to ascertain any depth lag in the data. In this study, the mineralogical composition of the Lark Formation mudstones was investigated and compared with the XRD data. The QEMSCAN data provides additional information other than mineralogy such as grain size distribution, high density mineral maps and textural characteristics (porosity, pore fillings, rock fabric etc) of the rock forming minerals contained in the mudstone samples. A particle image map and a high-density mineral map of sample 441-1 obtained at a depth of 540 m for well 4/4-1 is shown as an example (Figure 2.5). A continuous mineralogical profile was generated from the mineral maps of each sample from each well quantifying the mineralogy shown in Figure 5 from each sample analysed. The mineralogical profile is over an approximate depth of 360 m (-540 m - -900 m) in well 4/4-1 and 1030 m (-1350m - -2380m) in well 3/7-7 covering a total interval of ~1400 m at an average sampling interval/resolution of 50 m for each well. From the mineralogical data obtained, we observe that the samples are primarily composed of silica (quartz) and clay (mainly illite and mixed layer illite-smectite) minerals making up about 80% of the mineralogy in well 4/4-1 and almost 90% in well 3/7-7 and other minerals including pyrite, calcite, halite and sylvite making up 20% and 10% respectively in agreement with the data obtained from the XRD analysis. The samples analysed for well 4/4-1 appear slightly siltier with increasing depth while the values for well 3/7-7 remain almost constant with depth (Figure 2.7). A negative profile between illite, which is the dominant clay mineral and quartz is also observed in the QEMSCAN data especially in well 4/4-1. The mudstones of the lark formation have a 23 - 43% total illite mass composition in well 4/4-1 and about 35 - 52% in well 3/7-7 with an average of 31% and 45% respectively. Pyrite content also ranges from 3.7 – 7.7% and 2.2 – 7.8% with an average of 5.7% and 4.7% in the respective wells. These values obtained for the Lark formation are similar to values obtained for the Oligo-Miocene

Lark Formation equivalents of Arnum, Klintinghoved, Vejle Fjord and Branden formation from onshore Denmark obtained by Nielsen et. al. (2015).

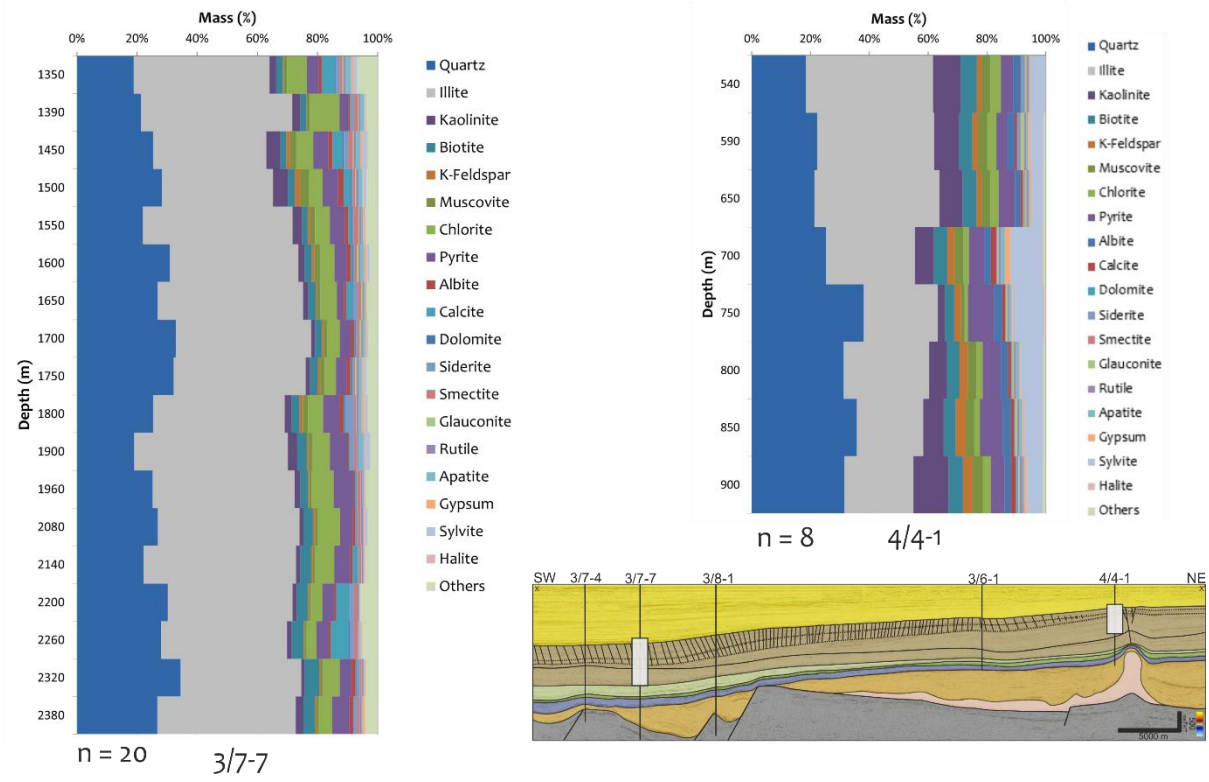

Figure 2.7: QEMSCAN data presented in Mass percentage for cutting samples from wells 3/7-7 and 4/4-1. The minerals represented in each sample for each well is from the defined primary SIP list using the iDiscover™ V5.2 software. The dominant minerals identified for the well 3/7-7 and 4/4-1 is mainly silica (quartz) and illite and mixed layer illite smectite with minor amounts of pyrite, sylvite, halite and other minerals. In well 3/7-7, the dominant minerals of illite and quartz make up about 90% of the composition while in well 4/4-1 they make up 80% of the total composition. Inset is a section showing the position of the wells 3/-7-7 and 4/4-1 and the coverage of the sampled interval.

2.5.2 The structure of the Opal-A/CT Boundary

A strong reflection event with a positive polarity is observed between -1150 and -1825 msTWT corresponding to average depths of 1 – 2 km below the seabed (Figure 2.3; 2.4). This strong reflection event is marked as the Opal-A/CT boundary and is initially mapped as the Intra-Lark I horizon within the Oligo-Miocene Lark formation in the Norwegian Danish Basin and parts of the Central Graben based on the 3D seismic data tied to well. The top of the Opal-A/CT boundary is not concordant with the present-day seabed but concordant with the mid-Miocene Unconformity (MMU) horizon mapped in this study as the Top of Lark (TL) formation. The Intra-Lark I formation is seen to be more concordant in geometry with other stratal reflections below the mid-Miocene Unconformity and is not seen to

crosscut other stratal reflections within the study area (Figure 2.4), a key feature of silica diagenetic boundaries observed on seismic data (Ireland et al., 2010). The depth of the positive polarity reflection marked as Intra-Lark is at about – 1620 mMD (-1620 msTWT) in the well 3/8-1 which we employed to tie the seismic to well in this study (Figure 2.3). The corresponding depth at well 3/8-1 is marked by an increase in the density log and a slight decrease on the sonic log over an interval of approximately 45 - 60 m (1595 – 1655 mMD) and a similar trend is observed in the western well 3/7-4 at depths of about 1730 – 1780 mMD (50 m) but a similar trend is hardly seen within the same mapped Intra-Lark I horizon in the eastern-most well 4/4-1 at depths of about 630 – 680 mMD (50 m) corresponding to the mappable Intra-Lark surface. Such a reflection with similar characteristics has been mapped on seismic data with the integration of well logs to correspond to the opal-A/CT diagenetic boundary in various basins across the Atlantic Margin (Davies & Cartwright, 2002; Neagu et al., 2010; Ireland et al., 2011; Wrona et al., 2017) and this is the first study that defines this interval as the opal-A/CT boundary in parts of the Norwegian-Danish Basin and Central Graben in the eastern Central North Sea. Regionally, the opal-A/CT boundary occurs within the greenish-grey to brown biosiliceous mudstone sediments of the informal upper Oligo-Miocene Lark formation of the Westray Group underlain by the red and green-grey basinal silty and sandy mudstone facies of the Horda Formation of the Stronsay Group and overlain by the grey, sandy, and shelly mudstones, siltstones, and sandstones of the Nordland Group (Deegan & Scull 1977, Knox & Holloway, 1992; Schiøler et al., 2007). The Oligo-Miocene Lark formation is seen to be offset in places by a wedge-tier polygonal fault system which thins out towards the northeast (Cartwright, 2011). The offset of the polygonal faults crosscutting the Oligo-Miocene Lark formation significantly reduces in throw towards the eastern-most well 4/4-1 within the study area (Malah et. al., this study, Chapter 3).

The opal-A/CT TWT structure map is smooth and laterally continuous over the study area but tends to appear with a topography of mesas separated by a network of troughs over a localised area within the study and remains significantly undisturbed over most of the study area (Figure 2.8) (Ireland et al., 2011). Figure 2.4 shows a SW-NE trending log correlation panel for the Lark formation showing a westward thickening of the Lark formation towards the Central Graben flattened on the underlying Top Balder Formation.

The figure shows a variation in the distribution of the Lark formation between the Central Graben (3/7-4 and 3/7-7), the Norwegian-Danish Basin and towards the Horda Platform to the east (3/8-1, 3/6-1, and 4/4-1) mainly because of the regional Coffee Soil Fault with the depocenter of the Lark formation being the central and northern part of the Norwegian Danish Basin (Schiøler et al., 2007). Furthermore, as highlighted, apart from small offsets across most of the individual polygonal faults, the silica diagenetic boundary reflection is remarkably smooth and laterally continuous over the study area with the offset of the polygonal faults increasing from the east to the west towards the Central Graben. The cellular geometry/pattern of the reaction front in the CNS can be seen to die out towards the east. Davies & Cartwright (2007) has investigated such a cellular geometry of the reaction front. The cellular geometry is described as generally circular in shape that formed elevations on the diagenetic front in parts of the study area and has been interpreted to have resulted from differential evolution and propagation of the reaction front.

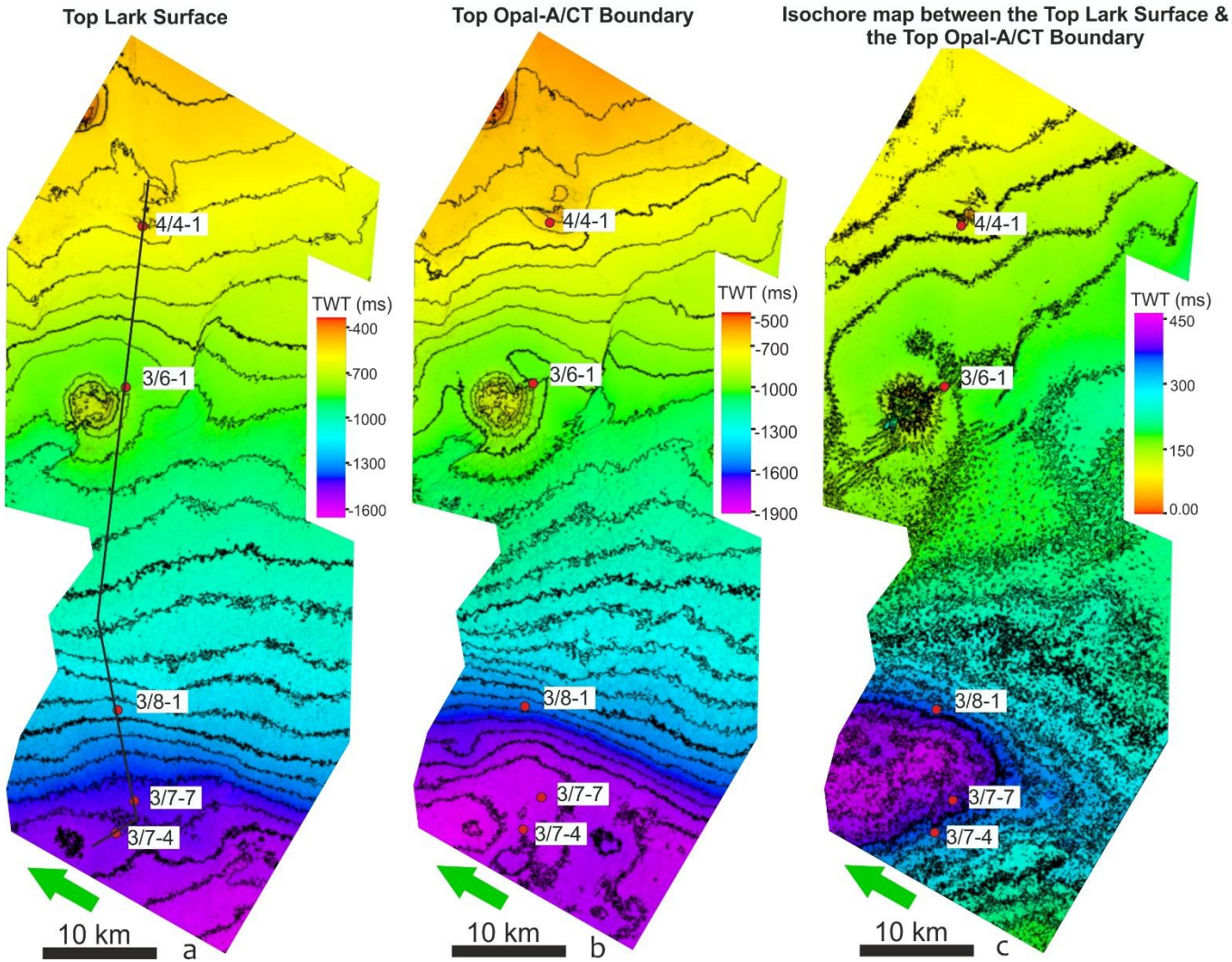

Figure 2.8: Two-way Travel (TWT) contour maps of the (a) Top Lark (TL) surface reflection mapped in an approximate Northwest to Southeast plan view and (b) the Opal-A/CT boundary reflection surface in the same direction. Note the almost similar nature of the Top Lark and the Opal-A/CT boundary TWT surface. (c) An isochore map between the Top Lark surface and the Opal-A/CT boundary showing the thickness variation of the sediments bounded by the two surfaces.

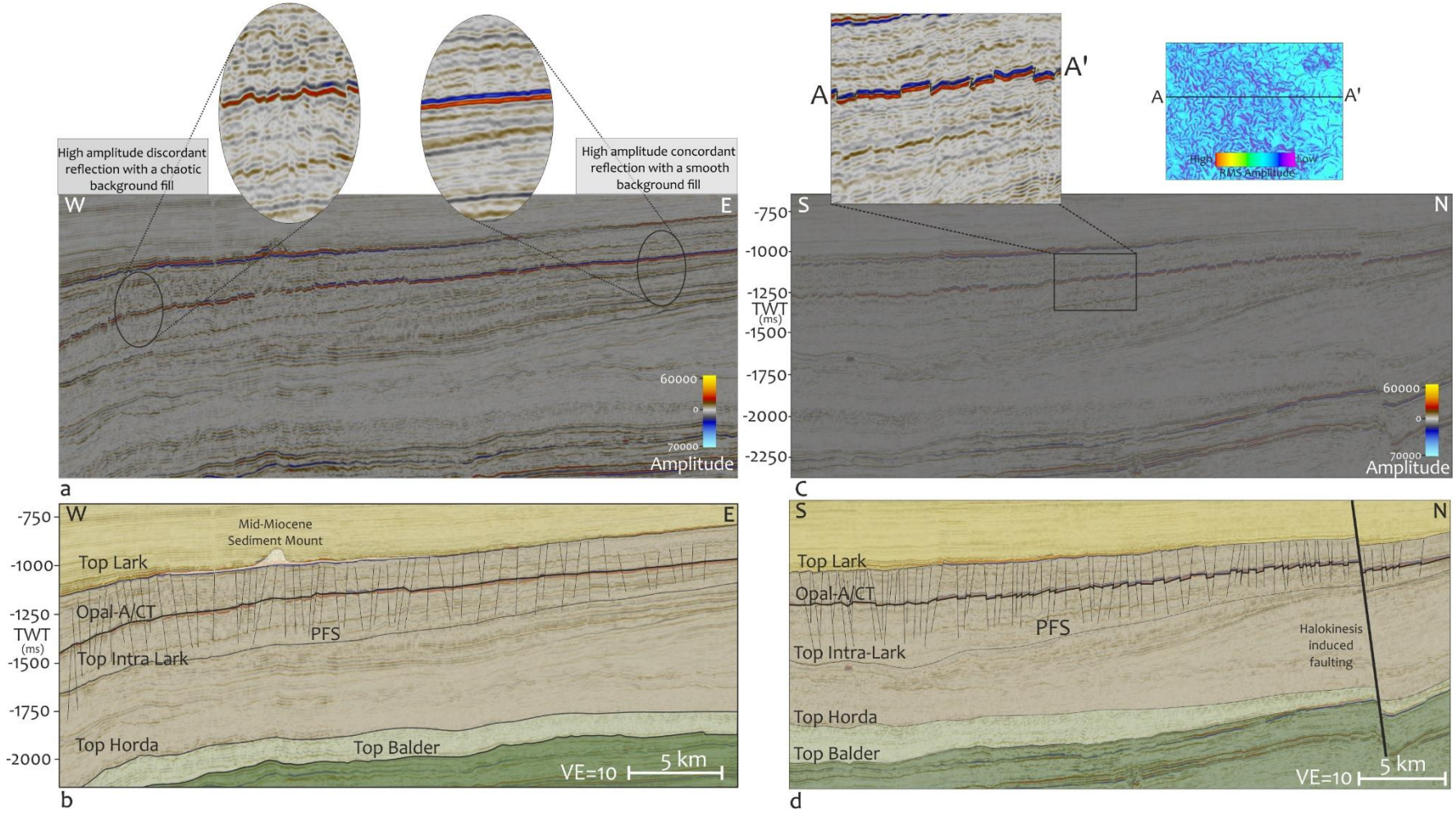

Figure 2.9: Seismic character of the opal-A/CT boundary in sections of the study area (a) highlighting the discordant nature of the identified Opal-A/CT reaction boundary towards the west which becomes more smoother towards the east (b) a n interpreted section from (a) above showing the numerous polygonal faults cross-cutting the opal-A/CT boundary and a mid-Miocene Mud Volcano at the Top of the Lark formation hosting the opal-A/CT boundary identified in the studies by Andresen et. al., (2009). (c) Shows the nature of the opal-A/CT boundary in a North – South trend with an inset plan view of line A-A' showing the nature of the boundary surface in RMS amplitude while (d) shows an interpreted section of (c) above with the numerous polygonal faults cross-cutting the opal-A/CT boundary and terminating at the Mid Miocene Top Lark surface. See figure 8 for approximate locations of the sections.

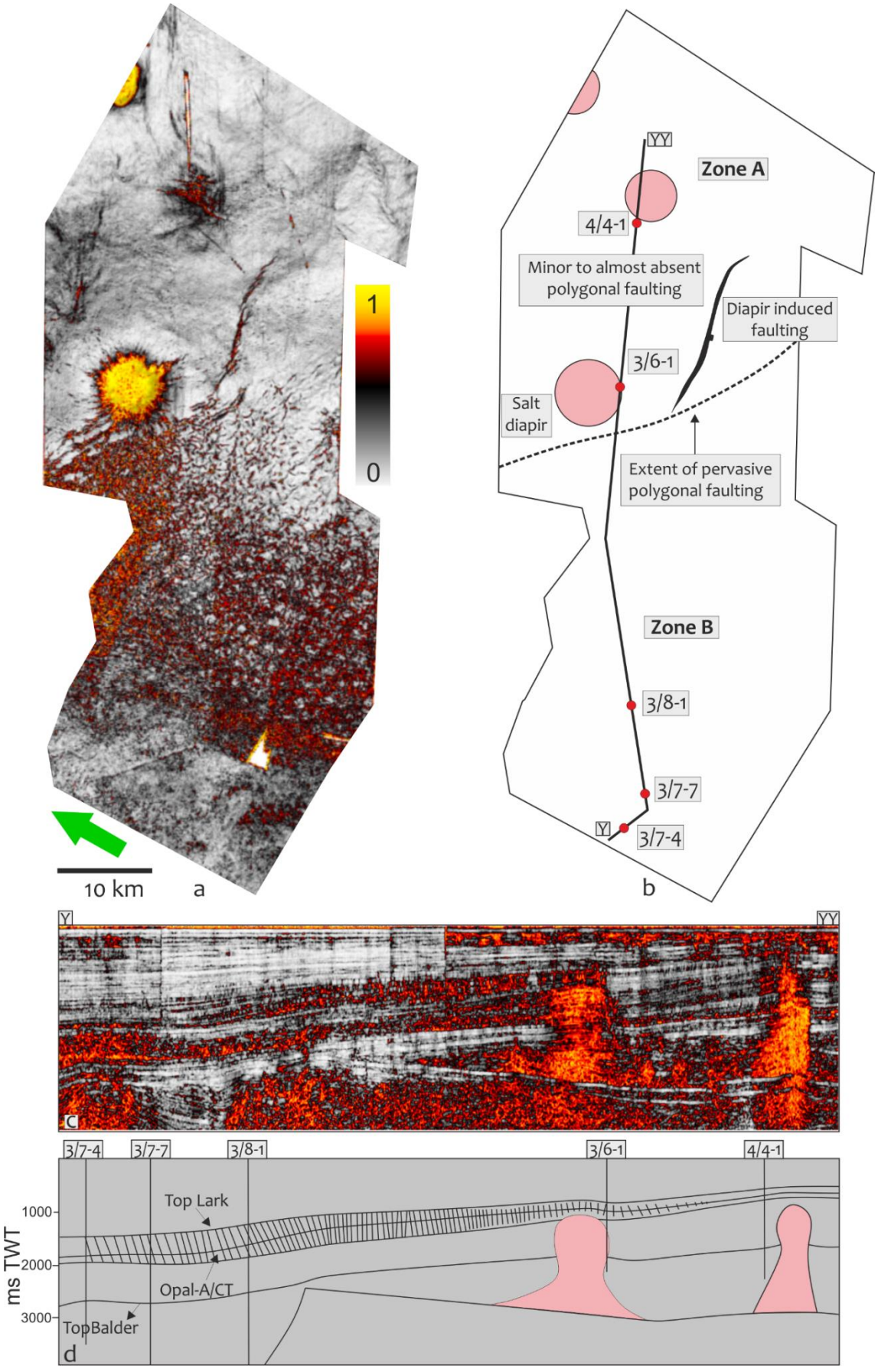
1
0
10 km
a
YY
Zone A
4/4-1
Minor to almost absent polygonal faulting
Diapir induced faulting
3/6-1
Salt diapir
Extent of pervasive polygonal faulting
Zone B
3/8-1
3/7-7
Y
3/7-4
b
Y
YY
c
3/7-4
3/7-7
3/8-1
3/6-1
4/4-1
Top Lark
Opal-A/CT
TopBalder
1000
2000
3000
ms TWT
d

Figure 2.10: (a) Variance attribute surface of the study area across the mapped Opal-A/CT boundary surface in plan view and approximately Northwest to Southeast direction showing the nature and extent of pervasive polygonal faulting in the study area. Note the absence of polygonal faulting beyond the salt diapirs in Zone A with respect to Zone B. (b) a sketch of the Opal-A/CT surface showing the spatial relationship of the pervasive polygonal faulting and the salt diapirs observed within the study area. (c) A cross section YY' taken through the Opal-A/CT surface showing the relationship of the opal-A/CT boundary and wedge tier polygonal faulting within the study area taken across the well intersect for the wells in Table 1. (d) a sketch of the cross-section in (c) showing the main relationship of the opal-A/CT boundary, the salt diapirs and the polygonal fault system.

2.6 Discussion

We draw inferences from the analysis and interpretation of the 3D seismic data and well data for the eastern CNS to discuss the characteristics of the opal-A/CT transformation boundary (the reaction front) in this study. The evolution, timing and propagation of the reaction front is also discussed and the impact of structural deformation of the reaction front is considered.

2.6.1 Opal-A/CT Transformation Zone Characteristics and controls on the Geometry of the Reaction front

In the eastern CNS, we show that the opal-A/CT reflection boundary appears sub-parallel to the MMU locally and at variable depths towards the Central Graben in an East – West transect. This is confined by the isochore map between the MMU and the opal-A/CT boundary presenting an almost uniform thickness with gentle thickening towards the Central Graben. The Characteristics of the reaction boundary is that it shows a vertical and lateral heterogeneity away from the Central Graben within the fine-grained mudstone succession of the Lark formation. These heterogeneities observed can be attributed to the variable rate of transformation of opal-A to opal-CT within the transformation zone away from the Central Graben where the Lark formation is buried at its deepest towards the east to the Stavanger Platform. The geometry of the Opal-A/CT reaction boundary can therefore be potentially related to the depositional environment of the Lark Formation which changes from a Neritic to a Bathyal setting. This can be inferred from the distribution and characteristics of the polygonal fault system within the unit which led to the division of the polygonal fault system distribution and geometry into two zones A & B (Figure 10), corresponding to the Oligocene and Miocene clinoforms break points within the study area. Numerous studies have established the presence of a similar silica diagenetic boundary (Opal-A/CT reaction front) using 3D seismic and well data across the east Atlantic margin (Davies & Cartwright., (2002); Neagu et al. (2010); Ireland et al., (2011); Wrona et al., (2017). The results of these study show such a silica diagenetic boundary is also present in the eastern Central North Sea across the Norwegian-Danish Basin and the Central Graben region. We characterize the opal-A/CT transformation boundary in this study seismically by a high amplitude positive polarity event with bright stratal reflections that dim out towards the east within the study area and is also characterized by enhanced

amplitudes at the boundary. However, the results presented here have not been previously described in the study area and it is observed that the evolution and propagation of the silica diagenetic boundary observed on seismic data in the eastern CNS might have been influenced locally by the effect of salt diapirism that affected parts of the CNS.

The findings in this study showed the preservation of opal-A and opal-CT below the silica diagenetic boundary contrary to that of other studies such as Ireland et al., (2010) and Wrona et al., (2017). An explanation for this might be that the silica diagenesis at the eastern CNS might have had a local control on the evolution and propagation of the reaction front. The reaction front has been known to be impacted primarily by temperature and time and the host sediments composition and the pore fluid to some extent (Kastner et. al. 1977). Also, subsurface temperature and lithostatic pressure have been shown to influence the possible generation of silica diagenesis (Kvenvolden & Claypool, 1988; Davies & Cartwright, 2007). Since the progression and propagation of the silica transformation is primarily temperature dependant, the effect of salt diapirism in the evolution and propagation of the reaction front in the eastern North Sea cannot be ruled out. Salt diapirism, currently active in the CNS has affected parts of the Cenozoic Succession through halokinesis influenced by differential sedimentary loading caused by prograding Cenozoic sequences which reactivated the Permian Zechstein salt (Andresen et al., 2011; Clausen et al. 2012). The reactivation of the salt bodies has affected locally the shallow geothermal gradient of the CNS leading to an increase in temperature across the study area.

2.6.2 Temperature as a controlling factor of Silica Diagenesis

To evaluate the role of temperature in the evolution of the opal-A/CT diagenetic boundary in the eastern CNS, we compiled bottom hole temperatures for the key wells used in these study (Table 5) to estimate the geothermal gradient of the study area. Variations observed in the lithological and mineralogical composition of the Lark formation from XRD and QEMSCAN data are not sufficient to exert the dominant controls on the propagation of the opal-A/CT reaction front and the characteristics of the pore fluid remain uncertain, hence leading us to conclude that other controls are dominant other than those mentioned. One of such dominant parameters considered is the role of temperature and

bottom hole temperatures (BHT) measured for wells 3/7-7, 3/6-1, 4/4-1, and other adjacent wells in the CNS. Published literature show that the present-day geothermal gradient is around 29 – 34.9 °C/km which is slightly higher than published geothermal gradients to adjacent parts of the North Sea basin (Kubala et al., 2003). Examining the geothermal gradient for the wells will put the present opal-A/CT transformation zone at approximately 65 °C which is outside the typical range of temperatures at which active transformation of opal-A to opal-CT usually take place (Hein et al., 1978; Behl., 2011). We observe an elevated increase in geothermal gradient towards the Central Graben which may be due to the insulating effects of the overburden. The elevated geothermal gradients within the sediments of the CNS have been attributed to the influence of a shallow Moho towards the centre of the basin and relative salt diapirism of the Permian Zechstein salt which transfers heat to shallower levels (Kubala et al., 2003). Davies & Cartwright, (2002) have speculated the effect of an elevated geothermal gradient leading to the initiation and fossilization of a silica diagenetic boundary in the Faroe Shetlands basin. Another plausible explanation for the arrest of the migration of the Opal-A/CT reaction front is the introduction of hydrocarbons into the basin by lateral transfer from the Central Graben (Rasmussen et al., 2005; Ohm et al., 2006). Factors which could have affected the geothermal gradient may include uplift and erosion, climatic deterioration, and the onset of cold deep-water circulation and the distribution of salt diapirs in the Central North Sea (Zanella & Coward., 2003; Miller at al., 2005).The elevated geothermal gradient for the CNS and the introduction of hydrocarbons to the basin might have likely led to the arrest of the evolution and propagation of the reaction front in the eastern North Sea.

2.6.3 Evolution, Timing and Propagation of the Opal-A/CT reaction front

The evolution of the Opal-A/CT reaction front in the CNS is summarised in Figure 2.11 according to the three stages of evolution of the reaction front namely (i) formation, (ii) migration and (iii) fossilization as previously described by Cartwright & Davies., (2002). The timing of formation of the silica diagenetic boundary in the eastern CNS is constrained by the present-day depth of burial of the reaction front and its relationship with the host strata. Given that the reaction front is within early Miocene sediments at depths of about 1 – 2 km below the seabed and discordant with the present-day seabed, it is safe to assume

that it is not active and therefore has been fossilized. Similar fossilized opal-A/CT reaction fronts have been described by Davies & Cartwright (2002) for the Faroe-Shetland basin, Neagu et al., (2010) for the mid-Norwegian Margin and Wrona et al., (2017) for the northern-North Sea. A parallel relationship between the opal-A/CT boundary and the mid-Miocene Unconformity observed within the study area and the dimming of the high amplitude reflection towards the east is interpreted to infer the extent of the preservation of the fossilized opal-A/CT or the limit of the phase transformation of the opal-A to opal-CT as we can see the presence of both phases from the mineralogical data. Of marked significance is the decrease in the offset of polygonal faulting in the same trend which highlights the important relationship between silica diagenesis and the formation of polygonal normal faults in the CNS. Furthermore, if the opal-A/CT boundary is considered fossilized and thought to be inactive since the late Miocene due to its relationship with the MMU and with no observed polygonal faulting exceeding this unit, it is paramount to establish the onset of silica diagenesis within the study area to fully constrain the evolution of the silica diagenetic boundary. This can be achieved with confidence through basin modelling such as in the study by Wrona et al., (2017) which is beyond the scope of this study. However, the presence of well-developed authigenic silica (quartz) morphologies due to silica digenesis within the study area have been observed from depths between ~1700 m to ~3000 m in the study by Weibel et al., (2010). This suggests that silica diagenesis probably commenced in the deeper parts of the basin within the deeper sediments of the Lower Lark formation. This is also supported by the presence of polygonal faults which emanate within the Horda Formation in deeper parts of the study area in the Central Graben (not shown) seen to be in connection with shallow polygonal faults of the Lark Formation that terminate at the Top Lark (MMU) surface.

From the above, we can infer that the silica diagenesis commenced within the Horda Formation since the Late Eocene times and migrated upwards with progressive sedimentation and burial within the basin. The arrest of this migration and the fossilization of the opal-A/CT boundary within the early Miocene sediments is thought to be probably due to the reactivation of salt diapirism due to continued sedimentation which led to a local increase in the temperature and geothermal gradient of the study area or the introduction of hydrocarbons. Changes in lithology and mineralogy within the study area

are thought to have no significant effect on the propagation of the opal-A/CT diagenetic boundary.

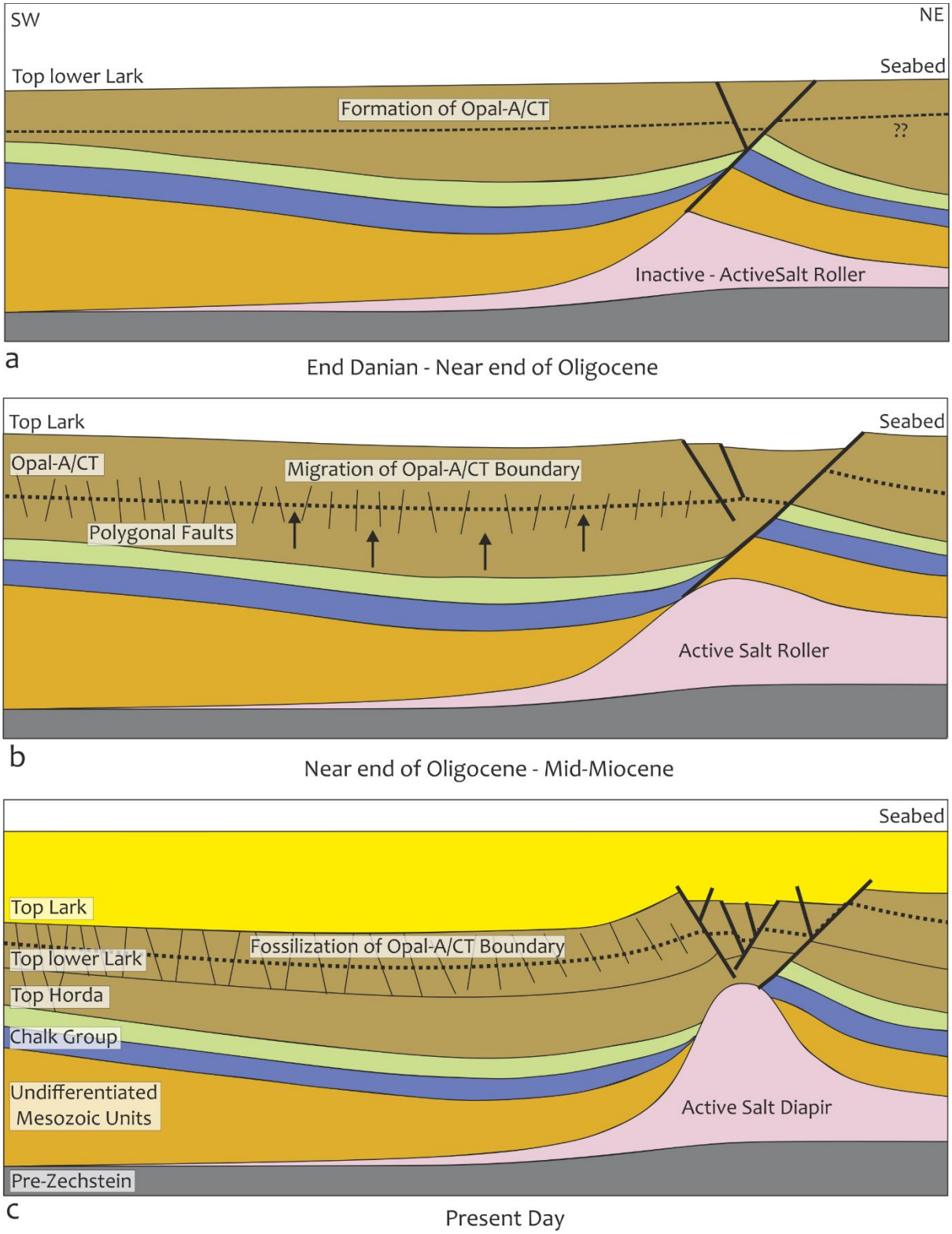

Figure 2.11: A structural reconstruction of a seismic section showing the approximate timing of formation of the Opal-ACT boundary, polygonal fault growth and the relationship with salt flow within the NDB after Sørensen (1998). Note that only

approximate timing of salt movement was considered to keep the model simple. (a) The opal-A/CT boundary initially formed in the Lower Lark formation when the salt roller across the study area was reactivated as a half pillow and became active. (b) Continued sedimentation lead to differential compaction and further growth of the salt roller accompanied with the migration of the earlier formed Opal-A/CT boundary towards the contemporaneous seabed. (c) Further sedimentation ensured the active salt continued development into a diapir for most parts of the study area and in turn influencing the shallow geothermal gradient which possibly lead to the fossilization of the Opal-A/CT boundary at its current position today.

2.7 Conclusions

In this study, using a combination of 3D seismic, wireline and mineralogical data, we were able to identify and characterize for the first time in the Central North Sea area the evidence and occurrence for silica diagenesis and a fossilized silica diagenetic reaction front. The silica diagenesis in the study area, i.e. the transition of Opal-A to Opal-CT and is associated with a change in physical properties of the host rock sediment leading to a reduction in porosity in the study area due to compaction and dewatering and thereby influencing seismic response. The compaction and dewatering led to the formation of polygonal normal faults mappable across the area but distinctively less pervasive towards the east which suggests a preferential evolution and propagation of the reaction front. The silica diagenesis in the study area is fossilized and this is attributed to the effect of local salt diapirism which affected the shallow geothermal gradient thereby impacting the evolution of the silica diagenetic boundary within the study area and possibly the introduction of hydrocarbons into the basin via the Siri canyon fairway.

This study also identified and quantified the presence of amorphous biogenic silica (opal-A) and its associated polymorphs, cristobalite-tridymite (opal-CT), quartz and other minerals from well cuttings and demonstrate the usefulness of well cuttings in otherwise un-cored sections of a sedimentary basin. The investigation of the Opal-A/CT reaction front suggests that the boundary initially formed probably during the Eocene – earliest Oligocene in the Horda Formation and Lower Lark formation and migrated upsection during the Mid-Miocene before being fossilized in its current position today during the Plio-Pleistocene. We propose that the migration and fossilization of the reaction front has been impacted by local salt diapirism within the study area and changes in mineralogical character within the Cenozoic mudstones could not account for the formation of polygonal fault systems within the host strata, hence the propagation of the silica diagenetic boundary impacted by the salt diapirism must have led to the preferential

present-day geometry of the PFS. These findings in this study have implications for both hydrocarbon resource exploitation and underground storage for hydrocarbon exploration, cardon dioxide and nuclear waste storage.

2.8 Acknowledgements

This work is part of MM's PhD research, which is funded by the Petroleum Technology Development Fund (PTDF) Scholarship of Nigeria (Research Grant: PTDF/ED/OSS/PHD/MMG/889/16). We are incredibly grateful to PGS for generously donating seismic datasets and Schlumberger for donating Petrel licenses and TGS for granting access to the Facies Map Browser to the University of Manchester for well data. We would further like to thank the Norwegian Petroleum Directorate (NPD) for making available cuttings samples for analysis. We would also like to thank John Waters, Heath Bagshaw and Stephen Stockley of the Williamson Research Centre at the University of Manchester for granting assistance during data preparation and analysis of the XRD and QEMSCAN data, respectively. Also, we would like to thank Dr. Kofi Owusu for rendering technical support during the period of the research.

2.9 References

Ayling, B., Rose, P., Petty, S., Zemach, E., & Drakos, P. (2012). QEMSCAN® (Quantitative Evaluation of Minerals by Scanning Electron Microscopy): Capability and Application to Fracture Characterization in Geothermal Systems. In *Thirty-Seventh Workshop on Geothermal Reservoir Engineering*.

Batchelder, M., & Cressey, G. (1998). Rapid, accurate phase quantification of clay-bearing samples using a position-sensitive X-ray detector. *Clays and Clay Minerals*, *46*(2), 183–194. https://doi.org/10.1346/CCMN.1998.0460209

Behl, R. J. (2011). Chert spheroids of the Monterey Formation, California (USA): Early-diagenetic structures of bedded siliceous deposits. *Sedimentology*, *58*(2), 325–351. https://doi.org/10.1111/j.1365-3091.2010.01165.x

Berner, R. A. (1980). Early Diagenesis. In *Early Diagenesis*. Princeton University Press. https://doi.org/10.1515/9780691209401

Brändén, R., & Deinum, J. (1978). The effect of pH on the oxygen intermediate and the dioxygen reducing site in blue oxidases. In *BBA - Enzymology* (Vol. 524, Issue 2). https://doi.org/10.1016/0005-2744(78)90166-3

Caroline M. Isaacs. (1981). Porosity Reduction During Diagenesis of Monterey Formation, Santa Barbara, California: ABSTRACT. *AAPG Bulletin*, *65*. https://doi.org/10.1306/2f919f0d-16ce-11d7-8645000102c1865d

Cartwright, J. (2007). The impact of 3D seismic data on the understanding of compaction, fluid flow and diagenesis in sedimentary basins. *Journal of the Geological Society*, *164*(5), 881–893. https://doi.org/10.1144/0016-76492006-143

Cartwright, J. (2011). Diagenetically induced shear failure of fine-grained sediments and the development of polygonal fault systems. In *Marine and Petroleum Geology* (Vol. 28, Issue 9, pp. 1593–1610). https://doi.org/10.1016/j.marpetgeo.2011.06.004

Chipera, S. J., & Bish, D. L. (2013). Fitting Full X-Ray Diffraction Patterns for Quantitative Analysis: A Method for Readily Quantifying Crystalline and Disordered Phases. *Advances in Materials Physics and Chemistry*, *03*(01), 47–53. https://doi.org/10.4236/ampc.2013.31a007

Clausen, O. R., & Huuse, M. (1999). Topography of the Top Chalk surface on- and offshore Denmark. *Marine and Petroleum Geology*, *16*(7), 677–691. https://doi.org/10.1016/S0264-8172(99)00003-3

Clausen, O. R., Nielsen, S. B., Egholm, D. L., & Gołedowski, B. (2012). Cenozoic structures in the eastern North Sea Basin - A case for salt tectonics. *Tectonophysics*, *514–517*, 156–167. https://doi.org/10.1016/j.tecto.2011.10.017

Compton, J. S. (1991). Porosity reduction and burial history of siliceous rocks from the Monterey and Sisquoc Formations, Point Pedernales area, California. *Geological Society of America Bulletin*, *103*(5), 625–636. https://doi.org/10.1130/0016-7606(1991)103<0625:PRABHO>2.3.CO;2

Davies, R. J., & Cartwright, J. (2002). A fossilized Opal A to Opal C/T transformation on the northeast Atlantic margin: Support for a significantly elevated palaeogeothermal gradient during the Neogene? *Basin Research*, *14*(4), 467–486. https://doi.org/10.1046/j.1365-2117.2002.00184.x

Davies, R. J., Goulty, N. R., & Meadows, D. (2008). Fluid flow due to the advance of basin-scale silica reaction zones. *Bulletin of the Geological Society of America*, *120*(1–2), 195–206. https://doi.org/10.1130/B26099.1

Davies, R. J., Huuse, M., Hirst, P., Cartwright, J., & Yang, Y. (2006). Giant clastic intrusions primed by silica diagenesis. *Geology*, *34*(11), 917–920. https://doi.org/10.1130/G22937A.1

Davies, R. J., & Ireland, M. T. (2011). Initiation and propagation of polygonal fault arrays by thermally triggered volume reduction reactions in siliceous sediment. *Marine Geology*, *289*(1–4), 150–158. https://doi.org/10.1016/j.margeo.2011.05.005

Dong, T., Harris, N. B., Ayranci, K., & Yang, S. (2017). The impact of rock composition on geomechanical properties of a shale formation: Middle and Upper Devonian Horn River Group shale, Northeast British Columbia, Canada. *AAPG Bulletin*, *101*(2), 177–204. https://doi.org/10.1306/07251615199

Eberl, D. D. (2003). User's guide to RockJock - A program for determining quantitative mineralogy from powder X-ray diffraction data. *U.S. Geological Survey Open-File Report 03-78*, 1–47. https://pubs.usgs.gov/of/2003/of03-078/pdf/RockMan7.pdf

Eidvin, T., Riis, F., & Rasmussen, E. S. (2014). Oligocene to Lower Pliocene deposits of the Norwegian continental shelf, Norwegian Sea, Svalbard, Denmark, and their relation to the uplift of Fennoscandia: A synthesis. *Marine and Petroleum Geology*, *56*, 184–221. https://doi.org/10.1016/j.marpetgeo.2014.04.006

Gottlieb, P., Wilkie, G., Sutherland, D., Ho-Tun, E., Suthers, S., Perera, K., Jenkins, B., Spencer, S., Butcher, A., & Rayner, J. (2000). Using quantitative electron microscopy for process mineralogy applications. *Jom*, *52*(4), 24–25. https://doi.org/10.1007/s11837-000-0126-9

Gross, M. R. (1995). Fracture partitioning: failure mode as a function of lithology in the Monterey Formation of coastal California. *Geological Society of America Bulletin*, *107*(7), 779–792. https://doi.org/10.1130/0016-7606(1995)107<0779:FPFMAA>2.3.CO;2

Guerin, G., & Goldberg, D. (1996). Acoustic and elastic properties of calcareous sediments across a siliceous diagenetic front on the eastern U.S. continental slope. *Geophysical Research Letters*, *23*(19), 2697–2700. https://doi.org/10.1029/96GL02188

Hamberg, L., Dam, G., Wilhelmson, C., & Ottesen, T. G. (2005). Paleocene deep-marine sandstone plays in the Siri Canyon, offshore Denmark-southern Norway. In *Petroleum Geology Conference Proceedings* (Vol. 6, Issue 0, pp. 1185–1198). https://doi.org/10.1144/0061185

Harris, N. B., Miskimins, J. L., & Mnich, C. A. (2011). Mechanical anisotropy in the Woodford Shale, Permian Basin: Origin, magnitude, and scale. *Leading Edge (Tulsa, OK)*, *30*(3), 284–291. https://doi.org/10.1190/1.3567259

Huuse, M., & Clausen, O. R. (2001). Morphology and origin of major Cenozoic sequence boundaries in the Eastern North Sea Basin: Top Eocene, near-top Oligocene, and the mid-Miocene unconformity. *Basin Research*, *13*(1), 17–41. https://doi.org/10.1046/j.1365-2117.2001.00123.x

Huuse, M., Lykke-Andersen, H., & Michelsen, O. (2001). Cenozoic evolution of the eastern Danish North Sea. *Marine Geology*, *177*(3–4), 243–269. https://doi.org/10.1016/S0025-3227(01)00168-2

Huuse, M., Le Heron, D. P., Dixon, R., Redfern, J., Moscariello, A., & Craig, & J. (n.d.). *Glaciogenic reservoirs and hydrocarbon systems: an introduction*. https://doi.org/10.1144/SP368.19

Ireland, M. T., Davies, R. J., Goulty, N. R., & Carruthers, D. (2011). Structure of a silica diagenetic transformation zone: The Gjallar Ridge, offshore Norway. *Sedimentology*, *58*(2), 424–441. https://doi.org/10.1111/j.1365-3091.2010.01170.x

Jarvie, D. M., Hill, R. J., Ruble, T. E., & Pollastro, R. M. (2007). Unconventional shale-gas systems: The Mississippian Barnett Shale of north-central Texas as one model for thermogenic shale-gas assessment. *American Association of Petroleum Geologists Bulletin*, *91*(4), 475–499. https://doi.org/10.1306/12190606068

Jordt, H., Faleide, J. I., Bjørlykke, K., & Ibrahim, M. T. (1995). Cenozoic sequence stratigraphy of the central and northern North Sea Basin: tectonic development, sediment distribution and provenance areas. *Marine and Petroleum Geology*, *12*(8), 845–879. https://doi.org/10.1016/0264-8172(95)98852-V

Keller, M. A., & Isaacs, C. M. (1985). An evaluation of temperature scales for silica diagenesis in diatomaceous sequences including a new approach based on the Miocene Monterey Formation, California. *Geo-Marine Letters*, *5*(1), 31–35. https://doi.org/10.1007/BF02629794

Knox, R. W. O., & Holloway, S. (1992). Paleogene of the central and northern North Sea. In *Lithostratigraphic nomenclature of the UK North Sea* (p. 206). https://scholar.google.co.uk/scholar?hl=en&q=Paleogene+of+the+central+and+northern+North+Sea&btnG=&as_sdt=1%2C5&as_sdtp=

Kuhlmann, G., & Wong, T. E. (2008). Pliocene paleoenvironment evolution as interpreted from 3D-seismic data in the southern North Sea, Dutch offshore sector. *Marine and Petroleum Geology*, *25*(2), 173–189. https://doi.org/10.1016/j.marpetgeo.2007.05.009

Meadows, D., & Davies, R. J. (2009). Predicting porosity reduction due to silica diagenesis using seismic reflection data. *Marine and Petroleum Geology*, *26*(8), 1543–1553. https://doi.org/10.1016/j.marpetgeo.2008.09.006

Michelsen, O., Thomsen, E., Danielsen, M., Heilmann-Clausen, C., Jordt, H., & Laursen, G. V. (2010). Cenozoic Sequence Stratigraphy in the Eastern North Sea. *Mesozoic and Cenozoic Sequence Stratigraphy of European Basins*. https://doi.org/10.2110/pec.98.02.0091

Miller, K. G., Kominz, M. A., Browning, J. V., Wright, J. D., Mountain, G. S., Katz, M. E., Sugarman, P. J., Cramer, B. S., Christie-Blick, N., & Pekar, S. F. (2005). The phanerozoic record of global sea-level change. *Science*, *310*(5752), 1293–1298. https://doi.org/10.1126/science.1116412

Mortimer-Lamb, M., (2018). Quantitative Compositional Characterization of the Biosiliceous Miocene Lark Formation, Danish North Sea, and Norwegian Margin. *Searchanddiscovery.Com*. http://www.searchanddiscovery.com/abstracts/html/2019/longbeach-90339/abstracts/2019.PS.22.html

Neagu, R. C., Cartwright, J., Davies, R., & Jensen, L. (2010). Fossilisation of a silica diagenesis reaction front on the mid-Norwegian margin. *Marine and Petroleum Geology*, *27*(10), 2141–2155. https://doi.org/10.1016/j.marpetgeo.2010.09.003

Nielsen, O. B., Rasmussen, E. S., & Thyberg, B. I. (2015). Distribution of clay minerals in the Northern North Sea Basin during the Paleogene and Neogene: A result of source-area geology and sorting processes. *Journal of Sedimentary Research*, *85*(6), 562–581. https://doi.org/10.2110/jsr.2015.40

Ohm, S. E., Karlsen, D. A., Roberts, A., Johannessen, E., & Høiland, O. (2006). The Paleocene sandy Siri Fairway: An efficient "pipeline" draining the prolific Central Graben? *Journal of Petroleum Geology*, *29*(1), 53–82. https://doi.org/10.1111/j.1747-5457.2006.00053.x

Ortoleva, P. J. (n.d.). *Ortoleva, P. J. (1994). Geochemical self-organization... - Google Scholar*. Retrieved May 1, 2021, from https://scholar.google.co.uk/scholar?hl=en&as_sdt=0%2C5&q=Ortoleva%2C+P.+J.+%281994%29.+Geochemical+self-organization+%28p.+411%29.+Oxford+University+Press%3A+Clarendon+Press.&btnG=

Overeem, I., Weltje, G. J., Bishop-Kay, C., & Kroonenberg, S. B. (2001). The Late Cenozoic Eridanos delta system in the Southern North Sea Basin: A climate signal in sediment supply? *Basin Research*, *13*(3), 293–312. https://doi.org/10.1046/j.1365-2117.2001.00151.x

Passey, Q. R., Bohacs, K. M., Esch, W. L., Klimentidis, R., & Sinha, S. (2010). From oil-prone source rock to gas-producing shale reservoir - Geologic and petrophysical characterization of unconventional shale-gas reservoirs. *Society of Petroleum Engineers - International Oil and Gas Conference and Exhibition in China 2010, IOGCEC*, *3*, 1707–1735. https://doi.org/10.2118/131350-ms

Pirrie, D., Butcher, A. R., Power, M. R., Gottlieb, P., & Miller, G. L. (2004). Rapid quantitative mineral and phase analysis using automated scanning electron microscopy (QemSCAN); potential applications in forensic geoscience. *Geological Society Special Publication*, *232*, 123–136. https://doi.org/10.1144/GSL.SP.2004.232.01.12

Rasmussen, E. S., VejbæK, O. V., Bidstrup, T., Piasecki, S., & DybkjæR, K. (2005). Late Cenozoic depositional history of the Danish North Sea basin: Implications for the petroleum systems in the Kraka, Halfdan, Siri and Nini fields. In *Petroleum Geology Conference Proceedings* (Vol. 6, Issue 0, pp. 1347–1358). https://doi.org/10.1144/0061347

Rasmussen, P., Petersen, K. S., & Ryves, D. B. (2007). *Geological Survey of Denmark and Greenland Bulletin 13, 2007, 21-24*. www.geus.dk/bulletin

Sulsbrück, H. & Toft, J. (2018). A new observation of a bio siliceous opal bearing sequence in the Miocene Lark Formation in the Danish North Sea.

Theodor, J. L., & Senelar, R. (1975). Cytotoxic interaction between gorgonian explants: Mode of action. *Cellular Immunology*, *19*(2), 194–200. https://doi.org/10.1016/0008-8749(75)90203-8

Thöle, H., Gaedicke, C., Kuhlmann, G., & Reinhardt, L. (2014). Late Cenozoic sedimentary evolution of the German North Sea - A seismic stratigraphic approach. *Newsletters on Stratigraphy*, *47*(3), 299–329. https://doi.org/10.1127/0078-0421/2014/0049

Thyberg, B., & Jahren, J. (2011). Quartz Cementation in Mudstones: Sheet-Like Quartz Cement from Clay Mineral Reactions during Burial. *Petroleum Geoscience*, *17*(1), 53–63. https://doi.org/10.1144/1354-079310-028

Weller, R. M. (2018). *Compositional and diagenetic controls of hardness in siliceous mudstones of the Monterey Formation, Belridge Oil Field, CA: Implications for fracture development* (Issue May).

Williams, L. A., Parks, G. A., & Crerar, D. A. (1985). Silica diagenesis: I. Solubility controls. *Journal of Sedimentary Petrology*, *55*(3), 301–311. https://doi.org/10.1306/212f86ac-2b24-11d7-8648000102c1865d

Wrona, T., Jackson, C. A. L., Huuse, M., & Taylor, K. G. (2017). Silica diagenesis in Cenozoic mudstones of the North Viking Graben: physical properties and basin modelling. *Basin Research*, *29*, 556–575. https://doi.org/10.1111/bre.12168

Ziegler, P. A. & Larminie, F. G., (1992). Geological Atlas of Western and Central Europe 1990. In *The Geographical Journal* (Vol. 158, Issue 3). https://doi.org/10.2307/3060311

Chapter 3

Second Paper Titled: Growth and propagation of polygonal normal faults due to silica diagenesis in the eastern Central North Sea

This paper will be submitted to the Journal of Marine and Petroleum Geology.

Growth and propagation of polygonal normal faults due to silica diagenesis in the eastern Central North Sea

Mohammed Malah[1, 2], Mads Huuse[3], Thilo Wrona[4].

4. Department of Earth and Environmental Science, University of Manchester.
5. Corresponding author: mohammed.malah@manchester.ac.uk
4. Department of Earth Science, University of Bergen, Bergen, Norway.

Abstract

Polygonal fault systems (PFS) have been studied widely in numerous sedimentary basins worldwide. Recently, there has been growing links between silica diagenesis of biosiliceous sediments and the nucleation, growth, and propagation of such polygonal fault systems. Silica diagenesis is found to be associated with a change in the chemical and mechanical properties of host lithologies, often leading to a loss in porosity and an increase in density and p-wave velocity. Using 3D seismic and well data, we mapped out the presence of an Opal-A/CT reaction front in the study area using conventional seismic mapping techniques to describe in detail, the nature of the polygonal fault system in the eastern CNS. We proposed a model for the nucleation, growth, and propagation of the polygonal fault system as a contemporaneous process happening alongside silica diagenesis and report that most of the faults are in-active at present by means of spatial and temporal evolution of the polygonal fault systems. Understanding the spatial, temporal, and kinematic evolution of polygonal faults have implications for basin analysis, carbon dioxide (CO_2) storage in the subsurface and nuclear waste disposal as they present a leakage risk in otherwise sealing sequences.

3.1 Introduction

Polygonal fault systems (PFS) have been studied widely in numerous sedimentary basins worldwide. They are often low displacement normal faults commonly found within fine grained successions of sedimentary basins around the world and they are made up of a network of faults forming a system of interconnected faults termed 'Polygonal Fault Systems' (PFS) which are non-tectonic in origin (Cartwright., 1994; Cartwright & Lonergan., 1996; Lonergan., 1998). They bare orientations which commonly form polygonal geometries on bedding planes confined within stratigraphic layers and they are sometimes referred to as layer-bound faults (Cartwright., 2007). They generally form in the first few hundred meters upon sediment burial and are characterized by vertically and laterally extensive arrays of numerous such polygonal normal faults within the host succession (Cartwright & Dewhurst., 1998; Cartwright., 2011). Several models have been put forward for the formation of polygonal faults such as gravitational sliding leading to internal layer-parallel extension (Higgs & McClay, 1993), hydraulic fracturing due to differential compaction and over-pressure build-up (Cartwright, 1994a), density inversion by differential compaction between the host strata and the overlying strata (Henriet et al., 1988; Watterson et al., 2000), spontaneous contraction of a sediment-water gel by syneresis (Dewhurst et al., 1999), low coefficients of residual friction that are too low to sustain in situ stresses along the fault plane due *to 'gravitational loading'* (Goulty, 2001; 2008) and particle dissolution during diagenesis which induces tensile stresses of sufficient magnitude for normal faulting termed *'diagenetically-induced shear failure'* (Shin et al., 2008; Cartwright., 2011). The lack of consensus portrays our poor understanding of polygonal fault networks in terms of their nucleation, growth & propagation, and the reason for their varied spatial and temporal distribution in numerous sedimentary basins of the world. Recently, the leading method in the understanding of the nucleation, growth and propagation of polygonal fault systems are the diagenetically induced shear failure nucleation hypothesis and the gravitational loading growth hypothesis. Diagenetic reactions have been studied widely for different hydrocarbon basins of the world, these diagenetic reactions, often associated with compaction and deformations in siliceous fine-grained sediments occur during early burial and affect the microstructural properties of the sediments. These diagenetic changes involve a two-step process (i) the transformation of biogenic silica (opal A) to cristobalite and tridymite (opal CT) and (ii) the transformation

of opal CT to quartz. Although both stages of the biogenic silica transformation affect the physical properties of the host rock, the first stage change involving the change of biogenic silica to crystalline cristobalite and tridymite have been associated with a loss in porosity and an increase in density and p-wave velocity (Isaacs 1981; Compton 1991; Guerin & Goldberg, 1996; Meadows & Davies, 2009; Thyberg & Jahren 2011). Silica diagenesis therefore plays a crucial role in reducing porosity and is often found to influence the style of deformation and fluid flow in sedimentary basins. As indicated earlier, several theories on the origin of polygonal faults have been proposed and recently the model most favoured is a diagenetically induced shear failure leading to the development of polygonal fault systems (Cartwright., 2011 and references therein). It is posited that the initiation of polygonal fault systems is linked to their host lithology where in clay-rich sediments, diagenesis can lead to shear fractures and normal faults under low confining stresses (Shin et al., 2008; Cartwright 2011, Wrona et al., 2017). Davies & Ireland (2011) before now linked the nucleation of polygonal fault systems to differential compaction associated with the transformation of Opal-A/CT. A much-debated question to date is the genesis of polygonal faults Cartwright (2011) and recently, there has been growing recognition of the vital links between diagenetic reactions and the growth of normal faults with a polygonal planform. This research aims to analyse the role diagenesis plays in the nucleation of such normal faults by means of a topological analysis of the polygonal system hosted within the Cenozoic mudstones in the eastern Central North Sea (Figure 3.1) to investigate the growth and propagation of such faults.

We employ a high-resolution 3D seismic data cropped from the PGS MegaSurvey™ to map out the thinning of a wedge-tier polygonally faulted unit using conventional seismic interpretation approaches to establish to what extent lithology and diagenesis affects the growth and propagation of the polygonal fault system within the study area. Polygonal faults often deform the fine-grained sedimentary successions hosting them which are otherwise low permeability and sealing sequences for most sedimentary basins which makes them important to the study of subsurface fluid flow in basin analysis (cartwright and Huuse., 2007; Jackson et al., 2014), carbon dioxide (CO_2) storage in the subsurface (Arts et al., 2004) and nuclear waste disposal sites (Dechandschutter et al., 2005a). Due to the potential of polygonal fault systems to decrease or increase the sealing capacity of

such fine-grained sedimentary successions hosting them, it is critical to understand their mode of nucleation and propagation.

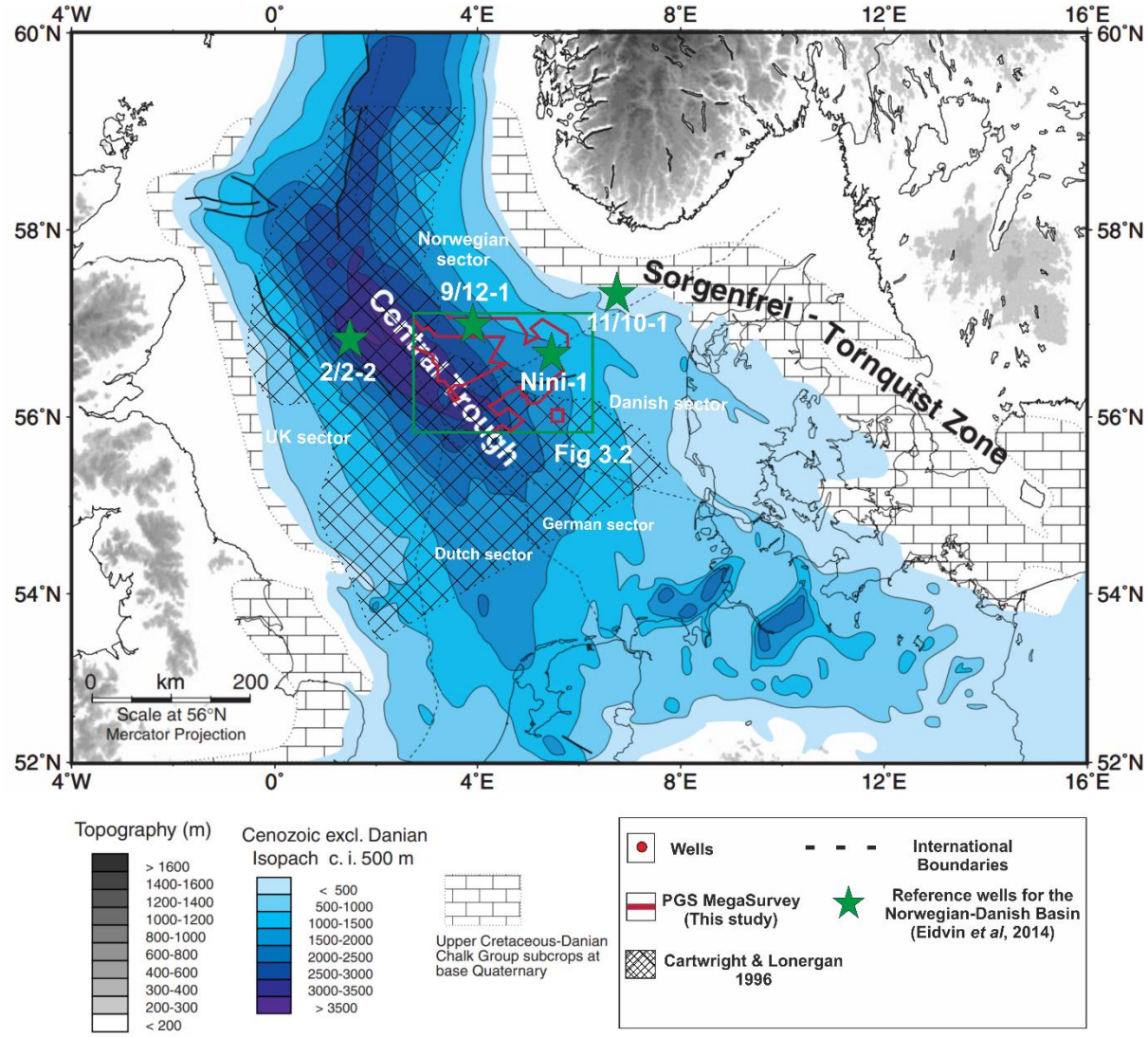

Figure 3.1: Location of study area in the eastern Central North Sea and some of the main structural elements including the sediment thickness of the Cenozoic sediments excluding the Danian with the coverage of the PGS MegaSurvey™ 3D Data used in this study. Also Indicated is the extent of Polygonal Faulting in part of the study area from Cartwright & Lonergan (1996).

3.2 Polygonal Faults and Silica Diagenesis

The formation of polygonal faults, although widely debated (Cartwright 2011 and references therein), have been linked to compaction in fine grained low permeability sediments with several controlling factors across sedimentary basins of the world. The mechanism of compaction results in a complex network of fault patterns interpreted to be polygonal normal faults (Cartwright, 1994; Lonergan et al., 1998). Polygonal faults,

along with silica diagenetic reaction front have been one of the enigmatic geological features identified and characterised since the advent of high-resolution 3D seismic data in the past century (Cartwright & Huuse., 2005). However, analysis for polygonal faults have recently shifted from characterisation and qualitative descriptions to quantified structural analysis of polygonal faults network (e.g. Morley & Nixon., 2016; Wrona et al., 2017). Factors controlling the initiation and propagation of polygonal normal faults in different geological settings are widely debated (Cartwright et al., 2003; Cartwright., 2011). Of the several factors, temperature is widely not considered in the development of normal faults, but for polygonal normal faults thought to form due to compaction of fine-grained sediments, temperature plays a vital role (Davies & Ireland., 2011). Temperature has been observed to be dominant in impacting the rate of diagenetic reactions along with time and composition of the host sediments and the chemistry of the pore fluid (Kastner et al., 1977). Silica diagenetic processes, primarily involving the transformation of amorphous biogenic silica (Opal-A) to ordered crystalline silica of Cristobalite/Tridymite (Opal-CT) is often impacted by an increase in temperature and a change in lithology (Williams et. al., 1985; Isaacs., 1981; Hesse., 1990). The transformation from Opal-A to Opal-CT usually occurs at temperatures between 25 °C to 55 °C corresponding to depths of 0.5 to 1.0 km in most sedimentary basins of the world (Hein et al., 1978; Behl., 2011). The conversion of Opal-A to Opal-CT is often associated with a reduction in porosity due to framework collapse of the biogenic silica and an increase in p-wave velocity and density which often impacts the acoustic impedance of seismic data giving rise to a distinct seismic character often referred to as the silica diagenetic reaction front (Hein et al., 1978; Davies & Cartwright., 2002; Cartwright., 2007; Ireland et al., 2011; Wrona et al., 2017). A link between silica diagenesis and the development of polygonal normal fault systems is still a subject of debate and have been documented for several sedimentary basins of the world (Cartwright., 1996; Hansen et al., 2005; Shin et al., 2008; Davies et al., 2008; 2009; Davies & Ireland., 2011; Cartwright 2011; Morley et al., 2017). Studies have shown that the development of normal polygonal fault arrays could form above or below Opal-A to Opal-CT reaction fronts, termed as the reaction zone by Ireland et al., (2011) by means of regular wavelength topological form which caused the differential subsidence of the overburden and leads to a systematic and irregular topology of the reaction front within the polygonally faulted interval (Ireland et al., 2011). The evolution of polygonal faults has been

linked to silica diagenesis in biosiliceous sediments due to the nature of the opal-A/CT reaction boundary necessary for the development of differential subsidence and growth of polygonal faults (Davies et al., 2009; Davies & Ireland., 2011). This study investigates the link between the initiation and propagation of polygonal fault systems and silica diagenesis by means of 3D seismic data analysis and topological analysis of the polygonal fault system within the Lark formation in the Central North Sea. Studying the geometry and kinematics of polygonal fault systems is important in investigating their evolution and the role that for example, lithology variations and factors such as depositional and stratigraphic setting, gravitational instability, post faulting compaction plays (Duffy et al., 2015).

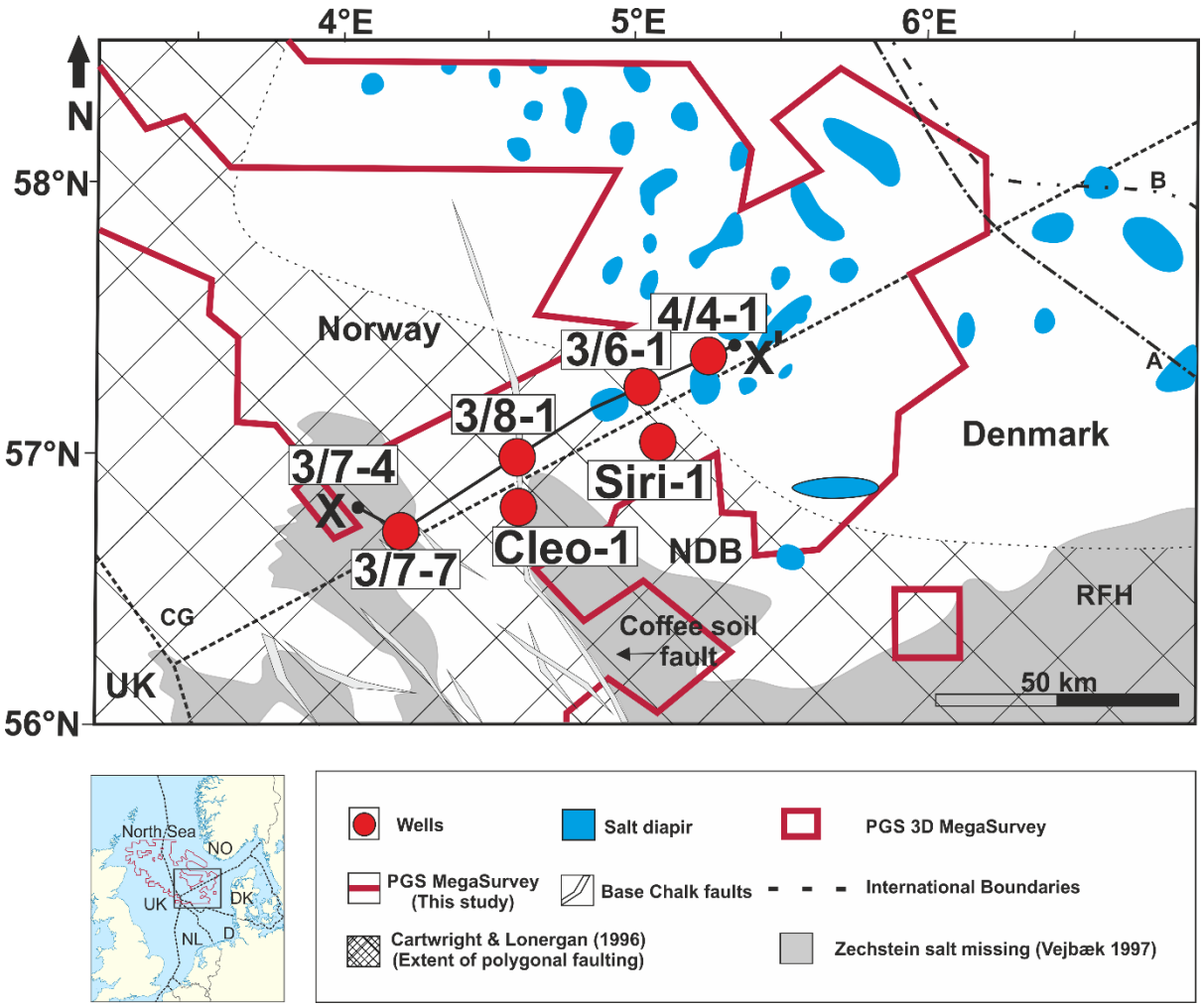

Figure 3.2: A zoom-in to the study area highlighting the positions of the wells 3/7-4, 3/7-7, 3/8-1, 3/6-1, and 4/4-1 employed for this study along with the local structural elements including the Coffee Soil Fault, The Ringkobing-Fyn High (RFH), the extent of the Permian Zechstein salt diapirism and mapped salt diapirs.

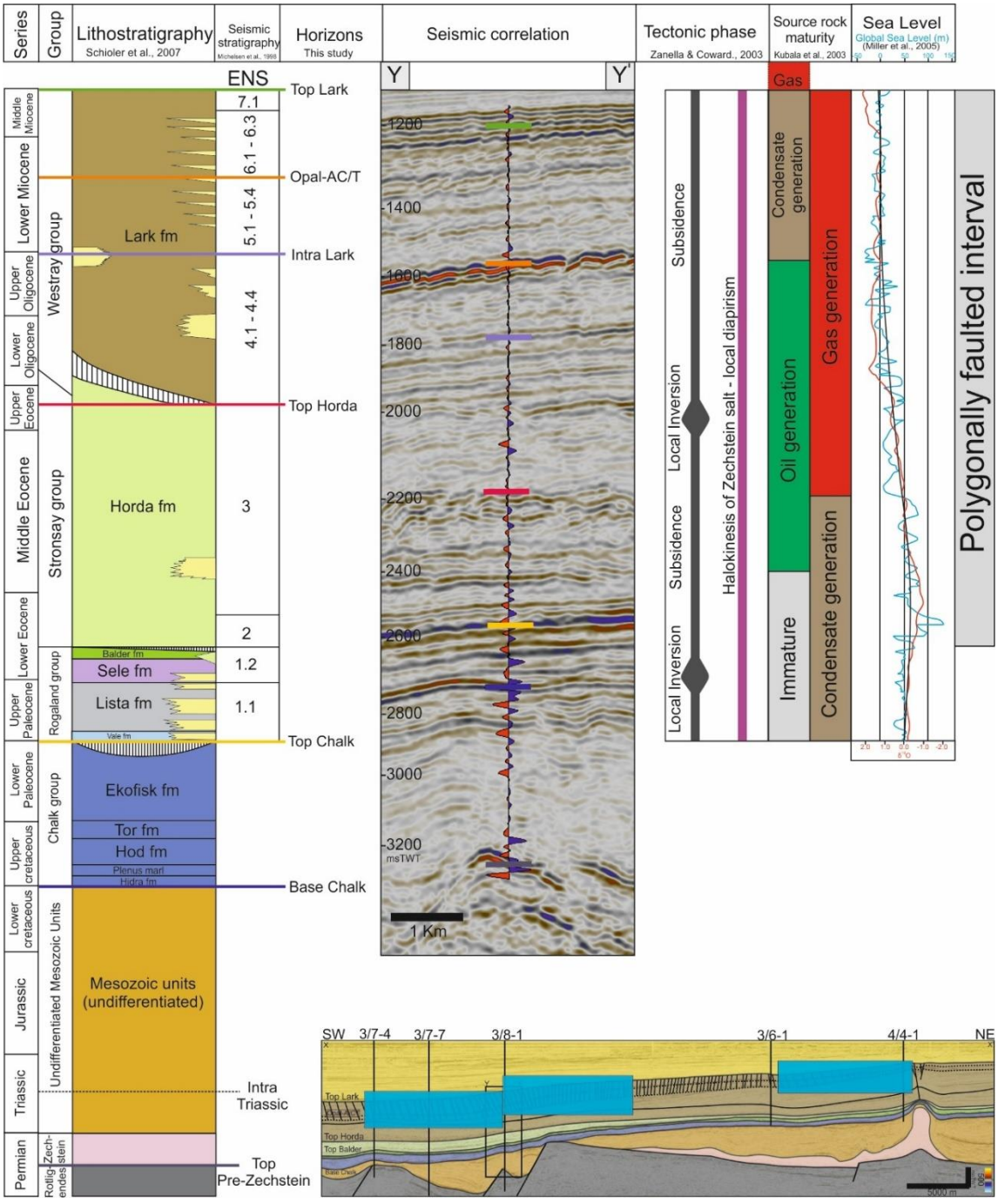

Figure 3.3: Stratigraphic position of horizons mapped and used in this study according to the lithostratigraphic subdivision of Schiøler et al., (2007) and seismic stratigraphy of Michelsen et al., (1998) by the aid of a seismic to well tie using well 3/8-1 (Inset: an interpreted seismic cross-section highlighting the position of the well 3/8-1, the key stratigraphic surfaces and other adjacent wells used in this study). (Note frequent thin sand stringers within the Westray Group Lark formation). Also shown are the local subsidence and inversion tectonics highlighting the tectonic evolution of the study area since the Cenozoic after Zanella & Coward., (2003), source rock maturation after Kubala et al., (2003) and the global sea level and δ^{18}O curves from Miller et al., (2005). In blue is the three segments and sub-volumes A, B and C cropped from the PGS 3D MegaSurvey for further topological analysis of the polygonal faults within the study area.

3.3 Geological Setting

The Central North Sea evolved due to a series of rifting episodes and has since been affected by a series of basin inversion, subsidence, uplift, and erosion during the Cenozoic (Ziegler, 1992; Huuse et al., 2001). Sediments supplied to the Cenozoic North Sea basin were influenced by tectonic movements of older structural elements and are sourced mainly from the east (Jordt et al., 1995; Michelsen et al., 1998; Ahmadi et al., 2003; Hamberg et al., 2005). The Cenozoic of the CNS preserves a complete record of Cenozoic sedimentation within depocenters characterised by prograding and delta slope systems and often affected by deep seated regional faults and salt diapirism (Jordt et al. 1995) (Figure 3.2). The Cenozoic succession in the CNS has been studied extensively by Jordt et al., (1995) and Michelsen et al., (1998) and subdivided into units based on seismic sequence stratigraphic principles. Large prograding deltas are believed to have covered the entire CNS during the Oligo-Miocene and later times, with sediment influx from the Baltic River system and its environs (Overeem et al., 2001), and partly controlled by subsidence and climatic conditions that created accommodation space for sediments during glacial and interglacial cycles at later times (Kuhlmann & Wong., 2008). The discovery of hydrocarbons in the Palaeocene - Eocene of the Norwegian-Danish basin outside the hydrocarbon-prone Central Graben demonstrates the importance of cross-stratal and lateral fluid migration from deeper and shallower source rocks of thermogenic and biogenetic fluids, coupled with pore fluid expelled by sediment compaction within the Central North Sea (Hamberg et al., 2005; Ohm et al., 2006) (Figure 3.2). The polygonal fault system investigated in this study is found within the Oligo-Miocene Lark formation in most parts of the eastern CNS and within the Horda formation in deeper parts of the basin towards the Central Graben. They are seen to terminate at the mid-Miocene Unconformity (MMU) surface, a prominent basin-wide seismic marker and sequence stratigraphic boundary defined by Michelsen et al., (1998). Immediately below the MMU surface is a dense network of polygonal fault system and an Opal-A/CT reaction boundary within the study area (Clausen & Korstgård., 1993; Cartwright., 1994; Malah et al., this study, Chapter 2). An extensive network of distributed Oligocene and Miocene pockmarks are also found below the MMU within the succession hosting the polygonal fault network in the study area (Andresen et al., 2008).

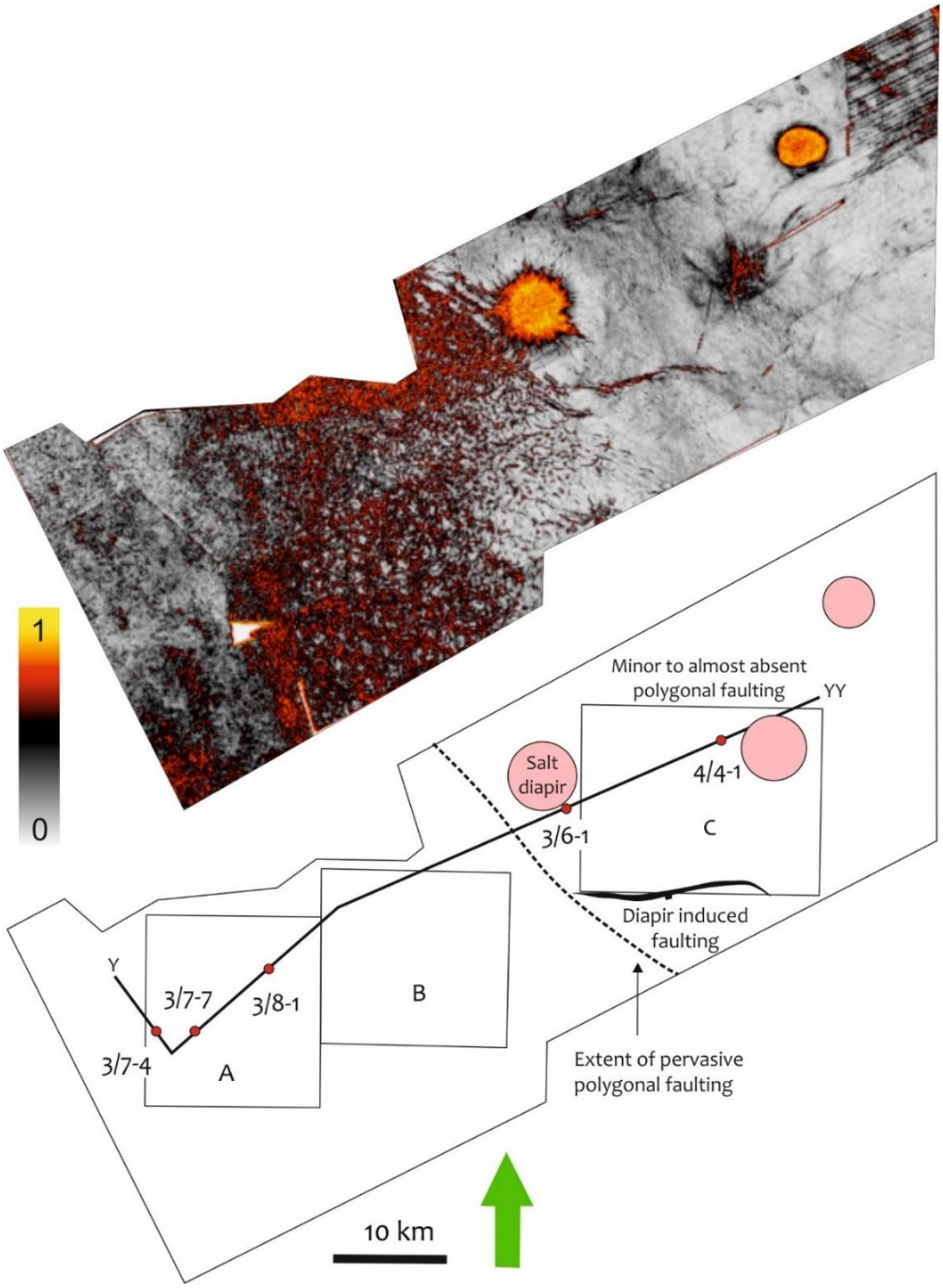

Figure 3.4: A variance surface attribute of the mapped Opal-A/CT reaction front in the study area (a) and the intricate relationship between salt diapirism and the polygonal faulting in the area is highlighted. In (b), we see an outline of the same surface with the three segments and sub-volumes cropped for further topological analysis of the polygonal faults within the study area with the extent of pervasive polygonal faulting clearly demarcated. See (Figure 3.1) for location. The image shows the development of the polygonal fault system at the Opal-A/CT boundary with the southwestern area having high variance values indicating significant seismic discontinuities excluding the areas with the salt diapirs piercing the surface at the interval. To the NE, the low variance values excluding the salt diapir areas indicate the almost missing polygonal faulting barring the skewed variance values induced by the salt diapirs.

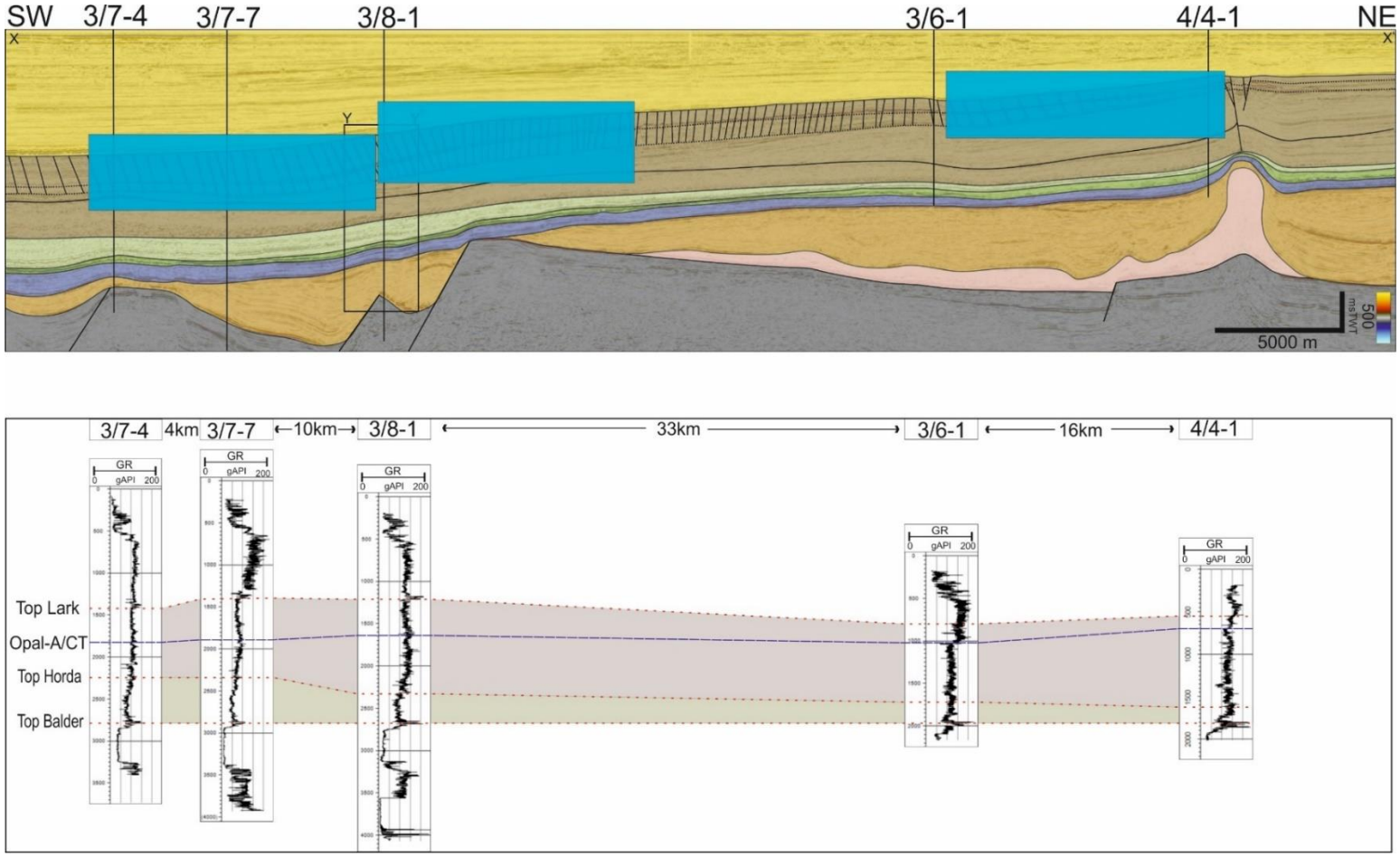

Figure 3.5: Top: Interpreted seismic cross-section with positions of the wells used in this study and the major stratal surfaces mapped and the outline of the Polygonal Fault System (PFS) within the Lark formation in an approximately SW – NE direction divided into three segments A, B & C (See figure 1 for the location of cross-section within the study area), Note the position of the opal-A/CT boundary and the prevalence of polygonal faults within the interval that progressively decreases in off-set towards the NE of the study area. Bottom: A simplified well log correlation panel across the wells 3/7-4, 3/7-7, 3/8-1, 3/6-1, and 4/4-1 displayed along the seismic cross section at the top covering an approximate 65 km from the Central Graben.

3.4 Data and Methods

Data for this study is a cropped volume of the PGS 3D MegaSurvey™ which covers an area of ~3,000 km^2 in the eastern Central North Sea (Figure 3.3). The 3D survey has a sub-sampled bin spacing of 50 m by 50 m, a sampling rate of 4 msTWT with a maximum vertical resolution ($\lambda/4$) of c. 12 – 15 m and a horizontal resolution ($\lambda/2$) of 20 – 30 m according to a dominant frequency of 50 – 70Hz. The CNS MegaSurvey™ is a normal polarity (zero phase) data where a hard kick i.e., a positive reflection (peak) is represented by red and a soft kick i.e., a negative reflection is represented by a negative reflection (trough). The Cenozoic has an average interval velocity of 2km/s (+/- 10%), thus allowing for the vertical measurements made in milliseconds two-way time (ms TWT) to be directly converted to depth in meters (m) as a first order approximation for the interval of interest for the North Sea (Japsen, 1999; Huuse et al., 2001).The data is sufficient for resolving the polygonal fault system (PFS) within the study area; however, the 3D seismic data is of variable data quality and polarity due to the post-stack merging of variable seismic cubes to achieve the extensive MegaSurvey™ data by PGS. In places, a phase rotation is applied to improve the match between different versions of seismic data, including adjacent surveys that were merged. A phase rotation of 180° produces a reverse polarity version of the input trace while a +90° or -90° rotation alters the seismic trace in such a way that a peak or trough on the input trace becomes a zero crossing on the output trace and vice versa. The phase rotation allows for an improved seismic-to-well tie and comparison of seismic data with well logs in other parts of the study area. Lithological and chronostratigraphic calibration for this study is provided by industry boreholes 3/7-4, 3/7-7, 3/8-1, 3/6-1, and 4/4-1 available from the Norwegian Petroleum Directorate (NPD) (Figure 4;5).

Key horizons were tied to the exploration well 3/8-1 also used to describe the lithology and other physical parameters within the Cenozoic section of interest (Figure 3.5). The horizons identified were employed to map a series of time structure surfaces from different stratigraphic reflections along with other geometrical properties and seismic attributes (Chopra & Marfurt, 2007; Bacon et al., 2007). The area of interest was divided into three segments/sub-volumes (Figure 3.4); A (306 Km^2), B (306 Km^2) and C (360 Km^2) to aid the detailed investigation of the topology of the polygonal faults. A further isoproportional slicing of the segments allowed for the mapping of different layers

(horizons, surfaces) within each segment. To analyse and quantify the fault orientation, ant-tracking fault extraction workflow was employed on the sub-volumes to resolve fully the extent of their polygonal form geometry and generate fault population statistics such as throw, dip, length, and azimuth. Ant Tracking™ seismic attribute is a fault enhancing and fault extraction attribute which helps delineate laterally continuous discontinuities based on a conditioned input while Variance Edge Method™ is a signal coherency analysis tool which aids with fault detection from a continuous variance response in seismic data related to stratigraphic terminations of structural lineaments in Petrel™. Detailed interpretations of the horizons, sub-volumes of the segments A, B, & C and the associated attribute maps allowed for resolving the nature and geometries of the polygonal faults to be mapped out in detail. We interpret the faults automatically using the Petrel™ automatic fault extraction workflow and subsequently extract fault properties such as strike, dip, and dip direction. The trend for this acquired values are subsequently imported via a spreadsheet into the Georose software application and plotted for visualization.

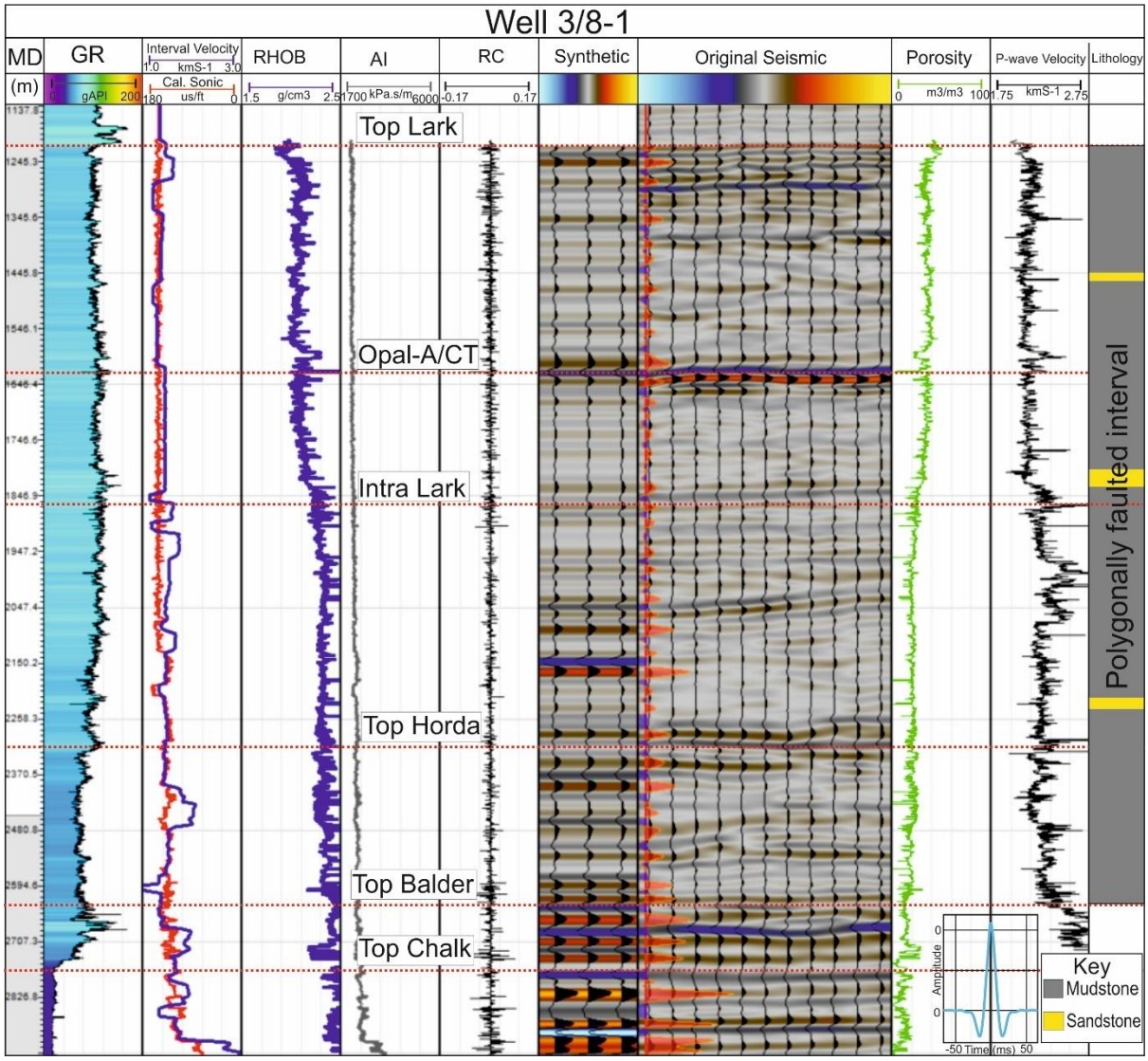

Figure 3.6: Seismic well correlation showing synthetic seismogram generated from well 3/8-1 and tied to the PGS 3D MegaSurvey™ Data. Also shown from left to right are the gamma ray log over the investigated section to the Top Chalk surface, the interval velocity, and the averaged sonic log over the interval as well as the density log over the interval. The acoustic impedance (AI) generated, and the wavelet (inset) convolved with the reflectivity coefficient (RC) to create the synthetic seismogram which aided with the seismic to well-tie at the well location. This was also used to model the synthetic response of the Opal-A/CT boundary. An estimated porosity log (green) was generated from the Neutron log and a p-wave Velocity from the sonic log over the interval. A lithological interpretation of the log is shown in the last panel.

3.5 Results

Three main horizons mapped within the study area to constrain the polygonal fault systems are the (i) Top Lark surface corresponding to the 'mid-Miocene unconformity surface,' the (ii) Opal-ACT reaction boundary 'reaction front,' and the (iii) Base Lark (Intra Lark) corresponding to the lower tips of the visible part of the polygonal faults within the study area. The surfaces were mapped to aid in the full resolution of the wedge tier polygonal fault system within the Lark formation. The seismic data is of variable quality and in places it allows for the full resolution of the seismic packages hosting the polygonal faults. All the surfaces mapped have good to moderate lateral continuity as all three can be easily traced across the study area and represent the top of the wedge tier or the base.

3.5.1 The seismic unit hosting the polygonal faults

Polygonal fault systems are known to be influenced by both lateral and vertical changes in facies, most notably the transition from fine-grained to coarse-grained sediments (Jackson et. Al., 2014). The polygonal faults imaged in this study is confined within the Cenozoic section of the eastern North Sea, mainly occurring within the Top Balder to the top of the Oligo-Miocene Lark formation (corresponding to the mid-Miocene unconformity surface) (Figure 3.2; 3.5). Approximately between 800 – 1800 msTWT (c. 800 – 1800m). Other studies acknowledged the deformation of the upper Paleocene to middle Miocene succession by a dense network of polygonal faulting attributed to volumetric contraction of the pelagic and hemi-pelagic mudstones within the succession identified by the seismic character of the hosting unit (Clausen & Korstgård, 1993; Cartwright, 1996; Cartwright & Lonergan, 1996). The succession immediately above the mid-Miocene unconformity surface in general is unfaulted with an overall west to southwest-ward prograding clinoform architecture and pierced by salt diapirs in places. The polygonal faults identified in this study are considered a simple wedge tier type of polygonal fault system which thins from the west towards the east in the study area i.e. from the Central Graben towards the Horda Platform and is evident from the fault offsets. The surface defining the top of the polygonal fault system within the eastern CNS is represented by a strong negative amplitude reflection and is generally concordant and continuous within the area. Majority of the polygonal faults (>97%) do not propagate above the mid-Miocene unconformity surface, the top or upper tip of the faults, which suggests that they have been inactive since the mid-Miocene time. This makes the upper tips of the polygonal faults easily

identifiable and are characteristics of the upper tips of similar normal blind faults observed in other basins (Baudon & Cartwright., 2008; Laurent et al., 2012). The base or lower tip of the polygonal faults is difficult to identify due to the seismic character of the underlying units within the formation. For this study, a similar concordant and continuous surface tagged the 'base of the PFS' or 'Intra-Lark' is mapped to constrain the wedge tier polygonal faults (Figure 3.4) (Cartwright., 2011). Numerous small normal faults which form a polygonal geometry in plan view on the seismic data are visible throughout the defined tier (Figure 3.4) with random strike patterns and displacement profiles with dips ranging from 25 - 70°. The internal reflection of the seismic unit is limited by the quality of the seismic data which is good to moderate and allows for the visualization of the polygonal faults in planform and cross section views. The seismic unit consists of chaotic moderate to high amplitude reflections with the intensity of the polygonal faulting varying with depth and the thickness of the hosting unit. Correspondingly, the density of the faulting also varies with areas of more pervasive polygonal faulting towards the west and less pervasive towards the east (Figure 3.3). Within the faulted succession, numerous pockmarks within the Oligocene and Miocene unit have been mapped extensively by Andresen et al., (2008) and are seen to be associated with the polygonal faults. Between the top of the polygonal faults and the base, a strong positive reflection defined in this study as the Opal-ACT reaction front is also mapped. This surface is continuous and runs parallel to the mid-Miocene unconformity surface dimming out towards the east (Figure 3.4). The study area was divided into three segments A, B and C according to the seismic character of the polygonal faults in cross section and plan view. The Opal-A/CT boundary surface is crosscut and offset by numerous normal polygonal faults throughout the study area.

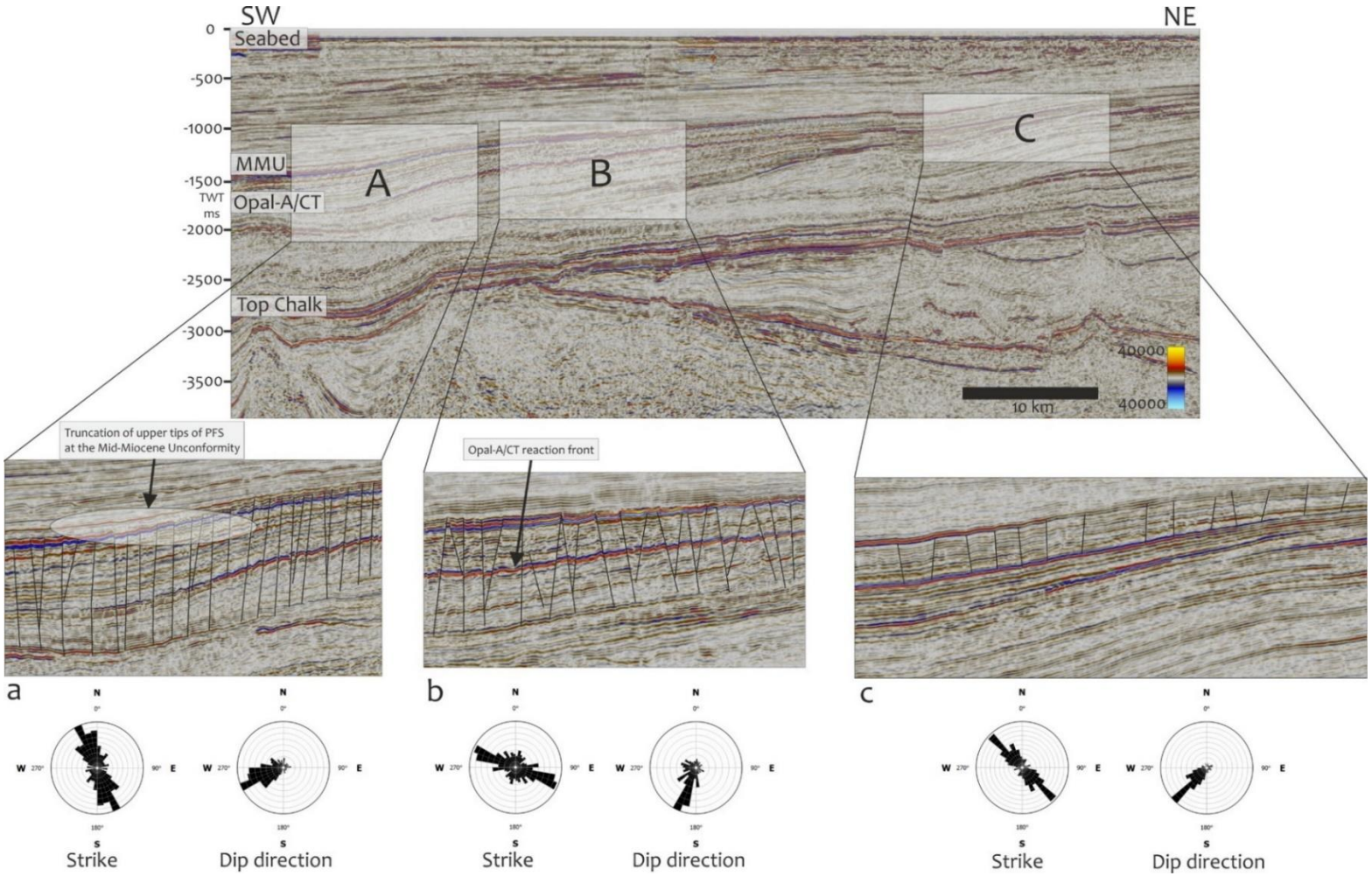

Figure 3.7: An arbitrary seismic line across the study area showing a side view of the three segments A, B and C defined in this study to characterise the polygonal fault systems. Below, is a section from each of the segment highlighting the polygonal faulting style within the unit with the faults striking mostly in a NW-SE trend and dipping towards the southeast for Segment A through to segment C, although with variable ranges of strike and dip directions.

3.5.2 Geometry and topology of the PFS around the reaction front

Sedimentary units hosting polygonal fault systems are subject to change over time as a result of diagenetic reactions, most notably of the transformation of biogenic silica (Opal-A) to crystals of cristobalite/tridymite (Opal-CT) (Davies et al., 2009; Davies and Ireland, 2011; Ireland et al., 2011; Neagu et al., 2010; Cartwright, 2011). Numerous normal faults were mapped in the 3D seismic data with strikes from NW – SE (Figure 3.6) for all the segments A, B and C. Majority of the faults terminate at the base of the surface mapped as the Base PFS in segment A and B, while in C, they mostly terminate at the Opal-A/CT boundary. In segment A & B, the PFS mapped have dip angles ranging from 15° - 29° below the Opal-A/CT boundary on seismic profile and dip ranges of 25° - 70°. On a segment-by-segment basis, when we investigate the polygonal faults in detail, we see that segment A has a denser network of faults less than 3 km long and dip in a south-westerly direction forming horst and graben like structures. The majority of the faults here do not terminate at the base of the mapped surface but are difficult to realise due to the chaotic nature of the seismic character. This can be attributed to different seismic facies relating to difference in the lithological composition of the underlying unit. The faults here show dip changes with depth based on the faults interaction with the three surfaces mapped (Top Lark, Opal-ACT surface and the Base PFS) (Figure 3.7; 3.8 and 3.9). In Segment B, the faults show a similar horst and graben feature on the surface maps to those mapped in segment A but appear more interlinked and connected with similar dip and strike to those in segment A. Towards the east, in segment C, the number of faults decreases sharply and are more widely spaced and hardly form the horst and graben feature seen in segments A & B, meaning a general decrease in the faults and fault throw. The faults mapped in segment C mostly originate at the Opal-ACT boundary and propagate upwards towards the Top Lark surface.

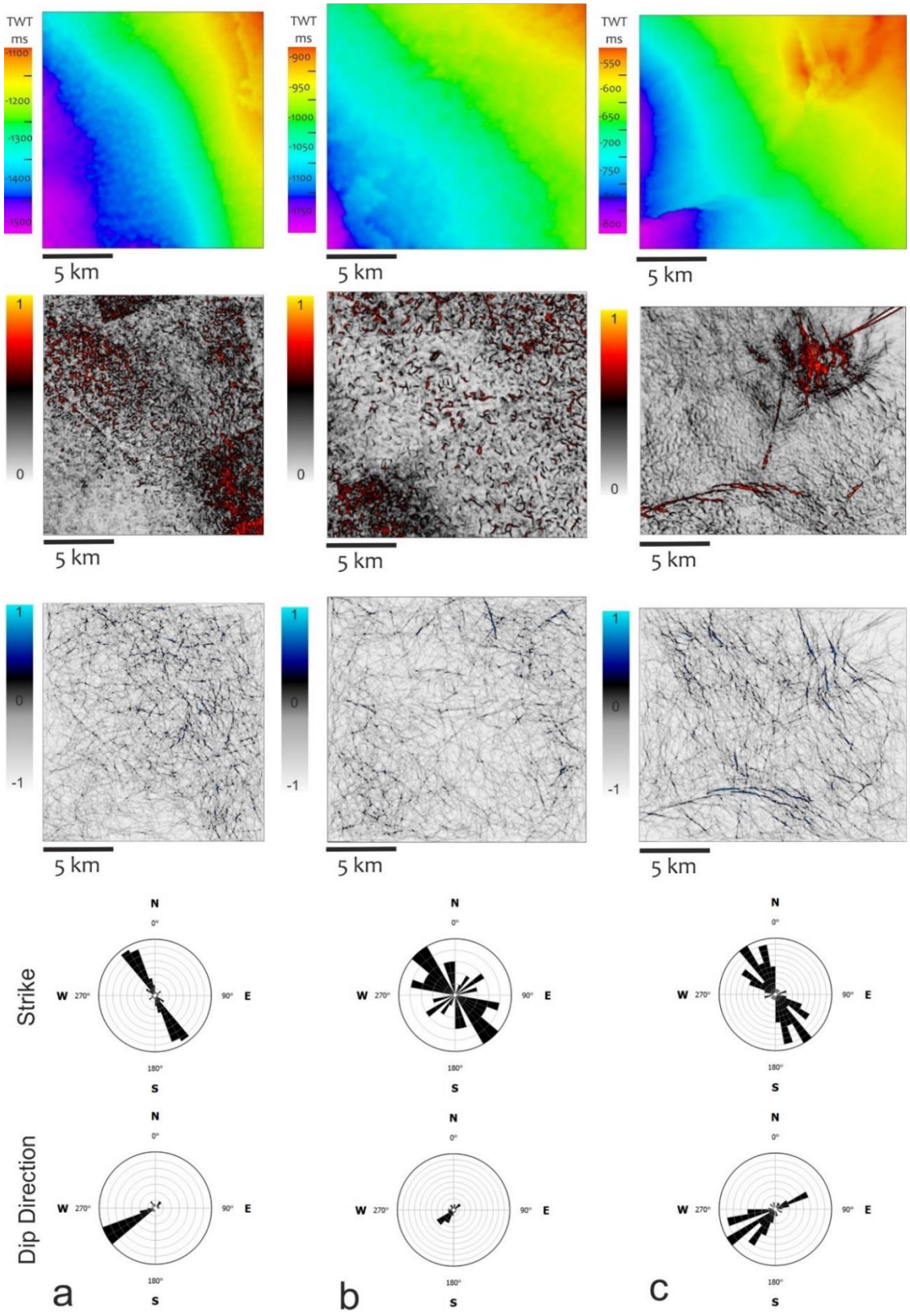

Figure 3.8: Time structure (TWT) and seismic amplitude maps (variance attribute and ant track surface maps) of the mid-Miocene unconformity surface across the three segments A, B and C highlighting the polygonal faults within the study area. Most of the faults terminate at the mid-Miocene unconformity surface with only a few exceptions. Generally, all segments A, B and C record only a few of the polygonal faults penetrating this surface.

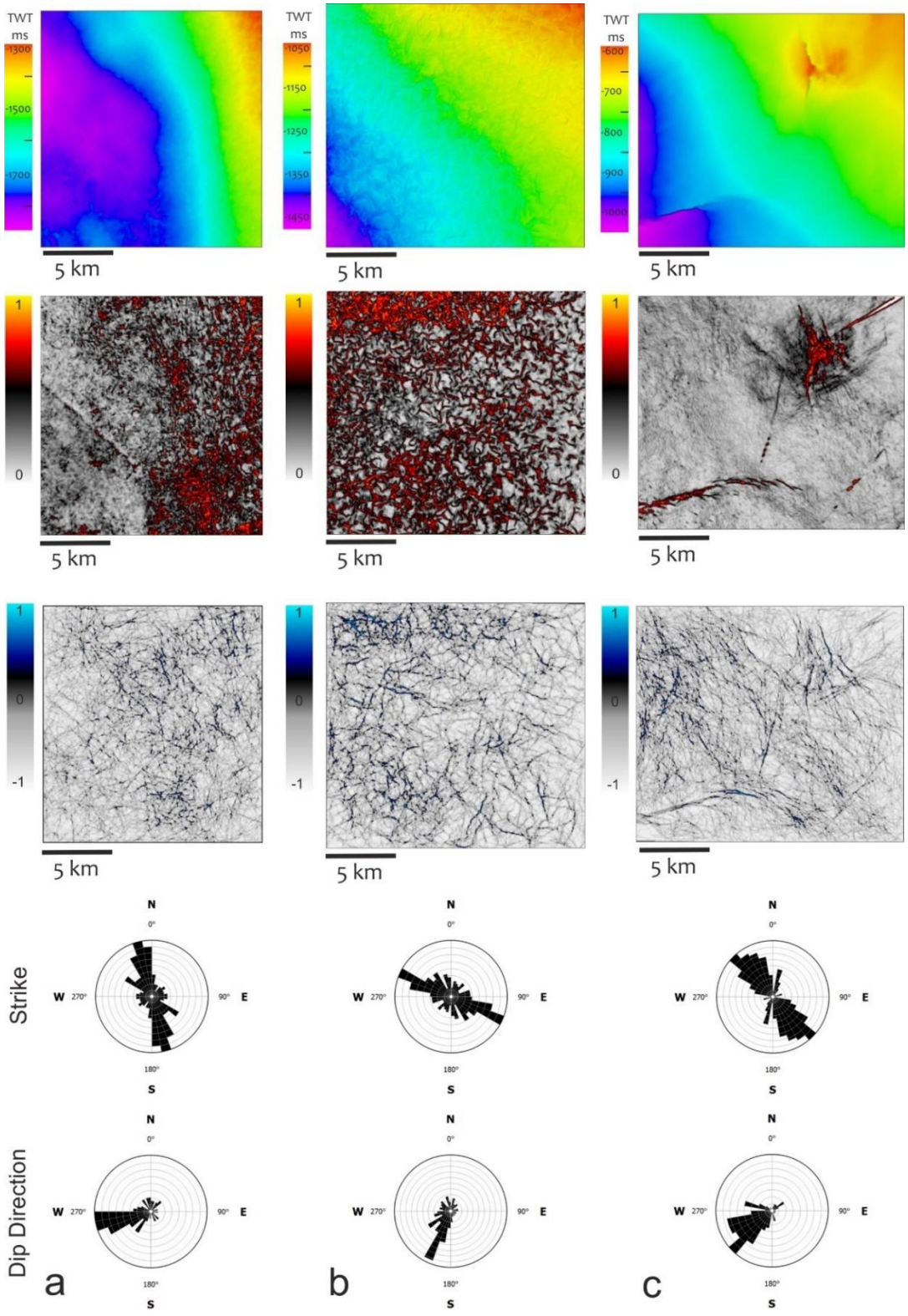

Figure 3.9: Time structure (TWT) and seismic amplitude maps (variance attribute and ant track surface maps) of the Opal-A/CT surface across the three segments A, B and C highlighting the polygonal faults within the study area. All the PFS mapped in this study cross-cut this surface. Segment A & B has a denser polygonal fault networks than segment C. Here, we see varied strike and dip directions, highlighting the complexity of the internal structure of the polygonal fault system across the Opal-A/CT surface.

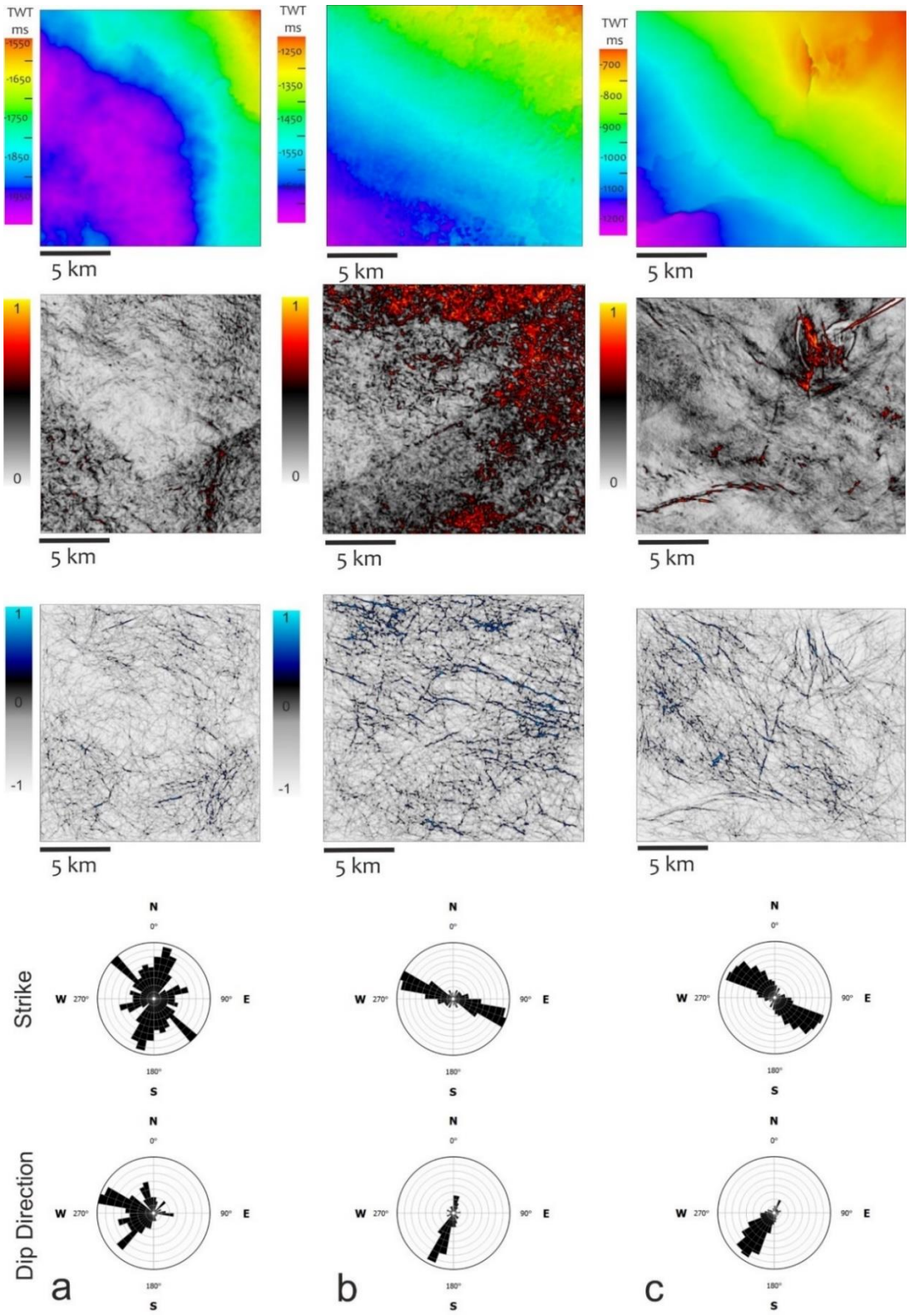

Figure 3.10: Time structure (TWT) and seismic amplitude maps (variance attribute and ant track surface maps) of the base of the PFS across the three segments A, B and C highlighting the polygonal faults likely terminations within the study area. Majority of the PFS mapped in this study terminate on this surface but some cut through into the underlying units. Here, we also see varied strike and dip directions, highlighting the complexity of the internal structure of the polygonal fault system across the Opal-A/CT surface.

3.6 Discussion

3.6.1 Polygonal Fault Systems and the Opal-A/CT reaction boundary

Since the discovery of polygonal fault systems on seismic data almost three decades ago, our knowledge of their formation and evolution have significantly progressed with several models of formation (nucleation) and propagation being presented. Recently, the most favoured is the 'diagenetically induced shear failure' model related to silica diagenesis within biosiliceous sediments in sedimentary basins.

3.6.2 Multi Attribute Fracture Analysis

The polygonal faults in this study are analysed via a multi attribute fracture analysis workflow using the Schlumberger Petrel Ant track workflow. The ant track workflow involves conditioning seismic data to achieve enhanced fault visibility and the extraction of fault patches and sticks and subsequently, fault statistics such as dip and azimuth which was subsequently used to estimate strike directions. The Ant Track fault interpretation technique is used to interpret regional and minor faults to a high degree of confidence using seismic data (Pedersen et al., 2002; Zhang et al., 2017). We employed the process multistep ant track workflow for the extraction of the fault patches and statistics to produce maps for the different sections A, B & C analysed and presented above. The Ant Tracking™ workflow is a fault enhancing and fault extraction attribute which helps delineate laterally continuous discontinuities based on a conditioned input while Variance Edge Method™ is a signal coherency analysis tool which aids with fault detection from a continuous variance response in seismic data related to stratigraphic terminations of structural lineaments in Petrel™. The workflow involved entails four main steps, (i) seismic data conditioning, (ii) fault detection and enhancement with conventional attributes such as variance and chaos, (iii) automated fault extraction and (iv) fault data analysis. This workflow allows for an efficient and automatic interpretation of the polygonal fault systems within the Cenozoic Succession in the three segments A, B and C. From the analysis in Figures 3.7. 3.8 and 3.8 for the three segments in this study, we see a slight difference influenced by the structural domains of the area with the Opal-A/CT boundary having the highest fault density as 90% the PFS pass through this surface. The Ant Track workflow enhances accurate and detailed mapping of the fault geometries across the seismic sections although it is difficult to distinguish between low-angle faults and other features with low angles such as amplitude anomalies and dipping beds.

3.6.3 Polygonal Fault Systems Growth and Kinematics

Polygonal faults thought to be initiated as a result of silica diagenesis are believed to occur in the initial stages of burial, although the timing of fault initiation is uncertain in several studies (Cartwright, 1994; Lonergan et al., 1998; Berndt et al., 2003; Gay et al., 2004; Morgan et al., 2015). Despite the uncertainty in the timing of the initiation of the polygonal faults, results from such studies agree that following a nucleation phase, polygonal fault systems often grow at the upper tip by upward propagation (Gay and Berndt, 2007; Davies and Ireland, 2011; Morgan et al., 2015). The downward propagation of polygonal fault systems is often limited by either a change in mechanical properties associated with a lithological transition or through a detachment of the lower tip into a mobile basal substrate (Cartwright et al., 2003; Cartwright, 2011). Due to the nature of polygonal faults, several driving mechanisms have been proposed for their growth and propagation in the theoretical sense without spatial and temporal constraints in their kinematics (Shin et al., 2010; Roberts et al., 2014; Roberts, 2014). Due to the constraints of the formation and propagation of polygonal fault systems, direct throw rates measurements are limited and only throw profiles are recorded across different basins of the world (Nicol et al., 2003; Stuevold et al., 2003; Neagu et al., 2010; Nixon., 2013; Wrona et al., 2017). All the models put forward for the formation of polygonal faults including gravitational sliding leading to internal layer-parallel extension by Higgs & McClay, (1993), hydraulic fracturing due to differential compaction and over-pressure build-up by Cartwright, (1994a), density inversion by differential compaction between the host strata and the overlying strata by Henriet et al., (1988) and Watterson et al., (2000), spontaneous contraction of a sediment-water gel by syneresis by Dewhurst et al., (1999), and low coefficients of residual friction that are too low to sustain in situ stresses along the fault plane due *to 'gravitational loading'* by Goulty, (2001; 2008) do not consider a genetic mechanism for the formation of polygonal faults, but the particle dissolution during diagenesis model which induces tensile stresses of sufficient magnitude for normal faulting termed *'diagenetically-induced shear failure'* by Shin et al., (2008) and Cartwright., (2011) do take into account the formation of polygonal faults to the intrinsic nature of their host rock lithology.

3.6.4 A theoretical model for the evolution of PFS in the eastern CNS

The upper tip of the PFS in the eastern CNS all terminate at the mid-Miocene unconformity surface with only a few breaching the mid-Miocene unconformity surface, indicating that

most of the polygonal faults ceased to be active since the late Miocene and as such are said to be fossilized. Although, the growth rate for the PFS in this study is not constraint due to a limitation of the data, we infer that the PFS were active, growing at the upper tip towards the paleo-seabed propagating dominantly upward while sedimentation continued. We based these assumptions in constraining the polygonal fault activity mainly with the nature of the evolution of the silica diagenetic boundary identified in the study area. These interpretation is consistent with that of Davies et al., (2009) and Neagu et al., (2010). We present a model (Figure 3.10) for the evolution of the PFS in the eastern CNS which can be used in interpreting similar PFS in other sedimentary basins of the world. Polygonal faults are thought to nucleate in the lower portions of their respective tiers early in their burial history and subsequently grow and propagate upwards throughout their growth history (Cartwright et al., 2003; Morgan et al., 2015). The polygonal faults in these study area appear with less pronounced changes in vertical throw compared to other similar systems in different basins and are thought to form a simple wedge-tier within the Cenozoic succession of the eastern CNS (Neagu et al., 2010; Ireland et al., 2011; Cartwright., 2011; Wrona et al., 2017). The implication of a diagenetically induced shear failure model for the mudstones of the Cenozoic section of the eastern CNS is far reaching especially in carbon dioxide storage and shale gas exploitation usually requiring an extensive understanding of natural fractures in fine grained sediments. This is because, as mentioned earlier, polygonal faults are important due to their enormous lateral extent and wherever they occur, they have the potential to enhance or occlude permeability (Cartwright., 2011). The polygonal faults in this study are found within an otherwise known 'good seal' for the petroleum system of the Central North Sea, however, polygonal faults tend to operate differently under different conditions such as that during their formation and growth which is why our model is important. In a studies conducted by Cartwright., (2019), they found that polygonal faults that formed in seals within the sedimentary strata functioned as fluid pathways during leakage events which occurred under different stress and pressure conditions than those prevailing during the growth and propagation of the polygonal fault systems. However, when these polygonal faults are under normal pressure conditions, they are mostly sealing along the fault planes.

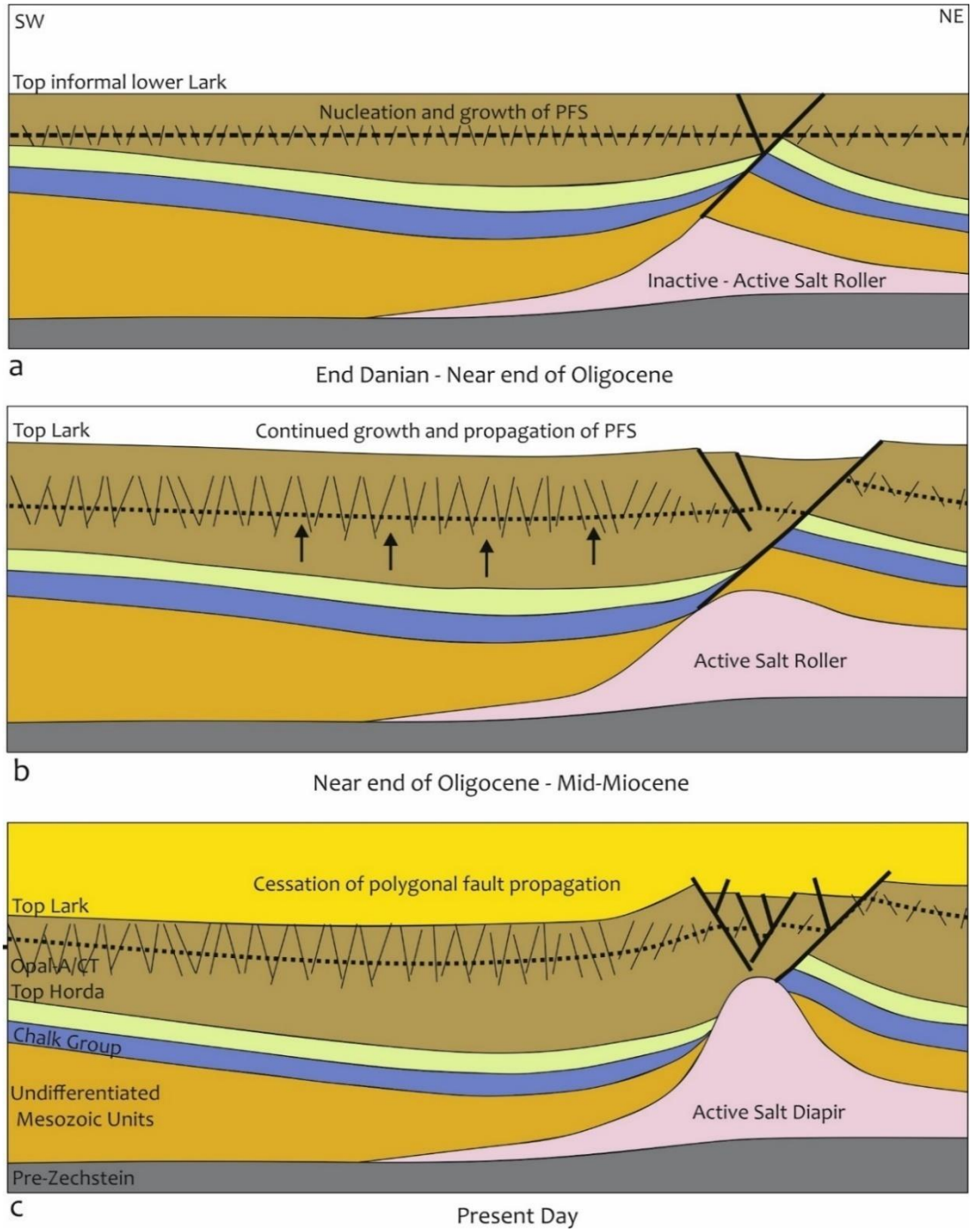

Figure 3.11: A model depicting the growth and propagation of the polygonal fault system approximately timed to be contemporaneous with the formation of the Opal-A/CT reaction front. (a) The polygonal faults are thought to nucleate at the approximate intersect of the formation of the Opal-A/CT front due to a diagenetically induced shear failure. (b) continued growth and propagation of the polygonal fault systems, mostly in the upward direction due to gravitational loading. (c) cessation of the polygonal fault propagation, except in a few cases where some faults are active breaching the mid-Miocene unconformity surface. This phase is thought to also be contemporaneous with the fossilization of the Opal-A/CT front in the eastern CNS.

3.7 Conclusion

This study presents a link between silica diagenesis and the growth and propagation of the polygonal fault systems within the eastern Central North Sea. Through a spatial, temporal, and kinematic study of the polygonal fault system, we propose that the polygonal fault systems nucleated contemporaneously with the formation of the Opal-A/CT reaction front due to a diagenetically induced shear failure within the Oligo-Miocene Lark formation and generally propagated upward through its growth history primarily due to gravitational loading. Changes in the dip across the profiles from the lower tip of the polygonal faults, the base of the polygonal faults, through the Opal-A/CT boundary to the upper tip at the mid-Miocene unconformity surface, coupled with observable changes in the throw profiles of the polygonal faults can be attributed to the chemical and mechanical changes which affected the biosiliceous Lark formation due to silica diagenesis.

3.8 Acknowledgement

This work is part of MM's PhD research, funded by the Petroleum Technology Development Fund (PTDF) Scholarship of Nigeria (Research Grant: PTDF/ED/OSS/PHD/MMG/889/16). We are incredibly grateful to PGS for generously donating seismic datasets and Schlumberger for donating Petrel licenses and TGS for granting access to the Facies Map Browser to the University of Manchester for well data.

3.9 References

Ahmadi, Z. M., Sawyers, M., Kenyon-Roberts, S., Stanworth, C. W., Kugler, K. A., Kristensen, J., & Fugelli, E. M. G. (2003). Paleocene. *The Millennium Atlas: Petroleum Geology of the Central and Northern North Sea. Geological Society, London*, 235–259.

Andresen, K. J., Huuse, M., & Clausen, O. R. (2008). Morphology and distribution of Oligocene and Miocene pockmarks in the Danish North Sea -implications for bottom current activity and fluid migration. *Basin Research*, *20*(3), 445–466. https://doi.org/10.1111/j.1365-2117.2008.00362.x

Bacon, M. (Michael), Simm, R. (Robert), & Redshaw, T. (Terence). (2007). *3-D seismic interpretation*. Cambridge University Press.

Baudon, C., & Cartwright, J. (2008). The kinematics of reactivation of normal faults using high resolution throw mapping. *Journal of Structural Geology*, *30*(8), 1072–1084. https://doi.org/10.1016/j.jsg.2008.04.008

Behl, R. J. (2011). Chert spheroids of the Monterey Formation, California (USA): Early-diagenetic structures of bedded siliceous deposits. *Sedimentology*, *58*(2), 325–351. https://doi.org/10.1111/j.1365-3091.2010.01165.x

Berndt, C., Bünz, S., & Mienert, J. (2003). Polygonal fault systems on the mid-Norwegian margin: A long-term source for fluid flow. *Geological Society Special Publication*, *216*(1), 283–290. https://doi.org/10.1144/GSL.SP.2003.216.01.18

Caroline M. Isaacs. (1981). Porosity Reduction During Diagenesis of Monterey Formation, Santa Barbara, California: ABSTRACT. *AAPG Bulletin*, *65*. https://doi.org/10.1306/2f919f0d-16ce-11d7-8645000102c1865d

Cartwright, J. A. (1994). Episodic basin-wide fluid expulsion from geopressured shale sequences in the North Sea Basin. In *Geology* (Vol. 22, Issue 5, pp. 447–450). https://doi.org/10.1130/0091-7613(1994)022<0447:EBWFEF>2.3.CO;2

Cartwright, J. A., & Dewhurst, D. N. (1998). Layer-bound compaction faults in fine-grained sediments. *Bulletin of the Geological Society of America*, *110*(10), 1242–1257. https://doi.org/10.1130/0016-7606(1998)110<1242:LBCFIF>2.3.CO;2

Cartwright, J. A., & Lonergan, L. (1996). Volumetric contraction during the compaction of mudrocks: A mechanism for the development of regional-scale polygonal fault systems. *Basin Research*, *8*(2), 183–193. https://doi.org/10.1046/j.1365-2117.1996.01536.x

Cartwright, J. (2011). Diagenetically induced shear failure of fine-grained sediments and the development of polygonal fault systems. In *Marine and Petroleum Geology* (Vol. 28, Issue 9, pp. 1593–1610). https://doi.org/10.1016/j.marpetgeo.2011.06.004

Cartwright, J. (2007). The impact of 3D seismic data on the understanding of compaction, fluid flow and diagenesis in sedimentary basins. *Journal of the Geological Society*, *164*(5), 881–893. https://doi.org/10.1144/0016-76492006-143

Cartwright, J. (2019). Polygonal Faults and Seal Integrity. In *Sixth EAGE Shale Workshop* (Vol. 2019, No. 1, pp. 1-4). European Association of Geoscientists & Engineers.

Cartwright, J., & Huuse, M. (2005). 3D seismic technology: The geological "Hubble." In *Basin Research* (Vol. 17, Issue 1, pp. 1–20). European Association of Geoscientists & Engineers. https://doi.org/10.1111/j.1365-2117.2005.00252.x

Cartwright, J., Huuse, M., & Aplin, A. (2007). Seal bypass systems. *American Association of Petroleum Geologists Bulletin*, *91*(8), 1141–1166. https://doi.org/10.1306/04090705181

Cartwright, J., James, D., & Bolton, A. (2003). The genesis of polygonal fault systems: A review. *Geological Society Special Publication*, *216*(1), 223–234. https://doi.org/10.1144/GSL.SP.2003.216.01.15

Chadwick, R. A., Arts, R., Eiken, O., Kirby, G. A., Lindeberg, E., & Zweigel, P. (2004). 4D Seismic Imaging of an Injected C02 Plume at the Sleipner Field, Central North Sea. *Geological Society Memoir*, *29*(1), 311–320. https://doi.org/10.1144/GSL.MEM.2004.029.01.29

Chopra, S., & Marfurt, K. J. (2007). Seismic Attributes for Prospect Identification and Reservoir Characterization. *Seismic Attributes for Prospect Identification and Reservoir Characterization*. https://doi.org/10.1190/1.9781560801900

Clausen, O. R., Andresen, K. J., Mauritzen, E. K., Connolly, D., & Korstgård, J. A. (2015). Hanging-wall deformation and gas-migration associated to a major salt detaching fault in the Norwegian Danish Basin. *Journal of Structural Geology*, *79*, 90–109. https://doi.org/10.1016/j.jsg.2015.08.003

Clausen, O. R., & Korstgåd, J. A. (1993). Small-scale faulting as an indicator of deformation mechanism in the tertiary sediments of the northern Danish Central Trough. *Journal of Structural Geology*, *15*(11), 1343–1357. https://doi.org/10.1016/0191-8141(93)90107-L

Compton, J. S. (1991). Porosity reduction and burial history of siliceous rocks from the Monterey and Sisquoc Formations, Point Pedernales area, California. *Geological Society of America Bulletin*, *103*(5), 625–636. https://doi.org/10.1130/0016-7606(1991)103<0625:PRABHO>2.3.CO;2

Davies, R. J., & Cartwright, J. (2002). A fossilized Opal A to Opal C/T transformation on the northeast Atlantic margin: Support for a significantly elevated palaeogeothermal gradient during the Neogene? *Basin Research*, *14*(4), 467–486. https://doi.org/10.1046/j.1365-2117.2002.00184.x

Davies, R. J., Goulty, N. R., & Meadows, D. (2008). Fluid flow due to the advance of basin-scale silica reaction zones. *Bulletin of the Geological Society of America*, *120*(1–2), 195–206. https://doi.org/10.1130/B26099.1

Davies, R. J., & Ireland, M. T. (2011). Initiation and propagation of polygonal fault arrays by thermally triggered volume reduction reactions in siliceous sediment. *Marine Geology*, *289*(1–4), 150–158. https://doi.org/10.1016/j.margeo.2011.05.005

Dehandschutter, B., Gaviglio, P., Sizun, J. P., Sintubin, M., Vandycke, S., Vandenberghe, N., & Wouters, L. (2005). Volumetric matrix strain related to intraformational faulting in argillaceous sediments. *Journal of the Geological Society*, *162*(5), 801–813. https://doi.org/10.1144/0016-764904-093

Dewhurst, D. N., Cartwright, J. A., & Lonergan, L. (1999). The development of polygonal fault systems by syneresis of colloidal sediments. *Marine and Petroleum Geology*, *16*(8), 793–810. https://doi.org/10.1016/S0264-8172(99)00035-5

Duffy, O. B., Bell, R. E., Jackson, C. A. L., Gawthorpe, R. L., & Whipp, P. S. (2015). Fault growth and interactions in a multiphase rift fault network: Horda Platform, Norwegian North Sea. *Journal of Structural Geology*, *80*, 99–119. https://doi.org/10.1016/j.jsg.2015.08.015

Evans et al., (2003). *The millennium atlas. Petroleum geology of the central and northern North Sea* (pp. 45–59).

Gay, A., & Berndt, C. (2007). Cessation/reactivation of polygonal faulting and effects on fluid flow in the Vøring Basin, Norwegian Margin. *Journal of the Geological Society*, *164*(1), 129–141. https://doi.org/10.1144/0016-76492005-178

Gay, A., Lopez, M., Cochonat, P., & Sermondadaz, G. (2004). Polygonal faults-furrows system related to early stages of compaction - upper Miocene to recent sediments of the Lower Congo Basin. *Basin Research*, *16*(1), 101–116. https://doi.org/10.1111/j.1365-2117.2003.00224.x

Goulty, N. R. (2008). Geomechanics of polygonal fault systems: A review. *Petroleum Geoscience*, *14*(4), 389–397. https://doi.org/10.1144/1354-079308-781

Goulty, N. R. (2001). Polygonal fault networks in fine-grained sediments - An alternative to the syneresis mechanism. *First Break*, *19*(2), 69–73. https://doi.org/10.1046/j.1365-2397.2001.00137.x

Guerin, G., & Goldberg, D. (1996). Acoustic and elastic properties of calcareous sediments across a siliceous diagenetic front on the eastern U.S. continental slope. *Geophysical Research Letters*, *23*(19), 2697–2700. https://doi.org/10.1029/96GL02188

Hamberg, L., Dam, G., Wilhelmson, C., & Ottesen, T. G. (2005). Paleocene deep-marine sandstone plays in the Siri Canyon, offshore Denmark-southern Norway. *Petroleum Geology Conference Proceedings*, *6*(0), 1185–1198. https://doi.org/10.1144/0061185

Hansen, J. P. V., Cartwright, J. A., Huuse, M., & Clausen, O. R. (2005). 3D seismic expression of fluid migration and mud remobilization on the Gjallar Ridge, offshore mid-Norway. *Basin Research*, *17*(1), 123–139. https://doi.org/10.1111/j.1365-2117.2005.00257.x

Heggland, R. (1998). Gas seepage as an indicator of deeper prospective reservoirs. A study based on exploration 3D seismic data. *Marine and Petroleum Geology*, *15*(1), 1–9. https://doi.org/10.1016/S0264-8172(97)00060-3

Hein, J. R., Scholl, D. W., Barron, J. A., Jones, M. G., & Miller, J. (1978). Diagenesis of late Cenozoic diatomaceous deposits and formation of the bottom simulating reflector in the southern Bering Sea. *Sedimentology*, *25*(2), 155–181. https://doi.org/10.1111/j.1365-3091.1978.tb00307.x

Henriet, J. P., De Batist, M., Van Vaerenbergh, W., & Verschuren, M. (1989). Seismic facies and clay tectonic features in the southern North Sea. *Bulletin of the Belgian Geological Society*, *97*, 457–472.

Hesse, R. (1990). Origin of chert: diagenesis of biogenic siliceous sediments. *Diagenesis*, *4*, 227–252.

Higgs, W. G., & McClay, K. R. (1993). Analogue sandbox modelling of Miocene extensional faulting in the Outer Moray Firth. *Geological Society Special Publication*, *71*(1), 141–162. https://doi.org/10.1144/GSL.SP.1993.071.01.07

Huuse, M., Lykke-Andersen, H., & Michelsen, O. (2001). Cenozoic evolution of the eastern Danish North Sea. *Marine Geology*, *177*(3–4), 243–269. https://doi.org/10.1016/S0025-3227(01)00168-2

Ireland, M. T. (2011). *3D seismic investigation of the diagenesis and deformation of siliceous sediments on the Eastern Atlantic Margin*. http://etheses.dur.ac.uk/712/

Ireland, M. T., Davies, R. J., Goulty, N. R., & Carruthers, D. (2011). Structure of a silica diagenetic transformation zone: The Gjallar Ridge, offshore Norway. *Sedimentology*, *58*(2), 424–441. https://doi.org/10.1111/j.1365-3091.2010.01170.x

Jackson, C. A. L., Carruthers, D. T., Mahlo, S. N., & Briggs, O. (2014). Can polygonal faults help locate deep-water reservoirs? *AAPG Bulletin*, *98*(9), 1717–1738. https://doi.org/10.1306/03131413104

Jordt, H., Faleide, J. I., Bjørlykke, K., & Ibrahim, M. T. (1995). Cenozoic sequence stratigraphy of the central and northern North Sea Basin: tectonic development, sediment distribution and provenance areas. *Marine and Petroleum Geology*, *12*(8), 845–879. https://doi.org/10.1016/0264-8172(95)98852-V

Kastner, M., Keene, J. B., & Gieskes, J. M. (1977). Diagenesis of siliceous oozes-I. Chemical controls on the rate of opal-A to opal-CT transformation-an experimental study.

Geochimica et Cosmochimica Acta, *41*(8). https://doi.org/10.1016/0016-7037(77)90099-0

Kuhlmann, G., & Wong, T. E. (2008). Pliocene paleoenvironment evolution as interpreted from 3D-seismic data in the southern North Sea, Dutch offshore sector. *Marine and Petroleum Geology*, *25*(2), 173–189. https://doi.org/10.1016/j.marpetgeo.2007.05.009

Laurent, D., Gay, A., Baudon, C., Berndt, C., Soliva, R., Planke, S., Mourgues, R., Lacaze, S., Pauget, F., Mangue, M., & Lopez, M. (2012). High-resolution architecture of a polygonal fault interval inferred from geomodel applied to 3D seismic data from the Gjallar Ridge, Vøring Basin, Offshore Norway. *Marine Geology*, *332–334*, 134–151. https://doi.org/10.1016/j.margeo.2012.07.016

Lonergan, L., Cartwright, J., & Jolly, R. (1998). The geometry of polygonal fault systems in Tertiary mudrocks of the North Sea. *Journal of Structural Geology*, *20*(5), 529–548. https://doi.org/10.1016/S0191-8141(97)00113-2

Lonergan, L., Cartwright, J., Laver, R., & Staffurth, J. (1998). Polygonal faulting in the Tertiary of the central North Sea: implications for reservoir geology. *Geological Society Special Publication*, *127*(1), 191–207. https://doi.org/10.1144/GSL.SP.1998.127.01.14

Meadows, D., & Davies, R. J. (2009). Predicting porosity reduction due to silica diagenesis using seismic reflection data. *Marine and Petroleum Geology*, *26*(8), 1543–1553. https://doi.org/10.1016/j.marpetgeo.2008.09.006

Michelsen, O., Thomsen, E., Danielsen, M., Heilmann-Clausen, C., Jordt, H., & Laursen, G. V. (2010). Cenozoic Sequence Stratigraphy in the Eastern North Sea. *Mesozoic and Cenozoic Sequence Stratigraphy of European Basins*, *60*(60), 91–118. https://doi.org/10.2110/pec.98.02.0091

Miller, K. G., Kominz, M. A., Browning, J. V., Wright, J. D., Mountain, G. S., Katz, M. E., Sugarman, P. J., Cramer, B. S., Christie-Blick, N., & Pekar, S. F. (2005). The phanerozoic record of global sea-level change. *Science*, *310*(5752), 1293–1298. https://doi.org/10.1126/science.1116412

Morgan, D. A., Cartwright, J. A., & Imbert, P. (2015). Perturbation of polygonal fault propagation by buried pockmarks and the implications for the development of polygonal fault systems. *Marine and Petroleum Geology*, *65*, 157–171. https://doi.org/10.1016/j.marpetgeo.2015.03.024

Morley, C. K., & Nixon, C. W. (2016). Topological characteristics of simple and complex normal fault networks. *Journal of Structural Geology*, *84*, 68–84. https://doi.org/10.1016/j.jsg.2016.01.005

Morley, C. K., von Hagke, C., Hansberry, R. L., Collins, A. S., Kanitpanyacharoen, W., & King, R. (2017). Review of major shale-dominated detachment and thrust

characteristics in the diagenetic zone: Part I, meso- and macro-scopic scale. *Earth-Science Reviews*, *173*, 168–228. https://doi.org/10.1016/j.earscirev.2017.07.019

Neagu, R. C., Cartwright, J., & Davies, R. (2010). Measurement of diagenetic compaction strain from quantitative analysis of fault plane dip. *Journal of Structural Geology*, *32*(5), 641–655. https://doi.org/10.1016/j.jsg.2010.03.010

Neagu, R. C., Cartwright, J., Davies, R., & Jensen, L. (2010). Fossilisation of a silica diagenesis reaction front on the mid-Norwegian margin. *Marine and Petroleum Geology*, *27*(10), 2141–2155. https://doi.org/10.1016/j.marpetgeo.2010.09.003

Nicol, A., Walsh, J. J., Watterson, J., Nell, P. A. R., & Bretan, P. (2003). The geometry, growth, and linkage of faults within a polygonal fault system from South Australia. *Geological Society Special Publication*, *216*(1), 245–261. https://doi.org/10.1144/GSL.SP.2003.216.01.16

Nixon, C. W. (2013). Analysis of fault networks and conjugate systems. *EPrints Soton*, 251. http://eprints.soton.ac.uk/359064/

Ohm, S. E., Karlsen, D. A., Roberts, A., Johannessen, E., & Høiland, O. (2006). The Paleocene sandy Siri Fairway: An efficient "pipeline" draining the prolific Central Graben? *Journal of Petroleum Geology*, *29*(1), 53–82. https://doi.org/10.1111/j.1747-5457.2006.00053.x

Overeem, I., Weltje, G. J., Bishop-Kay, C., & Kroonenberg, S. B. (2001). The Late Cenozoic Eridanos delta system in the Southern North Sea Basin: A climate signal in sediment supply? *Basin Research*, *13*(3), 293–312. https://doi.org/10.1046/j.1365-2117.2001.00151.x

Pedersen, S. I., Randen, T., Sonneland, L., & Steen, Ø. (2002). Automatic fault extraction using artificial ants. In *SEG Technical Program Expanded Abstracts 2002* (pp. 512-515). Society of Exploration Geophysicists.

Petersen, K., Clausen, O. R., & Korstgård, J. A. (1993). Evolution of a Salt-Related Tertiary Growth Fault in the Danish North Sea. In *Generation, Accumulation and Production of Europe's Hydrocarbons III* (pp. 69–78). Springer Berlin Heidelberg. https://doi.org/10.1007/978-3-642-77859-9_6

Roberts, D. T., Crook, A. J. L., Cartwright, J. A., Profit, M. L., & Ranee, J. M. (2014). The evolution of polygonal fault systems: Insights from geomechanical forward modelling. In *48th US Rock Mechanics / Geomechanics Symposium 2014* (Vol. 1, pp. 488–502). One Petro.

Schiøler, P., Andsbjerg, J., Clausen, O. R., Dam, G., Dybkjær, K., Hamberg, L., Heilmann-Clausen, C., Johannessen, E. P., Kristensen, L. E., Prince, I., & Rasmussen, J. A. (2007). Lithostratigraphy of the Palaeogene - Lower Neogene succession of the Danish North Sea. In *Geological Survey of Denmark and Greenland Bulletin* (Issue 12). https://doi.org/10.34194/geusb.v12.5249

Shin, H., Santamarina, C. J., & Cartwright, J. A. (2008). Contraction-driven shear failure in compacting uncemented sediments. *Geology*, *36*(12), 931–934. https://doi.org/10.1130/G24951A.1

Shin, H., Santamarina, J. C., & Cartwright, J. A. (2010). Displacement field in contraction-driven faults. *Journal of Geophysical Research: Solid Earth*, *115*(7). https://doi.org/10.1029/2009JB006572

Stuevold, L. M., Faerseth, R. B., Arnesen, L., Cartwright, J., & Möller, N. (2003). Polygonal faults in the Ormen Lange Field, Møre Basin, offshore Mid Norway. *Geological Society Special Publication*, *216*(1), 263–281. https://doi.org/10.1144/GSL.SP.2003.216.01.17

Thomas Roberts MEng, D. (2014). a Geomechanical Analysis of the Formation and Evolution of Polygonal Fault Systems. *PhD Thesis, University of Cardiff*, 1–243.

Thyberg, B., & Jahren, J. (2011). Quartz Cementation in Mudstones: Sheet-Like Quartz Cement from Clay Mineral Reactions during Burial. *Petroleum Geoscience*, *17*(1), 53–63. https://doi.org/10.1144/1354-079310-028

Vejbæk, O. V. (1997). Dybe strukturer i danske sedimentære bassiner. *Geologisk Tidsskrift*, *4*(4), 1–31.

Watterson, J., Walsh, J., Nicol, A., Nell, P. A. R., & Bretan, P. G. (1999). Geometry and origin of a polygonal fault system. *Journal of the Geological Society*, *157*(1), 151–162. https://doi.org/10.1144/jgs.157.1.151

Williams, L. A., Crerar, D. A., & Hall, G. (1985). SILICA DIAGENESIS, II. GENERAL MECHANISMS 1. In *pubs.geoscienceworld.org*. https://pubs.geoscienceworld.org/jsedres/article-lookup/55/3/312

Wrona, T., Jackson, C. A. L., Huuse, M., & Taylor, K. G. (2017). Silica diagenesis in Cenozoic mudstones of the North Viking Graben: physical properties and basin modelling. *Basin Research*, *29*, 556–575. https://doi.org/10.1111/bre.12168

Zhang, T., Lin, Y., Liu, K. H., Alhakeem, A., & Gao, S. (2017). Fault visualization enhancement using ant tracking technique and its application in the Taranaki basin, New Zealand. In *SEG Technical Program Expanded Abstracts 2017* (pp. 2350-2354). Society of Exploration Geophysicists.

Ziegler, P. A. (1992). North Sea rift system. In *Tectonophysics* (Vol. 208, Issues 1–3, pp. 55–75). https://doi.org/10.1016/0040-1951(92)90336-5

Chapter 4

Third Paper Titled: Shallow gas accumulations, focused fluid flow features and geochemical characterization of Cenozoic mudstones in the eastern Central North Sea

Journal of Frontiers in Earth Science Journal.

Part of the research from this paper has been presented as a talk at the EAGE Conference in Copenhagen in 2018.

Abstract

Mohammed Malah[1, 2], Mads Huuse[1], James Armstrong[1]

1. School of earth and environmental science, University of Manchester.
2. Corresponding author: mohammed.malah@manchester.ac.uk
3. Keywords: Shallow gas, bright spots, focused fluid flow, bright spots, fluid migration, hydrocarbon plumbing systems.

An analysis of an extensive set of the PGS 3D MegaSurvey™ seismic data from the Central North Sea shows evidence for numerous shallow gas accumulations appearing as 'bright spot' anomalies on seismic data within the Cenozoic succession. The shallow gas accumulations are classified based on their direct hydrocarbon indicator (DHI) characteristics, spatial and temporal distribution, and their relationship with other focused fluid flow related features. Such features include pockmarks, polygonal faults, gas pipes and chimneys, soft sediment remobilization and silica diagenesis. The shallow gas accumulations are classified mainly into two types, Type I and Type II. The Type I shallow gas anomalies are often found associated with the Zechstein salt diapirs while the Type II anomalies are found in discreet pockets within Delta Front sediments. Further, analysis of well data for organic richness and thermal maturity within the shallow sediments within the Cenozoic succession indicates average Total Organic Carbon content of 5% with a very good generative potential. This suggests the possibility of biogenic gas generation contributing to the charging of the shallow gas reservoirs in addition to gas from deep thermogenic sources. A geologic model is presented which may assist in mitigating risks associated with shallow gas accumulations whether they are considered as a shallow geohazard for the drilling of deeper targets or a potential new play where they are located near existing infrastructure. This study has implications for shallow geohazard assessment, subsurface storage of carbon dioxide and hydrocarbon exploration.

4.1 Introduction

Shallow hydrocarbon accumulations have been known to exist since the 70s and have been of great interest to the Exploration and Production (E&P) industry as its presence can either mean a drilling hazard or an indication for a deeper prospective reservoir. These shallow hydrocarbon accumulations, often referred to as 'shallow gas' as it is almost entirely 99% methane of either a thermogenic or biogenic origin or both are usually identified on seismic data as high amplitude anomalies known as 'bright spots' caused by a decrease in acoustic impedance at the top of a gas charged reservoir (Heggland et al., 1997; 1998). Shallow gas accumulation is defined in literature as gas within shallow sediments in the lithosphere at depths within the upper 1000m beneath the seabed within marine sediments (Davis, 1992; Judd & Hovland, 1992), but this study defines shallow gas accumulations as gas trapped within sediments above the top Chalk in the North Sea *c.* 2.5 km within the Cenozoic section. Recently, some shallow gas accumulations generally occurring in Oligo-Miocene to Pleistocene sands are being turned into resources in parts of the North Sea. Examples of such includes shallow gas in Lower Pleistocene sands of the Aviat field in the UK (Rose et al., 2016), gas in Pleistocene outwash fan in the Peon gas field Norway (Huuse et. al., 2012), mixed oil and gas in Miocene silty sandstones in the Lille John field in Denmark (Goffey et. al., 2018), producing A12-FA, A18, B13-FA and F02a fields from Miocene to Pliocene sands in the Netherlands (van den Boogard & Hoetz, 2012; 2015). These fields were largely undeveloped in the past due to technical challenges such as early water break through, low pressures and sand production due to unconsolidated nature of the reservoirs, but with the application of modern technology such as compressional drilling, directional drilling and expandable screens the shallow gas reservoirs were brought online in the last decade. Exploration for shallow gas in the Central North Sea has been intense since the last decade and is even thought to be considered as a new play especially where they are located near existing infrastructure (Teen Veen et al., 2014). The production of these shallow gas fields has been limited due to a lack of insight into their petroleum systems and hence the need to characterize their occurrence. In recent years, researchers have shown an increased interest in shallow gas accumulations particularly in the North Sea (Heggland, 1997; Schroot et al., 2003; Kuhlmann & Wong, 2008; ten Veen et al., 2014; Stuart & Huuse, 2012; Verweij et al., 2012, 2013; ten Veen et al., 2014; van Den Boogard & Hoetz, 2015; Williams & Gent., 2015; Clausen et al., 2015; Muller et al., 2018).

Shallow gas plays a vital role in the Exploration & Production (E&P) industry as a resource and a shallow geohazard during drilling for the location of offshore infrastructure, for climate change in the assessment of uncontrolled sources of greenhouse gas emissions from marine sources and of its impact on marine ecosystems (Romer et al., 2017; Lichtschlag et al., 2018). Results from earlier studies in parts of the Central North Sea, particularly the Dutch and German sectors have assessed and shown evidence for a working shallow gas petroleum system by the seismic characterisation of these so-called shallow gas accumulations (van den Boogard and Hoetz, 2015; Muller et al., 2018). These shallow gas accumulations do not occur in isolation in most cases but are often associated with focused fluid flow features within sedimentary basins (Sun et al., 2012; Andresen et al., 2012). Together, they all form the hydrocarbon plumbing systems within a sedimentary basin and the subject of the appearance, association and significance of the focused fluid flow features have been a subject of debate since the advent of high-quality 3D seismic data which allows for these features to be highlighted and resolved in great detail (Cartwright & Huuse., 2005). Focused Fluid flow features observed in this study, which form part of the hydrocarbon plumbing systems in the eastern CNS mainly within the Cenozoic succession include polygonal faults (Lonergan & Cartwright., 1998; Andresen et al., 2009; Clausen & Andresen., 2015; Malah et al., 2021 this study), late Palaeocene to Eocene sandstone injection complexes observed on core and seismic data (Duranti et. al., 2002; Hamberg et al., 2005; Svendsen et al., 2010; Huuse et al., 2004; Andresen & Clausen., 2014), Oligocene and Miocene pockmarks (Andresen et al., 2008), sediment mounds (Andresen et al., 2009), gas chimneys and pipes (Heggland 1998, Andresen et al., 2009; Clausen et al., 2015), silica diagenetic reaction front (Malah et al., 2021; This study, Chapter 2) and an extensive polygonal fault system (PFS) (This study, Chapter 3).

This study utilizes 3D seismic volumes combined with conventional and model-based interpretation approaches in providing a holistic view of the shallow hydrocarbon accumulations in the Eastern North Sea, their context, and likely plumbing systems by incorporating into the seismic-sequence stratigraphy of the Central North Sea by Michelsen et al., (1998) and lithostratigraphy by Schiøler et al., (2007). Examples of unexploited shallow hydrocarbon columns have been examined and the likely plumbing systems for the Cenozoic succession of the eastern Central North Sea and its relation to

the mobile Zechstein salt unit and detachment faults have been established, highlighting implications for both vertical and long-distance lateral migration in depositional fluid conduits embedded in the stratigraphy for the southern Norwegian and Danish sector of the Central North Sea in the Norwegian-Danish Basin. This study also sets out to determine the sources of hydrocarbons which make up the shallow gas accumulations in the Central North Sea. The origin of the shallow gas accumulations in the eastern CNS is not yet clear, however there is evidence of both a thermogenic, biogenic or a mixture of both for the origin of fluids. Although, geochemical and isotopic analysis on shallow gas samples from shallow gas fields in the Dutch sector of the CNS show that the gas is typically dry (>99% methane) and depleted in C13/C1 (-70% dC13/C1) pointing to a biogenic origin for the gas (Verweij et al., 2018). The presence of gas chimneys, pipes, and acoustic masking in the seismic section and the existence of several shallow gas accumulations in association with Zechstein salt domes and large regional faults, polygonal normal faults and clastic remobilization suggests there might have been migration of thermogenic gas from both deeper and shallow sources (teen Veen et al. 2014; Andresen & Clausen., 2014). No well have penetrated a shallow gas reservoir in the study area and therefore no tests data for the reservoirs in this area are available which results in an uncertainty around reservoir geometry and saturation levels, but gas shows have been reported for the study area in several studies and well reports (Heggland., 1998; Andresen et al., 2009; 2014). We analyse well cuttings samples for geochemical data to characterize and obtain information on hydrocarbon generation potential of the Cenozoic section under study, the type and maturity of the organic matter using Total Organic Carbon (TOC) and Rock-Eval pyrolysis analysis and the estimation of TOC using the method of Passey et al., (1990) from petrophysical well logs in this study.

In this study, we also document the occurrence and distribution of shallow gas accumulations and focused fluid flow systems such as polygonal faults, pockmarks, sediment mounds, gas chimneys & pipes, clastic sediment remobilization, intrusion, and silica diagenetic reaction front. We classify the shallow gas occurrences into two main types, with Type I being mainly associated with salt diapirs and Type II being isolated occurrences in Delta Top sediments. We further highlight the intricate relationship between the shallow gas occurrences and their relationship with focused fluid flow

features and how they influence the hydrocarbon plumbing system within the area. Furthermore, we were able to characterize and assess the organic matter richness, thermal maturity and source rock potential of the Cenozoic Mudstones and consider the role of a shallow biogenic source for the shallow gas accumulations. We summarise by presenting a model which can be useful in hydrocarbon exploration and risk assessment that highlight implications for the exploitation of shallow gas as a potential energy source, a shallow geohazard for the location of offshore infrastructure for drilling and offshore wind farm location, the storage of carbon dioxide in the subsurface and the assessment of the contributions of methane emissions to chemosynthetic benthic ecosystems and the climate.

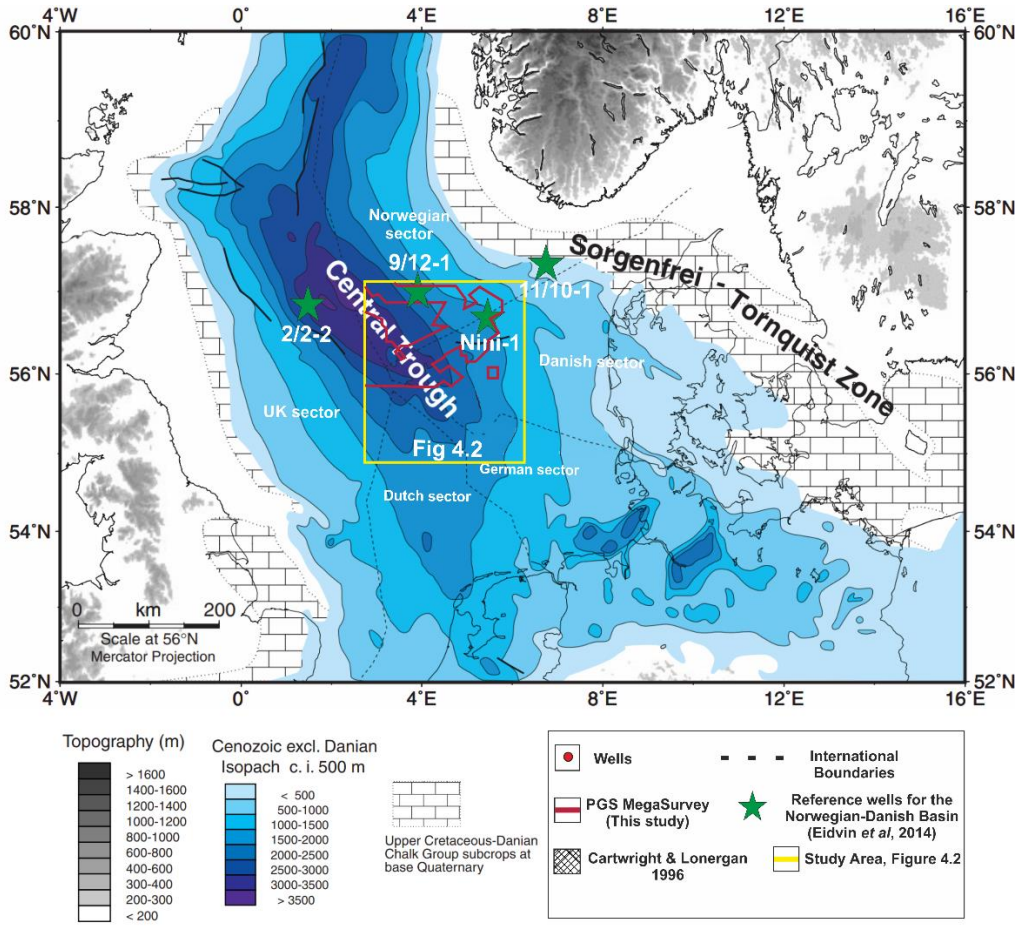

Figure 4.1: Location of the study area in the eastern corridor of the Central North Sea including the Norwegian, Danish, German, and Dutch sectors covered in the yellow polygon. Also shown is the extent and coverage of the PGS 3D MegaSurvey™ and the wells used in this study indicated by the green stars. The figure also shows some of the structural elements in the study area including the sediment thickness of the Cenozoic sediments in the North Sea excluding the Danian from Huuse., (2002).

4.2 Geological setting

The Central North Sea evolved due to a series of rifting episodes and has since been affected by a series of basin inversion, subsidence, uplift, and erosion during the Cenozoic (Ziegler, 1992; Huuse et al., 2001) (Figure 4.1). Sediments supplied to the Cenozoic North Sea basin were influenced by tectonic movements of older structural elements and are sourced mainly from the east (Jordt et al., 1995; Michelsen et al., 1998; Ahmadi et al., 2003; Hamberg et al., 2005). The Cenozoic of the CNS preserves a complete record of Cenozoic sedimentation within depocenters characterised by prograding and delta slope systems and often affected by deep seated regional faults and salt diapirism (Jordt et al. 1995). The Cenozoic succession in the CNS has been studied extensively by Jordt et al., (1995), Michelsen et al., (1998) and Thöle et al. (2014) and subdivided into units based on seismic sequence stratigraphic principles. Large prograding deltas are believed to have covered the entire CNS during the Oligo-Miocene and later times, with sediment influx from the Baltic River system and its environs (Overeem et al., 2001), and partly controlled by subsidence and climatic conditions that created accommodation space for sediments during glacial and interglacial cycles at later times (Kuhlmann & Wong., 2008). The discovery of hydrocarbons in the Palaeocene - Eocene of the Norwegian-Danish basin outside the hydrocarbon-prone Central Graben demonstrates the importance of cross-stratal and lateral fluid migration from deeper and shallower source rocks of thermogenic and biogenetic fluids, coupled with pore fluid expelled by sediment compaction within the Central North Sea (Hamberg et al., 2005; Ohm et al., 2006) (Figure 4.2).

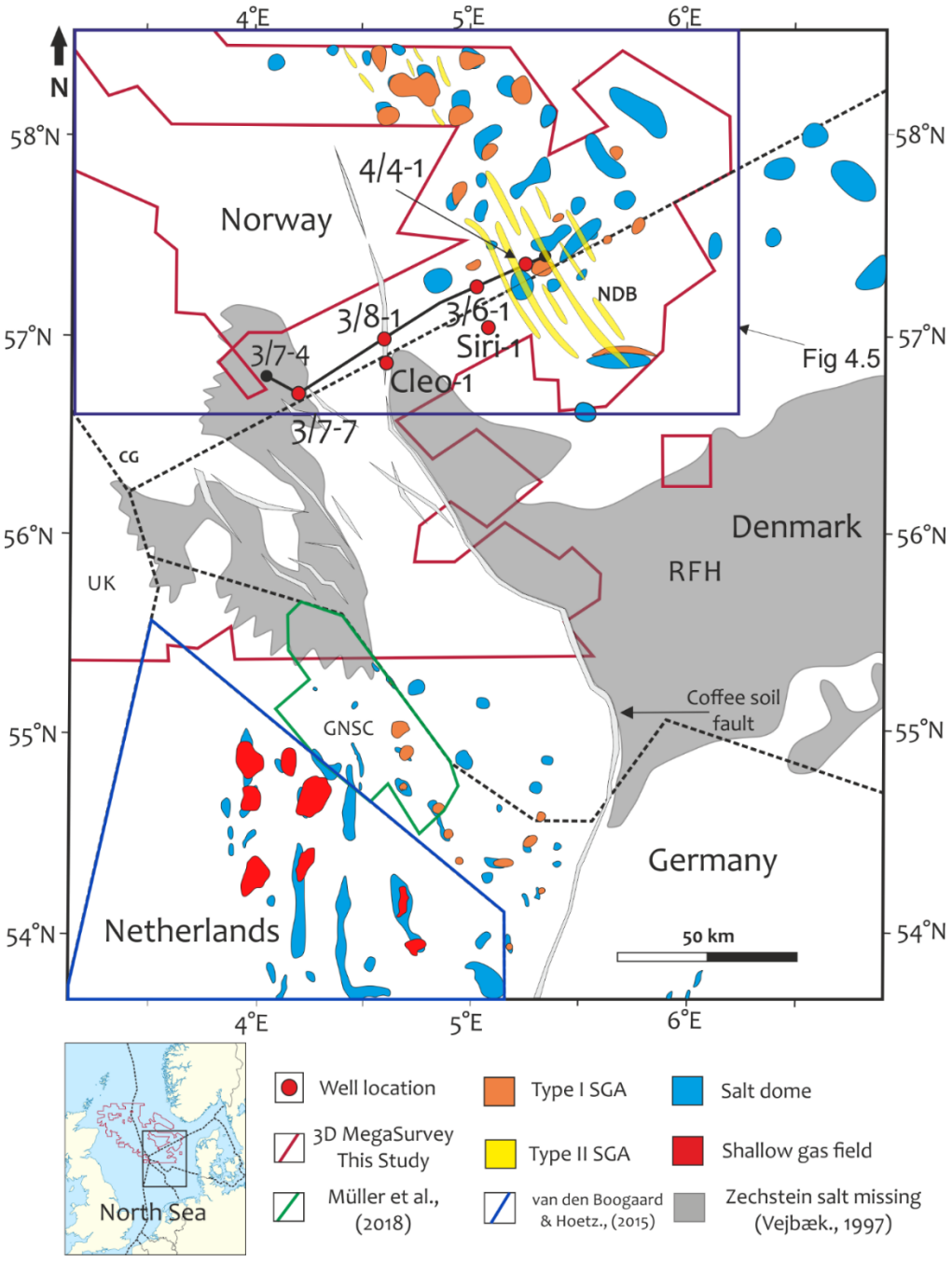

Figure 4.2: A zoom in to the study area shows the main structural elements in the eastern Central North Sea and the distribution of mapped shallow gas accumulations and salt diapirs for the Norwegian & Danish sectors (This study), the German sector (Muller et al., 2018) and the Dutch sector (van den Boogard & Hoetz., 2015). Also shown are other studies in the eastern CNS by Andresen., (2008), Andresen & Clausen., (2014) and Clausen et al., (2015) which have all highlighted the presence of shallow gas in the study area. The extent of mobile Zechstein salt pinch-out and non-deposition is highlighted by the grey area after Vejbæk., (1997), local areas missing the Zechstein salt at present day due to halokinesis is not shown but individual salt diapirs mapped across the study area are shown in blue. Also shown are the main depositional elements in the eastern CNS after Clausen & Huuse., (1999) and Andresen & Clausen., (2014) including the Coffee Soil Fault, Ringkobing-Fyn High and the Siri canyon, Ibenholt, and Luna valleys.

4.3 Stratigraphic Framework

Since the discovery of the Siri field by the Siri – 1 well in 1995 in the eastern Central North Sea, intense drilling activity followed to date and hence led to a better and improved understanding of the eastern Central North Sea (Hamberg *et al.,* 2005; Schiøler *et al.,* 2007). A detailed sequence stratigraphic framework for the Cenozoic of the Central North Sea used in this study is that by Michelsen *et al.,* (1998) and Lithostratigraphy by Schiøler *et al.,* 2007) (Figure 4.3). The Cenozoic of the Central North Sea is cut at the Palaeocene of the Norwegian-Danish basin by the Siri-canyon into the Top chalk group filling a submarine canyon in the eastern North Sea along with the Vidar, Ibenholt and Poul valleys (Clausen & Huuse *et al.,* 1999). Upper Palaeocene to Lower Eocene marlstone and mudstone successions dominate the Palaeocene in the Siri canyon comprising of the Vale, Lista, Sele and Balder formations that form part of the Rogaland group (Hamberg *et al.,* 2005; Schiøler *et al.,* 2007). Several sandstone rich members of the Bor, Tyr, Idun, Rind and Kolga are found intercalated within the marlstone and mudstone successions. The Eocene to present day stratigraphy of the Norwegian-Danish Basin is filled by progressive progradation of Cenozoic clinoforms sourced primarily from the north-east during the Oligocene and the east during the Miocene - Pliocene represented mainly by the overall coarsening upward of the Lark formation and the Nordland Group (Huuse *et al.,* 2001; Schiøler *et al.,* 2007). The Eocene to the present day is mostly dominated by mudstone successions with occasional stringers of sandstone members found within the Hordaland and Nordland group of the eastern Central North Sea.

The Lark formation is of Early-Oligocene to early Mid-Miocene age deposited in a distal shelf open marine (neritic) environment comprising mainly of mudstones and occasional sandstone stringers first divided into three informal units 4, 5 and 6 by Michelsen *et al.,* (1998) corresponding to sequences 4.1 to 6.3 (Figure 3). Recently, the Lark formation was further divided into four lithostratigraphic sub-units – L1 – L4 by Schiøler *et al.,* (2007) based on well logs, biostratigraphy, and seismic interpretations. Deegan & Scull., (1977) defined the group that represents the Lark formation in the Norwegian-Danish Basin as Hordaland group and is now represented by the Westray Group of Knox & Holloway., (1992). The Lark formation is underlain by the Horda formation and overlain by the Nordland group which corresponds to the Stronsay group and Nordland group of Knox &

Hollow., (1992) respectively. Where it is identified, the Lark formation has an overall stable gamma ray and sonic log motif with a relatively lower gamma-ray than that displayed by the underlying Balder formation. The Lark formation also studied by Jarsve *et al.,* (2015) based on sequence stratigraphic techniques, biostratigraphy, climate data, Sr-isotope stratigraphy described the Oligocene succession as having four main sequences that post-date the global cooling event at the Eocene-Oligocene boundary (Miller *et al.,* 2005) and the effect of tectonic uplift of the western part of Southern Norway that forced the drainage of large deltas eastward during the Rupelian and Chattian time. Halokinesis induced by differential loading in the basin (Stewart., 2007) influenced the lateral extension of sediment progradation and the creation of accommodation spaces (Japsen *et al.,* 2007; Jarsve *et al.,* 2015). These deltas are believed to have deposited thick succession of good reservoir unit sands in the Norwegian-Danish basin which are known as the informal Oligocene Sands (Michelsen *et al.,* 1998) and now introduced as the Freja and Dufa members by Schiøler *et al*., (2007) in parts of the eastern CNS. The Dufa member type well is the Inez-1 well which is about 120 km away from the Central Graben in the current study area within the Norwegian-Danish Basin and the Freja member type well is the Siri - 1, Frida - 1 and Francisca - 1 wells that are all within the extent of the current study area. The Freja member deposited in a submarine channel and levee environment is Chattian to Aquitanian and consists of thick and thin-bedded turbiditic sands where the reflection pattern and internal architecture of the Freja member with a clinoform downlap indicates its deltaic nature (Michelsen *et al.,* 1998; Huuse & Clausen., 2001; Schiøler *et al.,* 2007).

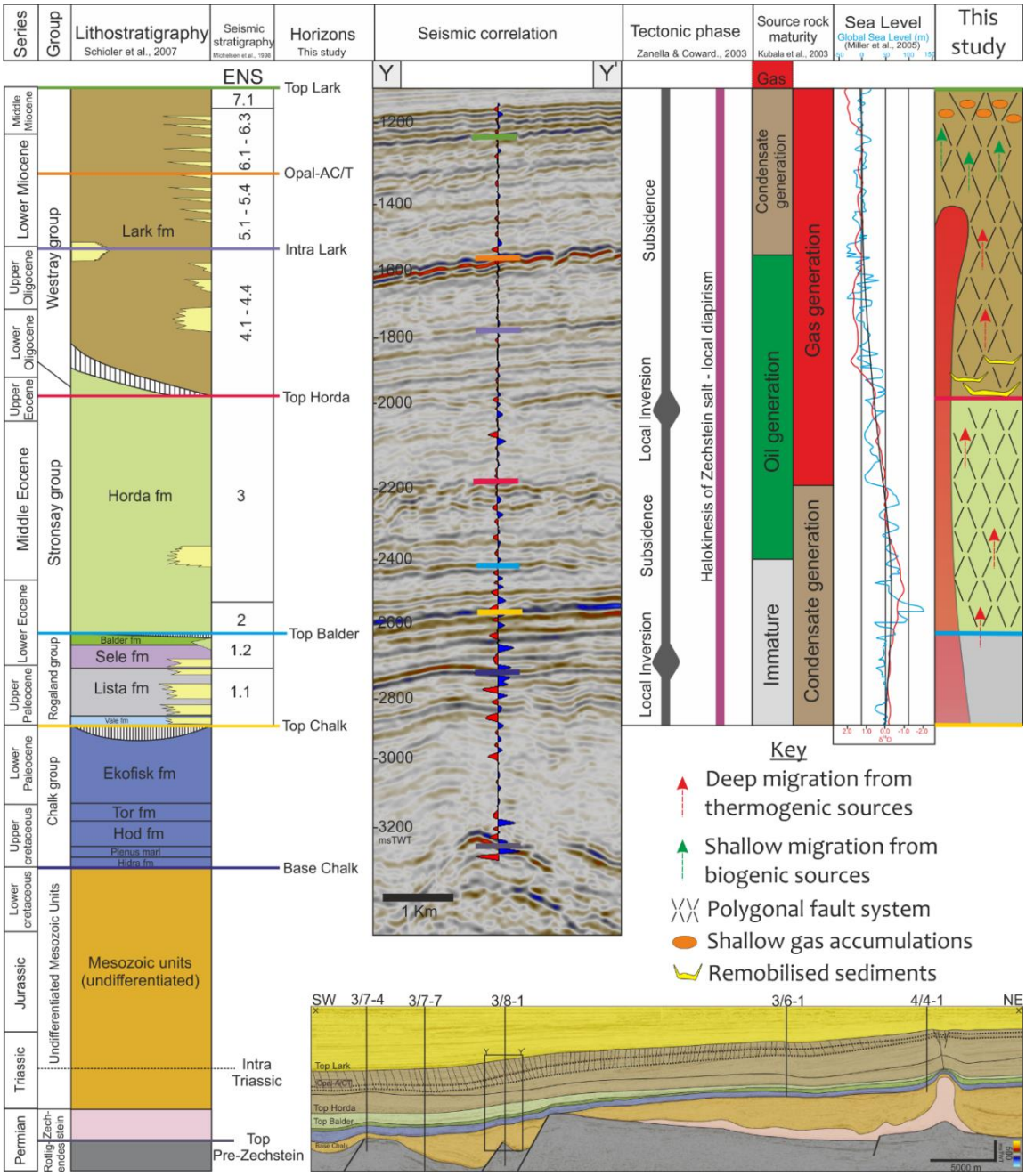

Figure 4.3: Stratigraphic framework of the eastern Central North Sea after Schiøler et al., (2007) and the main eastern North Sea sequences established by Michelsen et al., (1998) and the positions of horizons mapped in this study according to the lithostratigraphic subdivisions of Schiøler et al., (2007). The horizons were mapped by the aid of a seismic to well tie using the well 3/8-1 with the position of the well and the other adjacent wells used for this study shown inset along a transect (location of transect across the wells shown in Figure 2). Also shown is the tectonic evolution of the study area after Zanella & Coward., (2003), source rock maturation after Kubala et al., (2003), and the global sea level and $\delta^{18}O$ curves from Miller et al., (2005). Also shown in the last column is a simplified model of the occurrence of shallow gas accumulations and the relationship with salt diapirs, remobilised sediments (Andresen & Clausen., 2014), polygonal faults and migration from deep thermogenic and shallow biogenic sources within the study area. (Note the occurrence of frequent thin sand stringers in the Westray Group Lark formation in the Lithostratigraphic column).

4.4 Dataset and Methods

4.4.1 Seismic & Well Data

Data for this study includes the PGS MegaSurvey™ legacy seismic data that covers an area of about 128,000 km^2 in the CNS. A cropped 3D sub volume of the PGS MegaSurvey™ (Figure 4.2) covering an area of ~20,000 km^2 was employed for this study. The 3D survey has a bin spacing of 50 m by 50 m, a sampling rate of 4 msTWT with a maximum vertical resolution ($\lambda/4$) of c. 12 – 15 m and a horizontal resolution ($\lambda/2$) of 20 – 30 m according to a dominant frequency of 50 – 70Hz. The CNS MegaSurvey™ is a normal polarity (zero phase) data where a hard kick i.e., a positive reflection (peak) is represented by red and a soft kick i.e., a negative reflection is represented by a negative reflection (trough). The Cenozoic has an average interval velocity of 2km/s (+/- 10%), thus allowing for the vertical measurements made in milliseconds two-way time (ms TWT) to be directly converted to depth in meters (m) as a first order approximation for the interval of interest for the North Sea (Japsen, 1999; Huuse et al., 2001). The seismic data was integrated with well data from wells 3/6-1, 3/7-4, 3/7-7, 3/8-1, and 4/4-1 that cover the 3D sub volume to achieve a seismic to well tie and petrophysical logs and completion reports from the NPD were used to determine lithology. The quality of the seismic data is good to moderate but sufficient to resolve the shallow gas and focused fluid flow features mapped in this study. However, it is worthy to note that the PGS 3D MegaSurvey™ have irregular near offset distribution and low fold for shallow objectives and this is mainly because the source was designed during the acquisition for deeper targets. A temporal sampling of 4 ms and spatial sampling of 12.5m x 50m bin spacing is also likely too large for the target spectrum within 2 - 3 km below the seabed. This is further complicated by the presence of large tunnel valleys in the shallow section within the study area which often obscure seismic data quality.

Seismic sections were integrated with well data to establish the regional seismic horizons for the Cenozoic section and high amplitude anomaly interval. Conventional seismic interpretation technique of RMS amplitude mapping technique was employed to map high amplitude anomalies and establish the areal extent of the bright spots on horizon slice in plan (top) view. For the interpretation, the seismic stratigraphic framework of Michelsen et al., (1998) that subdivided the Cenozoic of the eastern North Sea into seven informal major unit based on the progradation or erosion of major surfaces was adopted and the

lithostratigraphic subdivision of the Paleogene to Lower Neogene of the Central North Sea by Schiøler et al., (2007) based on lithological, sedimentological and biostratigraphic evidence into seven formations from the Top Chalk surface to the base of the Nordland group is employed.

A systematic mapping/scanning for shallow gas accumulations was conducted using tools for assessing and mapping of focused fluid flow features and seismic anomalies or 'bright spots' for shallow gas occurrence by identifying direct hydrocarbon indicators (DHI's) such as velocity pushdown, seismic attenuation, bright spots, flat spots, phase/polarity reversal and gas chimneys according to Hilterman (2001), Bacon et al., (2007) and Brown (2011). A bright spot is often the result of the acoustic impedance contrast of gas-filled reservoirs while a flat spot is the contrast generated between a small acoustic impedance of a gas-filled reservoir and a greater acoustic impedance of a gas-filled porous reservoir unit with a horizontal gas-water contact. According to a study conducted by van den Boogaard & Hoetz (2012), even a 2% gas saturation in a reservoir can produce a high-amplitude anomaly that greatly affects the impedance contrast of the seismic character.

4.4.2 Geochemical Data

4.4.2.1 *Total Organic Carbon Estimation*

Total organic carbon content (TOC) analysis was conducted using a Schimadzu TOC-V CPN analyser system in the Williamson Research Centre at the University of Manchester. The system included an SSM-5000A solid sample module that contained a Total Carbon (TC) and Inorganic Carbon (IC) unit. The TC is measured putting a measured amount of the crushed dry mudstone samples into a sample boat and into a sample port in the analyser unit. The port is connected directly to a furnace which has already been preheated to 680° C. Upon insertion into the furnace, all the carbon in the sample is converted to carbon dioxide (CO_2) and is carried in a stream of high purity air to an infrared detector. The detector produces a signal which is directly proportional to the concentration of the carbon in the carbon dioxide and is measured on the workstation as the Total Carbon (TC). The Inorganic carbon is measured in the same fashion as for the TC, but in this case, the sample is treated with hydrochloric acid (HCL) to facilitate the liberation of the inorganic carbon from the sample once inserted into the TC port in the analyser unit. Prior to running the samples through the analyser for the following study, a calibration was done using

three (3) different weigh outs of pure glucose ($C_6H_{12}O_6$) of 12.5 mg, 25 mg and 50 mg corresponding to 5 mg, 10 mg, and 20 mg of carbon in each sample before running the analysis for Total Carbon (TC). In a similar fashion for the Inorganic Carbon (IC), a calibration of the analyser was conducted using sodium carbonate ($NaCO_3$) standards of 44.2 mg, 88.4 mg and 176.8 mg corresponding to 5 mg, 10 mg, and 20 mg of carbon in each sample. This initial calibration is to align the '*calibration curve*' of the detectors to keep error margins below 3% and a calibration standard was run after every tenth sample analysed to ensure the consistency of the analyser system. All the data generated from the analyser system is stored on the TOC-V CPN software on a workstation and downloaded as an excel file for further processing.

For this study, a total of twenty-one (21) samples were analysed from two wells 3/6-1 and 4/4-1 from the CNS (Figure 1), the samples are collected from well cuttings from the Norwegian Petroleum Directorate (NPD) for the analysis. The mudstone samples were washed & dried, dry crushed and measured out to 50 mg (+/- 5) using a metric balance accurate to four decimal places into the sample boat before onward insertion into the analyser port unit. Results obtained for TOC values for the samples analysed are presented in Table 1.

4.4.2.2 *Rock-eval Pyrolysis*

Four samples where further selected for Rock-eval pyrolysis to determine the hydrocarbon potential of the Cenozoic mudstones. They were analysed at the Applied Petroleum Technology (APT) laboratories in Stavanger, Norway using the Rock-eval 6 HAWK instruments according to procedures set by The Norwegian Industry Guide to Organic Geochemical Analysis (NIGOGA), 4th edition. Results from the analysis that include the following are presented in Table 2 and Figure 10.

S1: Amount of hydrocarbons thermally extracted at 300°C (Kg of free oil (unexpelled) /tonne rock).

S2: Amount of hydrocarbons produced from pyrolysis up to 550°C (Kg pyrolysate/tonne rock)

S3: Amount of CO_2 released from organic matter at higher temperatures. (Kg CO_2 from organic oxygen/tonne rock)

Tmax: Temperature at maximum S2 peak.

The primary data obtained above will be used to derive ratios as such:

Hydrogen Index (HI) = S2/TOC (mg/gTOC)

Oxygen Index (OI) = S3/TOC (mg/gTOC)

Production Index (PI) = S1/ (S1 + S2)

4.4.2.3 *CARPLOT*

The wells 3/6-1 and 4/4-1 were further studied and analysed for TOC from petrophysical logs and to compare and validate values obtained from the laboratory analysis of well cuttings samples. The TOC results obtained from the log analysis used the CARPLOT software based on Passey et al., (1990) methodology. The Passey et al., method estimates TOC from either sonic/resistivity, neutron/resistivity or density/resistivity logs based on the log separation that occurs between the resistivity and other logs due to the presence of organic matter. The mathematical equation to quantify this separation is given by the equation below and the results presented in Figure 11.

$$\boldsymbol{\Delta logR} = \log\left(\frac{R}{\mathrm{R_{baseline}}}\right) - P(\Delta t - \Delta t_{\mathrm{baseline}})$$

Where,

ΔlogR is the separation between the two logs measured in logarithmic resistivity circle.

R is the resistivity in Ωm

Δt is the sonic measurement in μs/ft.

P is the ratio of -50 μs/ft per one resistivity cycle.

$\Delta t_{baseline}$ is the sonic corresponding to $R_{baseline}$ in the lean shale interval (non-source rock).

With the log separation quantified.

Thus, the TOC can be calculated using the equation below:

$TOC = \Delta logR \times 10^{[2.297 - (0.1688 \times LOM]}$

Where LOM is the level of maturity, for any specific *ΔlogR*, TOC decreases as LOM increases.

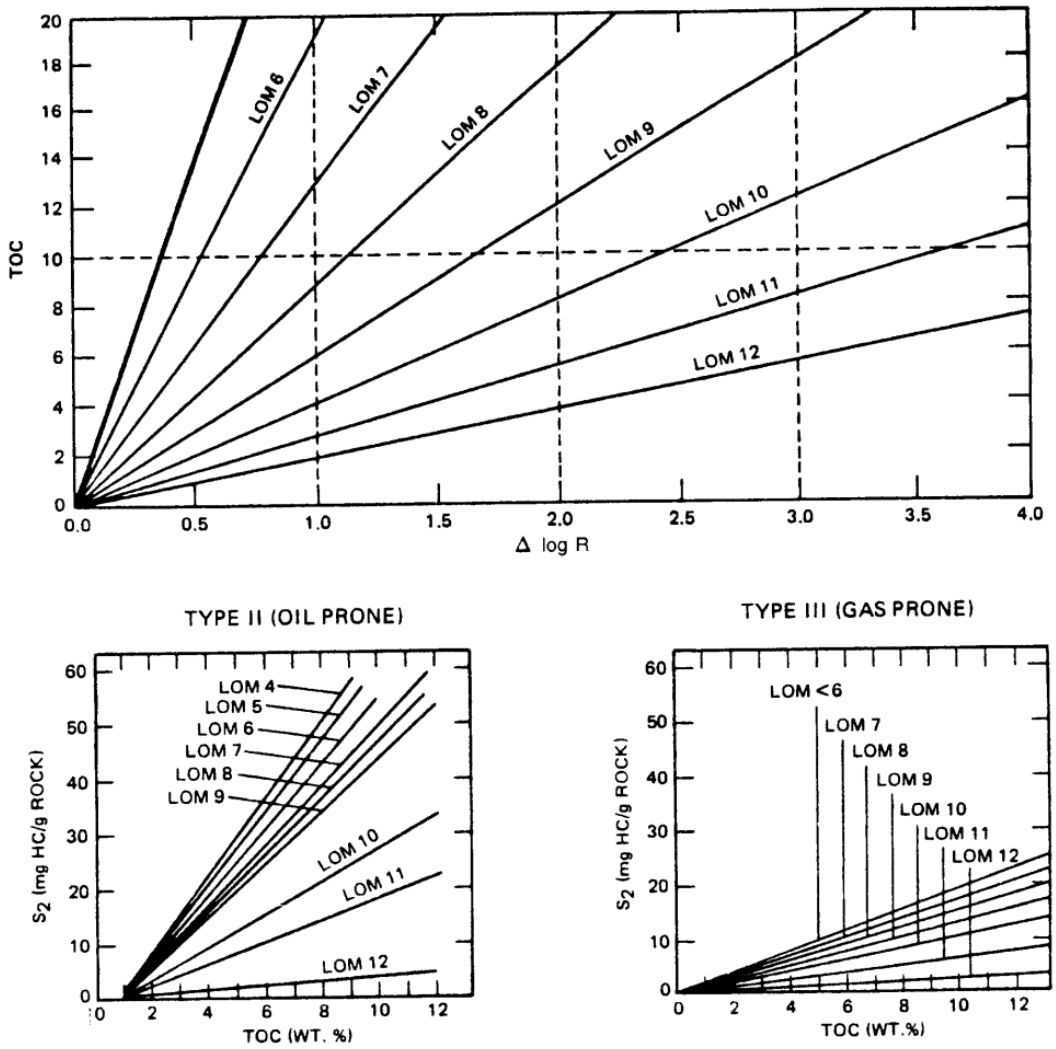

Figure 4.4: (a) ΔlogR diagram relating ΔlogR to TOC via maturity used for organic matter with <6 LOM. (b) TOC vs S_2 via maturity plot for Type II (Oil Prone) Kerogen used for both Type I and Type II kerogen. (c) TOC vs S_2 via maturity plot used for Type III (gas prone) kerogen. Sourced from Passey et al., (1990).

4.5 Results and Observations

4.5.1 Seismic Characterization of Shallow Gas

Seismic anomalies appearing as 'bright spots' on seismic data have been mapped and characterized, numerous of such bright spots have been identified based on their seismic character and through RMS amplitude scanning. They appear mainly within the Oligo-Miocene and occurrence within the Plio-Pleistocene where salt diapirs pierce beyond the Middle-Miocene Unconformity within the Cenozoic succession in the study area (Figure 4.4). This contrasts with similar seismic anomalies observed from the Dutch and German sectors of the CNS mainly found within the Plio-Pleistocene succession (ten Veen et al., 2014; Muller et al., 2018). The bright spot anomalies are thought to represent shallow hydrocarbon accumulations within shallow reservoirs containing gas rich pore fluids. The

character of the so-called amplitude anomalies 'bright spots' are defined as shallow gas accumulations based on direct hydrocarbon indicators (DHIs) parameters defined by Hilterman (2001), Bacon et al., (2007) and Brown (2011). According to a study conducted by van den Boogard et. al. (2012), even a 2% gas saturation in a reservoir can produce a high-amplitude anomaly that greatly affects the impedance contrast of the seismic character.

The bright spot anomalies mapped as shallow gas accumulations in this study are broadly classified into two types according to DHI characteristics, their spatial and temporal distribution, and their relationship with other focused fluid flow systems within the eastern CNS. The two main classifications are the **Type I** anomalies which are shallow gas found directly associated with salt diapirs and the **Type II** anomalies which are isolated shallow gas anomalies found associated with delta front (topset) sequences within the study area.

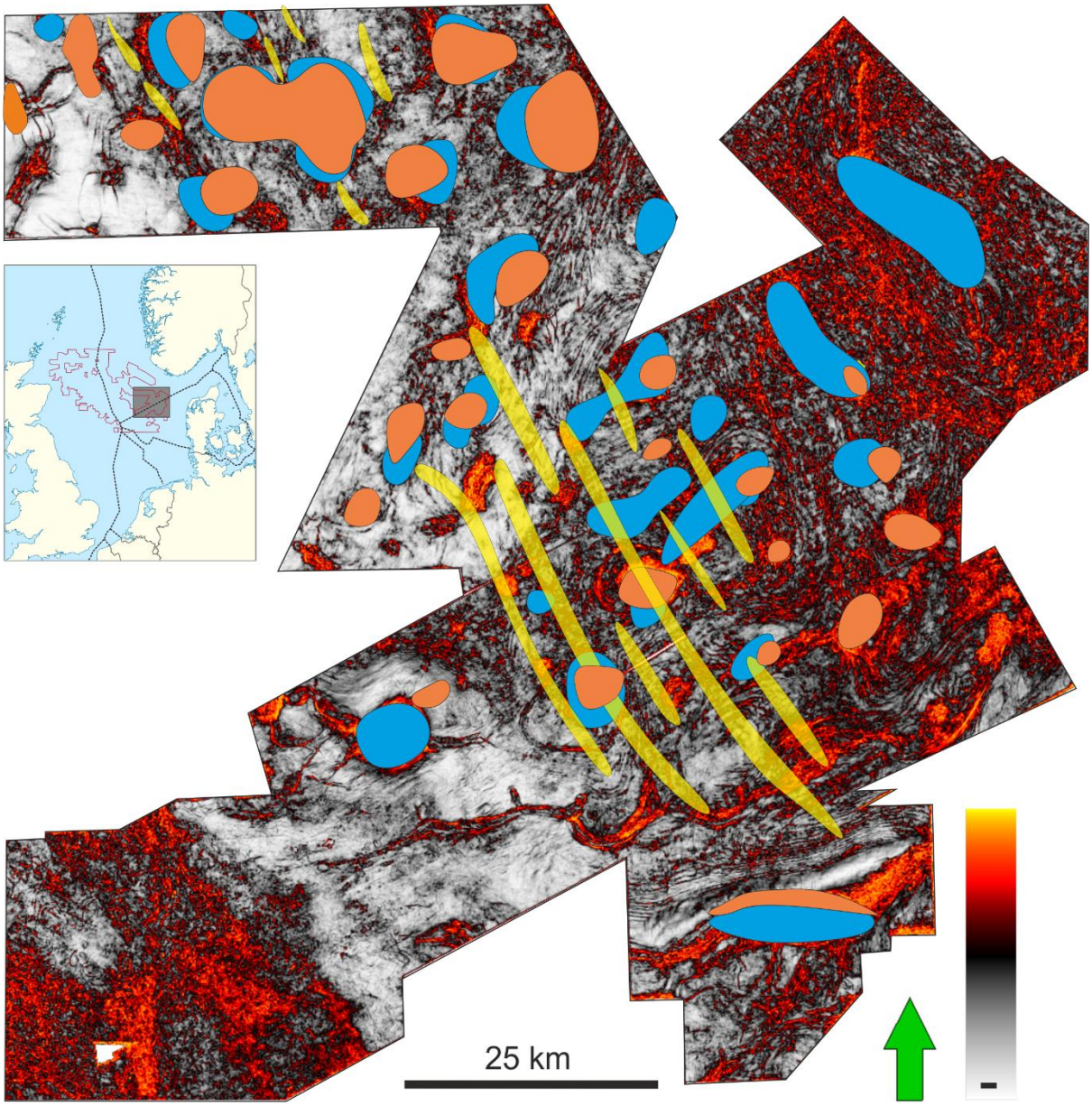

Figure 4.5: A variance attribute surface map of the Top Chalk surface in the study area highlighting the approximate positions of salt diapirs piercing the Top Chalk surface and mapped shallow gas accumulations, mainly Type I accumulations which are seen across the study area to be associated with salt diapirs. Important to note that not all diapirs are associated with a shallow gas accumulation. Type II shallow gas accumulations mapped in this study are less impacted by the salt diapirs and are thought to occur in shallow delta top sediments. Inset is a map of the North Sea showing the location of the mapped study area.

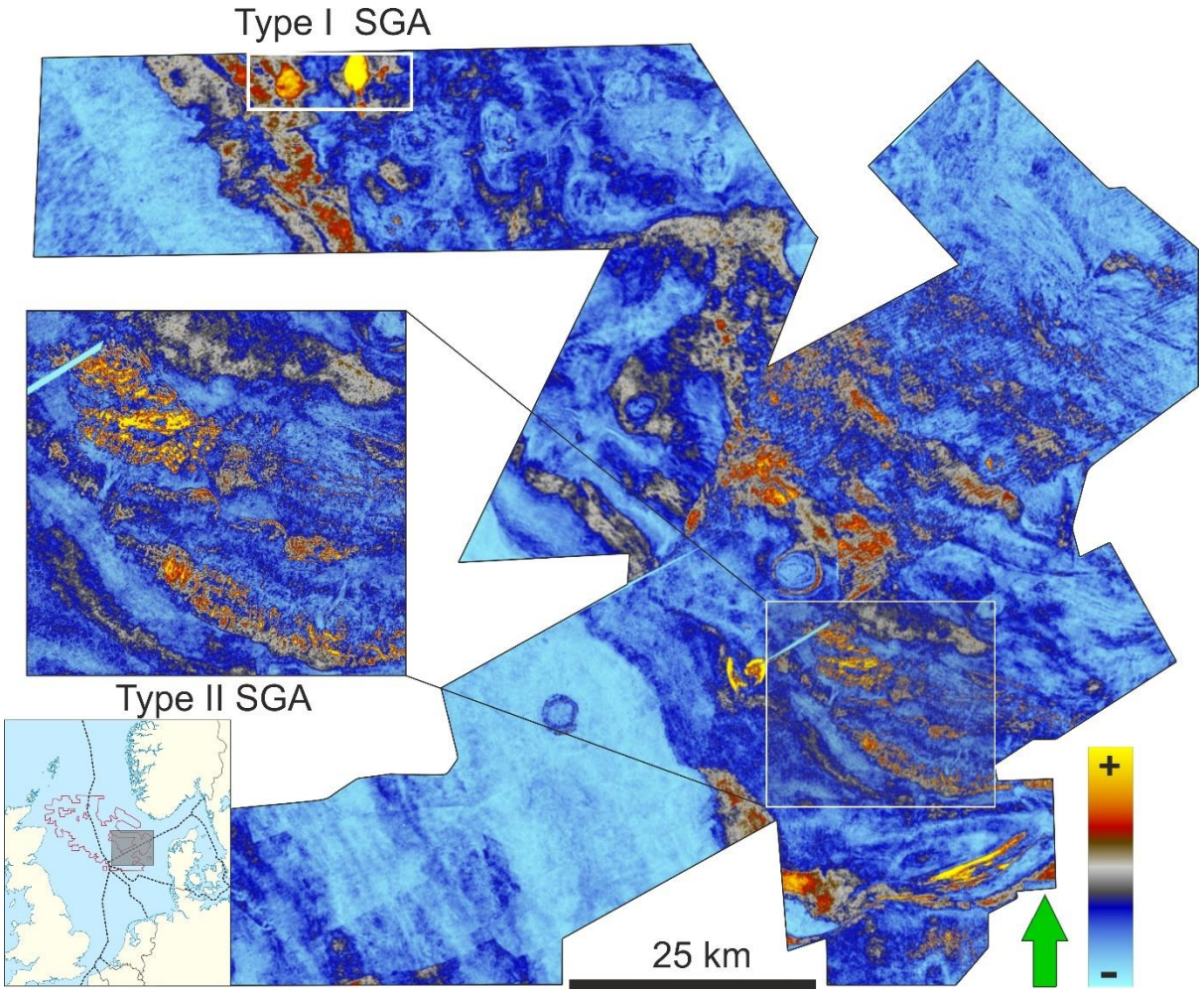

Figure 4.6: An RMS amplitude map at – 704 msTWT in the study area highlighting the settings and nature of both Type I and Type II shallow gas accumulations in the study area.

4.5.2 Type I: Bright Spot Anomalies Associated with Salt Diapirs

The first type of bright spot anomalies mapped in this study are often found directly associated with Zechstein Salt Diapirs in the study area. They are high amplitude seismic reflections termed bright spots and are thought to be enhanced due to the presence of gas within the sediments. This is because the presence of gas in a reservoir strongly affects the acoustic properties of the reservoir unit thereby creating a high amplitude anomaly within in the seismic data (Heggland, 1998; van den Boogaard & Hoetz, 2015; Muller et al., 2018). Geometrically, they appear as large discreet high amplitude sections discernible on seismic time slices and profiles (Figure 4.5). They occur widely within the study area and are found usually in low lying anticlines or fault dip closures often stacked in nature above the Zechstein salt diapirs associated with other focused fluid flow features such as pipes, gas chimneys, faults, and silica diagenetic boundaries. The accumulations are unevenly

distributed within the Cenozoic succession in sediments at depths between 350 – 900 ms TWT below the seabed. The bright spots reveal DHI characteristics such as bright spot, seismic attenuation, phase change, polarity reversal; seismic gas chimney and velocity pull down in places. The Type I shallow gas accumulations mapped are dispersed within the study area and geometrically, they vary in depth, area covered, trapping geometry and size in addition to the seismic characteristics. The lateral extent of these Type I anomalies can reach up to 5 km in length and are often found stacked characterized by high amplitude, associated with deep seated focused fluid flow features. The Type I anomalies are mainly associated with four types of direct hydrocarbon indicators (DHIs) according to their seismic character; bright spots (high amplitude anomalies), gas chimneys, seismic attenuation, and velocity push downs. In seismic time slices and seismic profiles analysed, the bright spots representing high amplitudes are localized on the seismic profiles and have been interpreted to indicate the presence of free gas in sediments on seismic data (Hilterman, 2001; Bacon et al., 2007; Brown., 2011). The rising of the salt diapirs by halokinesis is often associated with the deformation in the overburden post deposition which leads to the formation of structures necessary for the accumulation of the Type I shallow gas accumulations above the salt diapirs. The movement of salt diapirs also influences the creation of accommodation space and the maturation of source rocks within the study area (Hamberg et al., 2005). Faults induced by halokinesis strike in a NW-SE direction and are seen to be associated to the shallow gas by means of the bright spots concentrating along the fault flanks and tip where the faults terminate at the accumulations (Figure 4.6a).

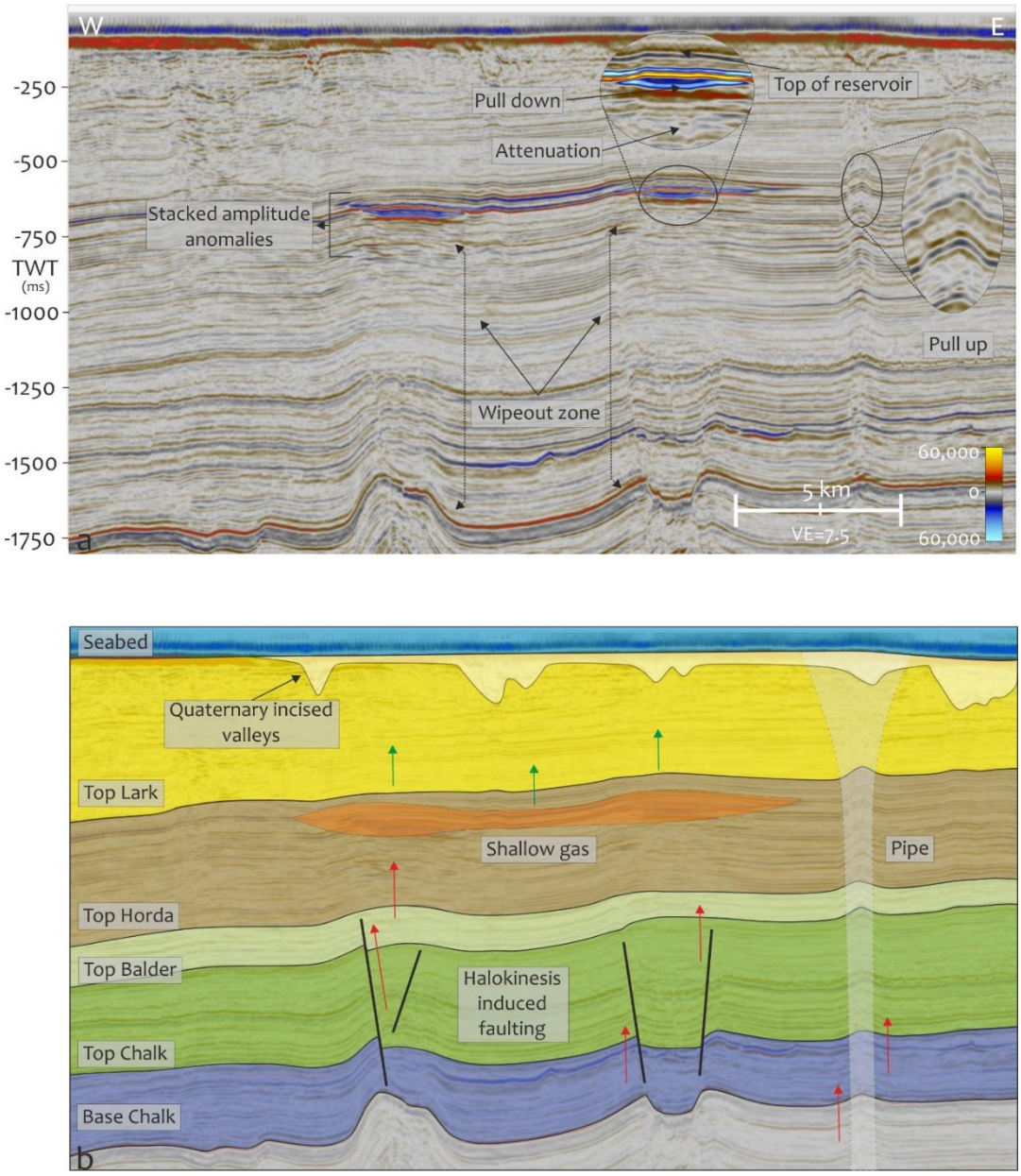

Figure 4.7: (a) shows an uninterpreted section from the PGS 3D MegaSurvey™ in two-way-time highlighting the main seismic character associated with the interpreted bright spots as shallow gas accumulations including a chimney (Wipeout zone), attenuation and pull down. The polarity of the seismic data used in this study is shown so that an increase in acoustic impedance at the seabed is represented by a positive amplitude red peak and the bright spots represented by a decrease in acoustic impedance is represented by a negative amplitude blue trough character. The pull up here is associated with high velocity infill of quaternary incised tunnel valleys after Haavik & Landro., (2014) rather than a pipe for the migration of hydrocarbons. (b) shows an interpreted version of (a) with the main stratigraphic intervals mapped for this study and the occurrence of the shallow gas accumulations within the Oligo-Miocene Lark formation. Note the relationship of the Zechstein salt diapirs piercing the Top Chalk surface and the location of normal faults induced by halokinesis which might serve as a migration route for deep thermogenic sources within the study area indicated by the red arrows. Also, the shallow plumbing within the study area includes the possible migration of hydrocarbons from shallow biogenic sources indicated by the green arrows. The location of the seismic line is shown in Figure 4.

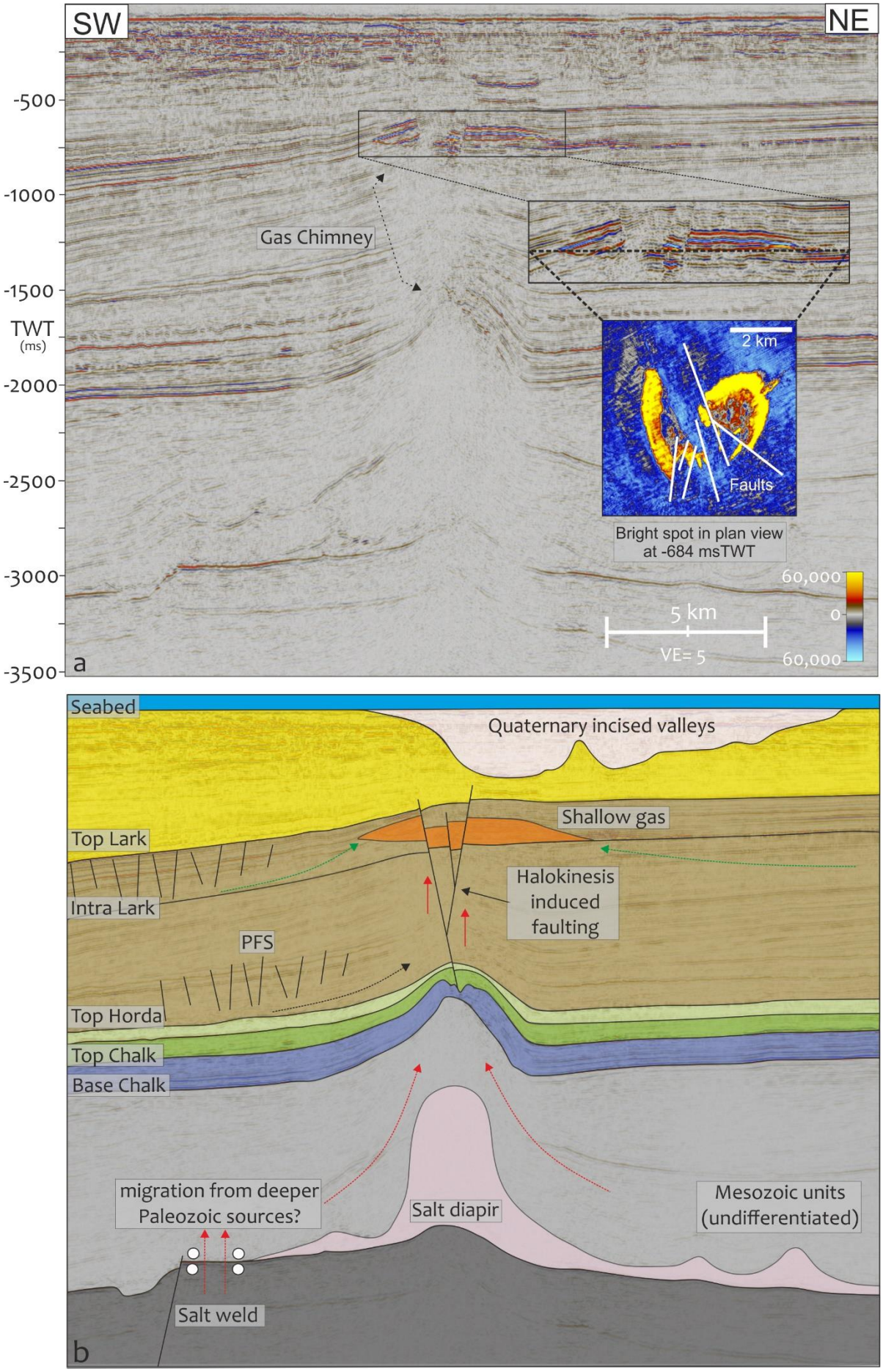
SW
NE
-500
-1000
-1500
TWT
(ms)
-2000
-2500
-3000
-3500
Gas Chimney
2 km
Faults
Bright spot in plan view
at -684 msTWT
60,000
0
60,000
5 km
VE= 5
a
Seabed
Quaternary incised valleys
Shallow gas
Top Lark
Intra Lark
Halokinesis
induced
faulting
PFS
Top Horda
Top Chalk
Base Chalk
migration from deeper
Paleozoic sources?
Salt diapir
Mesozoic units
(undifferentiated)
Salt weld
b

Figure 4.8: (a) An uninterpreted section from the PGS 3D MegaSurvey™ in two-way-time also highlighting the main seismic character associated with the interpreted bright spots as shallow gas accumulations and the view of the shallow gas in plan view with the associated fault demarcating the accumulations into compartments above the salt diapirs. (b) an interpretation of the section (a) above with the main lithostratigraphic horizons mapped and the stratigraphic position of the shallow gas within the Oligo-Miocene Lark formation and its association with the Zechstein salt diapir in the area. A migration is considered in this model from deeper Palaeozoic sources along salt welds and along salt flanks within the Mesozoic unit that form part of deep plumbing system in the study area indicated by the red arrows. A possible shallow plumbing system highlighting potential for migration from shallow biogenic sources is also highlighted in relation to the polygonal fault system thought to form a part of the shallow plumbing system indicated by the green arrows. The black arrows show potential for lateral migration from deeper thermogenic sources in the Central Graben area as demonstrated in the studies by Hamberg et al., (2005) and Ohm et al., (2006). The location of the seismic line is shown in Figure 3.

4.5.3 Type II: Isolated Bright Spot Anomalies in Delta Front Sediments

The second type of bright spots are seen often dispersed towards the easternmost (proximal) part of the study area, away from the piercing salt diapirs and are rarely associated with the underlying salt diapirs (Figure 4.7). They appear as bright, negative amplitude anomalies within a background of low amplitude seismic sections, often displaying the trough-over-peak pattern associated with gas charged units identified on seismic data (Muller et al., 2018; Hilterman et al., 2001). They are often isolated, in discreet pockets and only laterally continuous in places (Figure 4.7). The Type II anomalies are not restricted to a specific stratigraphic interval but occur at depths between -500 - -1000 msTWT corresponding to depths of about 500 m – 1Km below the seabed within Oligo-Miocene sediments of the Cenozoic Succession. However, the Type II anomalies are often restricted in vertical extent to about 12 – 15m (the maximum vertical resolution of the PGS 3D MegaSurvey™ data) and often lacking the stacking nature seen in Type I anomalies (Figure 4.7) which highlights the thin nature of the sands hosting these bright spots. These Type II bright spots anomalies are thought to indicate the accumulations of gas in shallow porous sediments and the charging of these sediments could have been possible either laterally or vertically through sub-seismic faults from either deeper thermogenic sources or shallow biogenic sources (Rasmussen et al., 2005). The Type II anomalies here are thought to be trapped in sands transported to the delta front which are intercalated within mudstone units that form the sealing units for these sands. During the Oligocene – Middle Miocene, the eastern Central North Sea basin was progressively filled by sediments

supplied by ancient rivers which fed large deltas along the eastern basin margin (Huuse., 2002) (Figure 4.8).

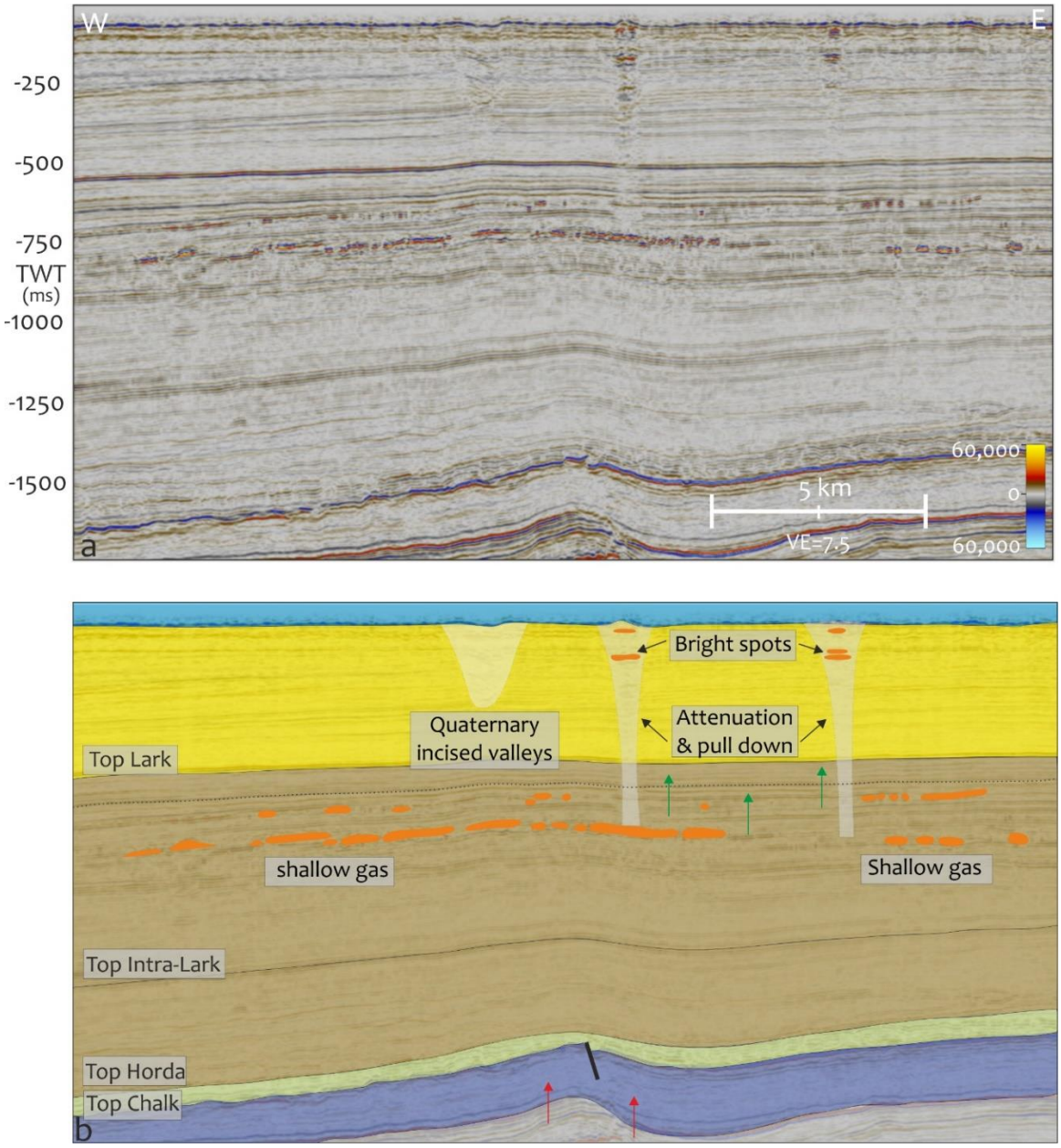

Figure 4.9: (a) shows an uninterpreted section from the PGS 3D MegaSurvey™ in two-way-time highlighting the main seismic character associated with the interpreted bright spots as shallow gas accumulations in delta top sediments. The shallow gas accumulations here appear in discreet mounded depositional features often elongate and parallel to the direction of slope depositions.

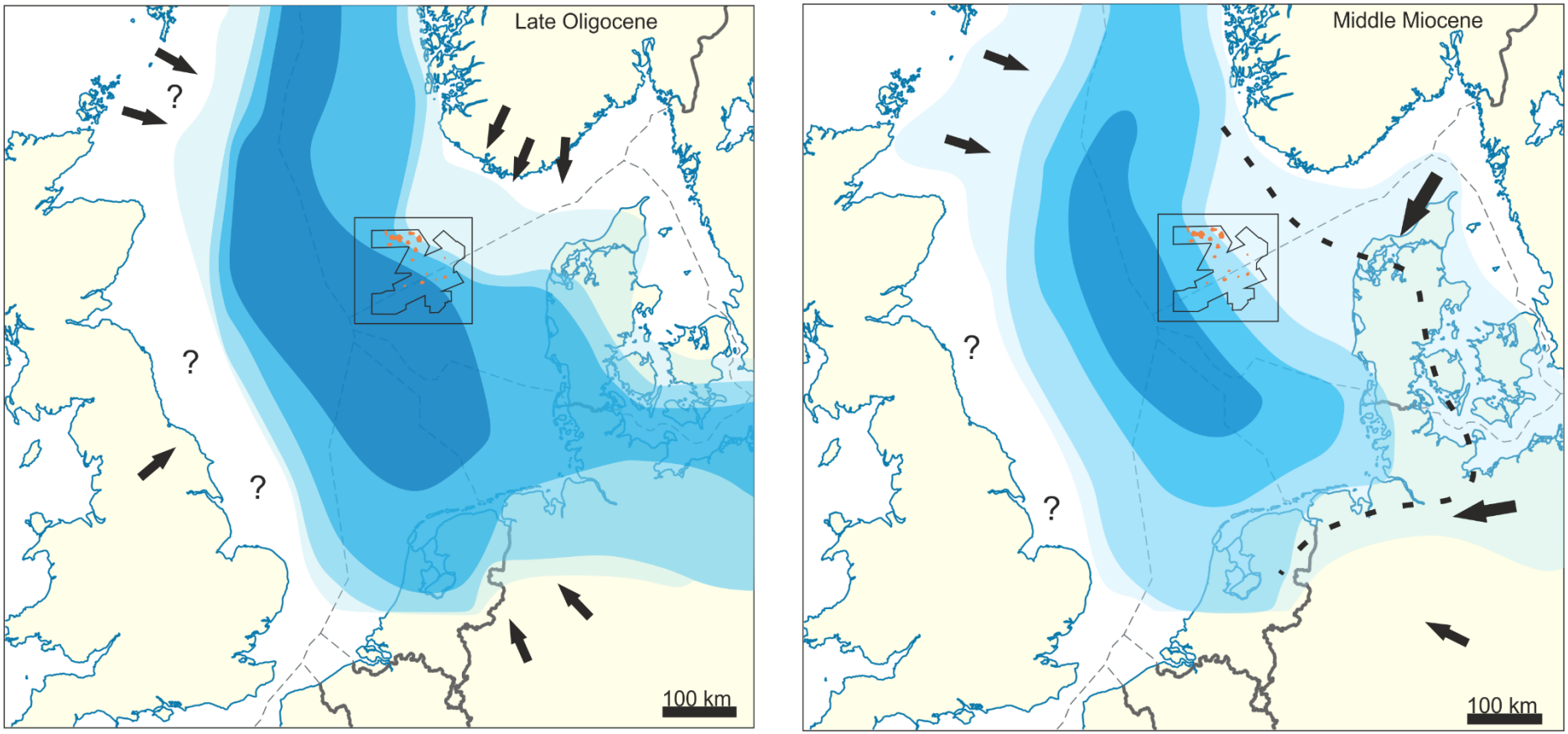

Figure 4.10: Late Oligocene and Middle Miocene paleogeographic maps after Huuse., (2002) with the approximate location of the mapped shallow gas accumulations within the Cenozoic succession in the eastern North Sea. Black arrows indicate major sediment supply sources for the Late Oligocene and Middle Miocene.

4.5.4 Shallow gas and other related focused fluid flow features

The **Type I & II** shallow gas accumulations mapped in this study for the eastern Central North Sea do not occur in isolation for most of the cases. They are seen to be in interaction with the hydrocarbon plumbing systems within the area associated with focused fluid flow features such as polygonal faults, pockmarks, sediment mounds, gas chimneys, sediment intrusions and silica diagenetic reaction fronts which all emanated from the flow of fluids in the subsurface. These fluid flow features therefore form a dynamic component of the sedimentary basin and the identification of each fluid flow feature associated with the shallow gas accumulations will be discussed in this section and their impact on the presence of shallow gas within the study area in subsequent sections.

4.5.4.1 *Polygonal Faults*

Polygonal faults occur typically in restricted stratigraphic intervals within fine grained mudstone dominated sections and are thought to have formed due to differential compaction during basin dewatering (Cartwright et al., 2003; 2007; Cartwright., 2011). They are hence a direct product of fluid flow within the basin and are often found associated with other fluid flow related phenomena such as pockmarks and diagenetic reaction fronts (Gay et al., 2006). Within the study area, polygonal faults are found in the Cenozoic section within the Horda and Lark formation.

4.5.4.2 *Pockmarks*

Pockmarks are circular/cone-like depressions associated with ascending fluids to seabed and they appear at the seabed as expressions of focused vertical fluid flow which occur predominantly in fine-grained mudstone dominated sections attributed to various geological structures and processes of formation such as joints, faults, faulted anticlines, buried channels, mud diapirs, current and tidal influences, gas hydrate dissolution and dissociation (King & Maclean., 1970; Hovland & Judd., 1988; Judd & Hovland., 1992; 2007; Hovland et al., 2005).

4.5.4.3 *Gas Chimneys & Pipes*

Gas chimneys are seismic artefacts which are vertical regions of low amplitude and acoustic masking on a seismic profile, while pipes are narrow vertical zones of stacked high amplitude anomalies within a seismic section (Berndt et al., 2003; Løseth et al., 2009).

4.5.4.4 *Clastic Sediment Remobilization and Injection*

Clastic sediment intrusions and extrusions are often the result of the forcible extrusion and injection of remobilised sandstone sediments which may have developed due to pore fluid overpressure in buried unconsolidated bodies within less permeable unit (Hurst et al., 2003). They form dykes or sills and cross-cut depositional stratigraphy and are often connected with high permeable units within otherwise low-permeability strata and form significant hydrocarbon reservoirs in sedimentary basins around the world (Andresen et al., 2012; Andresen & Clausen., 2014).

4.5.4.5 *Silica Diagenetic Reaction Fronts*

Diagenetic reaction fronts form due to the diagenesis and deformation of siliceous sediments from the transformation of biogenic silica (opal-A) to crystalline silica (opal-CT (Ireland et al., 2011). They are often found associated with other geological features such as polygonal faults, sandstone intrusions, submarine slope failures, pockmarks, and fluid expulsion (Davies & Cartwright., 2002; Malah et al., 2021, This study, Chapter 2).

4.5.5 TOC & Rock-Eval Pyrolysis Results

To obtain Geochemical information about the investigated section within the Lark formation, cutting samples from two wells 3/6-1 and 4/4-1 were analysed for Total Organic Carbon (TOC) and Rock-Evaluation pyrolysis for the mudstone sections of the Lark formation within the Cenozoic succession and integrated with Mineralogical Data for the same sample sets analysed by (Malah et al., 2021; This study, Chapter 2). The TOC & Rock-Eval results are summarized in Table 6 and analysed further in Figure 4.9. TOC values were also obtained for the interval under investigating within the Cenozoic section from well logs using CARPLOT software based on the methodology outlined by Passey et al., (1990) and the results are presented in Figure 9. The geochemical information obtained from the analysis of the cuttings samples is analysed to ascertain the hydrocarbon potential of the Lark formation and is presented in terms of the thermal maturity, and amount and type of organic matter. Furthermore, the hydrogen index (HI) and kerogen type are presented. TOC values were also obtained for both wells using the CARPLOT methodology. CARPLOT is sensitive to both log responses and to thermal maturity of the sample analysed (Murphy et al., 1995). The underlying algorithm in CARPLOT uses the Level of Maturity (LOM) index instead of the more familiar Vitrinite reflectance (VR) index and for the assessment of the following samples, a LOM of 8 corresponding to a VR value of ~ 0.56% was selected based on data from the rock-eval pyrolysis analysis (TOC vs S2) and the age of the mudstone samples from both wells 3/6-1 and 4/4-1 (Figure 4.9).

Well ID	Depth (m)	TOC (%)	S1 (mg HC/g)	S2 (mg HC/g)	S3 (mg CO_2/g)	HI (mg/g TOC)	OI (mg CO_2/g TOC)	T_{max} (° C)	PI
4/4-1	650	4.73	5.94	10.47	5.33	221.35	112.68	354	0.36
4/4-1	800	4.99	6.87	9.69	4.99	194.19	100.00	353	0.41
3/6-1	1050	4.85	1.74	5.16	4.87	106.39	100.41	425	0.25
3/6-1	1250	2.59	2.06	5.37	3.43	207.34	132.43	370	0.28

Table 6: Summary of Rock-Eval results from the analysis of cutting samples from well 3/6-1 and 4/4-1 within the study area.

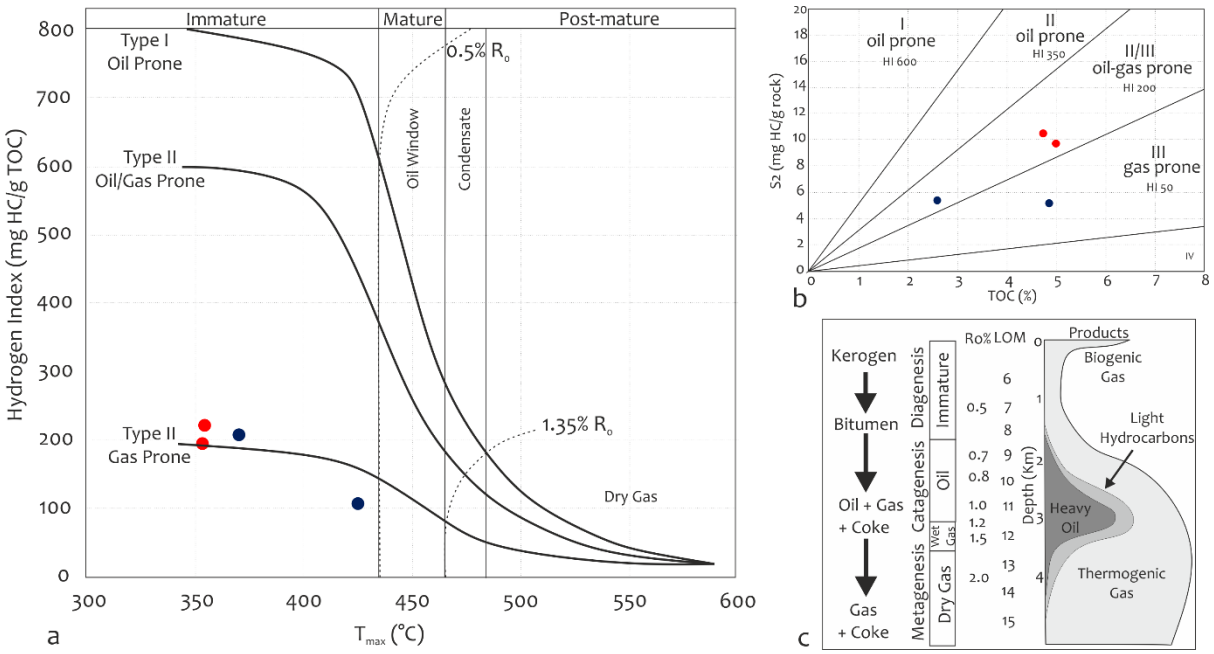

Figure 4.11: Kerogen type and maturity of the lark formation mudstones from Rock-Eval pyrolysis data shown in (a) the plot of Hydrogen Index (HI) versus Tmax. Also shown in (b) is a TOC versus Rock-Eval S2 plot which shows their relationship between and characterises the samples analysed as being of type II/III and type III organic matter type meaning they are oil-gas and gas prone. The red dots show samples for well 4/4-1 and the purple for samples from well 3/61. Shown in (c) a generalised thermal maturation plot after Clifford et al., (2003) showing typical depths at which kerogen is converted into liquid and gaseous hydrocarbons. The plot was instructive in the determination of the Level of Maturity (LOM) assigned to the sections analysed in both wells using the CARPLOT application.

4.5.5.1 *Thermal Maturity and Organic Richness of the Lark Formation*

The Rock-Eval data presented in Table 1 are used to assess the thermal maturity of the Lark formation within the study area. The Rock-eval Tmax values were used as an indicator for thermal maturity of the Cenozoic mudstones and these values range from 353 – 425 °C with a mean of 378 °C across the two sampled wells. Tmax values of less than 430 °C are indicative of an immature source (Copestake et al., 2003; Cornford., 2009). The Hydrogen and Oxygen indices (Table 6) suggests that the kerogen type is of terrestrial type II/III composition thought to be oil/gas prone. Although the samples analysed are considered immature, they have good to very good generative potential according to the S2 peaks and values analysed. TOC values are shown in table 6 and they range from 2.59 – 4.99 wt% and a mean of 4.29 wt% which is on a scale of 'good to very good' values for the mudstone sections according to industrial standards for the North Sea (Cornford., 2009). The TOC values are not surprising for a mudstone dominated sample and the values obtained here fall within the range of reported values obtained from core data for the Lark formation by

Sulsbrück & Toft., (2018). A further analysis for the potential of the Lark formation using the CARPLOT application agrees with the measured data for the TOC with average TOC values estimated to be between 1 – 5 % over the interval in both wells 3/6-1 and 4/4-1 analysed (Figure 4.10). A good agreement is also obtained between S2 values obtained by Rock-Eval pyrolysis (Table 6) and the estimation by the CARPLOT application indicating very good potential for the generation of hydrocarbons with values > 5.0 mg/g S2 over the interval in both wells analysed. It is worthy to note that although TOC values obtained by means of measurement in the lab shows further potential in well 4/4-1 below the depths of 700m, this potential is not borne out by the log analysis. The disparity seen from the measured and estimated values from the logs below 700m may be indicate of caving of the well cutting samples in the well.

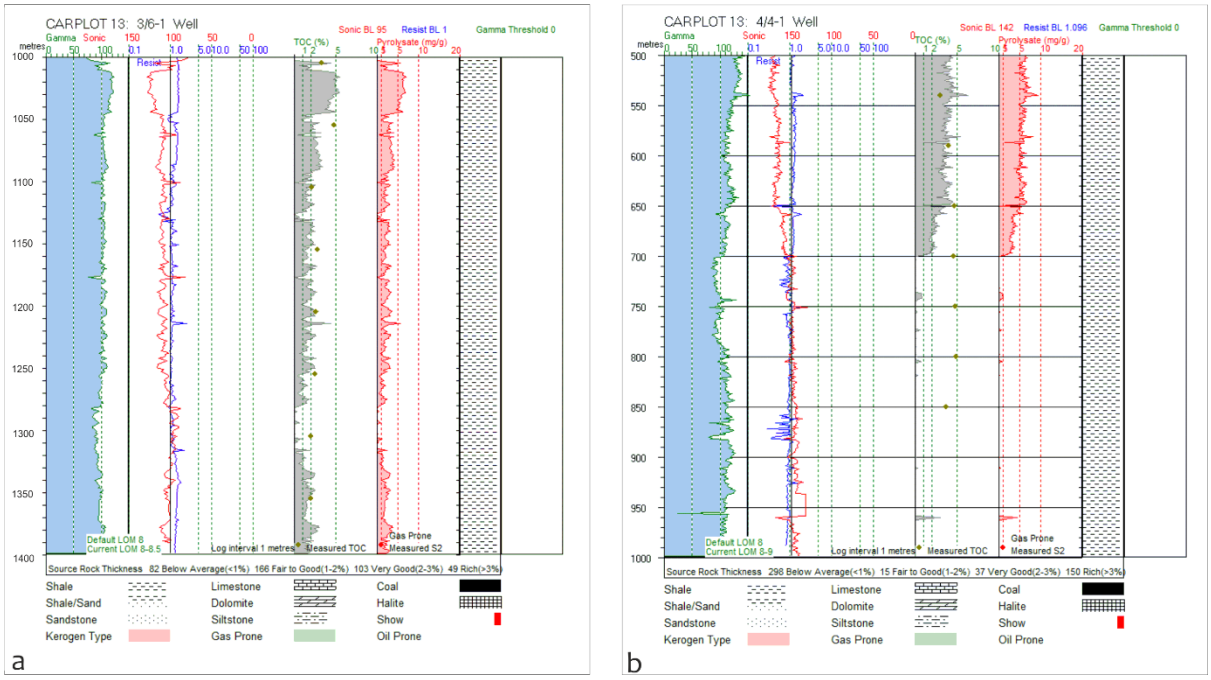

Figure 4.12: Source rock potential estimations based on well log responses for the intervals covering sections of the Cenozoic mudstones within the study area. (a) Log responses over an interval of 400 m (1000 – 1400m) in the well 3/6-1 indicating the average TOC and S2 (pyrolysate) estimations over the interval. (b) log responses over an interval of 500 m (500 – 1000m) in the well 4/4-1 indicating the average TOC and S2 (pyrolysate) estimations over the interval. Note potential of caving indicated below 700m in the well 4/4-1 analysis.

4.6 Discussion

The results presented in this study shows the evidence of shallow gas occurrence with respect to other focused fluid flow systems such as pockmarks, polygonal faults, gas chimneys and pipes in the CNS. The results also show the potential for generation of

biogenic gas from shallow sources within the shallow plumbing system in the CNS. The discussion will focus on highlighting the importance of the shallow gas mapped and other related fluid flow features and their implications to the Petroleum System of the eastern CNS.

4.6.1 Occurrence of shallow gas

As mentioned in the literature review, shallow gas occurrence in the CNS has been identified by several studies in the past by means of Direct Hydrocarbon Indicators (DHI's). The shallow gas occurrences have been uncharacterized on this part of the eastern CNS. This study characterizes the shallow gas anomalies and put them in the context of the petroleum system and hydrocarbon plumbing system of the eastern CNS into Type I and Type II anomalies according to their appearance and spatial distribution within the eastern CNS. On seismic data, both the Type I & II investigated bright spot anomalies are obvious features on RMS amplitude map and have similar characteristics to other such bright spot anomalies from other parts of the Central North Sea. These bright spot anomalies have been largely interpreted to be shallow gas accumulations due to their seismic character in several studies (Heggland, 1997; Schroot et al., 2003; Kuhlmann & Wong, 2008; ten Veen et al., 2014; Stuart & Huuse, 2012; Verweij et al., 2012, 2013; ten Veen et al., 2014; van Den Boogard & Hoetz, 2015; Williams & Gent., 2015; Clausen et al., 2015; Muller et al., 2018). The bright spot anomalies found throughout the study area (Figure 4.4), occur within the Oligo-Miocene succession in this study and are interpreted to be shallow gas accumulations trapped within sediments. The enhanced reflections (bright spots), and other seismic expressions such as gas chimneys, pipes, seismic attenuation, phase/polarity reversals and velocity pushdowns are all typical expressions of the presence of gas in sediments and form the seismic expressions related to shallow gas anomalies and fluid flow (Brown et al., 2011). However, it is noteworthy to mention that the presence of bright spots rarely outrightly indicates presence of gas within sediments and this is because other features such as coal beds, organic-rich mudstones, diatomaceous ooze, Bottom Simulating Reflectors (BSRs) and Opal-A/CT boundaries also create distinct bright spot anomalies with the signature trough-over-peak polarity (depending on the SEG convention) which largely indicates as a first pass, the presence of gas within sediments due to the impedance contrast between the reservoir hosting the gas and the surrounding

lithology (Ireland et al., 2011; Andresen & Huuse, 2011;). Beyond the identification of shallow gas anomalies using geophysical methods and primarily seismic data, evidence for the occurrence of shallow gas within marine sediments can be obtained using geochemical analysis of drilling mud, seabed sediment and seawater samples (Judd & Hovland, 1992; 2007). Although this study is limited by the identification of the occurrence of shallow gas employing only geophysical data, geochemical evidence for the occurrence of gas within shallow sediments have been reported for other parts of the CNS (Lichtschlag et al., 2018) and the production of shallow gas reservoirs from the Dutch sector of the CNS (van den Boogard & Hoetz., 2015).

4.6.2 Origin and sources of fluids

The results and observations from the study area indicates the presence of fluids involved in the formation of the shallow gas accumulations. These observations are used to constrain the origin of the fluids and discuss their relationships with the bright spot anomalies and other related fluid flow features within the context of the structural and stratigraphic setting of the eastern CNS.

The seismic evidence of widespread fluid flow features already gives credence to the presence of hydrocarbons and other fluid types such as biogenic hydrocarbons, pore fluids and even groundwater within the study area. The main source rock within the study area is the Upper Jurassic and Cretaceous Bo member of the Farsund formation which is age equivalent to the Kimmeridge Clay considered to be generating hydrocarbons from deep thermogenic sources (Kubala et al., 2003). The potential for lateral hydrocarbon migration from the Central Graben area up-dip into shallow traps located eastward on the Ringkobing-Fyn High has also been demonstrated for the eastern CNS area with the Siri Canyon and other canyons acting as effective drains for the generated hydrocarbons (Rasmussen et al., 2005; Hamberg et al., 2005; Ohm et al., 2006). Although the seismic data can be used to infer the main periods of fluid flow and fluid migration routes, what is not clear from the seismic data alone is the fluid sources. Even though fluid sources can be inferred to some extent from seismic data by such features as pockmarks, sediment mounds, sediment remobilization (Heggland, 1998; Andresen et al., 2008; 2011; Andresen & Clausen., 2014), it remains speculative. For this study, to evaluate the hypothesis for the possibility of the Cenozoic Mudstones analysed generating hydrocarbons in situ, well

cutting samples were analysed for thermal maturity and organic richness. The geochemical data was integrated with mineralogical data from Malah et al., (2021, This study, Chapter 2) for the same sample sets and interval and then analysed. The Cenozoic Mudstones analysed from the well cutting samples using XRD and QEMSCAN techniques by Malah et al., (This study, Chapter 2) suggests that the samples are dominated by clays (illite and mixed layer illite-smectite), silicates (quartz) and pyrite and other minerals in minor amounts including calcite, halite and sylvite.

From the TOC & Rock-eval pyrolysis results presented in Table 6 and Figures 4.9 & 4.10, we see in terms of overall organic richness that the mudstones from the well cutting samples have good to very good organic richness according to the TOC values based on industrial standards (Copestake et al., 2003; Conford., 2009). The Rock-Eval Tmax and S2 values were used as an indicator of thermal maturity and generative potential. The results indicate that although the organic matter contained in the samples are considered immature, they have good to very good generative potential and hence are likely to have contributed to the sources of fluids. These results are significant as it gives the potential for the consideration of a shallow biogenic source to be included in the shallow petroleum system of the eastern CNS. Often, the presence and role of organic matter in shallow sediments is overlooked and poorly studied and the origin/type of organic matter in the shallow sediments hardly ever established. However, the evidence for the type of organic matter is usually determined by Carbon Isotope analysis which is beyond the scope of this study. But results from the adjacent part of the eastern CNS within the Central Graben area from petroleum systems modelling and carbon isotope analysis carried out on samples from producing fields from the Dutch Sector and modelling from the German sector shows the possibility of a shallow biogenic source contributing to the accumulation of gas in the shallow sections (Verweij et al., 2012;2013; Teen Veen et al., 2014; Muller et al., 2020). Consequently, we posit that the evidence from the geochemical data indicates the potential for the generation of hydrocarbons within the Cenozoic mudstones in the eastern CNS.

The evidence for deep thermogenic sources of hydrocarbons within the plumbing system coming from pre-Cenozoic sources is evident with the presence of migration routes and gas chimneys observed on the seismic data. Mature candidate source rocks from the Palaeozoic and Mesozoic have also been studied for the study area along with

contributions from known source rocks charging major fields in the CNS from the Central Graben area (Hamberg et al., 2005; Hemmet, 2005; Ohm et al., 2006; Pedersen et al., 2006). The thermogenic fluids from these mature Palaeozoic and Mesozoic source rocks are a source of generating fluids which we believe to also be contributing to the shallow plumbing system and impacting the presence of the shallow gas anomalies within the study area. Due to the presence of an Opal-A/CT reaction front in the study area and occurring within the Oligo-Miocene succession, the likelihood of expelled pore water due to differential compaction impacting fluid flow and the shallow reservoirs cannot be discounted (Davies & Cartwright, 2007). The diagenesis of siliceous sediments leading to the transformation of amorphous opal (Opal-A) to well-ordered crystalline opal (Opal-CT) is known to be associated with fluid expulsion, multiple fracture populations, brecciation and cementation. The diagenesis can lead to the formation of fluid flow features such as polygonal faults which if not sealing, can serve as migration routes for hydrocarbons into the shallow reservoirs leading to the formation of the bright spot anomalies. From the analysis of the fluid sources in the study area, we infer that the fluid sources of major importance are the hydrocarbons, both thermogenic and biogenic and the expelled pore water. The bright spot anomalies characterised in this study and interpreted to be shallow gas accumulations are likely to contain a mixture of both thermogenic and biogenic gases.

4.6.3 Shallow gas & the hydrocarbon plumbing system in the eastern CNS

The bright spot anomalies in this study along with the other fluid flow related features (pockmarks, polygonal faults, etc) supports the evidence of a working hydrocarbon plumbing system within the eastern CNS along with other depositional elements such as the Siri Canyon. The shallow gas accumulations and the fluid flow features are employed here to facilitate an understanding of the evolution of the eastern CNS petroleum system. The hydrocarbon plumbing system is divided into a deep and a shallow system based on the sources of fluids, migration routes and timing.

4.6.3.1 *The deep plumbing system*

The deep hydrocarbon plumbing system associated with the shallow gas accumulations include the deep Palaeozoic and Mesozoic source rocks, the large regional faults, gas chimneys, the Palaeocene canyons, and the salt diapirs within the eastern CNS. This deep system is seen to be associated with the Type I shallow gas accumulations in the study

area. The deep system includes the upward migration of hydrocarbons from deep source rocks through deep seated large normal faults, salt welds and along the flank of salt diapirs which is evident by the stratal deformations and disturbances on seismic data appearing as gas chimneys or pipes and where they terminate at the seabed, they form sediment mounds and pockmarks on the seabed. The evidence for thermogenic hydrocarbons charging Paleogene Reservoirs in the eastern CNS is well established, with the Siri Canyon serving as an effective drain for the mature source rocks from the Central Graben area (Hamberg et al., 2005; Ohm et al., 2006). The Type I shallow gas anomalies in this study are seen to be directly linked to salt diapirs and the migration routes which form part of the deep-seated plumbing system believed to be charging shallow reservoirs within the Cenozoic succession. However, this does not discount the contribution of biogenic sources to charging the reservoirs as well as data from finger printing of such similar reservoirs indicate a 99% methane (dry gas) concentration (Rice & Claypool., 1981; Verweij et al., 2018). The intricate relationship between the Type I anomaly and the Zechstein salt and a listric normal fault charging the shallow reservoirs studied extensively by Clausen et al., (2015) in the study area and this represents a primary relationship of the deep-seated plumbing system along with the other critical elements in the study area (Malah et al., 2018).

4.6.3.2 *The shallow plumbing system*

The shallow hydrocarbon plumbing system is associated with the shallow features of the plumbing system such as polygonal faults, pockmarks, sediment remobilisation, and the salt diapirs. Where these features are found related to shallow gas accumulations within the shallow system, they provide evidence for the activity of fluids within the sections (Andresen & Huuse., 2011). The polygonal normal faults can transmit fluids either vertically or horizontally when they are not sealing due to reduced effective stress increasing their permeability (Cartwright., 1994; Cartwright et al., 2003; Wrona et al., 2017) and the formation of pockmarks often represent the expression of focused fluid flow (Andresen & Huuse., 2011). The pockmarks have been extensively studied by Andresen et al., (2008) and is attributed to thermogenic gas venting and sediment loading. The polygonal normal faults have been studied by Malah et al., (This study, chapter 3) and they have been attributed to be controlled by primarily by the evolution of the silica diagenetic reaction

boundary in the study area. The shallow system is associated with the Type II anomaly in this study and the anomalies appear discreetly in contrast to Type I anomalies. The gas charging these so-called bright spot anomalies we believe is a mixture of both a thermogenic and biogenic source within the study area. This is to say that the shallow plumbing system does not occur in isolation to the deep plumbing system highlighted earlier but rather, together, they form a comprehensive mechanism for the hydrocarbon plumbing system within the eastern CNS.

4.6.4 Model for a shallow gas petroleum system

Due to the availability of a large set of both 3D seismic and well data, results and observations allowed us to make inferences into generating a model which can be used for other passive continental margins around the world. The observations of the shallow gas anomalies and focused fluid flow features in the eastern CNS allowed for the evaluation of the basin in terms of its evolution (Andresen et al., 2012), although controls for the specific fluid flow features highlighted is still poorly understood and will require further research. For the conceptual model, the following assumptions (Table 7) and deductions from the analysis were employed:

Table 7: Summary of assumptions and deductions influencing the formation of shallow gas anomalies and key focused fluid flow features within the study area.

Main periods of fluid flow	Continuous, initially from the Mesozoic to Recent and then Paleocene to present day.
Fluid sources	Palaeocene to present day: Thermogenic oil and gas. Oligocene to middle Miocene: Thermogenic oil & gas, expelled pore water and biogenic gas. Present day: Thermogenic oil & gas, expelled pore water and biogenic gas.
Trigger & driving mechanisms	Overpressure build up remobilization due to differential loading Silica diagenesis and the onset of polygonal faulting Lateral transfer of pressure Thermogenic fluid venting Salt diapirism/Halokinesis

Migration routes	Primary: Deep seated faults and salt flanks Secondary: Diffused through PFS and sandstone intrusions.
Timing	Thermogenic: Late Miocene to Recent Biogenic: Recent

The simplified 2D model (Figure 4.11) puts the shallow gas anomalies and focused fluid flow features into the stratigraphic and depositional context of the eastern CNS. Several factors as highlighted in Table 7 control the development of the shallow gas anomalies and the focused fluid flow features within the eastern CNS. The controls impacting the shallow gas anomalies are to do with thermogenic and biogenic gas generation within the study area and the impact of salt diapirism creating migration pathways for the migration of hydrocarbons from the deep-seated plumbing systems. Sandstone intrusions widespread within the study area due to sediment remobilization have been studied extensively by Andresen & Clausen., (2014) and they also represent important fluid migration pathways where they occur in association with the shallow gas anomalies and polygonal normal faults. The shallow gas anomalies in this study are characterized and classified both as a potential hydrocarbon resource where they are located close to existing infrastructure and a shallow geohazard for the drilling of deep targets. Also, the model presented in this study further enhances our understanding of the petroleum system within the eastern CNS and can be beneficial in de-risking hydrocarbon exploration, geohazard assessment for the location of offshore wind farms and the subsurface storage of carbon dioxide.

Observations from the seismic reflection data influenced the model and suggests that the shallow reservoirs might have been charged from the deep source rock through the deep-seated fault networks above the Zechstein salt domes forming part of the deep plumbing system within the study area. Few of the shallow gas accumulations analysed are seen to be linked directly to these deep-seated faults. An assumption that will lend credence to the previous assertion is the evidence for the mixture of thermogenic and biogenic gas in similar reservoirs from the Dutch sector. Further, the shallow gas analysed occur within strata in the Lark formation deformed by intense polygonal faulting. The reduction of effective stress due to pore pressure collapse in polygonal faults causes them to transmit

fluids. This will allow for effective further migration of thermogenic sources and migration from shallower biogenic sources and form part of the shallow plumbing system. The relationship between polygonal faults and shallow gas have been confirmed in the Lower Congo Basin, Great South Basin in New Zealand, and the Norwegian Margin. A mechanism for the migration of hydrocarbons from both deep and shallow sources is inferred to be driven by a combination of trigger and driving mechanisms including overpressure build-up within the fine-grained mudstones of the Lark formation, remobilization of soft sediment due to differential loading, the lateral transfer of pressure due to fluid flow, silica diagenesis and the onset of polygonal faulting and salt diapirism within the study area. This has implications for shallow geohazard assessment, subsurface storage of carbon dioxide and hydrocarbon exploration within the study area and other similar settings.

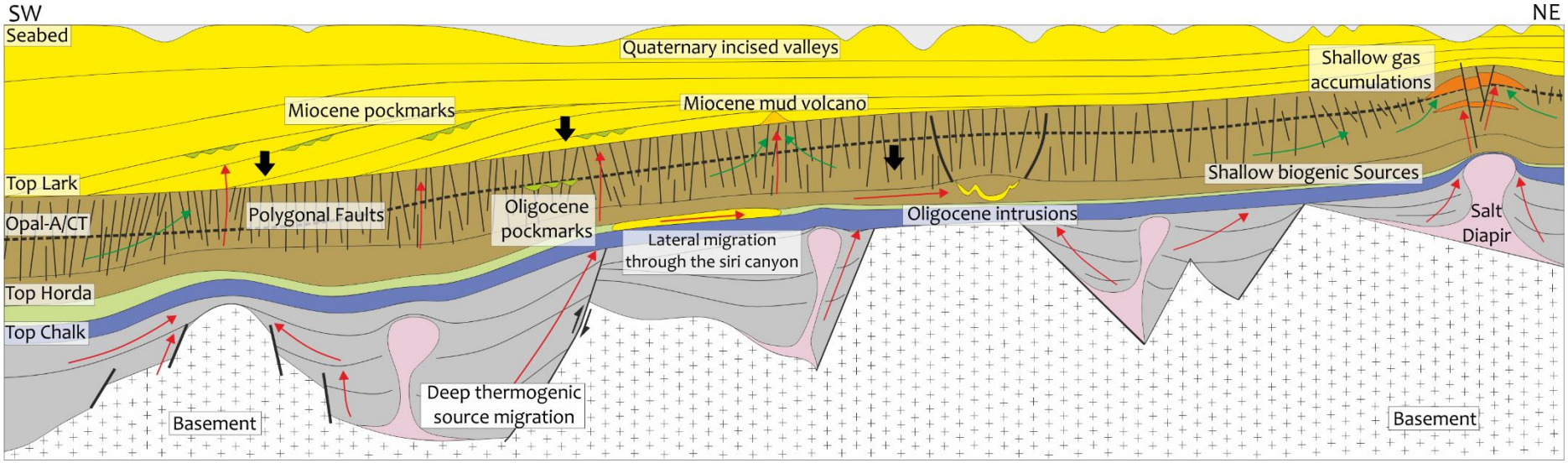

Figure 4.13: A simplified model southwest – northeast highlighting the occurrence of shallow gas and the other focused fluid flow features in the eastern Central North Sea. The model summarizes the intricate relationship between the shallow gas and the various fluid features including the polygonal fault systems, pockmarks, gas chimneys and pipes, sediment remobilization and silica diagenetic fronts. Red arrows indicate likely migration of hydrocarbons from deeper thermogenic sources and green arrows indicate migration from shallow biogenic sources. The significance of lateral fluid migration is also highlighted.

4.7 Conclusion

In this study, we document the occurrence and distribution of numerous bright spot anomalies on the high resolution PGS 3D MegaSurvey™ seismic data within the Cenozoic Section in the eastern CNS. These bright spot anomalies are interpreted to have been as a result of gas trapped within sediments in the shallow section of the study area. The shallow gas accumulations are classified based on their occurrence, spatial distribution, DHI characteristics and relationship with other fluid flow related features within the study area into **Type I and Type II**. The Type I shallow gas accumulations appear as bright spot anomalies on the seismic data associated with Zechstein salt diapirs within the study area and the Type II accumulations appear as isolated bright spot anomalies within Delta Front sediments. The Type I anomalies are more widely distributed within the study area while the Type II anomalies are restricted to the easternmost section of the study area towards the Delta Top. The investigation of these shallow gas anomalies allows us to incorporate the existence of these shallow gas systems into the petroleum system of the eastern CNS using the seismic stratigraphy of Michelsen et al., (1998) and lithostratigraphy of Schiøler et al., (2007). It is inferred that the shallow gas accumulations along with other fluid flow related features identified including gas pipes, chimneys, polygonal faults, pockmarks, silica diagenesis and sediment remobilisation all form a critical part of the hydrocarbon plumbing system within the study area.

The second aim of this study was to determine the sources of hydrocarbons charging the shallow reservoirs. Although the origin of the shallow gas accumulations is not clear, there is evidence of either a thermogenic or biogenic origin or both. Well cutting samples analysed for mudstone samples of the Lark formation hosting the shallow gas accumulations indicate that they are found to have very good organic matter content and generative potential. We can draw conclusions from these that there might be a potential for biogenic gas generation charging the shallow gas reservoirs. There is no well tests data from a well penetrating a shallow gas reservoir within the study area but evidence from the Dutch and German sectors of the Central North Sea suggests the contribution of a shallow biogenic source to producing shallow gas reservoirs (teen even et al., 2014; Muller et al., 2018). Whilst this study did not confirm explicitly the type of organic matter within the study area, it did partially substantiate the evidence for a very good organic matter

content and generative potential for the studied section and this is an area of future research within the study area.

4.8 Acknowledgements

This work is part of MM's Ph.D. research, which is funded by the Petroleum Technology Development Fund (PTDF) Scholarship of Nigeria (Research Grant: PTDF/ED/OSS/PHD/MMG/889/16). We are incredibly grateful to PGS for generously donating seismic datasets and Schlumberger for donating Petrel licenses and TGS for granting access to the Facies Map Browser to the University of Manchester for well data. We would further like to thank the Norwegian Petroleum Directorate (NPD) for making available cuttings samples for analysis.

4.9 References

Ahmadi, Z. M., Sawyers, M., Kenyon-Roberts, S., Stanworth, C. W., Kugler, K. A., Kristensen, J., & Fugelli, E. M. G. (2003). Paleocene. *The Millennium Atlas: Petroleum Geology of the Central and Northern North Sea. Geological Society, London*, 235–259.

Andresen, K. J., & Clausen, O. R. (2014). An integrated subsurface analysis of clastic remobilization and injection; a case study from the Oligocene succession of the eastern North Sea. *Basin Research*, *26*(5), 641–674. https://doi.org/10.1111/bre.12060

Andresen, K. J., Huuse, M., & Clausen, O. R. (2008). Morphology and distribution of Oligocene and Miocene pockmarks in the Danish North Sea -implications for bottom current activity and fluid migration. *Basin Research*, *20*(3), 445–466. https://doi.org/10.1111/j.1365-2117.2008.00362.x

Andresen, K. J., Huuse, M., Schødt, N. H., Clausen, L. F., & Seidler, L. (2011). Hydrocarbon plumbing systems of salt minibasins offshore Angola revealed by three-dimensional seismic analysis. *AAPG Bulletin*, *95*(6), 1039–1065. https://doi.org/10.1306/12131010046

Andresen, K. J. (2012). Fluid flow features in hydrocarbon plumbing systems: What do they tell us about the basin evolution? *Marine Geology*, *332–334*, 89–108. https://doi.org/10.1016/j.margeo.2012.07.006

Andresen, K. J., Clausen, O. R., & Huuse, M. (2009). A giant (5.3 × 107 m3) middle Miocene (c. 15 Ma) sediment mound (M1) above the Siri Canyon, Norwegian-Danish Basin: Origin and significance. *Marine and Petroleum Geology*, *26*(8), 1640–1655. https://doi.org/10.1016/j.marpetgeo.2009.02.005

Bacon, M. (Michael), Simm, R. (Robert), & Redshaw, T. (Terence). (2007). *3-D seismic interpretation*.

Berndt, C., Bunz, S., & Mienert, J. (2003). Polygonal fault systems on the mid-Norwegian margin: a long-term source for fluid flow. *Geological Society, London, Special Publications*, *216*(1), 283–290. https://doi.org/10.1144/GSL.SP.2003.216.01.18

Brown, A. R. (2011). Interpretation of Three-Dimensional Seismic Data. *AAPG Memoir*, *42*, 1–528. https://doi.org/10.1190/1.9781560802884

Brown, A. R., Sheriff, R. E., Geldart, L. P., Weimer, P., & Slatt, R. M. (2004). Interpretation of Three-Dimensional Seismic Data. *Continuing Education*. http://library.seg.org/doi/pdf/10.1190/1.9781560802884.index

Brown, K. M. (1990). The nature and hydrogeologic significance of mud diapirs and diatremes for accretionary systems. *Journal of Geophysical Research*, *95*(B6), 8969. https://doi.org/10.1029/JB095iB06p08969

Cartwright, J. (2007). The impact of 3D seismic data on the understanding of compaction, fluid flow and diagenesis in sedimentary basins. *Journal of the Geological Society*, *164*(5), 881–893. https://doi.org/10.1144/0016-76492006-143

Cartwright, J. A. (1994). Episodic basin-wide fluid expulsion from geopressured shale sequences in the North Sea Basin. In *Geology* (Vol. 22, Issue 5, pp. 447–450). https://doi.org/10.1130/0091-7613(1994)022<0447:EBWFEF>2.3.CO;2

Cartwright, J. A., & Lonergan, L. (1996). Volumetric contraction during the compaction of mudrocks: A mechanism for the development of regional-scale polygonal fault systems. *Basin Research*, *8*(2), 183–193. https://doi.org/10.1046/j.1365-2117.1996.01536.x

Cartwright, J. (2011). Diagenetically induced shear failure of fine-grained sediments and the development of polygonal fault systems. In *Marine and Petroleum Geology* (Vol. 28, Issue 9, pp. 1593–1610). Elsevier. https://doi.org/10.1016/j.marpetgeo.2011.06.004

Cartwright, J., & Huuse, M. (2005). 3D seismic technology: The geological "Hubble." In *Basin Research* (Vol. 17, Issue 1, pp. 1–20). Blackwell Science Ltd. https://doi.org/10.1111/j.1365-2117.2005.00252.x

Cartwright, J., James, D., & Bolton, A. (2003). The genesis of polygonal fault systems: a review. *Geological Society, London, Special Publications*, *216*(1), 223–243. https://doi.org/10.1144/GSL.SP.2003.216.01.15

Clausen, O. R., Andresen, K. J., Mauritzen, E. K., Connolly, D., & Korstgård, J. A. (2015). Hanging-wall deformation and gas-migration associated to a major salt detaching fault in the Norwegian Danish Basin. *Journal of Structural Geology*, *79*, 90–109. https://doi.org/10.1016/j.jsg.2015.08.003

Clausen, O. R., & Huuse, M. (1999). Topography of the Top Chalk surface on- and offshore Denmark. *Marine and Petroleum Geology*, *16*(7), 677–691. https://doi.org/10.1016/S0264-8172(99)00003-3

Copestake, P., Sims, A., Crittenden, S., & Hamar, G. (2003). *The Millennium Atlas: petroleum geology of the central and northern North Sea*. https://www.academia.edu/download/54483353/Atlas_fig12p5.pdf

Cornford, C. (2009). Source Rocks and Hydrocarbons of the North Sea. *Petroleum Geology of the North Sea: Basic Concepts and Recent Advances: Fourth Edition*, 376–462. https://doi.org/10.1002/9781444313413.CH11

Davies, R. J., & Cartwright, J. (2002). A fossilized Opal A to Opal C/T transformation on the northeast Atlantic margin: Support for a significantly elevated palaeogeothermal gradient during the Neogene? *Basin Research*, *14*(4), 467–486. https://doi.org/10.1046/j.1365-2117.2002.00184.x

Davies, R., Letters, J. C.-E., and P. S., (2007). Kilometer-scale chemical reaction boundary patterns and deformation in sedimentary rocks. *Elsevier*. Retrieved October 2, 2021, from https://www.sciencedirect.com/science/article/pii/S0012821X07004670

Davis, A. M. (1992). Shallow gas: an overview. *Continental Shelf Research*, *12*(10), 1077–1079. https://doi.org/10.1016/0278-4343(92)90069-V

Deegan, C. E., & Scull, B. J. (1977). A standard lithostratigraphic nomenclature for the Central and Northern North Sea / compiled by C.E. Deegan and B.J. Scull. *A STANDARD LITHOSTRATIGRAPHIC NOMENCLATURE FOR THE CENTRAL AND NORTHERN NORTH SEA.*, 36.

Dudley D. Rice, G. E. C. (1981). Generation, Accumulation, and Resource Potential of Biogenic Gas. *AAPG Bulletin*, 65. https://doi.org/10.1306/2F919765-16CE-11D7-8645000102C1865D

Duranti, D., Hurst, A., Bell, C., Groves, S., & Hanson, R. (2002). Injected and remobilized Eocene sandstones from the Alba Field, UKCS: core and wireline log characteristics. *Petroleum Geoscience*, *8*(2), 99–107. https://doi.org/10.1144/PETGEO.8.2.99

Gay, A., Lopez, M., Cochonat, P., Séranne, M., Levaché, D., & Sermondadaz, G. (2006). Isolated seafloor pockmarks linked to BSRs, fluid chimneys, polygonal faults and stacked Oligocene-Miocene turbiditic palaeochannels in the Lower Congo Basin. *Marine Geology*, *226*(1–2), 25–40. https://doi.org/10.1016/j.margeo.2005.09.018

Goffey, G., Attree, M., Curtis, P., Goodfellow, F., Lynch, J., MacKertich, D., Orife, T., & Tyrrell, W. (2018). New exploration discoveries in a mature basin: Offshore Denmark. *Petroleum Geology Conference Proceedings*, *8*(1), 287–306. https://doi.org/10.1144/PGC8.1

Haavik, K. E., & Landrø, M. (2014). Iceberg ploughmarks illuminated by shallow gas in the central North Sea. *Quaternary Science Reviews*, *103*, 34–50. https://doi.org/10.1016/J.QUASCIREV.2014.09.002

Hamberg, L., Dam, G., Wilhelmson, C., & Ottesen, T. G. (2005). Palaeocene deep-marine sandstone plays in the Siri Canyon, offshore Denmark-southern Norway. In *Petroleum Geology Conference Proceedings* (Vol. 6, Issue 0, pp. 1185–1198). https://doi.org/10.1144/0061185

Heggland, R. (1997). Detection of gas migration from a deep source by the use of exploration 3D seismic data. *Marine Geology*, *137*(1–2), 41–47. https://doi.org/10.1016/S0025-3227(96)00077-1

Heggland, R. (1998). Gas seepage as an indicator of deeper prospective reservoirs. A study based on exploration 3D seismic data. *Marine and Petroleum Geology*, *15*(1), 1–9. https://doi.org/10.1016/S0264-8172(97)00060-3

Hemmet, M. (2005). The hydrocarbon potential of the Danish Continental Shelf. In *Petroleum Geology: North-West Europe and Global Perspectives – Proceedings of the 6th Petroleum Geology Conference* (Vol. 6, Issue 1, pp. 85–97). Geological Society of London. https://doi.org/10.1144/0060085

Hilterman, F. (2001). Seismic amplitude interpretation. In *Quantitative Seismology-Theory and Methods* (Vol. 1). Society of Exploration Geophysicists and European Association of Geoscientists and Engineers. https://doi.org/10.1190/1.9781560801993.ch9

Hovland, M., Svensen, H., & Forsberg, C. (2005). Complex pockmarks with carbonate-ridges off mid-Norway: products of sediment degassing. *Marine Geology*. http://www.sciencedirect.com/science/article/pii/S0025322705001180

Hovland, M., Hill, A., & Stokes, D. (1997). The structure and geomorphology of the Dashgil mud volcano, Azerbaijan. *Geomorphology*, *21*(1), 1–15. https://doi.org/10.1016/S0169-555X(97)00034-2

Hurst, A., Cartwright, J., Huuse, M., Jonk, R., Schwab, A., Duranti, D., & Cronin, B. (2003). Significance of large-scale sand injectites as long-term fluid conduits: evidence from seismic data. *Geofluids*, *3*(4), 263–274. https://doi.org/10.1046/j.1468-8123.2003.00066.x

Huuse, M., Le Heron, D. P., Dixon, R., Redfern, J., Moscariello, a., & Craig, J. (2012). Glaciogenic reservoirs and hydrocarbon systems: an introduction. *Geological Society, London, Special Publications*, *368*(1), 1–28. https://doi.org/10.1144/SP368.19

Huuse, M., Lykke-Andersen, H., & Michelsen, O. (2001). Cenozoic evolution of the eastern Danish North Sea. *Marine Geology*, *177*(3–4), 243–269. https://doi.org/10.1016/S0025-3227(01)00168-2

Huuse, M. (2002). Late Cenozoic palaeogeography of the eastern North Sea Basin: Climatic vs tectonic forcing of basin margin uplift and deltaic progradation. *Bulletin of the Geological Society of Denmark*, *49*(2), 145–170.

Huuse, M., & Mickelson, M. (2004). Eocene sandstone intrusions in the Tampen Spur area (Norwegian North Sea Quad 34) imaged by 3D seismic data. *Marine and Petroleum Geology*, *21*(2), 141–155. https://doi.org/10.1016/j.marpetgeo.2003.11.018

Ireland, M. T., Davies, R. J., Goulty, N. R., & Carruthers, D. (2011). Structure of a silica diagenetic transformation zone: The Gjallar Ridge, offshore Norway. *Sedimentology*, *58*(2), 424–441. https://doi.org/10.1111/j.1365-3091.2010.01170.x

Japsen, P. (1999). Overpressured Cenozoic shale mapped from velocity anomalies relative to a baseline for marine shale, North Sea. *Petroleum Geoscience*, *5*(4), 321–336. https://doi.org/10.1144/petgeo.5.4.321

Japsen, P., Green, P. F., Nielsen, L. H., Rasmussen, E. S., & Bidstrup, T. (2007). Mesozoic-Cenozoic exhumation events in the eastern North Sea Basin: A multi-disciplinary study based on palaeothermal, palaeoburial, stratigraphic and seismic data. *Basin Research*, *19*(4), 451–490. https://doi.org/10.1111/j.1365-2117.2007.00329.x

Jarsve, E. M., Eidvin, T., Nystuen, J. P., Faleide, J. I., Gabrielsen, R. H., & Thyberg, B. I. (2015). The Oligocene succession in the eastern North Sea: Basin development and depositional systems. *Geological Magazine*, *152*(4), 668–693. https://doi.org/10.1017/S0016756814000570

Jordt, H., Faleide, J. I., Bjørlykke, K., & Ibrahim, M. T. (1995). Cenozoic sequence stratigraphy of the central and northern North Sea Basin: tectonic development, sediment distribution and provenance areas. *Marine and Petroleum Geology*, *12*(8), 845–879. https://doi.org/10.1016/0264-8172(95)98852-V

Judd, A. G., & Hovland, M. (1992). The evidence of shallow gas in marine sediments. *Continental Shelf Research*, *12*(10), 1081–1095. https://doi.org/10.1016/0278-4343(92)90070-Z

Judd, A., & Hovland, M. (2007). Seabed fluid flow: The impact on geology, biology, and the marine environment. In *Seabed Fluid Flow: The Impact on Geology, Biology, and the Marine Environment*. Cambridge University Press. https://doi.org/10.1017/CBO9780511535918

King, L. H., & MacLean, B. (1970). Pockmarks on the Scotian Shelf. *Geological Society of America Bulletin*, *81*(10), 3141. https://doi.org/10.1130/0016-7606(1970)81[3141:POTSS]2.0.CO;2

Knox, R. W. O., & Holloway, S. (1992). Paleogene of the central and northern North Sea. In *Lithostratigraphic nomenclature of the UK North Sea* (p. 206).

Kubala, M., Bastow, M. A., Thompson, S., Scotchman, I. C., & Øygard, K. (2003). Geothermal regime, petroleum generation and migration. In *The Millennium Atlas: petroleum geology of the central and northern North Sea*.

Kuhlmann, G., & Wong, T. E. (2008). Pliocene paleoenvironment evolution as interpreted from 3D-seismic data in the southern North Sea, Dutch offshore sector. *Marine and Petroleum Geology*, *25*(2), 173–189. https://doi.org/10.1016/j.marpetgeo.2007.05.009

Lichtschlag, A., Cevatoglu, M., Connelly, D. P., James, R. H., & Bull, J. M. (2018). Increased Fluid Flow Activity in Shallow Sediments at the 3 km Long Hugin Fracture in the Central North Sea. *Geochemistry, Geophysics, Geosystems*, *19*(1), 2–20. https://doi.org/10.1002/2017GC007181

Lonergan, L., Cartwright, J., Laver, R., & Staffurth, J. (1998). Polygonal faulting in the Tertiary of the central North Sea: implications for reservoir geology. *Geological Society, London, Special Publications*, *127*(1), 191–207. https://doi.org/10.1144/GSL.SP.1998.127.01.14

Løseth, H., Gading, M., & Wensaas, L. (2009). Hydrocarbon leakage interpreted on seismic data. *Marine and Petroleum Geology*, *26*(7), 1304–1319. https://doi.org/10.1016/j.marpetgeo.2008.09.008

Michelsen, O., Thomsen, E., Danielsen, M., Heilmann-Clausen, C., Jordt, H., & Laursen, G. V. (1998). Cenozoic Sequence Stratigraphy in the Eastern North Sea. *Mesozoic and Cenozoic Sequence Stratigraphy of European Basins*. https://doi.org/10.2110/pec.98.02.0091

Malah, M., Huuse, M., & Kane, I. (2018). Characterization of shallow hydrocarbon accumulations in the central North Sea. In *80th EAGE Conference and Exhibition 2018* (Vol. 2018, No. 1, pp. 1-5). European Association of Geoscientists & Engineers. https://doi.org/10.3997/2214-4609.201801049

Miller, K. G., Kominz, M. A., Browning, J. V., Wright, J. D., Mountain, G. S., Katz, M. E., Sugarman, P. J., Cramer, B. S., Christie-Blick, N., & Pekar, S. F. (2005). The

phanerozoic record of global sea-level change. *Science*, *310*(5752), 1293–1298. https://doi.org/10.1126/science.1116412

Müller, S., Arfai, J., Jähne-Klingberg, F., Bense, F., & Weniger, P. (2020). Source rocks of the German Central Graben. *Marine and Petroleum Geology*, *113*, 104120. https://doi.org/10.1016/J.MARPETGEO.2019.104120

Müller, S., Reinhardt, L., Franke, D., Gaedicke, C., & Winsemann, J. (2018). Shallow gas accumulations in the German North Sea. *Marine and Petroleum Geology*, *91*, 139–151. https://doi.org/10.1016/j.marpetgeo.2017.12.016

Murphy, N. J., Sauer, M. J., & Armstrong, J. P. (1995). Toarcian source rock potential in the North Celtic Sea Basin, offshore Ireland. *Geological Society, London, Special Publications*, *93*(1), 193–207. https://doi.org/10.1144/GSL.SP.1995.093.01.14

NIGOGA: The Norwegian Guide to Organic Geochemical Analyses. http://www.npd. no/engelsk/nigoga/default.htm (Last accessed 2019).

Norwegian Petroleum Directorate (NPD). Available online: http://www.npd.no/en/ (Last accessed 2018).

Ohm, S. E., Karlsen, D. A., Roberts, A., Johannessen, E., & Høiland, O. (2006). The Palaeocene sandy Siri Fairway: An efficient "pipeline" draining the prolific Central Graben? *Journal of Petroleum Geology*, *29*(1), 53–82. https://doi.org/10.1111/j.1747-5457.2006.00053.x

Overeem, I., Weltje, G. J., Bishop-Kay, C., & Kroonenberg, S. B. (2001). The Late Cenozoic Eridanos delta system in the Southern North Sea Basin: A climate signal in sediment supply? *Basin Research*, *13*(3), 293–312. https://doi.org/10.1046/j.1365-2117.2001.00151.x

Passey, Q. R., Creaney, S., Kulla, J. B., Moretti, F. J., & Stroud, J. D. (1990). A practical model for organic richness from porosity and resistivity logs. In *American Association of Petroleum Geologists Bulletin* (Vol. 74, Issue 12, pp. 1777–1794). Geoscience World. https://doi.org/10.1306/0c9b25c9-1710-11d7-8645000102c1865d

Pedersen, J. H., Karlsen, D. A., Backer-Owe, K., Lie, J. E., & Brunstad, H. (2006). The geochemistry of two unusual oils from the Norwegian North Sea: implications for new source rock and play scenario. *Petroleum Geoscience*, *12*(1), 85–96. https://doi.org/10.1144/1354-079305-658

Rasmussen, E., Vejbæk, O., Bidstrup, T., Piasecki, S., & Dybkjær, K. (2005). Late Cenozoic depositional history of the Danish North Sea Basin: implications for the petroleum

systems in the Kraka, Halfdan, Siri and Nini fields. In *Petroleum Geology: North-West Europe and Global Perspectives – Proceedings of the 6th Petroleum Geology Conference* (pp. 1347–1358). https://doi.org/10.1144/0061347

Römer, M., Wenau, S., Mau, S. & M. V.-G., (2017). Assessing marine gas emission activity and contribution to the atmospheric methane inventory: A multidisciplinary approach from the Dutch Dogger Bank seep area. *Wiley Online Library*, *18*(7), 2617–2633. https://doi.org/10.1002/2017GC006995

Rose, P., Byerley, G., Vaughan, O., Cater, J., Rea, B. R., Spagnolo, M., & Archer, S. (2016). Aviat: A Lower Pleistocene shallow gas hazard developed as a fuel gas supply for the Forties Field. *Geological Society, London, Petroleum Geology Conference*, *8*, PGC8.16. https://doi.org/10.1144/PGC8.16

Schiøler, P., Andsbjerg, J., Clausen, O. R., Dam, G., Dybkjær, K., Hamberg, L., Heilmann-Clausen, C., Johannessen, E. P., Kristensen, L. E., Prince, I., & Rasmussen, J. A. (2007). Lithostratigraphy of the Palaeogene - Lower Neogene succession of the Danish North Sea. In *Geological Survey of Denmark and Greenland Bulletin* (Issue 12). https://doi.org/10.34194/geusb.v12.5249

Schroot, B. M., & Schüttenhelm, R. T. E. (2003). Shallow gas and gas seepage: Expressions on seismic and other acoustic data from the Netherlands North Sea. *Journal of Geochemical Exploration*, *78–79*, 305–309. https://doi.org/10.1016/S0375-6742(03)00112-2

Stewart, S. A. (2007). Salt tectonics in the North Sea Basin: a structural style template for seismic interpreters. *Geological Society, London, Special Publications*, *272*(1), 361–396. https://doi.org/10.1144/GSL.SP.2007.272.01.19

Stolt, R., & Benson, A. (1986). *Seismic migration: Theory and practice*.

Stuart, J. Y., & Huuse, M. (2012). 3D seismic geomorphology of a large Plio-Pleistocene delta - "Bright spots" and contourites in the Southern North Sea. *Marine and Petroleum Geology*, *38*(1), 143–157. https://doi.org/10.1016/j.marpetgeo.2012.06.003

Sulsbrück, H. & Toft, J. (2018). A new observation of a bio siliceous opal bearing sequence in the Miocene Lark Formation in the Danish North Sea.

Sun, Q., Wu, S., Cartwright, J., & Dong, D. (2012). Shallow gas and focused fluid flow systems in the Pearl River Mouth Basin, northern South China Sea. *Marine Geology*, *315*, 1–14. https://doi.org/10.1016/j.margeo.2012.05.003

Svendsen, J. B., Hansen, H. J., Staermose, T., & Engkilde, M. K. (2010). Sand remobilization and injection above an active salt diapir: the Tyr sand of the Nini Field, Eastern North Sea. *Basin Research*, *22*(4), 548–561. https://doi.org/10.1111/j.1365-2117.2010.00480.x

Teen Veen, J. H., Verweij, H., Bruin, G. De, Geel, K., & Donders, T. H. (2014). *Integrated Exploration Workflow for Maturing the Shallow Gas Play*. *10595*, 10–12. http://www.searchanddiscovery.com/documents/2014/10595veen/ndx_veen.pdf

Thöle, H., Gaedicke, C., Kuhlmann, G., & Reinhardt, L. (2014). Late Cenozoic sedimentary evolution of the German North Sea – A seismic stratigraphic approach. *Newsletters on Stratigraphy*, *47*(3), 299–329. https://doi.org/10.1127/0078-0421/2014/0049

Van den Boogaard, M., & Hoetz, G. (2012). Shallow Gas Play in the Netherlands Takes Off. *74th EAGE Conference & Exhibition 2012*, *June 2012*, 4–7. https://doi.org/10.3997/2214-4609.20148764

Van den Boogaard, M., & Hoetz, G. (2015). Seismic characterisation of shallow gas in The Netherlands. *Abstract FORCE Seminar Stavanger 8-9 April 2015*, *April 2015*, 1–3. www.dana-petroleum.com

Vejbæk, O. V. (1997). Dybe strukturer i danske sedimentære bassiner. *Geologisk Tidsskrift*, *4*(4), 1–31.

Verweij, J. M., Nelskamp, S. N., Ten Veen, J. H., De Bruin, G., Geel, K., & Donders, T. H. (2018). Generation, migration, entrapment, and leakage of microbial gas in the Dutch part of the Southern North Sea Delta. *Marine and Petroleum Geology*, *97*, 493–516. https://doi.org/10.1016/J.MARPETGEO.2018.07.034

Verweij, J. M., Veen, J. H. Ten, Bruin, G. De, Nelskamp, S. N., Donders, T., Kunakbayeva, G., & Geel, K. (2012). Shallow Gas Migration and Trapping in the Cenozoic Eridanos Delta Deposits, Dutch Offshore. *74th European Association of Geoscientists and Engineers Conference and Exhibition 2012 Incorporating SPE EUROPEC 2012: Responsibly Securing Natural Resources*, cp-293-00875. https://doi.org/10.3997/2214-4609.20148871

Verweij, J. M., Nelskamp, S., & Sarmiento, M. A. G. (2013). Timing and Distribution of Biogenic Gas Generation in the Shallow Gas Play in the Dutch Offshore. *75th European Association of Geoscientists and Engineers Conference and Exhibition 2013 Incorporating SPE EUROPEC 2013: Changing Frontiers*, cp-348-00053. https://doi.org/10.3997/2214-4609.20130100

Walters, C. C., Isaksen, G. H., & Peters, K. E. (2003). Applications of Light Hydrocarbon Molecular and Isotopic Compositions in Oil and Gas Exploration. *Analytical Advances for Hydrocarbon Research*, 247–266. https://doi.org/10.1007/978-1-4419-9212-3_10

Walters, C. C., Isaksen, G. H., & Peters, K. E. (2003). Applications of Light Hydrocarbon Molecular and Isotopic Compositions in Oil and Gas Exploration. *Analytical Advances for Hydrocarbon Research*, 247–266. https://doi.org/10.1007/978-1-4419-9212-3_10

Williams, J., … C. G.-I. C. on F. and T., & 2015, undefined. (n.d.). Shallow Gas Offshore Netherlands-the role of faulting and implications for CO2 storage. *Earthdoc.Org*. Retrieved August 3, 2021, from https://www.earthdoc.org/content/papers/10.3997/2214-4609.201414058

Wrona, T., Jackson, C. A. L., Huuse, M., & Taylor, K. G. (2017). Silica diagenesis in Cenozoic mudstones of the North Viking Graben: physical properties and basin modelling. *Basin Research*, *29*, 556–575. https://doi.org/10.1111/bre.12168

Zanella, E., Coward, M.P., 2003. Structural framework. In: Evans, D., Armour, C. G. A., Bathurst, P. (Eds.), T. M. A. P. G. of the C. and, & Sea., N. N. (2003). *The Millennium Atlas: Petroleum Geology of the Central and Northern North Sea* (pp. 45–59).

Ziegler, P. A. (1992). North Sea rift system. *Tectonophysics*, *208*(1–3), 55–75. https://doi.org/10.1016/0040-1951(92)90336-5

Chapter 5

5.1 Summary & Conclusions

To summarise, this study employed the use of seismic, petrophysical well data, mineralogical and geochemical evidence to analyse multifaceted subsurface fluid flow phenomena associated with the hydrocarbon plumbing systems in the eastern Central North Sea. Specifically, this study investigates the eastern CNS in terms silica diagenesis, polygonal fault systems and shallow gas accumulations. By combining multiple data types and different methodologies, this study attempted to analyse fully the following research questions:

- Identifying and documenting the extent of silica diagenesis in the eastern Central North Sea to understand the controls on silica diagenesis within the NDB.
- Determine the influence of silica diagenesis on the physical host rock properties and establish its relationship to polygonal faulting.
- Characterize the existence and distribution of comparable shallow gas accumulations in the eastern Central North Sea and compare to adjacent parts and investigate the influence of polygonal fault as a migration pathway.

To investigate the above objectives, analytical techniques employed for this study include traditional 3D seismic interpretation approaches and analytical techniques such as XRD, QEMSCAN, TOC and RockEval pyrolysis were employed. The summary for the main findings of each paper (chapter -2, -3 & -4) for the main papers in this study are presented below by means of a brief overview and the main findings and conclusions.

5.1.1 Paper 1: Silica diagenesis in Cenozoic Mudstones of the eastern Central North Sea: Physical properties and the effect of salt diapirism.

Brief overview: This paper focused on the identification and characterization of a silica diagenetic boundary on seismic data within the eastern Central North Sea. Silica diagenesis has been proven to play a significant role in understanding host rock properties of siliceous sediments in numerous hydrocarbon basins of the world. Silica diagenesis involves a two-step process which involves first, the conversion of biogenic silica (Opal-A) to crystalline silica of cristobalite or tridymite (CT) and secondly, the conversion of Opal-CT to Quartz

((Williams et al., 1985; Isaacs, 1981; Keller & Isaacs, 1985). The most important to seismic studies is the first step, involving the change of biogenic silica (Opal-A) to Opal-CT which is often associated with a loss in porosity leading to an increase in the density of the host rock which in turns leads to an increase in p-wave velocity thereby affecting the acoustic properties of the host rock unit and producing a distinct seismic character mappable over hundreds to thousands of kilometres on seismic data.

Main findings & conclusions: In this study, we employed the use of a combination of techniques including 3D seismic mapping, petrophysical well log investigation, and analysing samples from well cuttings using x-ray diffraction (XRD) and quantitative evaluation of minerals by scanning electron microscope (QEMSCAN) techniques to identify and map out the presence of a silica diagenetic boundary for the first time in the eastern Central North Sea over an area of ~20,000 km^2. The identified silica diagenetic boundary is found to be associated with numerous polygonal faults within the area and we posit that it is not a bottom simulating reflector (BSR). The identified silica diagenetic reaction boundary is not parallel to the present-day seabed and as such is thought not to be in equilibrium with the present-day seabed, indicating that the silica diagenetic boundary is fossilized and has seized to be active. We also presented a link to the fossilization of the silica diagenetic boundary to the local salt diapirism by Zechstein evaporites which affected the thermal equilibrium of the study area locally and led to the fossilization of the reaction front and preservation of both Opal-A and Opal-CT within the host rock.

5.1.2 Paper 2: Growth and propagation of polygonal normal faults due to silica diagenesis in the eastern Central North Sea

Brief overview: Silica diagenesis is a two-step process involving the transformation of biogenic silica (Opal-A) to crystals of Cristobalite or Tridymite (Opal-CT) and the subsequent change of Opal-CT to crystals of quartz. The first step is known to impact the chemical and mechanical properties of the host rock lithology and influence the style of deformation. Silica diagenesis therefore plays a critical role in the formation of polygonal fault systems, which have been widely studied in numerous sedimentary basins of the

world. Polygonal faults are often low displacement normal faults commonly found within fine grained successions of sedimentary basins around the world and they are made up of a network of faults forming a system of interconnected faults termed 'Polygonal Fault Systems' (PFS) which are non-tectonic in origin. A link between silica diagenesis and the development of polygonal normal fault systems is still a subject of debate and here, we study the growth and propagation of a network of polygonal fault systems due to silica diagenesis. In this paper, we analysed the role diagenesis plays in the nucleation of such normal faults by means of a topological analysis of the polygonal system hosted within the Cenozoic mudstones in the eastern Central North Sea to investigate the evolution (nucleation, growth, and propagation) of such faults through spatial, temporal, and kinematic analysis of the host rock interval by the use of 3D seismic and well data.

Main findings & conclusions: In this study, we studied the evolution of the polygonal fault systems and the relationship with a silica diagenetic reaction front over an area of 3,000 Km^2. We divide the hosting unit along a northeast – southwest trend into three segments A, B & C to understand the evolution of the polygonal fault systems across three key surfaces by generating strike and dip direction plots for each interval using the Georose software application. We present a model summarising our findings and the polygonal fault systems are thought to have nucleated contemporaneously with the formation of the Opal-A/CT reaction front due to a diagenetically induced shear failure within the Oligo-Miocene Lark formation. The polygonal faults subsequently grow and propagate upward primarily through gravitational loading and are thought to have ceased further growth since the Miocene (except for a few active faults), which is also contemporaneous with the fossilization of the Opal-A/CT reaction front within the study area.

5.1.3 Paper 3: Shallow gas accumulations, focused fluid flow features and geochemical characterization of Cenozoic mudstones in the eastern Central North Sea

Brief overview: This paper focused on the characterisation of the numerous shallow gas accumulations visible on the 3D seismic data within the study area. Shallow hydrocarbon accumulations, often referred to as shallow gas which can be either of thermogenic or biogenic origin have been reported for adjacent parts of the Central North Sea with some

producing shallow gas fields in the Dutch sector of the CNS. Shallow gas is a critical part of the hydrocarbon plumbing systems of many sedimentary basins and is a tool used extensively in analysing a basin and for geohazard assessment.

Main findings & conclusions: In this study, we document the occurrence and distribution of twenty-six such shallow gas accumulations in the eastern Central North Sea and analyse their impact to the hydrocarbon plumbing system and fluid flow of the study area using a range of techniques including traditional 3D seismic amplitude mapping, petrophysical well log investigation and the analysis of well cuttings samples for total organic carbon content (TOC) and Rock-eval pyrolysis to ascertain organic matter content and thermal maturity of the Cenozoic mudstones found to be hosting 95% of the identified shallow gas accumulations. Employing the 3D seismic analysis by means of direct hydrocarbon indicators (DHIs) screening to map the spatial and temporal distribution of the shallow gas, we classified the shallow gas within the study area into two main types: Type I and Type II. The Type I shallow gas anomalies are often found associated with the Zechstein salt diapirs within the study area while the Type II anomalies are found in discreet pockets within Delta Front sediments. Analysis of well cuttings samples indicate that the Cenozoic mudstones have an average organic matter richness of 5% which is within the range of other similar studies and indicate a very good generative potential which does not rule out the contribution of biogenic gas to the shallow gas accumulations in addition to thermogenic gas from deeper sources within the study area.

Appendix

6.1 Data Inventory, sampled intervals and tools/techniques used in data analysis

Table 8: Database employed in this study and analytical techniques used for well 4/4-1.

S/N		Well	Sample ID	Depth (m)	Seismic	Wireline	XRD	QEMSCAN	TOC	RE
1		4/4-1	441-1	540	•	•	•	•	•	
2		4/4-1	441-2	550	•	•	•			
3		4/4-1	441-3	560	•	•	•			
4		4/4-1	441-4	570	•	•	•			
5		4/4-1	441-5	580	•	•	•			
6		4/4-1	441-6	590	•	•	•			
7		4/4-1	441-7	600	•	•	•	•	•	
8		4/4-1	441-8	610	•	•	•			
9		4/4-1	441-9	620	•	•	•			
10		4/4-1	441-10	630	•	•	•			
11		4/4-1	441-11	640	•	•	•			
12		4/4-1	441-12	650	•	•	•	•	•	•
13		4/4-1	441-13	660	•	•	•			
14		4/4-1	441-14	670	•	•	•			
15		4/4-1	441-15	680	•	•	•			
16		4/4-1	441-16	690	•	•	•			
17		4/4-1	441-17	700	•	•	•	•	•	
18		4/4-1	441-18	710	•	•	•			
19		4/4-1	441-19	720	•	•	•			
20		4/4-1	441-20	730	•	•	•			
21		4/4-1	441-21	740	•	•	•			
22		4/4-1	441-22	750	•	•	•	•	•	
23		4/4-1	441-23	760	•	•	•			
24		4/4-1	441-24	770	•	•	•			

25		4/4-1	441-25	780	•	•	•			
26		4/4-1	441-26	790	•	•	•			
27		4/4-1	441-27	800	•	•	•	•	•	•
28		4/4-1	441-28	810	•	•	•			
29		4/4-1	441-29	820	•	•	•			
30		4/4-1	441-30	830	•	•	•			
31		4/4-1	441-31	840	•	•	•			
32		4/4-1	441-32	850	•	•	•	•	•	
33		4/4-1	441-33	860	•	•	•			
34		4/4-1	441-34	870	•	•	•			
35		4/4-1	441-35	880	•	•	•			
36		4/4-1	441-36	890	•	•	•			
37		4/4-1	441-37	900	•	•	•	•	•	

Table 9: Database employed in this study and analytical techniques used for well 3/6-1.

S/N	Well	Sample ID	Depth (m)	Seismic	Wireline	XRD	QEMSCAN	TOC	RE
1	3/6-1	361-1	810	•	•	•		•	
2	3/6-1	361-2	820	•	•	•			
3	3/6-1	361-3	840	•	•	•			
4	3/6-1	361-4	860	•	•	•		•	
5	3/6-1	361-5	880	•	•	•			
6	3/6-1	361-6	900	•	•	•		•	
7	3/6-1	361-7	920	•	•	•			
8	3/6-1	361-8	940		•	•			
9	3/6-1	361-9	950	•	•	•		•	
10	3/6-1	361-10	960	•	•	•			
11	3/6-1	361-11	980	•	•	•			
12	3/6-1	361-12	990	•	•	•			
13	3/6-1	361-13	1000	•	•	•		•	
14	3/6-1	361-14	1020		•	•			

15	3/6-1	361-15	1040	•	•	•			
16	3/6-1	361-16	1050	•	•	•		•	
17	3/6-1	361-17	1060	•	•	•			
18	3/6-1	361-18	1070	•	•	•			
19	3/6-1	361-19	1080	•	•	•			
20	3/6-1	361-20	1090	•	•	•			
21	3/6-1	361-21	1100	•	•	•		•	
22	3/6-1	361-22	1110	•	•	•			
23	3/6-1	361-23	1120	•	•	•			
24	3/6-1	361-24	1130	•	•	•			
25	3/6-1	361-25	1140	•	•	•			
26	3/6-1	361-26	1150	•	•	•		•	•
27	3/6-1	361-27	1160	•	•	•			
28	3/6-1	361-28	1170	•	•	•			
29	3/6-1	361-29	1180	•	•	•			
30	3/6-1	361-30	1190	•	•	•			
31	3/6-1	361-31	1200	•	•	•		•	
32	3/6-1	361-32	1210	•	•	•			
33	3/6-1	361-33	1220	•	•	•			
34	3/6-1	361-34	1230	•	•	•			
35	3/6-1	361-35	1240	•	•	•			
36	3/6-1	361-36	1250	•	•	•		•	•
37	3/6-1	361-37	1260	•	•	•			
38	3/6-1	361-38	1270	•	•	•			
39	3/6-1	361-39	1280	•	•	•			
40	3/6-1	361-40	1290	•	•	•			
41	3/6-1	361-41	1300	•	•	•		•	
42	3/6-1	361-42	1310	•	•	•			
43	3/6-1	361-43	1320	•	•	•			
44	3/6-1	361-44	1330	•	•	•			
45	3/6-1	361-45	1340	•	•	•			

46	3/6-1	361-46	1350	•	•	•		•	
47	3/6-1	361-47	1360	•	•	•			
48	3/6-1	361-48	1370	•	•	•		•	
49	3/6-1	361-49	1380	•	•	•			
50	3/6-1	361-50	1390	•	•	•			

Table 10: Database employed in this study and analytical techniques used for well 3/7-7.

S/N	Well	Sample ID	Depth (m)	Seismic	Wireline	XRD	QEMSCAN	TOC	RE
1	3/7-7	377-1	1350	•	•	•	•	•	•
2	3/7-7	377-2	1360	•	•	•			
3	3/7-7	377-3	1370	•	•	•			
4	3/7-7	377-4	1380	•	•	•			
5	3/7-7	377-5	1390	•	•	•			
6	3/7-7	377-6	1400	•	•	•	•	•	
7	3/7-7	377-7	1410	•	•	•			
8	3/7-7	377-8	1420	•	•	•			
9	3/7-7	377-9	1430	•	•	•			
10	3/7-7	377-10	1440	•	•	•			
11	3/7-7	377-11	1450	•	•	•	•	•	
12	3/7-7	377-12	1460	•	•	•			
13	3/7-7	377-13	1470	•	•	•			
14	3/7-7	377-14	1480	•	•	•			
15	3/7-7	377-15	1490	•	•	•			
16	3/7-7	377-16	1500	•	•	•	•	•	
17	3/7-7	377-17	1510	•	•	•			
18	3/7-7	377-18	1520	•	•	•			
19	3/7-7	377-19	1530	•	•	•			
20	3/7-7	377-20	1540	•	•	•			
21	3/7-7	377-21	1550	•	•	•	•	•	
22	3/7-7	377-22	1560	•	•	•			

23	3/7-7	377-23	1570	•	•	•			
24	3/7-7	377-24	1580	•	•	•			
25	3/7-7	377-25	1590	•	•	•			
26	3/7-7	377-26	1600	•	•	•	•	•	
27	3/7-7	377-27	1610	•	•	•			
28	3/7-7	377-28	1620	•	•	•			
29	3/7-7	377-29	1630	•	•	•			
30	3/7-7	377-31	1650	•	•	•	•	•	
31	3/7-7	377-32	1660	•	•	•			
32	3/7-7	377-33	1670	•	•	•			
33	3/7-7	377-34	1680	•	•	•			
34	3/7-7	377-36	1700	•	•	•	•	•	
35	3/7-7	377-38	1720	•	•	•			
36	3/7-7	377-39	1730	•	•	•			
37	3/7-7	377-40	1740	•	•	•			
38	3/7-7	377-41	1750	•	•	•	•	•	
39	3/7-7	377-42	1760	•	•	•			
40	3/7-7	377-44	1780	•	•	•			
41	3/7-7	377-46	1800	•	•	•	•	•	
42	3/7-7	377-47	1810	•	•	•			
43	3/7-7	377-48	1820	•	•	•			
44	3/7-7	377-49	1830	•	•	•			
45	3/7-7	377-50	1840	•	•	•			
46	3/7-7	377-51	1850	•	•	•	•	•	
47	3/7-7	377-52	1860	•	•	•			
48	3/7-7	377-56	1900	•	•	•	•	•	
49	3/7-7	377-58	1920	•	•	•			
50	3/7-7	377-60	1940	•	•	•			
51	3/7-7	377-62	1960	•	•	•	•	•	
52	3/7-7	377-64	1980	•	•	•			
53	3/7-7	377-66	2000	•	•	•			

54	3/7-7	377-68	2020	•	•	•	•	•	
55	3/7-7	377-70	2040	•	•	•			
56	3/7-7	377-72	2060	•	•	•			
57	3/7-7	377-74	2080	•	•	•	•	•	
58	3/7-7	377-76	2100	•	•	•			
59	3/7-7	377-78	2120	•	•	•			
60	3/7-7	377-80	2140	•	•	•	•	•	
61	3/7-7	377-82	2160	•	•	•			
62	3/7-7	377-84	2180	•	•	•			
63	3/7-7	377-86	2200	•	•	•	•	•	
64	3/7-7	377-88	2220	•	•	•			
65	3/7-7	377-90	2240	•	•	•			
66	3/7-7	377-92	2260	•	•	•	•	•	
67	3/7-7	377-94	2280	•	•	•			
68	3/7-7	377-96	2300	•	•	•			
69	3/7-7	377-98	2320	•	•	•	•	•	
70	3/7-7	377-100	2340	•	•	•			
71	3/7-7	377-102	2360	•	•	•			
72	3/7-7	377-104	2380	•	•	•	•	•	
73	3/7-7	377-106	2400	•	•	•			

6.2 Geochemical Data and Analysis

Table 11: TOC values obtained for well 3/7-7.

Sample ID	UWI	Depth (m)	TOC (%)
377-1	3/7-7	1350	4.45
377-6	3/7-7	1400	6.82
377-11	3/7-7	1450	6.56
377-16	3/7-7	1500	6.32
377-21	3/7-7	1550	7.58
377-26	3/7-7	1600	6.23
377-31	3/7-7	1650	6.67
377-36	3/7-7	1700	6.45
377-41	3/7-7	1750	6.59
377-46	3/7-7	1800	7.88
377-51	3/7-7	1850	5.57
377-56	3/7-7	1900	6.72
377-62	3/7-7	1960	5.70
377-68	3/7-7	2020	6.41
377-74a	3/7-7	2080	4.19
377-80	3/7-7	2140	3.24
377-86	3/7-7	2200	4.01
377-92	3/7-7	2260	4.70
377-98	3/7-7	2320	4.72
377-104	3/7-7	2400	5.04

Table 12: TOC Values obtained for well 3/6-1.

Sample ID	UWI	Depth (m)	TOC (%)
361-1	3/6-1	810	2.14
361-4	3/6-1	860	1.25
361-6	3/6-1	900	4.71
361-9	3/6-1	950	4.38

361-13	3/6-1	1000	3.39
361-16	3/6-1	1050	4.85
361-21a	3/6-1	1100	2.16
361-26	3/6-1	1150	2.82
361-31	3/6-1	1200	2.61
361-36	3/6-1	1250	2.59
361-41	3/6-1	1300	2.09
361-46	3/6-1	1350	2.08
361-50	3/6-1	1390	2.33

Table 13: TOC Values obtained for well 4/4-1.

Sample ID	UWI	Depth (m)	TOC (%)
441-1	4/4-1	540	3.08
441-7	4/4-1	590	4.03
441-12	4/4-1	650	4.73
441-17	4/4-1	700	4.69
441-22	4/4-1	750	4.87
441-27	4/4-1	800	4.99
441-32	4/4-1	850	3.72
441-37	4/4-1	900	3.31

Table 14: TOC and Rock-eval results for samples analysed from well 3/6-1, 3/7-7, and 4/4-1.

Sample type	UWI	Depth (m)	S1 (mg/g)	S2 (mg/g)	S3 (mg/g)	Tmax (°C)	PP (mg/g)	PI (wt ratio)	HI (mg HC/g TOC)	OI (mg CO_2/g TOC)	TOC (%)
441-12	4/4-1	650	5.94	10.47	5.33	354	16.41	0.36	2.21	1.13	4.73
441-27	4/4-1	800	6.87	9.69	4.99	353	16.56	0.41	1.94	1.00	4.99
361-16	3/6-1	1050	1.74	5.16	4.87	425	6.9	0.25	1.06	1.00	4.85
361-36	3/6-1	1250	2.06	5.37	3.43	370	7.43	0.28	2.07	1.32	2.59
377-6	3/7-7	1400	29.12	16.54	2.28	430	45.66	0.64	2.43	0.33	6.82
377-46	3/7-7	1800	29.22	12.67	2.37	429	41.89	0.7	1.61	0.30	7.88
377-104	3/7-7	2380	25.38	8.04	1.21	432	33.42	0.76	1.60	0.24	5.04

S2

>20.0	Excellent generative potential
10.0 - 20.0	Very good generative potential
5.0 - 10.0	Good generative potential
2.5 - 5.0	Fair generative potential
<2.0	Poor generative potential

Tmax

<430	Immature
430 - 455	Oil Window
<456 -475	Condensate
>475	Dry gas

TOC

HI vs OI

Interpretation key (Source, Millennium Atlas).

6.3 QEMSCAN Images and Data Analysis

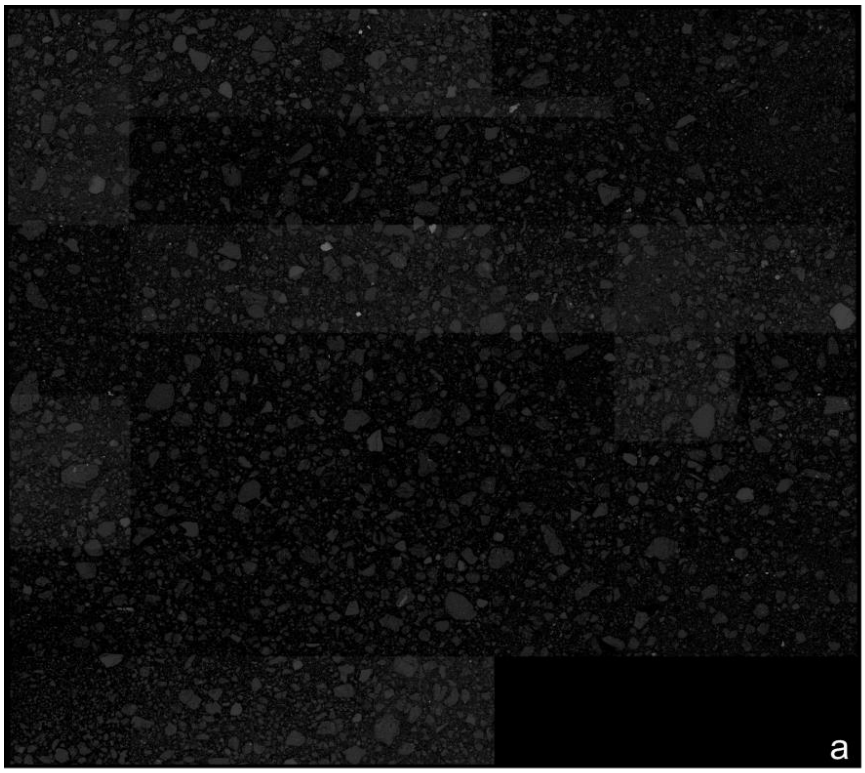

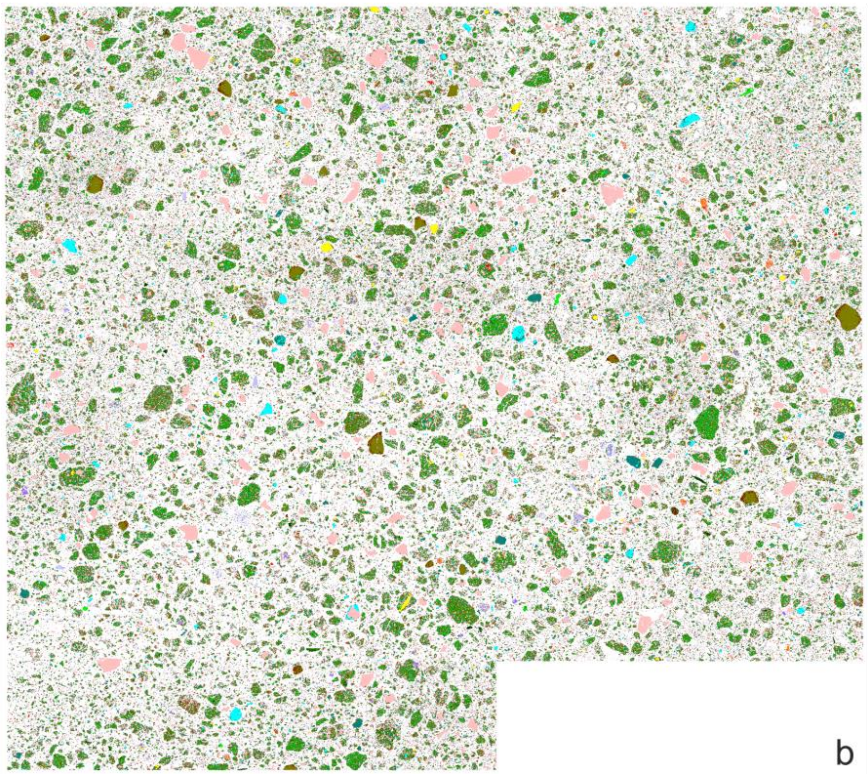

Mineral name	Area %
Quartz	22.10
Illite	31.17
Kaolinite	8.42
Hornblende	10.78
Biotite	4.02
K-Feldspar	2.08
Muscovite	2.82
Chlorite	3.21
Pyrite	1.91
Albite	2.53
Calcite	0.62
Dolomite	0.20
Siderite	0.55
Smectite	0.52
Glauconite	1.12
Rutile	0.38
Apatite	0.48
Gypsum	0.60
Kcl Mud	5.88
NaCl Mud	0.12
Others	0.52
Background	3.90
Unclassified	0

4.8 µm
1000.0µm

Figure 6.1: a) BSE map of polished section from drill cuttings of mudstone particles from a depth of 590m in well 4/4-1 and b) false colour map of the same polished thin section showing a mineralogical map and the distribution of main mineral species with Quartz in pink, Illite in green and Pyrite in yellow.

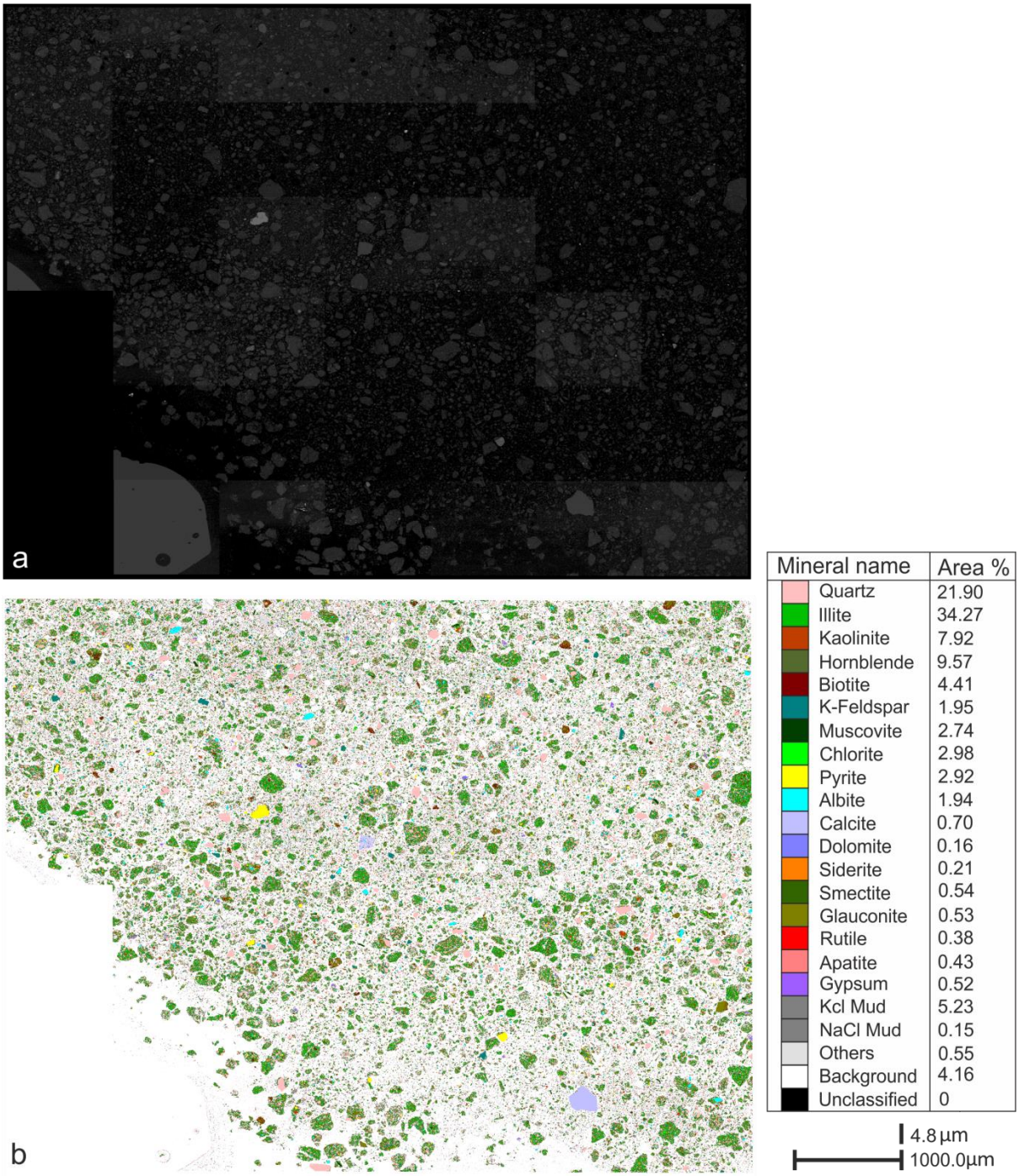

Figure 6.2: a) BSE map of polished section from drill cuttings of mudstone particles from a depth of 650m in well 4/4-1 and b) false colour map of the same polished thin section showing a mineralogical map and the distribution of main mineral species with Quartz in pink, Illite in green and Pyrite yellow.

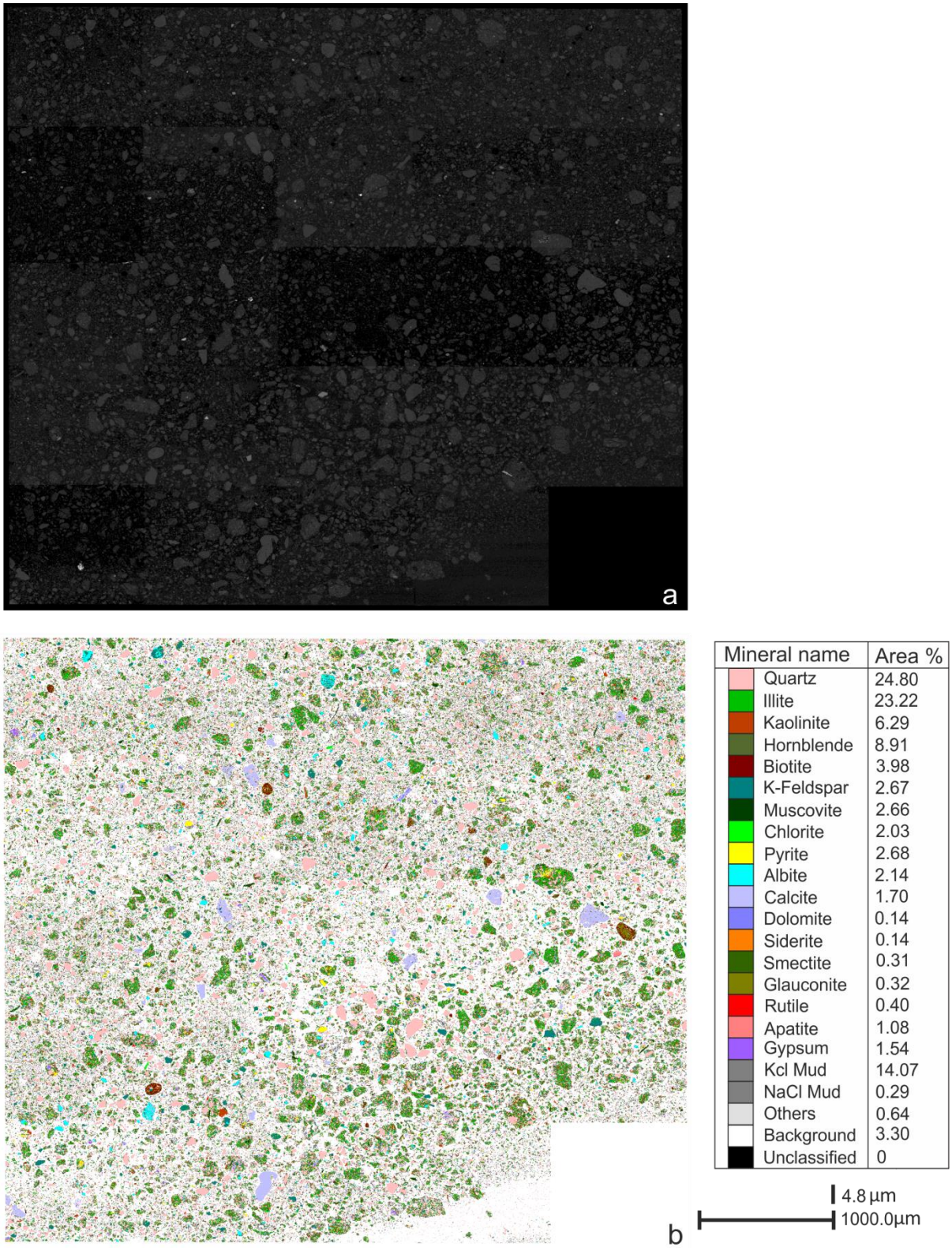

Figure 6.3: a) BSE map of polished section from drill cuttings of mudstone particles from a depth of 700 m in well 4/4-1 and b) false colour map of the same polished thin section showing a mineralogical map and the distribution of main mineral species with Quartz in pink, Illite in green and Pyrite in yellow.

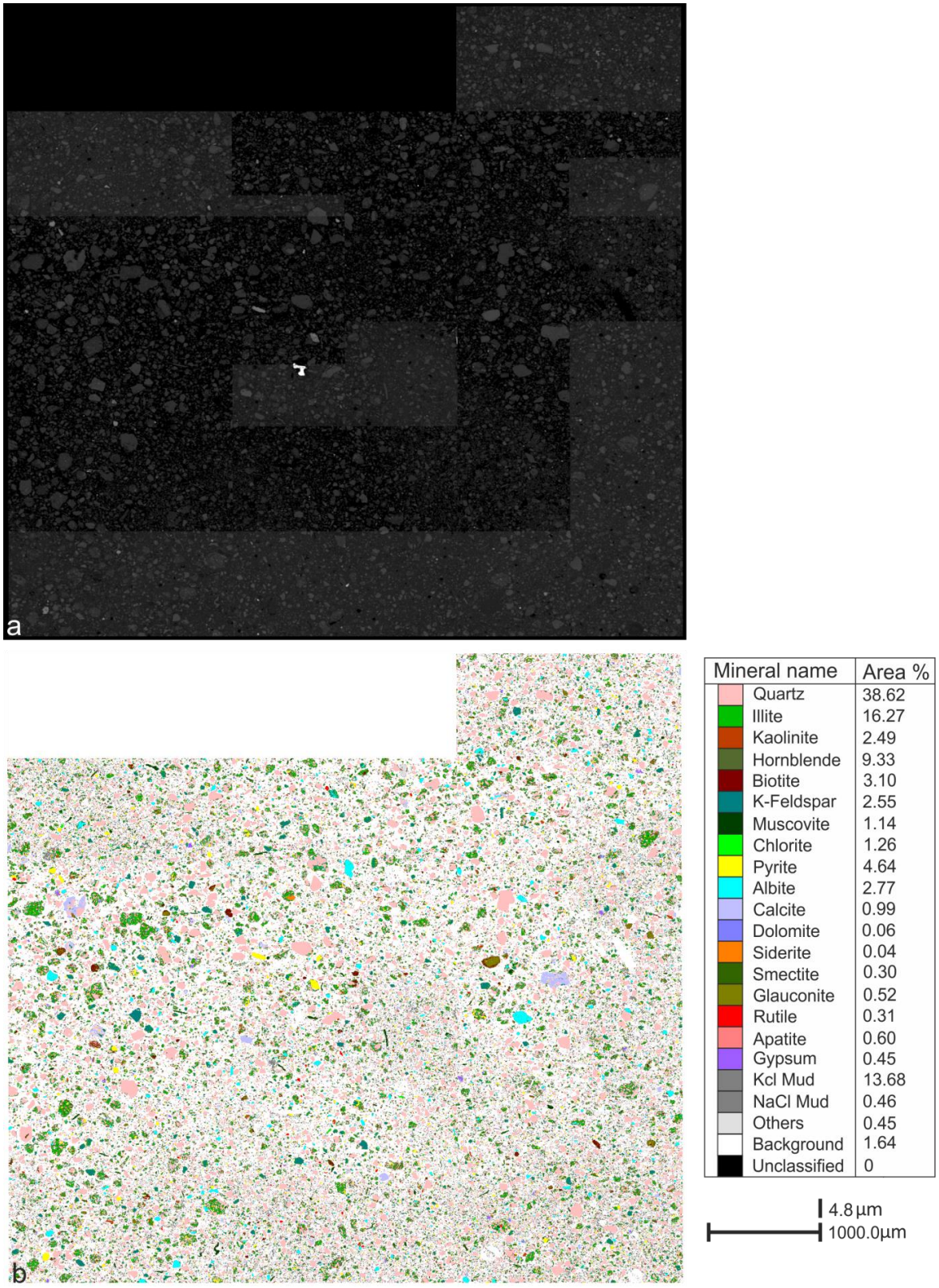

Figure 6.4: a) BSE map of polished section from drill cuttings of mudstone particles from a depth of 750 m in well 4/4-1 and b) false colour map of the same polished thin section showing a mineralogical map and the distribution of main mineral species with Quartz in pink, Illite in green and Pyrite in yellow.

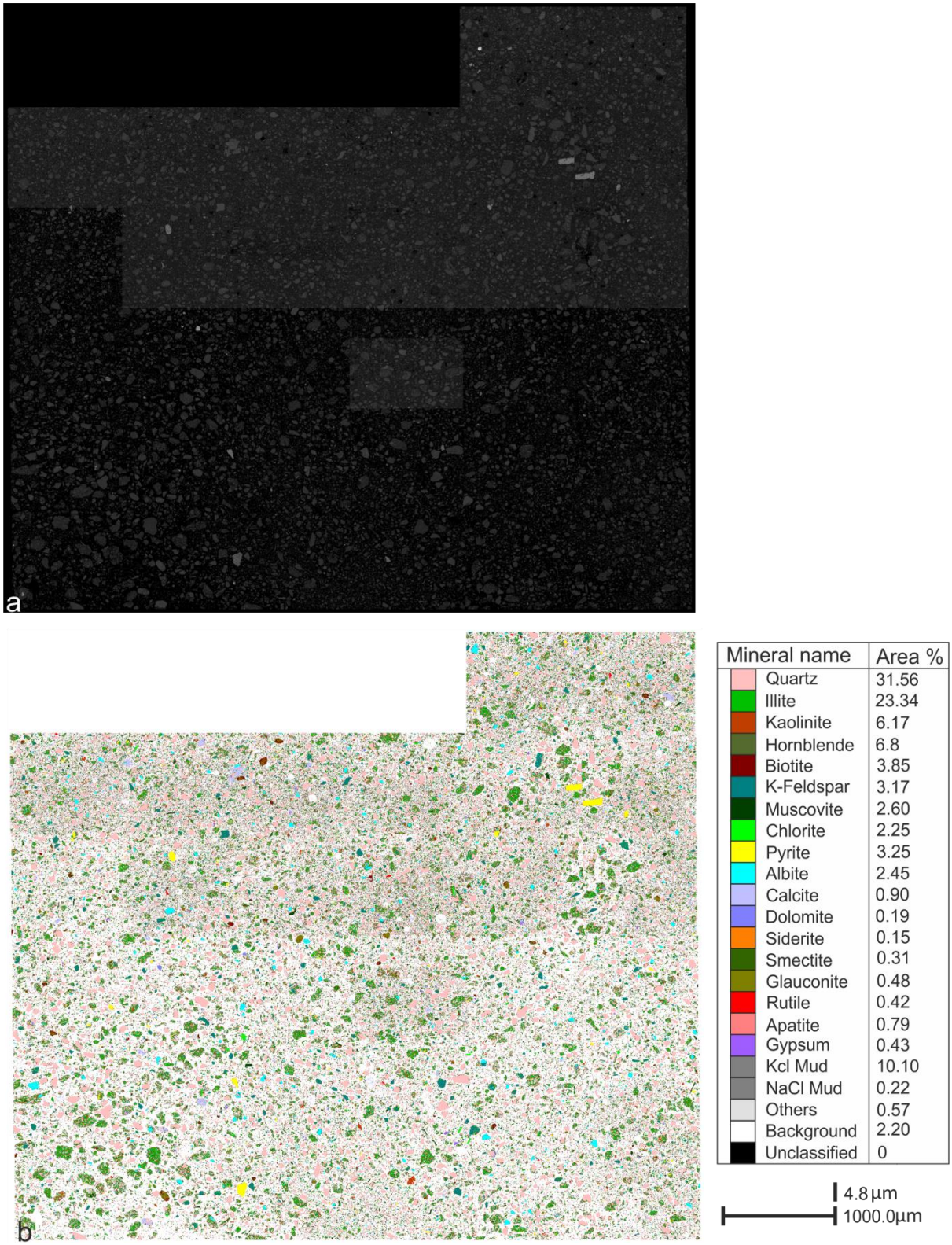

Figure 6.5: a) BSE map of polished section from drill cuttings of mudstone particles from a depth of 800 m in well 4/4-1 and b) false colour map of the same polished thin section showing a mineralogical map and the distribution of main mineral species with Quartz in pink, Illite in green and Pyrite in yellow.

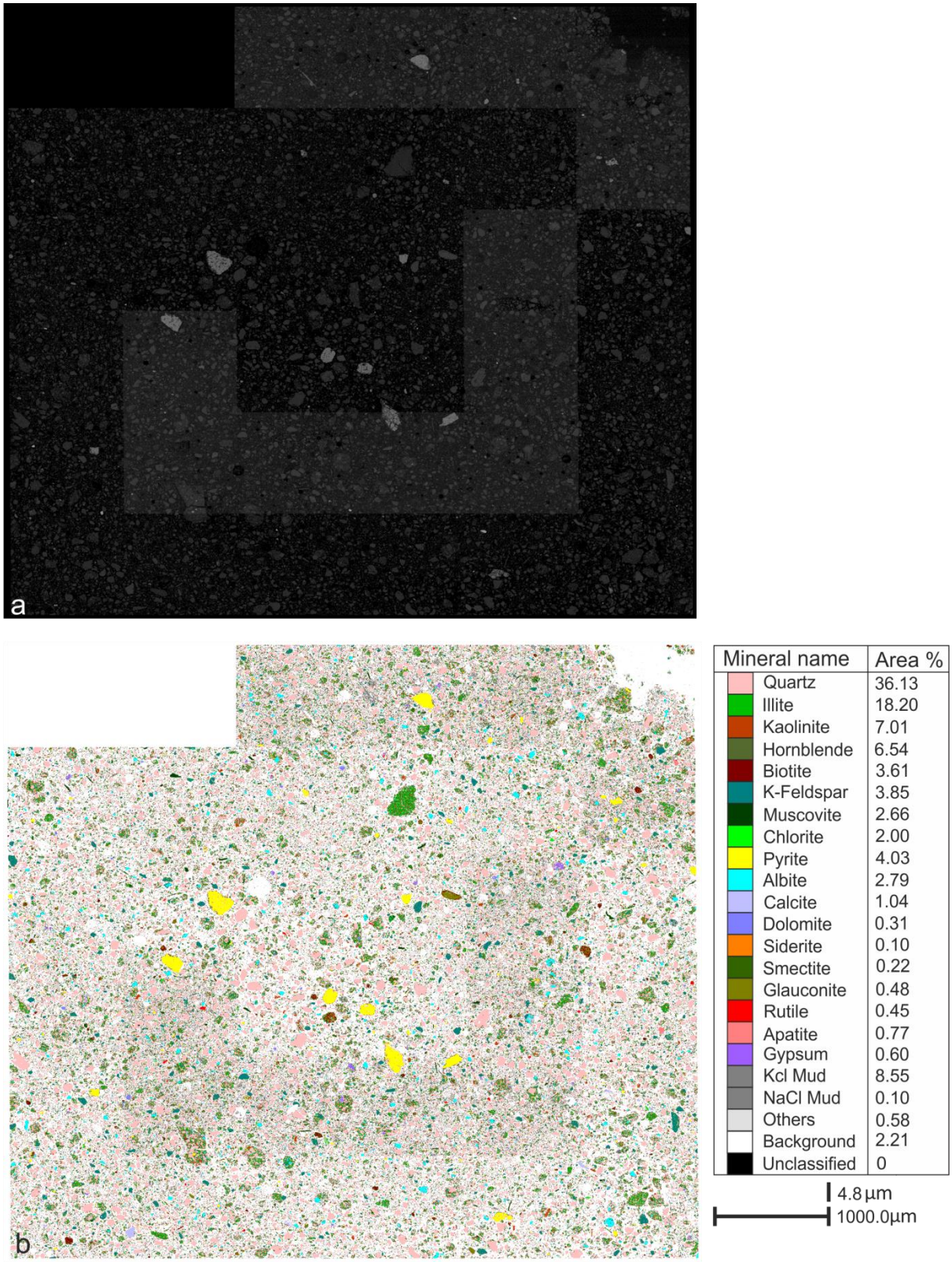

Figure 6.6: a) BSE map of polished section from drill cuttings of mudstone particles from a depth of 850 m in well 4/4-1 and b) false colour map of the same polished thin section showing a mineralogical map and the distribution of main mineral species with Quartz in pink, Illite in green and Pyrite in yellow.

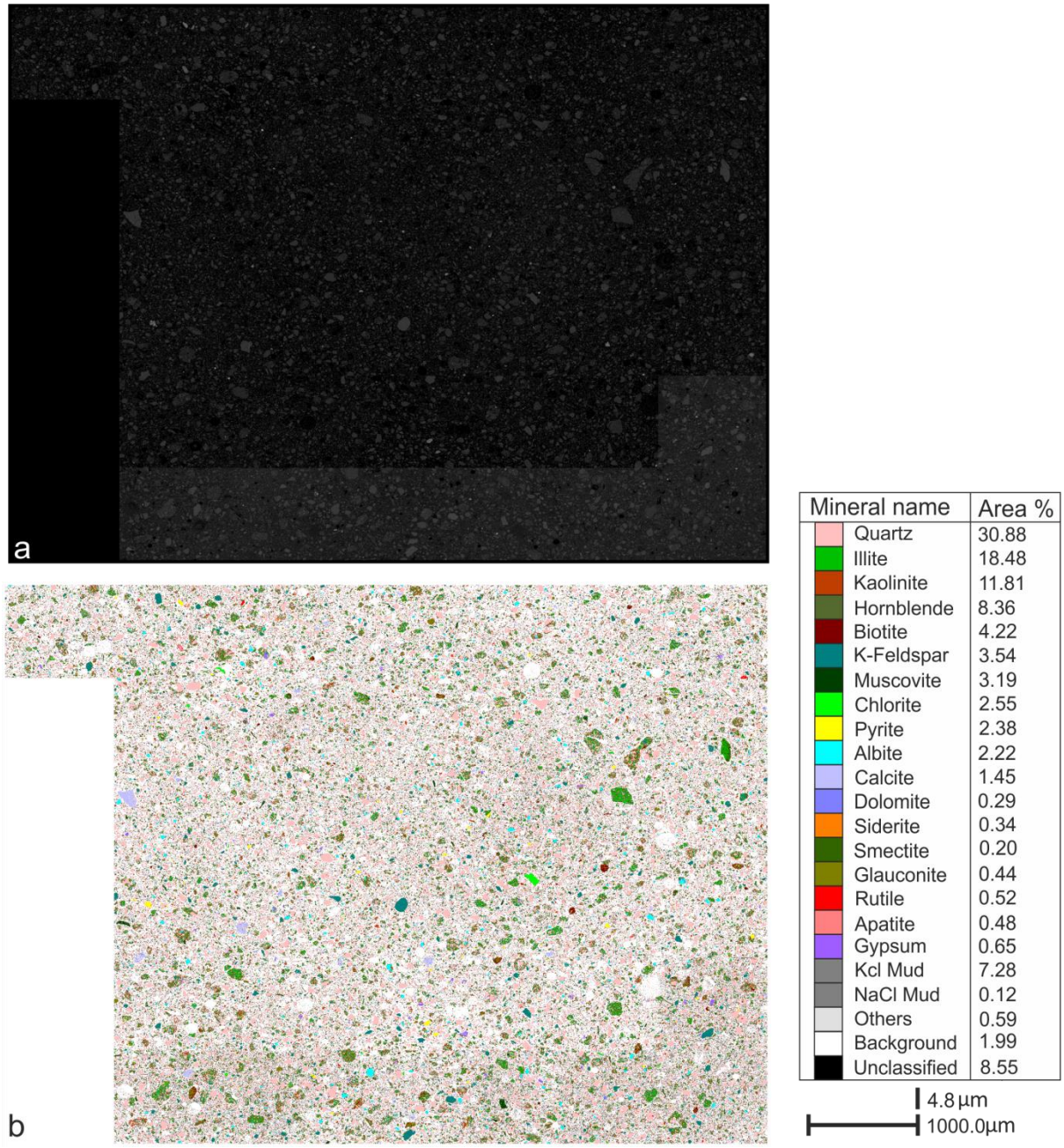

Figure 6.7: a) BSE map of polished section from drill cuttings of mudstone particles from a depth of 900 m in well 4/4-1 and b) false colour map of the same polished thin section showing a mineralogical map and the distribution of main mineral species with Quartz in pink, Illite in green and Pyrite in yellow.

6.4 XRD Data and QEMSCAN Data

All the raw data files acquired for the XRD and QEMSCAN analysis in this study can be requested at https://zenodo.org/record/5746050 and cited as:

Malah M. (2021). Silica diagenesis, polygonal faulting, and shallow gas: implications for fluid migration, storage, and shallow hazards [Zenodo]. https://doi.org/10.5281/zenodo.5746050